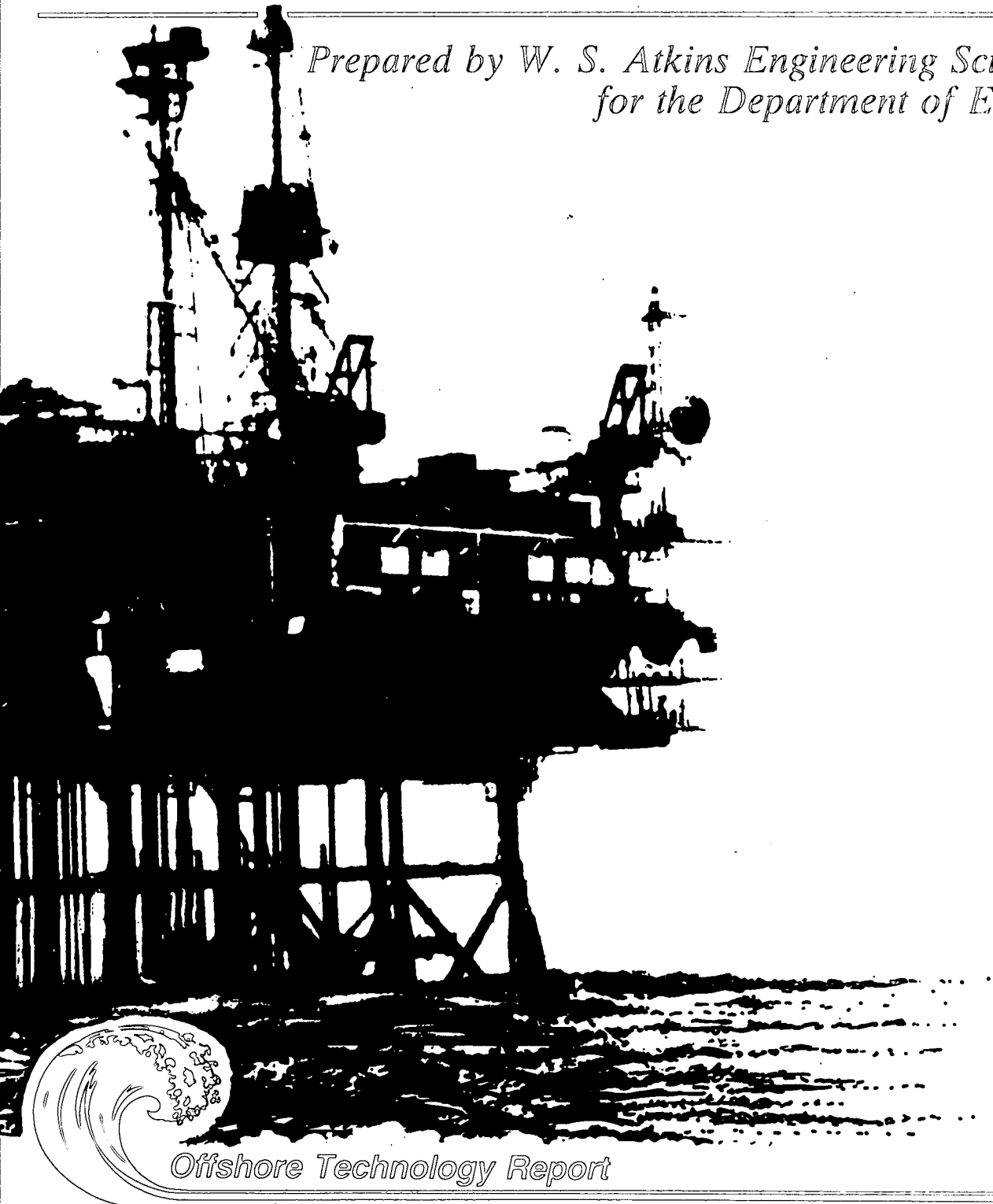

FLUID LOADING ON FIXED OFFSHORE STRUCTURES VOLUME I

Background to the 4th edition of Offshore
Installations: Guidance on Design and Construction

*Prepared by W. S. Atkins Engineering Sciences
for the Department of Energy*



Offshore Technology Report

<p>A SUMNER 15/7/2004 Returned to Library 28/6/04</p>	
---	--

Please return by the date indicated

FLUID LOADING ON FIXED OFFSHORE STRUCTURES VOLUME I

Background to the 4th edition of Offshore
Installations: Guidance on Design and Construction

COPY ID: 195462-1001

Authors

N.D.P. BARLTROP, G.M. MITCHELL and J.B. ATKINS

Prepared for publication by
W.S. ATKINS ENGINEERING SCIENCES

***Woodcote Grove
Ashley Road
Epsom
Surrey KT18 5BW***

London: HMSO

© *Crown copyright 1990*
First published 1990
ISBN 0 11 413324 7

This publication forms part of a series of reports to the Department of Energy of work which has been wholly or in part supported by funds provided by the Department. Neither the Department nor the contractors concerned assume any liability for the reports nor do they necessarily reflect the views or policy of the Department.

Results, including detailed evaluation and, where relevant, recommendations stemming from these research projects, are published in the OTH series of reports.

Background information and data arising from these research projects are published in the OTI series of reports.

This publication has been prepared from camera ready copy supplied by the Department of Energy

HMSO

Standing order service

Placing a standing order with HMSO BOOKS enables a customer to receive other titles in this series automatically as published. This saves the time, trouble and expense of placing individual orders and avoids the problem of knowing when to do so.

For details please write to HMSO BOOKS (PC 13A/1), Publications Centre, PO Box 276, London SW8 5DT quoting reference X12.01.025

The standing order service also enables customers to receive automatically as published all material of their choice which additionally saves extensive catalogue research. The scope and selectivity of the service has been extended by new techniques, and there are more than 3,500 classifications to choose from. A special leaflet describing the service in detail may be obtained on request.

ACKNOWLEDGEMENT TO STEERING GROUP

This document has been prepared by WS Atkins Engineering Sciences (previously Atkins R & D) for the Department of Energy, and directed by the Fluid Loading Guidance Notes Revision Group set up by the Petroleum Division of the Department.

The Steering Group members were:

- Mr A R McIntosh Petroleum Engineering Division – Department of Energy,
 Chairman.
- Mr G Lawrence MaTSU, Secretary (to 30.6.86)
- Mr R Vaux MaTSU, Secretary (from 30.6.86)
- Mr J Franklin (from 1.2.87)
- Dr R G Guy
- Mr D Harris
- Dr F Ramzan
- Dr R G Standing
- Mr G Tickell
- Dr W Visser
- Mr R M Webb
- Mr M K Wilsdon

Support was given by:

- Prof J Chaplin
- Mr M Birkinshaw
- Dr R Robinson
- Mr J R Potter
- Mr J Shuurman

The Department and WS Atkins Engineering Sciences would like to express their appreciation of the efforts made by these contributors and thank the organisations which permitted them to take part.

ACKNOWLEDGEMENT

This document has drawn on many sources of information and we acknowledge the contribution of all the research workers, their organisations and publishers.

In particular we thank the following for permitting us to reproduce information first published by themselves:

American Society of Civil Engineers (ASCE)

British Marine Technology Ltd (BMT) (previously the National Maritime Institute (NMI))

Construction Industry Research and Information Association, Underwater Engineering Group (CIRIA-UEG)

Elsevier Science Publishers BV

Engineering Sciences Data Unit (ESDU)

Institution of Civil Engineers (ICE)

Cambridge University Press

Springer - Verlag

Offshore Technology Conference (OTC)

National Physical Laboratory (NPL)

Naval Postgraduate School, Monterey

Van Nostrand Reinhold Company

SUMMARY

This document reviews the experimental work performed on wave particle kinematics and fluid loading in the context of the design of fixed offshore structures. It compares various methods (spectral, deterministic etc) of estimating loading conditions for extreme and fatigue strength calculations and describes the sensitivity of the calculations to various fluid loading parameters.

a. Determination of Particle Kinematics in Waves (Sections 2.1 and 2.2)

Regular wave theories are compared and recommendations are made for the selection of a suitable theory. The recommendations have been established by comparing wave properties that are significant for the design of offshore structures; e.g. velocities, accelerations, crest height and wave length. The errors involved in using Airy theory outside its range of applicability are quantified.

Particle velocities predicted by regular wave theories have been compared with measurements made in the sea. Near the water surface some approximate agreement was found but at depth the regular wave theories overpredicted the kinematics.

Linear random wave theories are described and the problems of representing finite height waves in the splash zone are discussed. The results of random wave theory are compared with sea measurements and generally reasonable agreement is found, especially if directional spreading is taken into account.

Theoretical comparisons between random wave theory and regular waves have been made by comparing the extremes of random wave particle kinematics with the regular wave particle kinematics for regular waves having a corresponding extreme height with a range of steepness. This suggests that near the surface very steep regular waves are needed to obtain the predicted highest particle kinematics. At depth, shallower (i.e. longer) regular waves are needed.

b. Wave - Current Interaction (Section 2.3)

The structure of currents is discussed in Section 3.4 of Meteorological and Oceanographic Design Parameters, Proposed Revision to Offshore Installations : Guidance on Design and Construction Part II Section 2, Department of Energy, July 1987. However the intensity and profile of the near surface wind driven current in the presence of waves is still uncertain.

This report considers various approximate methods of allowing for wave-current interaction. Methods which reduce the current velocity under the wave crest, on the basis of continuity arguments, are shown to be incorrect. A better approximation considers the wave to 'ride' on the current. It is recommended that the current velocity profile is vectorially added to the wave velocity profile in such a way that the instantaneous surface current is constant.

c. Breaking Waves (Section 2.4)

The mechanism and causes of wave breaking are discussed. Guidance is given on the characteristics of breaking waves that may be expected at any site. The kinematics of breaking waves are still the subject of research but guidance is given for spilling breakers and some tentative guidance is given for plunging breakers.

d. Morison's Equation (Section 3.2)

The applicability of Morison's equation and the factors affecting C_d and C_m , the drag and inertia coefficients, are discussed in relation to experiments performed in the laboratory and in the sea. Realistic values of C_d , for circular cylinders are shown to be markedly higher than those generally used for design purposes but, as shown later (in Appendix P), the low C_d value can be regarded as allowing for (1) the small probability of extreme wave and current occurring at the same time and (2) the conservative use of unidirectional and, usually, regular wave theories in the determination of particle kinematics.

C_d and C_m are shown to be affected by many parameters; Reynolds number: R_e , Keulegan Carpenter number: K_c , surface roughness and current all significantly affect C_d . Most loading of significance to offshore structures is in the post super-critical range of R_e and the loading then becomes independent of R_e . C_d still appears to be sensitive to K_c , surface roughness and current but we have taken advantage of the link between K_c and the ratio of drag to inertia loading in order to present C_d and C_m pairs which

will give approximately correct loading over the whole range of K_c and current. The approximate C_d and C_m values are therefore dependent on surface roughness alone. Member inclination may also have an effect on C_d but there is at present insufficient data to allow for this effect. Additional possibly important changes to loading occur where a member penetrates the water surface. This is the subject of ongoing research.

e. Vortex Shedding (Section 3.3)

Vortex shedding, structural response and 'lock-on' are described for steady flow and wave flow. The significance of Strouhal number, the response parameter and K_c are demonstrated. Recommendations are made for the avoidance of vortex shedding induced oscillation. This includes tentative guidance on vortex shedding in waves and the case of intermittent lock-on. References are given to guidance on the use of strakes etc to cure existing vortex induced oscillations.

f. Diffraction Loading (Section 3.4)

Wave diffraction by large members is briefly discussed and guidance is given on when diffraction theory should be used and how in some circumstances modified Morison inertia coefficients may be used instead. The situations in which diffracting members modify the loading on adjacent Morison regime members are described. Some examples of diffraction theory results are given and reference is made to more detailed texts.

g. Wave Slam and Wave Slap (Section 3.5)

Wave slam and slap forces, pressures, probabilities and structural response are discussed and guidance (some tentative) is given. The considerable scatter in measured slap pressure is noted. This large scatter would favour a reliability based analysis approach but at present deterministic methods are used and this is recognised in the guidance given.

h. Hydrostatic and Hydrodynamic Pressure (Section 3.6)

Hydrostatic and hydrodynamic pressures are discussed. It is recommended that stresses are calculated from the applied pressure distribution in preference to using buoyancy arguments which may neglect e.g. hydrostatically induced punching shear forces acting on the connection of a horizontal brace to its chord members.

The interaction of member curvature, external pressure and internal pressure is noted although this is only likely to be significant for members subject to pressures of more than 100m water.

i. Interference (Section 3.7)

Interference effects on the total load acting on conductor groups are shown to be usually small (less than 20%) providing the centre line spacing is greater than three diameters. Individual conductors may still be subject to higher loading and a 50% increase for checking extreme loading on individual members is recommended.

Similarly no interference effect need be taken into account when calculating the global load on structures with attachments standing off (with a gap) from the structural members. However for the calculation of the load on the attachment itself it is necessary to consider the increased velocities caused by the presence of the member and the 'convective' acceleration in the water as it accelerates and decelerates in its path around the member. Diagrams are given to enable both the increased velocities and convective accelerations to be easily calculated.

Where there is no gap between the member and attachment the member should be considered to have a modified shape. Some guidance on the calculation of increased forces in these circumstances is given.

j. Extreme and Fatigue Analysis Methods (Section 4)

The link between environmental data, hydrodynamics and structural behaviour is discussed in relation to deterministic, semi-probabilistic (a type of deterministic), spectral and other methods for extreme and fatigue analysis.

None of the methods are found to be ideal but deterministic analysis is shown to be a useful technique for extreme loading analysis. The semi-probabilistic and spectral methods are shown to be useful for the fatigue analysis of structures which respond quasistatically and dynamically respectively.

The semi probabilistic method is also shown to be a useful basis for the analysis of vortex shedding and wave slam/slap.

This section also contains the results of a numerical comparison of the methods and a description of experiments in which the total hydrodynamic load on structures has been compared with the calculated loads. These experiments allow some confidence in the existing methods of design for wave loading.

k. Sensitivity (Section 5)

The sensitivity of typical members and structures to assumed wave theory, wave length, height and period, selected wave phase angle, current, tide and storm surge, C_d and C_m , wave current directionality and crest length is, mainly qualitatively, described.

NOMENCLATURE

A	area of cross section	t	time
b	diameter of particle orbit	T	wave period
B_r	breaker index	T_z	mean zero crossing period
c	wave celerity	u,w	particle velocities
C_a	added mass coefficient	U	normal particle velocity (see Figure 3.2.1)
C_d	drag coefficient (time averaged)	U_r	reduced velocity
C'_d	fluctuating drag coefficient	x,z	co-ordinates (see Figure 2.1.1)
C_f	total force coefficient		
C_l	lift coefficient (time averaged)	δ	logarithmic decrement = $2\pi\xi$
C'_l	fluctuating lift coefficient	η	water surface elevation above MWL
C_m	inertia coefficient (frequently $C_m = 1+C_a$)	θ	angle
C_s	slap coefficient	μ	viscosity
C_p	slap pressure coefficient	ν	kinematic viscosity
d	water depth	ξ	damping ratio
D	cylinder diameter (see Figure 3.2.6)	ρ	density
E	ellipticity : 0 = planar, 1 = circular	σ	standard deviation, stress
f	force	ϕ	velocity potential
g	gravity acceleration	ω	angular velocity (rad/sec)
H	wave height		
H_s	significant wave height		
k	roughness height (see Figure 3.2.6)		
K_c	Keulegan Carpenter number		
K_1	velocity enhancement factor		
K_2	convective acceleration factor		
m	sea bed slope		
M	mean, spectral moment		
MWL	mean water level		
N	frequency (H_z)		
R_e	Reynolds number		
R_p	response parameter		
s	height above mudline		
S	spacing of members, spectral ordinate		
S_t	Strouhal Number		

Subscripts

b	breaking
c	curent
d	drag
i	inertia
m	maximum value
o	deep water values
p	pair
w	wave

CONTENTS

VOLUME I

	Page
1.0 INTRODUCTION	25
2.0 DETERMINATION OF PARTICLE KINEMATICS	27
2.1 REGULAR WAVES	27
2.1.1 Introduction	27
2.1.2 Regular wave theories	27
2.1.3 Comparison of wave theories	33
2.1.4 Regular waves: conclusion	38
2.2 RANDOM WAVES	43
2.2.1 Introduction	43
2.2.2 Random wave theory	43
2.2.3 Finite wave height effects in random wave analysis	45
2.2.4 Comparison of random wave theory with experiments in the sea	47
2.2.5 Comparison of regular wave theory with experiments in the sea	59
2.2.6 Comparison of regular wave and random wave theories	63
2.2.7 Random waves: conclusion	64

	Page
2.3 WAVE – CURRENT INTERACTION	65
2.3.1 Introduction	65
2.3.2 Effect of a uniform current	65
2.3.3 Effect of a steady current which varies with depth	66
2.3.4 Effect of unsteady and non uniform currents	69
2.3.5 Wave – current interaction: conclusion	69
2.4 BREAKING WAVES	71
2.4.1 Introduction	71
2.4.2 Waves breaking in shoaling water	72
2.4.3 Wave breaking caused by wind	77
2.4.4 Wave breaking caused by wave–wave interaction	81
2.4.5 Wave breaking caused by currents	83
2.4.6 Plunging wave after breaking	83
2.4.7 Breaking wave kinematics	83
2.4.8 Breaking waves: conclusion	85
2.5 REFERENCES	86

	Page
3.0 FLUID LOADING	93
3.1 INTRODUCTION	93
3.1.1 General	93
3.1.2 Vortex Formation, Drag and Lift Forces	93
3.1.3 Inertia Forces	95
3.1.4 Diffraction Loading	96
3.1.5 Wave Slam, Slap and Impulsive Buoyancy	96
3.1.6 Hydrostatic and Hydrodynamic Pressure	97
3.1.7 Loading Regimes	97
3.2 DRAG AND INERTIA LOADING ON CIRCULAR CYLINDERS	98
3.2.1 Morison's Equation	98
3.2.2 Flow Conditions	100
3.2.3 Marine Growth and Surface Roughness	109
3.2.4 Steady Flow	110
3.2.5 Accelerating flow	117
3.2.6 Planar Oscillating Flow	119

	Page
3.2.7 Cylinders in Simulated Waves	132
3.2.8 Laboratory Waves	135
3.2.9 Sea Waves	149
3.2.10 Summary and Discussion of C_d and C_m Results for Circular Cylinders	166
3.2.11 The Selection of C_d and C_m for Circular Cylinders in Waves and Currents	185
3.2.12 Approximate C_d and C_m Values for Circular Cylinders in Waves and Current	191
3.2.13 Drag, Inertia and Steady Lift Coefficients for Non-circular Members	191
3.3 VORTEX SHEDDING INDUCED OSCILLATION	202
3.3.1 General	202
3.3.2 Steady Flow with No Member Oscillation	204
3.3.3 Steady Flow with Vortex Induced Member Oscillation	210
3.3.4 Lift Forces in Planar Oscillating Flow and Waves, with No Member Oscillation	220
3.3.5 Frequency of Vortex Shedding in Planar Oscillating Flow and Waves	224

	Page
3.3.6 Planar Oscillating and Wave Flow with Vortex Induced Member Oscillation	228
3.3.7 Recommendations for Avoiding Vortex Induced Member Oscillation	231
3.3.8 Fatigue Analysis of Members Excited by Vortex Shedding	234
3.3.9 Vortex Shedding : Conclusion	235
 3.4 DIFFRACTION LOAD EVALUATION	 236
3.4.1 Introduction	236
3.4.2 Analytical and Numerical Methods	236
3.4.3 Effects of Currents	239
3.4.4 Differences between Diffraction and the Inertia Term in Morison's Equation	240
3.4.5 Influence of Diffracting Members on Other Members	241
3.4.6 Comparison of Diffraction Theory with Experiment	241
3.4.7 Jarlan Walls	241
 3.5 WAVE SLAM AND WAVE SLAP	 242
3.5.1 General	242
3.5.2 Slam Coefficients for Cylinders	243

	Page
3.5.3 Member Response to Slam	245
3.5.4 Probability of Wave Slam	249
3.5.5 Slam Coefficients for Non-Cylindrical Members	249
3.5.6 Pressure Distributions from Wave Slam	250
3.5.7 Wave Slap	252
3.5.8 Probability of Wave Slap from Breaking Waves	257
3.5.9 Recommendations for the Calculation of Wave Slam and Slap Forces and Pressure	257
 3.6 HYDROSTATIC AND HYDRODYNAMIC PRESSURE	 260
3.6.1 Hydrostatic Pressure	260
3.6.2 Hydrodynamic Pressure	260
 3.7 INTERFERENCE BETWEEN MEMBERS	 261
3.7.1 General	261
3.7.2 Forces on Arrays of Cylinders in Steady Flow	261
3.7.3 In Line Forces on Arrays of Cylinders in Oscillating Flow	266
3.7.4 Inertia and Diffraction Forces on Arrays of Cylinders in Inviscid Flow	269

	Page
3.7.5 Lift Forces on Arrays of Cylinders	270
3.7.6 Conclusion for Arrays of Cylinders	271
3.7.7 Interference Between Non Cylindrical Shapes	274
3.7.8 Attachments	274
3.7.9 Total Load on a Member with Attachments	274
3.7.10 Force on Attachments to Members	278
3.7.11 Joints	279
3.7.12 Interference : Conclusions	282
 3.8 REFERENCES	 284

VOLUME II

4.0 METHODS FOR THE ANALYSIS OF EXTREME AND FATIGUE LOADING	297
4.1 INTRODUCTION	297
4.2 RELEVANT ENVIRONMENTAL DATA	297
4.2.1 H_s and T_z Scatter Diagrams	297
4.2.2 Wave Height Exceedence Data	300
4.2.3 Individual Wave Height-Period Scatter Diagrams	303
4.2.4 Directionality Data	303

	Page
4.2.5 Current Data	303
4.2.6 Water Levels	304
4.2.7 Combination of Extremes	304
4.3 METHODS FOR ESTIMATING EXTREME LOADS	305
4.3.1 Introduction	305
4.3.2 Deterministic Extreme Load Analysis	309
4.3.3 Semi-Probabilistic – Extreme Load Analysis	311
4.3.4 Spectral: Linear Probabilistic Extreme Load Analysis	313
4.3.5 Non-Linear Probabilistic Extreme Load Analysis	319
4.3.6 Random Wave Time History Analysis	321
4.3.7 Comparison of Extreme Load Analysis Methods	322
4.4 METHODS FOR ESTIMATING FATIGUE LOADS	323
4.4.1 Introduction	323
4.4.2 Deterministic Fatigue Load Analysis	328
4.4.3 Semi-Probabilistic Fatigue Load Analysis	331
4.4.4 Spectral: Linear Probabilistic Fatigue Load Analysis	337
4.4.5 Non-Linear Probabilistic Fatigue Load Analysis	343
4.4.6 Random Wave Time History	345

	Page
4.4.7 Comparison of Fatigue Load Analysis Methods	345
4.5 THEORETICAL COMPARISONS OF ANALYSIS METHODS	347
4.5.1 General	347
4.5.2 Comparison of Predicted Extreme Loading	348
4.5.3 Comparison of Predicted Fatigue Loading	348
4.6 COMPARISON OF THEORETICAL ESTIMATES OF STRUCTURAL LOADING WITH MEASURED VALUES	348
4.6.1 General	348
4.6.2 OTS Measurements	351
4.6.3 Eugene Island Measurements	352
4.6.4 Forties Field Experiment	353
4.6.5 Conclusion	354
4.7 REFERENCES	354
5.0 SENSITIVITY OF RESULTS TO VARIOUS FACTORS AFFECTING FLUID LOADING	357
5.1 INTRODUCTION	357
5.2 WAVE THEORY	357
5.2.1 General	357

	Page
5.2.2 Sensitivity of Extreme Loading to the Selected Wave Theory	357
5.2.3 Sensitivity of Fatigue Loading to the Selected Wave Theory	357
5.3 WAVE LENGTH	358
5.3.1 General	358
5.3.2 Sensitivity of Extreme Loading to Wave Length	359
5.3.3 Sensitivity of Fatigue Loading to Wave Length	361
5.4 WAVE HEIGHT	361
5.4.1 General	361
5.4.2 Sensitivity of Extreme Loading to Wave Height	362
5.4.3 Sensitivity of Fatigue Loading to Wave Height	362
5.5 WAVE PERIOD	362
5.5.1 General	362
5.5.2 Sensitivity of Extreme Loading to Wave Period	363
5.5.3 Sensitivity of Fatigue Loading to Wave Period	363
5.6 EFFECTS OF CURRENTS	363
5.6.1 General	363

	Page
5.6.2 Sensitivity of Extreme Loading to Current	364
5.6.3 Sensitivity of Fatigue Loading to Current	366
5.7 WAVE PHASE	368
5.7.1 General	368
5.7.2 Sensitivity of Extreme Loading to Wave Phase Angle	369
5.7.3 Sensitivity of Fatigue Loading to Wave Phase Angle	369
5.8 LOADING COEFFICIENTS (FOR MORISON'S EQUATION)	371
5.9 TIDE AND STORM SURGE (EFFECT ON MEAN WATER LEVEL)	371
5.9.1 General	371
5.9.2 Sensitivity of Extreme Loading to Tide and Storm Surge	371
5.9.3 Sensitivity of Fatigue Loading to Tide and Storm Surge	373
5.10 WAVE AND CURRENT DIRECTIONALITY	373
5.11 CREST LENGTH	376
5.11.1 General	376
5.11.2 Sensitivity of Extreme Loading to Crest Length	376
5.11.3 Sensitivity of Fatigue Loading to Crest Length	376
5.12 REFERENCES	378

APPENDICES

	Page
A	SOME PROPERTIES OF AIRY WAVES 381
B	DERIVATION OF THE WAVE THEORY SELECTION DIAGRAM 384
C	COMPARISONS OF AIRY AND HIGHER ORDER WAVE THEORIES 389
D	THEORETICAL COMPARISON OF PEAK VELOCITIES AND ACCELERATIONS IN A SEA STATE AND IN REPRESENTATIVE REGULAR WAVES (BY R. G. STANDING, BMT) 397
E	EFFECT OF A UNIFORM CURRENT ON WAVE PERIOD : WAVE LENGTH RELATIONSHIP 400
F	CALCULATION OF PARTICLE KINEMATICS IN A WAVE OF SPECIFIED PERIOD (ENCOUNTERED BY A STATIONARY OBSERVER) IN THE PRESENCE OF A CURRENT 408
G	BREAKING WAVES: DERIVATION OF FIGURE 2.4.6 AND ESTIMATION OF PARTICLE KINEMATICS IN PLUNGING BREAKERS 411
H	EFFECT OF CURRENT ON C_d AND C_m IN WAVES 415
I	EFFECT OF IGNORING THE AXIAL FROUDE KRYLOV FORCE 423
J	DAMPING 425
K	OSCILLATION OF CIRCULAR CYLINDERS. RESPONSE AMPLITUDE FROM A SIMPLE WAKE OSCILLATOR MODEL 431
L	TRANSVERSE OSCILLATION OF CIRCULAR CYLINDERS WHEN THE INCIDENT FLOW VELOCITY IS INTERMITTENTLY IN THE LOCK-ON RANGE 438

	Page	
M	RELATIONSHIP BETWEEN WAVE IMPACT EXPERIMENTAL RESULTS AND THE COEFFICIENT C_p	447
N	CALCULATION OF SLAP PRESSURES ALLOWING FOR WAVE CURVATURE	451
O	POTENTIAL FLOW VELOCITY AND ACCELERATION FIELD AROUND A CIRCULAR CYLINDER	455
P	A STUDY FOR THE VALIDATION OF FORCE COEFFICIENTS USED IN THE STRUCTURAL DESIGN OF FIXED STEEL OFFSHORE PLATFORMS (BY D. HARRIS, LRS)	461

1. INTRODUCTION

This report for the Department of Energy, provides supporting documentation for the hydrodynamic and hydrostatic loading on rigid structures sections of the Department's Guidance Notes. Atkins Engineering Sciences prepared the report under the supervision of a small Steering Group which consisted of representatives from oil companies, certifying authorities, designers and research institutions. The Steering Group members are listed on page 3.

Most aspects of fluid loading calculations are subject to uncertainty but the normal industry design practice is based on the results of experiments, theory and to a limited extent, full scale tests. An exception to this has been the selection of drag and inertia coefficients. Over the last 10 years experiments have shown that the C_d values for marine roughened cylinders are significantly greater than 0.7, which is usually used for design purposes. Designers have, however, not increased C_d values in line with the research results. The general opinion of the Steering Group and Authors is that the use of low C_d values is probably acceptable for conventional structures because the current industry practice also contains some compensatory conservative methodology:

- a) Separate extreme values of wave height, wave period, current and mean water level are combined.
- b) Regular wave theories are used.
- c) The seas are assumed unidirectional.
- d) Possible benefits from shielding effects are excluded.

However, it is by no means certain that the balance would be maintained for unconventional structures and if any of the items (a) to (d) above are replaced by realistic but less conservative assumptions the design process may be unsatisfactory unless more realistic C_d values are also used.

Any guidance is bound to contain a certain amount of engineering judgement and to change with time. Designers and analysts will therefore still need to satisfy themselves that the guidance is applicable to their problem and they remain free to justify their own methods and data to their clients and the certifying authorities.

2. DETERMINATION OF PARTICLE KINEMATICS

2.1 REGULAR WAVES

2.1.1 Introduction

The approximation of an irregular random sea by regular waves is the basis for the deterministic and semi-probabilistic methods for the design and analysis of offshore structures. Regular wave theories are also the basis of the random wave methods discussed in Section 2.2. Random wave theories are used in the spectral and probabilistic methods. The choice between regular or random wave theory is therefore determined by the type of analysis being performed. This is discussed in Sections 4.3 and 4.4.

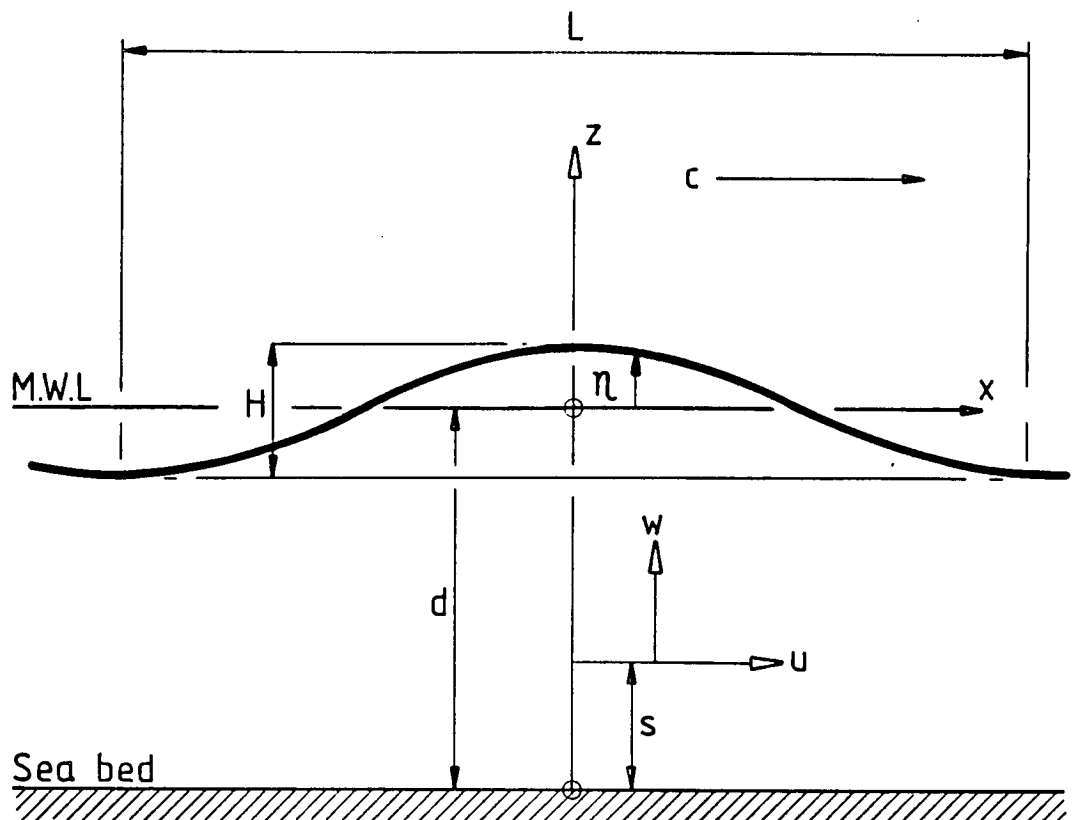
2.1.2 Regular wave theories

Regular waves have recurring profiles and particle kinematics. The profile is usually symmetric about a vertical plane through the crest. The water must be deep enough for the sea bed not to affect the wave or the sea bed must be horizontal; otherwise the profile will change as the wave propagates and the wave will not be regular.

The symbols used to describe waves are given in Figure 2.1.1.

The characteristics of regular waves are defined as follows:-

- Wave Length** The distance between successive crests, troughs, or up-crossings of the wave profile through the mean water level.
- Wave Period** The elapsed time, as recorded by a stationary observer, between the passage of successive crests, troughs or up-crossing points.
- Celerity** The propagation speed of the wave crest, i.e. the ratio of the wave length to the period.



c : Wave celerity or speed of propagation = L/T

d : Depth from mean still water level to seabed

H : Wave height from crest to trough

L : Wave length or distance between successive crests

s : $z + d$, height above mudline

T : Wave period

u : Horizontal particle velocity

w : Vertical particle velocity

x : Horizontal axis

z : Height measuring positively above MWL

η : Free water surface profile at time t above mean water level

MWL : Mean water level

Subscript c : Refers to the current

Subscript w : Refers to the wave

Subscript m : Refers to the maximum value

Figure 2.1.1. Definition of wave and current symbols

- Steepness** The ratio of the wave height to wave length.
- Long Crest** A wave with all crests parallel and long in relation to the wave-length.
- Short Crest** Short crests are produced when a sea contains waves propagating in several directions.
- Particle Orbit** The path taken by a water particle during a wave cycle. The form of these orbits, for long crested waves of small steepness with no current, are depicted in Figure 2.1.2.

Regular wave theories describe the flow in a train of waves of a given height and period. The flow itself is assumed to be unaffected by any viscous forces and to have no initial rotation, it is therefore 'irrotational'. The water is also assumed incompressible. These two assumptions expressed mathematically: in the form of a velocity potential or a stream function, become Laplace's equation.

The boundary conditions to be satisfied are:-

- a) No flow through the seabed, i.e. vertical velocity at the seabed equals zero.
- b) A 'kinematic' condition at the surface which requires that, in the direction normal to the free surface, the wave particle velocity should be equal to the wave surface velocity.
- c) A 'dynamic' condition at the free surface which is expressed in terms of Bernoulli's equation and usually assumes a constant atmospheric pressure.
- d) A periodic condition - that the wave should be regular.
- e) A condition of prescribed average current.

Different wave theories are based on different approximations to the boundary conditions at the free surface. In linear theories, the free surface boundary conditions are simplified by assuming that the departure of the water surface from the mean water level is very small.

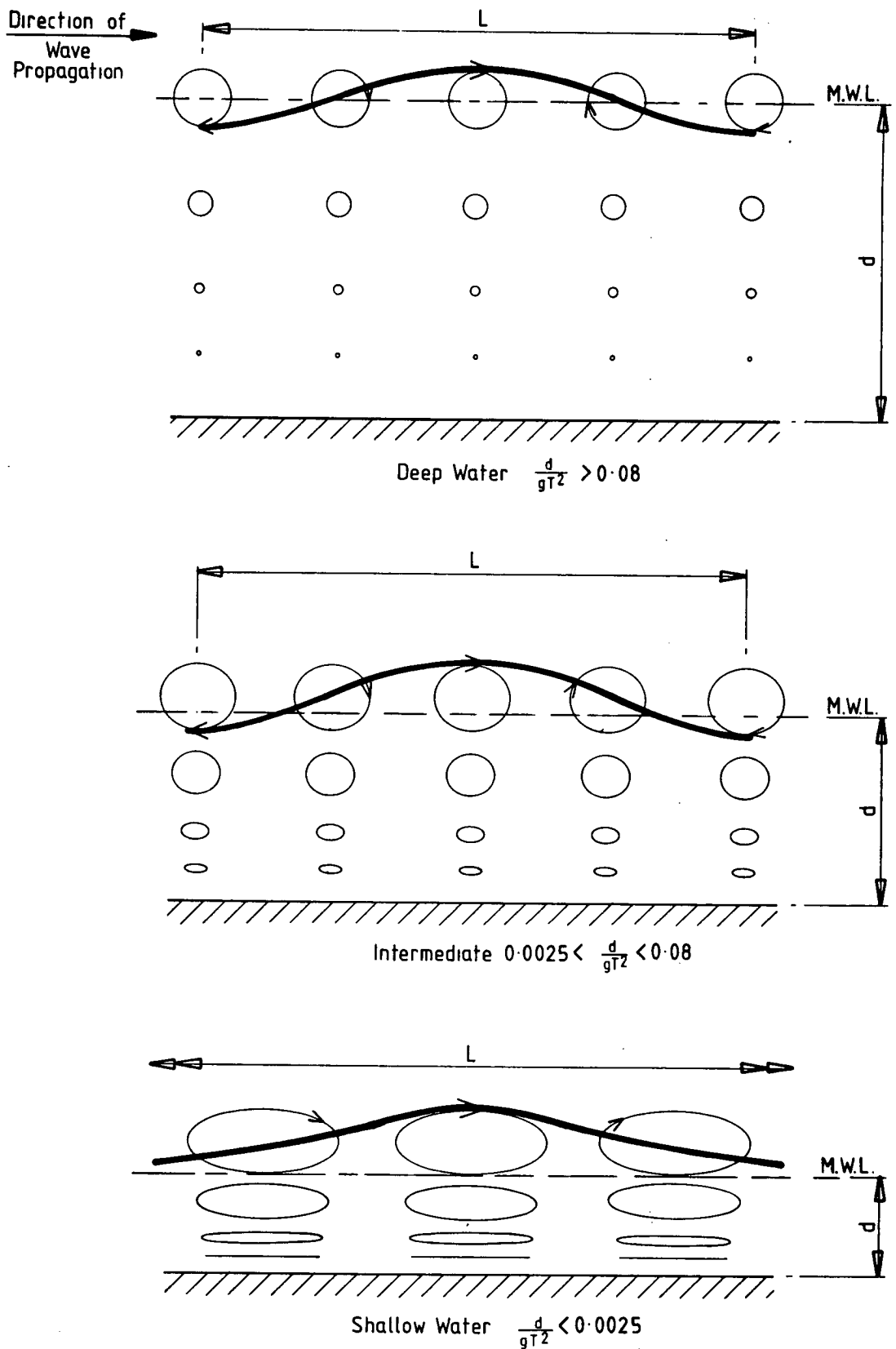


Figure 2.1.2. Wave particle orbits in different water depths as predicted by linear theory (Higher order theories predict some horizontal translation of the particles in each wave cycle)

Non-linear or higher order theories satisfy more closely the fluid conditions at the surface, and give a better approximation to waves of finite amplitude, (Sarpkaya and Isaacson, 1981).

Usually regular wave theories are derived for the case of average zero current. There are two definitions of average zero current in use which give slightly different results:-

1. The average horizontal velocity of any particle in the wave equals zero.
2. The average current taken over one wavelength between the seabed and the water surface equals zero.

The method of defining zero current affects the overall wave characteristic including the celerity. Frequently the first or second zero current definition is referred to as the first or second definition of celerity. The effects of non zero currents are described in Section 2.3.

Some commonly used, or referenced, wave theories are described below:

AIRY Theory - This is a velocity potential method also known as linear or sinusoidal wave theory. It is assumed that the wave height is small relative to both the wave length and the water depth. The velocity potential and the particle kinematics then reduce to first-order expressions which are straightforward to calculate.

Airy Theory is strictly only valid for waves of very small height. As an approximation the theory may be applied to waves of finite height, either by extrapolating the cosh and sinh functions up to the instantaneous water surface or by empirical modification to Airy Theory e.g. Wheeler (1970). The errors involved in applying linear wave theory outside its theoretical range of applicability are discussed in Appendix C where the method of calculating kinematics above MWL was to apply the hyperbolic functions with positive values of z .

The theory is simple and stable and works quite well over a wide range of conditions. It can be easily extended to model irregular multidirectional seas (Section 2.2) and the diffraction of waves by large members.

STOKES Theory – This is a velocity potential method in which successive approximations are developed to satisfy the boundary conditions. The potential is calculated in powers of wave steepness (H/L) and is usually carried to the fifth order on the basis of work by Bretschneider (1960) or Skjelbreia & Hendrickson (1960). The original Skjelbreia & Hendrickson paper contains an error in the formulae (Nishimara et al 1977, and Fenton 1985).

Stokes theory predicts a longer wave with peakier crests and flatter troughs than Airy theory. Particle velocities are greater at the crest than at the trough and the maximum horizontal acceleration occurs nearer the crest. The resulting wave is longer than an Airy wave of the same period (see Appendix C).

STREAM FUNCTION Theory – Dean (1965) described a numerical method for predicting two dimensional wave characteristics that is based on a stream function representation of the flow. The stream function expression is expanded as a series and the free surface boundary conditions are satisfied numerically by minimising the least-squares error. The theory is capable of extension to any desired order.

The stream function method is capable of modelling an asymmetric or a prescribed individual wave form. However, the theory cannot model a wave which changes shape as it propagates. A free surface pressure distribution may be prescribed. For research purposes these features allow a closer approximation to measured wave profiles to be made.

CNOIDAL Theory – Korteweg and de Vries (1895), expressed the wave characteristics in terms of the Jacobian elliptic function (cn), hence the term 'cnoidal'. This is essentially a shallow water theory in which the velocity potential is expanded in powers of H/d (the ratio of wave height to water depth). Keulegan and Patterson (1940), Keller (1948), Laitone (1961) and Fenton (1979) have extended the theory. It is suited to shallow and intermediate water depths.

HYPERBOLIC Theory is a simplification of CNOIDAL Theory.

SOLITARY Wave Theory may be considered to be a special case of the CNOIDAL theory in which the wave length and period become infinite. (Therefore it is arguably not a regular wave). This wave lies wholly above the still water level. It never exhibits horizontal particle velocities in the reverse direction to wave advance so that there is always a nett displacement of fluid in the sense of the wave advance. SOLITARY Wave Theory may approximate waves caused by land or ice slides.

LONG WAVE Theory has application to tsunami propagation, tidal motion, storm surge, flood waves etc, but is not of primary interest in the present context. Usually a linear version is used which is based on the assumption that the wave length is much longer than the water depth, the vertical particle acceleration is also neglected. This gives a flow in which the horizontal particle velocity is constant with depth and the pressure is hydrostatic.

GODA Theory - a form of Stokes theory empirically modified on the basis of tank tests. (Goda, 1964).

TROCHOIDAL WAVE Theory is largely of historical interest even though it has, to a limited extent, been applied to engineering problems. Unlike most other wave theories it involves a rotational fluid motion.

Recently developed wave theories, for instance, Cokelet (1977), Schwartz (1974), Longuet-Higgins (1973) and Chaplin (1980), have advantages when applied to near breaking waves. They all require extensive computation and, as a result, have not yet found widespread application.

For research purposes extended velocity potential theory (Lambrakos and Branon, 1974) allows a wave to be modelled which changes shape as it propagates.

When the seabed is not horizontal the waves may change direction and height. This 'refraction' and 'shoaling' is not discussed in detail in this document. See Sarpkaya and Isaacson (1981) for a well referenced introduction to the subject.

2.1.3 Comparison of wave theories

The validity, or range of application, of a regular wave theory may be evaluated on the basis of its ability to satisfy the boundary conditions. It should be noted, however, that a better numerical 'fit' does not necessarily mean that the theory is better for the calculation of wave loading.

14

In the evaluation of wave theories, the wave characteristics H and d are normally reduced to dimensionless parameters. The wave height may be expressed in terms of H/gT^2 , the wave steepness H/L or the relative height H/d . In a similar manner, the water depth may be expressed in terms of the depth parameters d/gT^2 , $kd = 2\pi d/L$ or the relative depth d/L .

The results of linear wave theory may be used to create a distinction between shallow, intermediate and deep water depth to wavelength ratios. Simplifications of linear theory become possible in 'shallow' ($d/gT^2 < 0.0025$) and deep water ($d/gT^2 > 0.08$). These occur as a result of approximations that can be made to the hyperbolic functions involved.

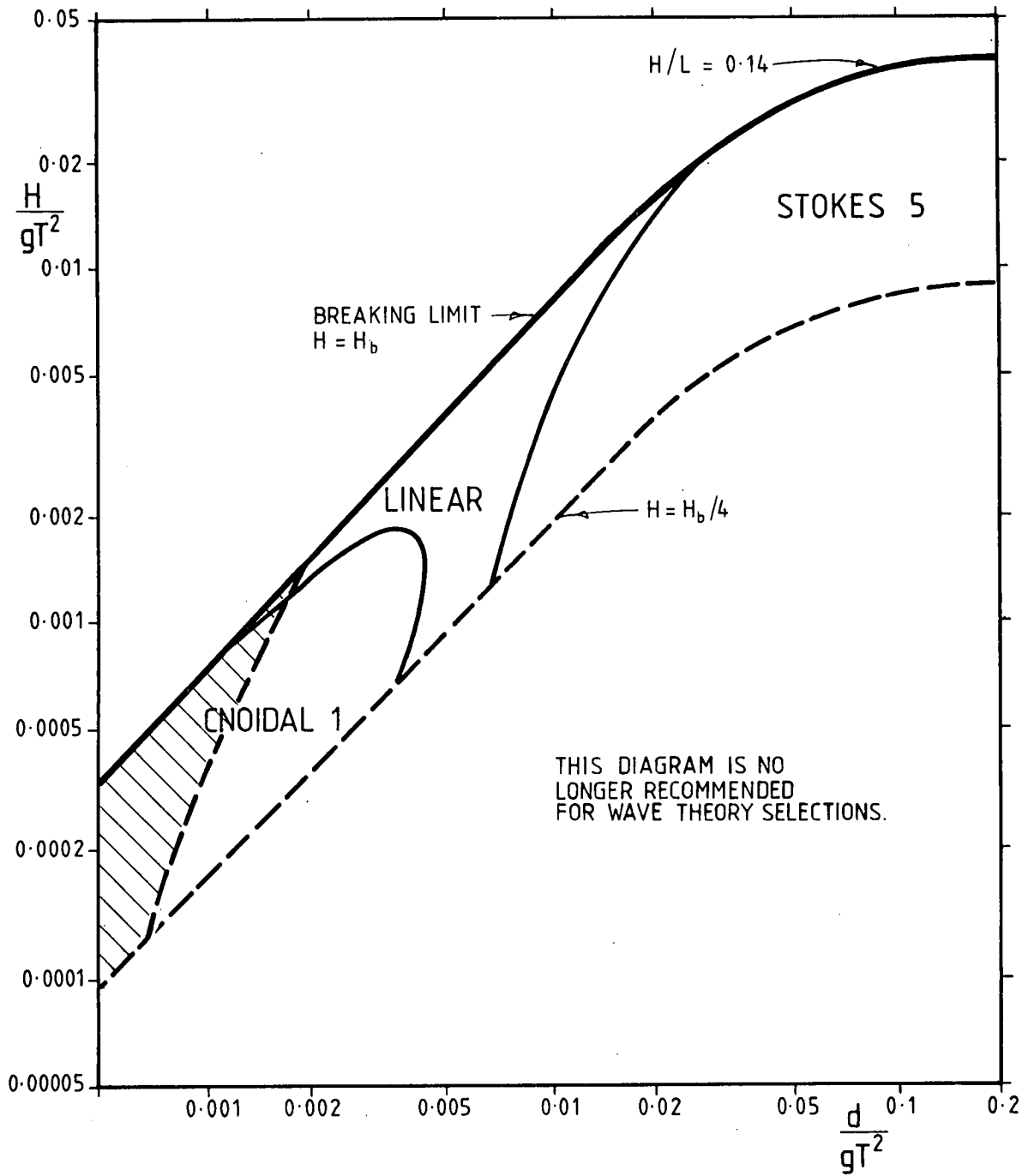
Only a few of the theories described above are commonly used in current design practice. This is because only a small number of theories are required to cover the usual range of relative wave heights and water depths to acceptable accuracies. The range of validity of presently used theories has been investigated by several researchers.

A comparison of Airy, Stokes (3rd and 5th), cnoidal (1st and 2nd), solitary (1st and 2nd) and stream function theories has been made by Dean (1970). This was made on the basis of the closeness of fit to the dynamic free-surface boundary condition. It was found that Airy, Stokes 5th, cnoidal 1st and stream function were generally the most suitable and had ranges of validity as indicated in Figure 2.1.3.

Le Mehaute (1976) also summarised the approximate limits of wave theories. This, reproduced in Figure 2.1.4, shows some agreement with the results of Dean.

Cnoidal 5th order theory has been compared with Cokelet's (1977) theory by Fenton (1979). He found that the wave celerities were well predicted by 5th order Cnoidal up to H/d of 0.6 and d/gT^2 of 0.01.

Stokes 5th order theory has been studied by Ebbesmeyer (1974) who showed that 'bumps' in the profile and multiple crests in a wavelength (Figure 2.1.5) occur when d/gT^2 is less than 0.01 to 0.02. Dalrymple (1986) has shown that multiple crest solutions can also be produced by stream function theory.



H/gT^2 : Dimensionless wave steepness

d/gT^2 : Dimensionless relative depth

H : Wave height

d : Mean water depth

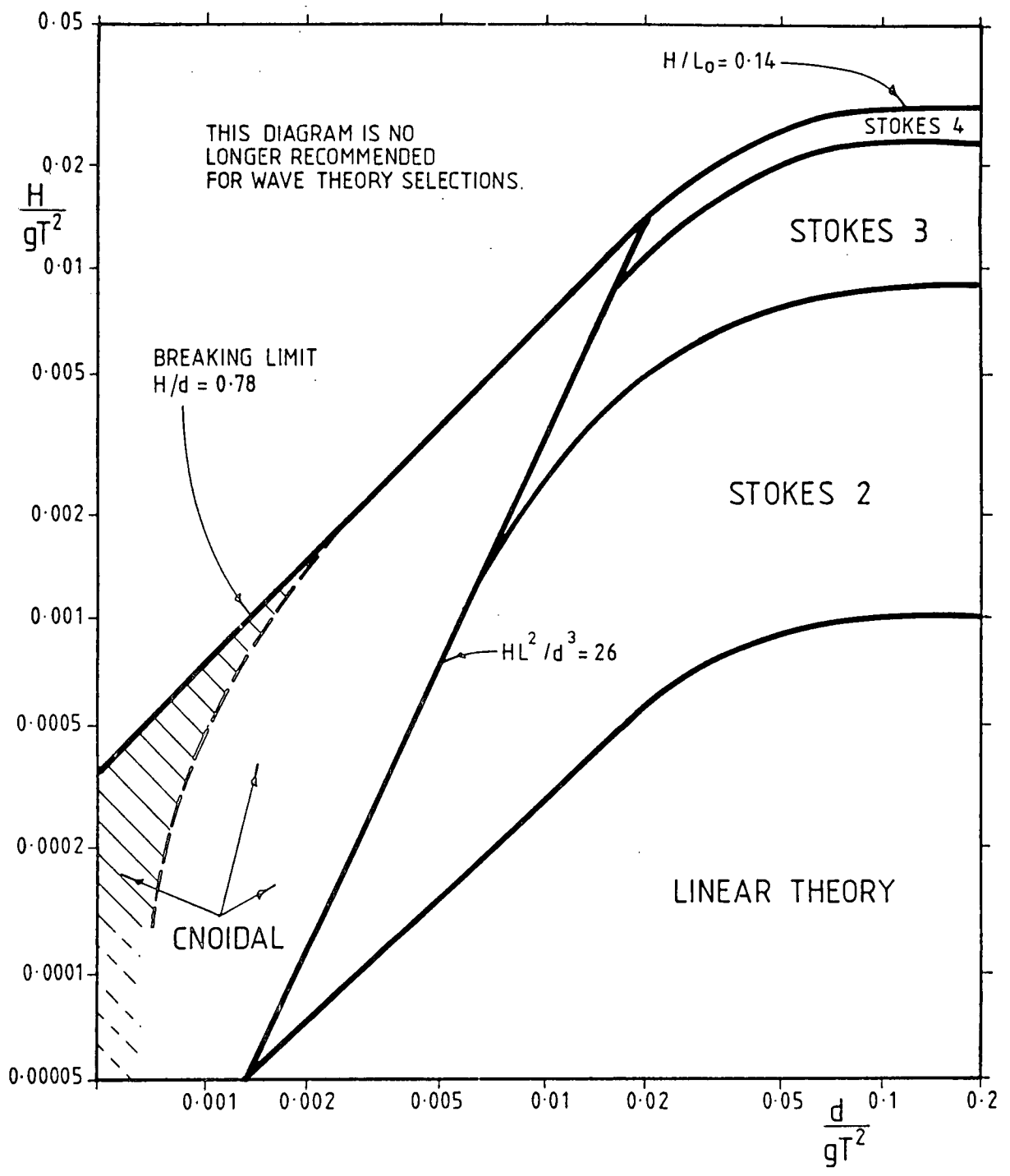
L : Wave length

T : Wave period

Subscript b : Breaking conditions

Stream function 5 is suggested as being valid except in shaded area

Figure 2.1.3 Range of wave theories giving the best fit to the dynamic free surface boundary condition (Dean, 1970)

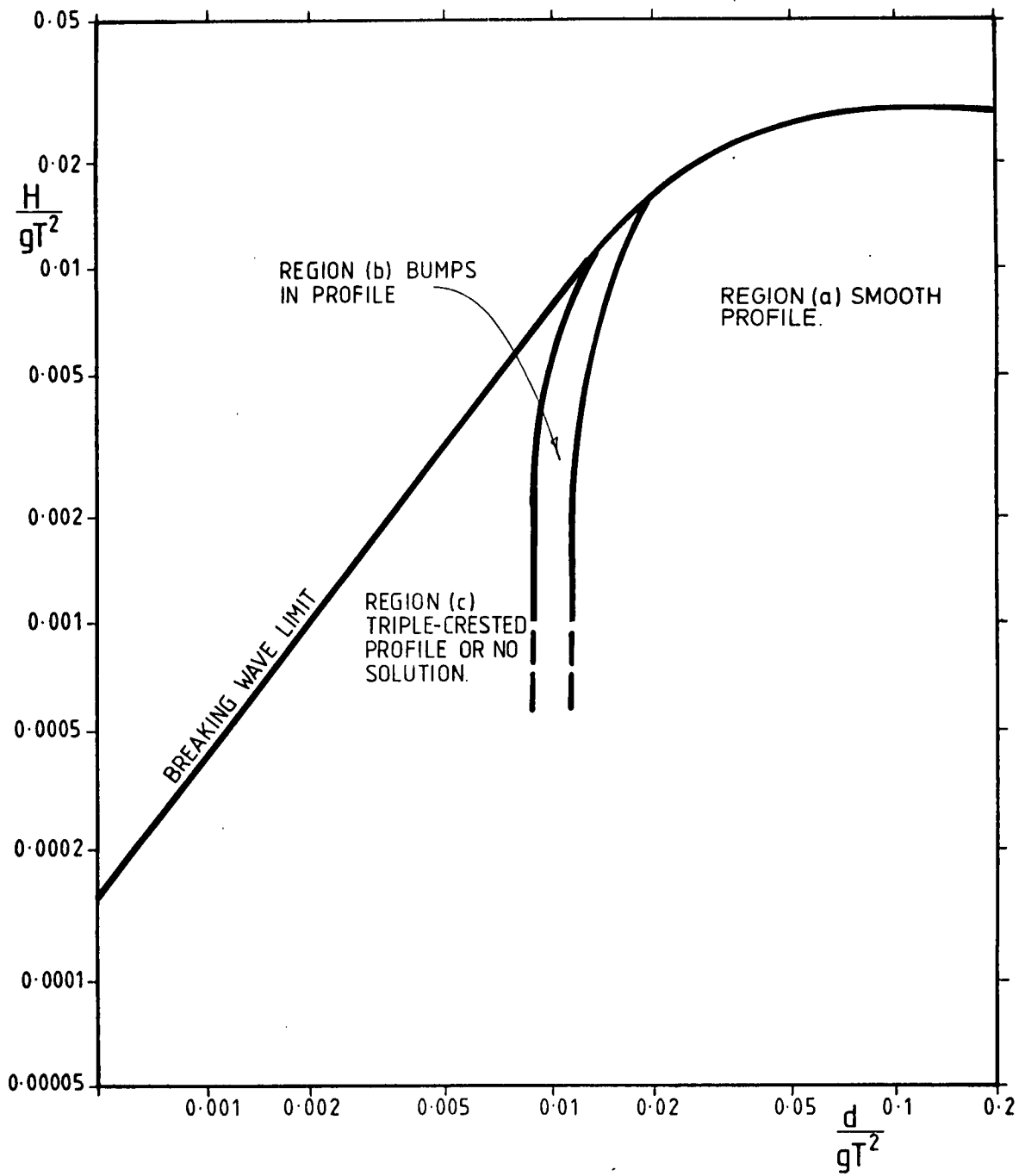


Notes

- H/gT^2 : Dimensionless wave steepness
- d/gT^2 : Dimensionless relative depth
- H : Wave height
- d : Mean water depth
- L : Wave length
- T : Wave period

- 1) o Subscript indicates deep
- 2) Stream function 5 is suggested as being valid except in shaded area

Figure 2.1.4 Ranges of suitability for various wave theories as suggested by Le Mehaute (1976)



Note: Ebbesmeyer does not give any information about profiles for $H/gT^2 < 0.001$

Figure 2.1.5. Regions of characteristic Stokes 5 wave profiles (Ebbesmeyer, 1974)

A comparison of linear, Stokes 5 and stream function theories is presented in Appendices B and C. The comparison was based on particle velocity and acceleration under the wave crest, wave length and wave crest height above mean water level. The comparison led to the wave theory selection diagram: Figures 2.1.6a and b.

Wave theories have also been compared under laboratory conditions.

Le Mehaute, Divoky and Lin (1968) measured the velocity distribution under the crest of waves, in shallow and intermediate water depths, and compared the results with a number of theories including Airy, Cnoidal 1 and 2; Stokes 2, 3 and 5; and Goda's theory. The agreement between the measured data and the shallow water Cnoidal 1 or 2 was found to be poor. Airy theory generally performed better than Cnoidal theory or Stokes theories in the shallow water depths. Goda's theory was found to be one of the better theories for the waves considered.

Dean (1974) compares his stream function theory results with the data of Le Mehaute et al. This showed that stream function theory performed well and, on average, matched the results better than the other theories considered.

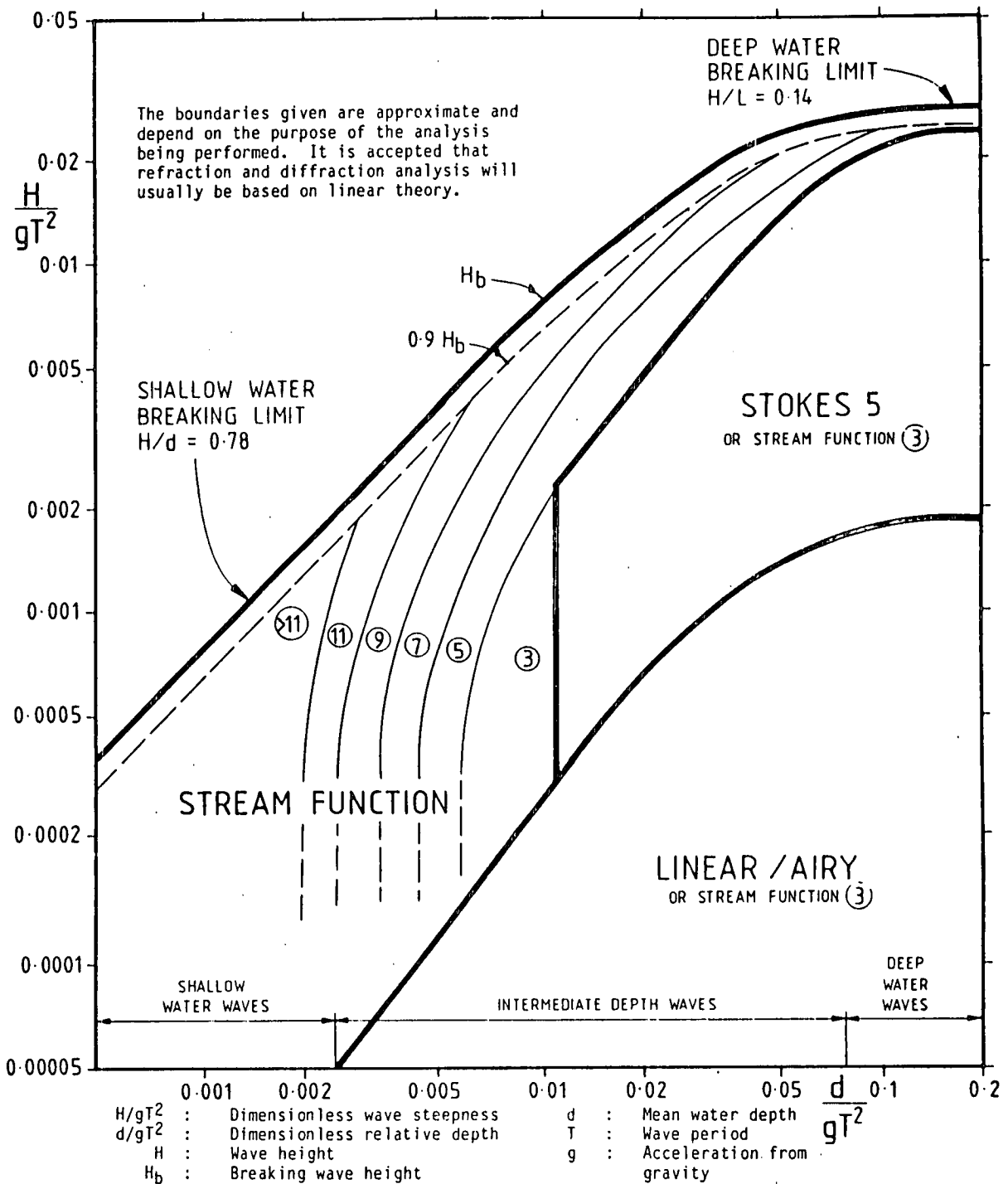
Standing (1981) presented the results and theories of Dean (1974), Fenton (1979), Iwagki and Sakai (1970) and Le Mehaute, Divoky and Lin (1968). He made comparisons of the maximum particle velocity: see Figure 2.1.7. In shallow water there was found to be poor agreement between the experimental results and all the wave theories, however stream function and Goda's theories were found to give the best estimates of particle velocity.

For deeper water and for the levels at which experimental results were obtained, the correlation between theory and experiment was quite reasonable. There were only small differences between linear and Stokes 5 and stream function theories for this case, which is typical of a North Sea 'design wave'.

Comparisons have also been made between regular wave theories and measured kinematics in random seas. These are discussed further in Section 2.2.4.

2.1.4 Regular waves: conclusion

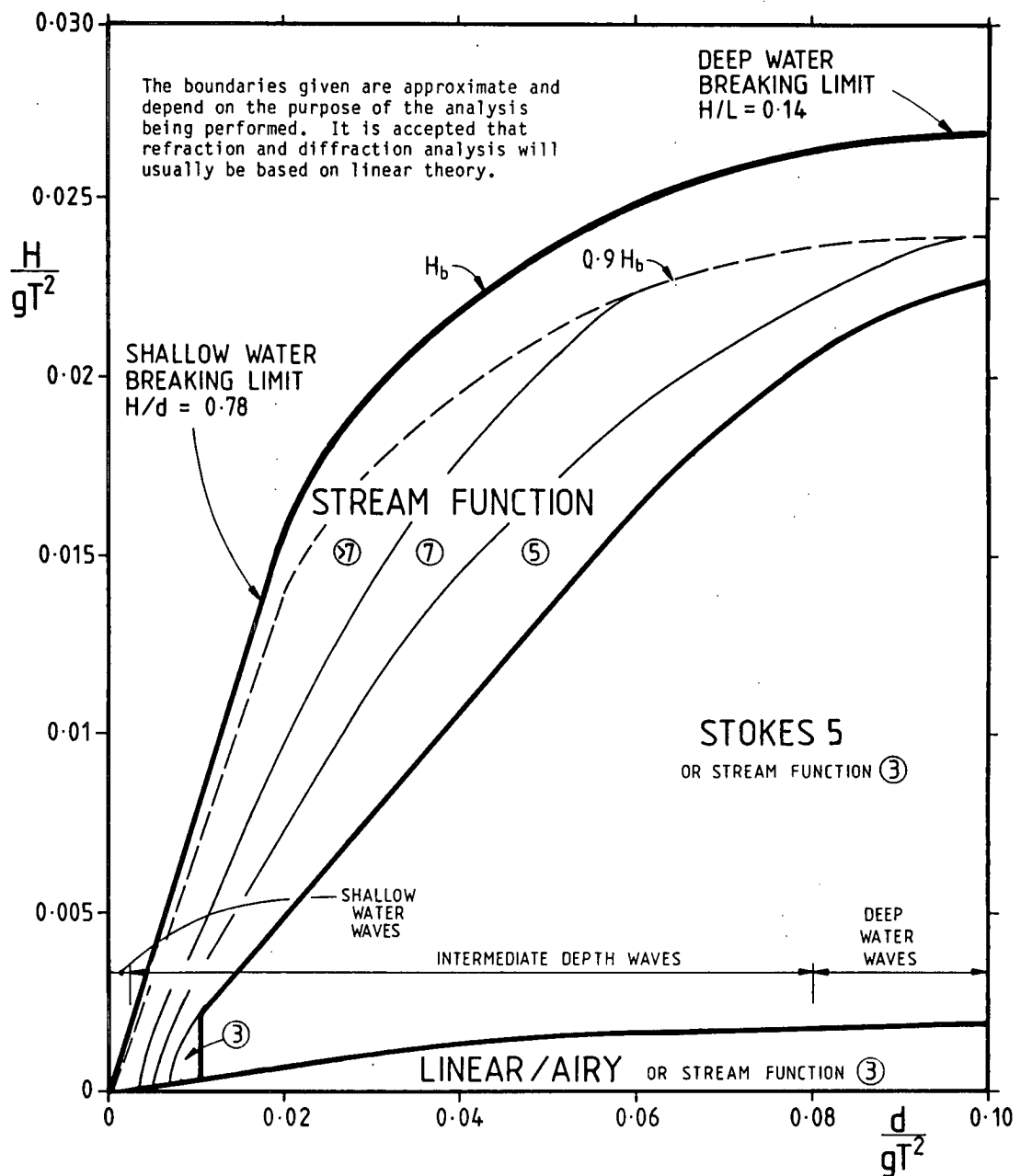
The wave theory selection diagram, Figure 2.1.6 should be used as a basis for the selection of an appropriate regular wave theory. Programmes which generate wave particle kinematics should be treated with caution. Changes in the method of



Notes

- 1) None of these theories is theoretically correct at the breaking limit.
- 2) Wave theories intended for limiting height waves should be referenced for waves higher than $0.9 H_b$ when stream function theory may underestimate the kinematics.
- 3) Stream function theory is satisfactory for wave loading calculations over the remaining range of regular waves. However stream function programs may not produce a solution when applied to near breaking waves or deep water waves.
- 4) The order of stream function theory likely to be satisfactory is circled. Any solution obtained should be checked by comparison of the results with a higher order solution.
- 5) The error involved in using Airy theory outside its range of applicability is discussed in the background notes, Appendix C.

Figure 2.1.6a Regular wave theory selection diagram (log scales)



H/gT^2 :	Dimensionless wave steepness	d :	Mean water depth
d/gT^2 :	Dimensionless relative depth	T :	Wave period
H :	Wave height	g :	Acceleration from gravity

Notes

- 1) None of these theories is theoretically correct at the breaking limit.
- 2) Wave theories intended for limiting height waves should be referenced for waves higher than $0.9 H_b$ when stream function theory may underestimate the kinematics.
- 3) Stream function theory is satisfactory for wave loading calculations over the remaining range of regular waves. However stream function programs may not produce a solution when applied to near breaking waves or deep water waves.
- 4) The order of stream function theory likely to be satisfactory is circled. Any solution obtained should be checked by comparison of the results with a higher order solution.
- 5) The error involved in using Airy theory outside its range of applicability is discussed in Appendix C.

Figure 2.1.6b Regular wave theory selection diagram (linear scales)

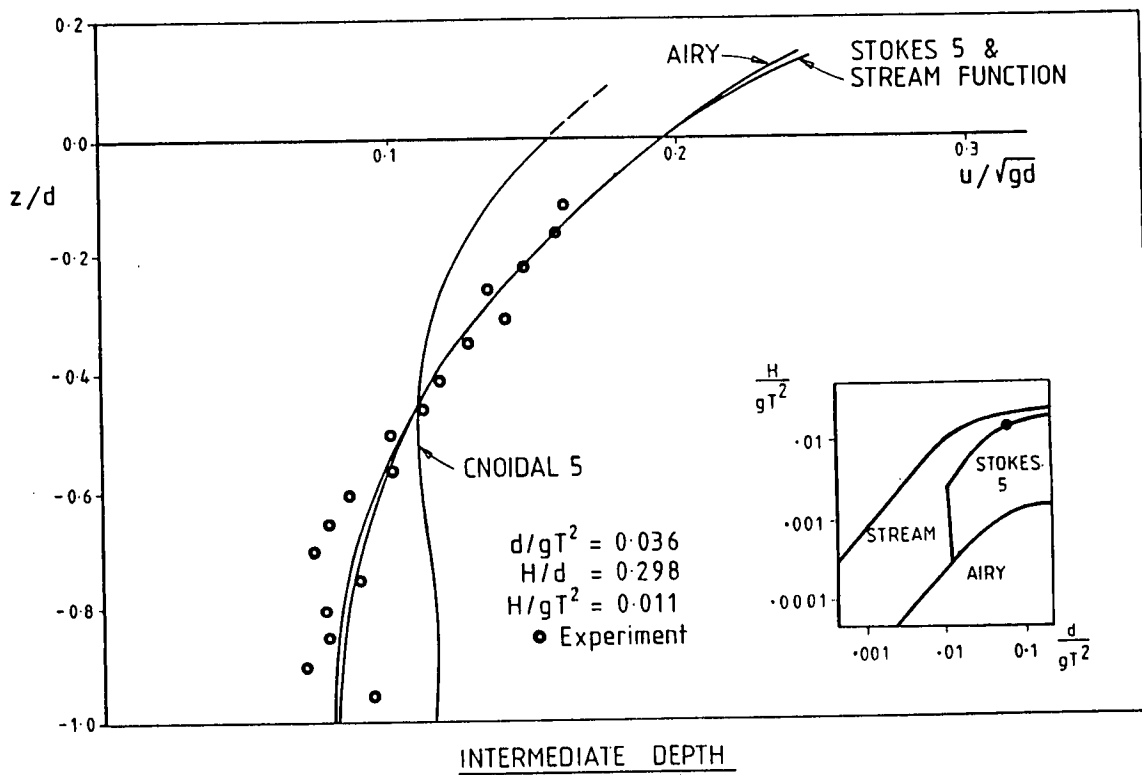
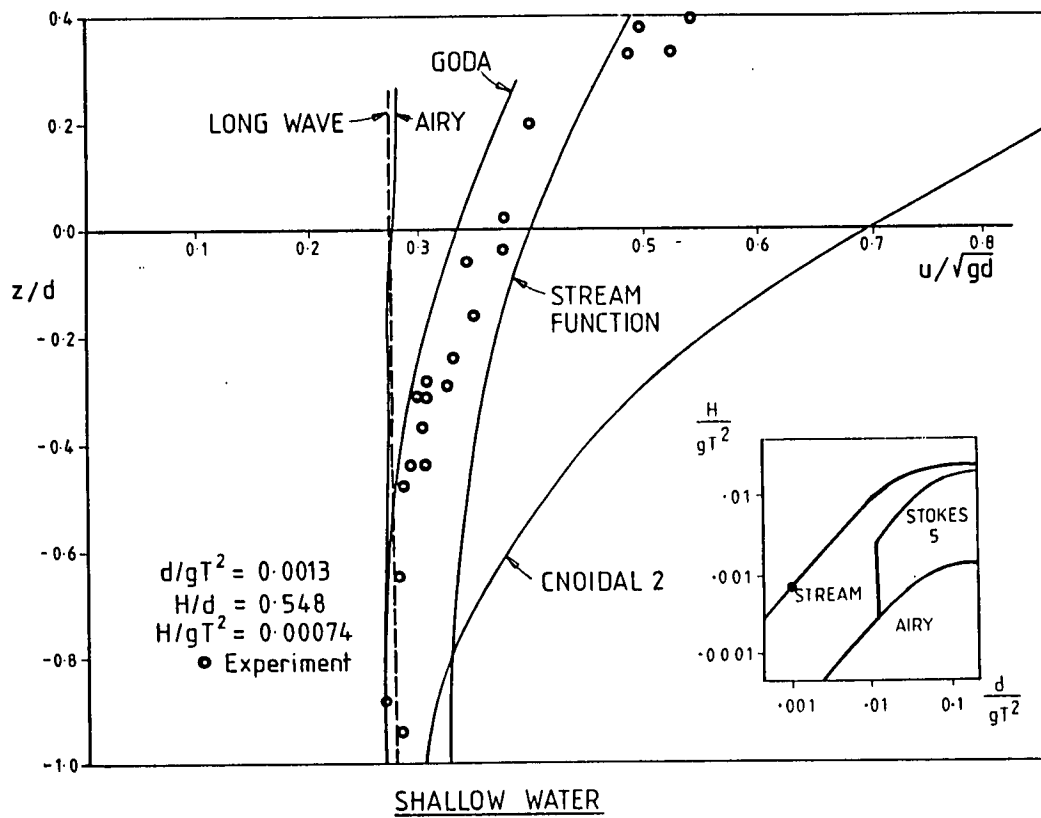


Figure 2.1.7. Horizontal particle velocity under the wave crest (Standing, 1981)

programming the Theory can lead to significantly different results, especially near or outside the validity limits of the Theory. The surface profile of the generated wave should always be checked to ensure that no intermediate crests or troughs have been formed and the kinematics should be compared with a different Theory or order of Theory that is theoretically valid for the same conditions.

Airy should preferably be used only in the indicated validity range. However, it is accepted that, for refraction and diffraction analysis Airy theory may be the only practical choice.

Airy theory is useful for initial design purposes because it is applicable by hand. However, in shallow water and near the breaking limit it considerably underestimates particle velocities and accelerations. (See Appendix B).

Stokes 5 is applicable to the moderate steepness and deeper water waves. Its validity range would be expected to cover most North and Central North Sea extreme wave conditions.

The limited number of terms included in Stokes 5 wave theory suggests that even in deep water it may not properly model the steepest waves. In some organisations therefore the use of Stokes 5 has been limited to waves of less than 0.675 times the breaking wave height. However, in deep water the results of Stokes 5 and Stream Function theory are close although at the breaking limit both are in error (Chaplin and Anastasiou, 1980).

Cnoidal 5 (Fenton, 1979) is applicable to moderate steepness waves in the shallower water depths. However, Cnoidal 5 computer programmes are not yet commonly available and the useful range is outside that relevant to most offshore structures therefore a region of applicability of Cnoidal 5 has not been identified in Figure 2.1.6.

For waves approaching the breaking limit Stream Function Theory is recommended. A convergence check (using progressively higher order theories) should be performed to ensure that the overall solution has converged. Multiple crest solutions can also sometimes occur with Stream Function theory (Dalrymple, 1986). The shape of the wave should therefore be checked. If available, the more advanced theories mentioned at the end of 2.1.2 may be used to model near breaking regular waves more accurately. For a discussion of the particle kinematics at the crest of a steep wave see Longuet-Higgins & Fox (1977 and 1978) and Longuet-Higgins (1985).

2.2 RANDOM WAVES

2.2.1 Introduction

The statistical properties of the random waves in a sea are found to be approximately constant for short periods of time (of the order of an hour). During this time a 'sea state' is said to exist. The sea state may be defined by a frequency spectrum of water surface elevation and ideally, although rarely in practice, the spectrum would contain information about the spread of direction as well as the spread of frequency. The spectrum is usually characterised by the significant height: H_s and mean zero (up crossing) period: T_z of the waves. The long term distribution of sea states is defined by a scatter diagram showing the proportion of time for which any given H_s and T_z occurs.

The shape of the frequency spectra vary considerably, from sea state to sea state, even for the same values of H_s and T_z . However, for design purposes various typical spectral shapes are used, e.g. JONSWAP or Pierson Moskowitz (see Section 4 and the Metocean Appendix). Only limited information is available about the directions of waves within sea states. It is common practice to estimate a mean direction for each sea state based on wind and fetch or ship's observations. Some measurements have been made of the spread of direction within a sea state. These tend to show a narrow spread of direction at the peak frequency but a wider spread away from the peak frequency, e.g. Atkins (1979). However, because of the limited amount of spreading data it is at present normal design practice to assume no spreading of direction within a sea state. This results in identical wave particle kinematics, at any instant, on any line perpendicular to the wave direction.

2.2.2 Random wave theory

Random wave theory is usually based on Airy wave theory in which case it is known as linear random wave theory (LRWT). The method models the required frequency spectrum of water surface elevation by the superposition of regular linear 'wavelets' having the range of frequencies required by the spectrum. The random wave model may be based on a continuous function of wave frequency. Alternatively, discrete regular wavelets, with selected heights and frequencies but random phases, may be used in order to obtain an approximation to the required water surface elevation spectrum. In either case the randomness in the modelled wave is caused by the various fixed amplitude wavelets occurring in and out of phase with one another. This causes waves of various heights and zero crossing periods to occur.

It is possible to produce approximate random wave theories which include some of the characteristics of higher order regular wave theories. Dean, Lo and Johansson (1979) propose a method in which they sum the particle kinematics of a Stokes 5 wave and Airy wavelets. However it is only capable of predicting the particle kinematics for one wave at a time and is probably more useful as an aid to understanding some effects of the higher order waves than as a design tool.

Several methods, and several variations of each method, are available for calculating the effect of a random sea on a structure:-

- a. The particle kinematics may be calculated, from the water surface elevation spectrum, as a time history. Used with a loading model, usually Morison's equation, and a structural analysis the time history of the internal stresses in the structure may be obtained; see 4.3.6 and 4.4.6. This method is computationally very time consuming but there are some types of analysis, e.g. of drag loading response of a dynamically sensitive structure, which are difficult to calculate by other means. The method is also used for the analysis of experimental measurements.
- b. The statistics of the particle kinematics may be determined and used in conjunction with a loading model and load-stress influence coefficients (from a structural analysis) to determine the statistics of the stress at any point in the structure. This is the Non Linear Probabilistic Analysis method which is described in 4.3.5 and 4.4.5.
- c. If the structure responds linearly to wave particle kinematics (in practice this requires that the loading is dominated by diffraction or the inertia term in Morison's Equation) and finite wave height effects are not important then the response of the structure to a random sea may be determined from the water surface elevation spectrum and a transfer function based on the response to regular waves over the range of frequencies of interest. This is the Linear Probabilistic analysis method, described in 4.3.4 and 4.4.4, which is the basis of the spectral analysis method commonly used for the calculation of fatigue life of dynamically responsive structures.

2.2.3 Finite wave height effects in random wave analysis

a. Time history analysis

Linear random wave theory (LRWT) is, in principle, only applicable to very small waves, for the reasons that Airy theory itself is only applicable to small waves. However the application of LRWT to finite height waves has an additional problem associated with how the wavelets add together.

The simplest method (1) is to assume that members above MWL are never loaded and members below MWL are always loaded whatever the specified wave height.

Method (1) is not very satisfactory for most surface piercing structures therefore an extension of LRWT (Method 2) is to extrapolate the cosh and sinh functions of each wavelet to the instantaneous water surface, as described for a regular wave in 2.1.2. Unfortunately this method leads to unrealistically high values of particle kinematics above MWL. This is caused by the extrapolation of the hyperbolic function beyond the highest water level that would ever be associated with the individual higher frequency wavelets if they existed as isolated waves.

Various empirical modifications to Airy wave theory have been proposed in order to avoid the problem of overestimation. However, these may lead to an underestimation of the above MWL particle kinematics when frequencies are closely spaced. The alternative empirical modifications are to the mud-line vertical ordinate $s = d + z$, or to the water depth, d , used in the Airy wave formulation. They are described in Figure 2.2.1 and below:

$$s' = s \frac{d}{(d + \eta)} \quad - \text{method (3)}$$

$$s'_i = s \frac{(d + \eta_i)}{(d + \eta)} \quad - \text{method (4)}$$

$$d'_i = d + (\eta - \eta_i) \quad - \text{method (5)}$$

where:

η is the total water surface elevation above MWL

η_i is the water surface elevation from the wavelet i

The prime indicates a modified value

The i subscript indicates that s_i and d_i are used with linear wave theory to obtain the particle kinematics of the i th wavelet component in the random sea representation.

See Pawsey & Dello Stritto (1983) and Dean, Lo & Johansson (1979).

The various modifications have the following effect on the velocity at the instantaneous water surface.

Method (3) results in the velocities that would have been calculated as occurring at mean water level being applied to the instantaneous water surface. This may underestimate crest particle velocities when there is a dominant frequency in the wave.

Method (4) amounts to the addition of the surface velocities occurring in each wavelet being applied to the instantaneous water surface. This helps to avoid the underestimation when there is a dominant wave frequency but the result is dependent on the number of wavelets selected and would need the dominant frequency to be included as one wavelet alone. When the spectrum being modelled is a continuous function of frequency this method will result for locations above MWL, in lower estimates of surface particle velocities if a larger number of smaller wavelets are used to model the same spectrum. In the limit the results of method (4) will coincide with those of method (3) as the number of wavelets becomes large.

Method (5) assumes that each wavelet can be regarded as having an instantaneous water depth which is determined by all the other wavelets which are to be superimposed. Like method (4) the results will be dependent on the number of wavelets and above MWL, the calculated particle velocities will decrease as the number of wavelets increases. The results will not however tend to the method (3) values.

Note: Equation (5) as given by Pawsey and Dello Stritto is given as

$d'_i = d - (\eta - \eta_i)$. This would seem to be incorrect or associated with a z down sign convention.

b. Non-linear probabilistic analysis

In work carried out to date the Airy wave theory equations have been used in the unmodified form. Intermittent loading has however been taken into account probabilistically.

c. Linear probabilistic analysis: 'spectral analysis'

The method of applying spectral analysis usually involves the definition of a transfer function using finite height waves. Each wave is analysed independently of the other waves and the kinematics are determined only to the surface of each wave that is used. The results will therefore be highly dependent on the wave heights selected for the analysis. In general the results for any intermittently loaded member will be poor.

2.2.4 Comparison of random wave theory with experiments in the sea

a. Christchurch Bay

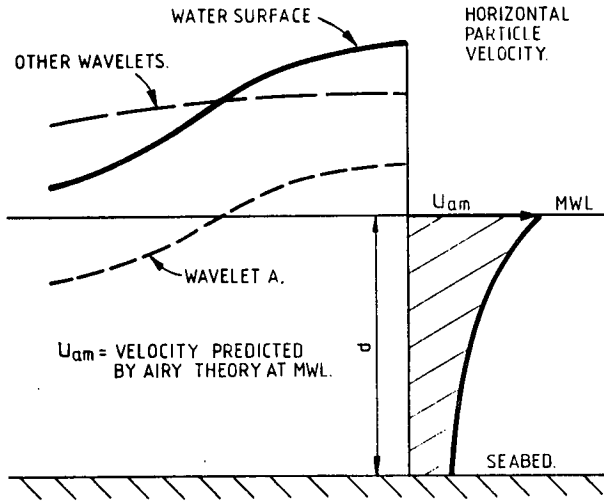
As part of the Christchurch Bay Experiment (Bishop et al, 1980 and Bishop, 1984), see Figure 2.2.2, water surface elevation, wave particle velocity and acceleration were measured. This data has been used to evaluate linear random wave theory. Velocity and acceleration spectra were predicted from the water surface elevation spectra. The measured water surface elevation did not allow directional spreading to be estimated so the velocities and accelerations were calculated assuming no spreading.

Comparison of the measured (in line with the predominant wave direction) and predicted velocity and acceleration spectra, Figure 2.2.3, showed good agreement near the spectral peak but a tendency for overestimation at high frequencies and underestimation at low frequencies. Bishop notes that the underprediction occurs in the shallow water range of water depth to wave period.

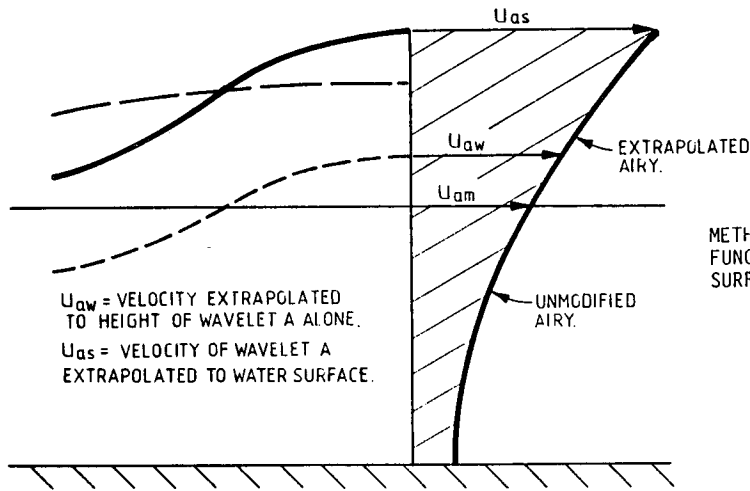
Bishop has also produced plots of peak velocities and accelerations. These show that:-

- The in-line peaks of velocity and acceleration also show a tendency to be overestimated from the water surface elevation; see Figure 2.2.4.
- Part of the overestimate may be caused by directional spreading since the error in the in-line peak values is of similar size to the difference between the in-line and total velocity; see Figure 2.2.5.

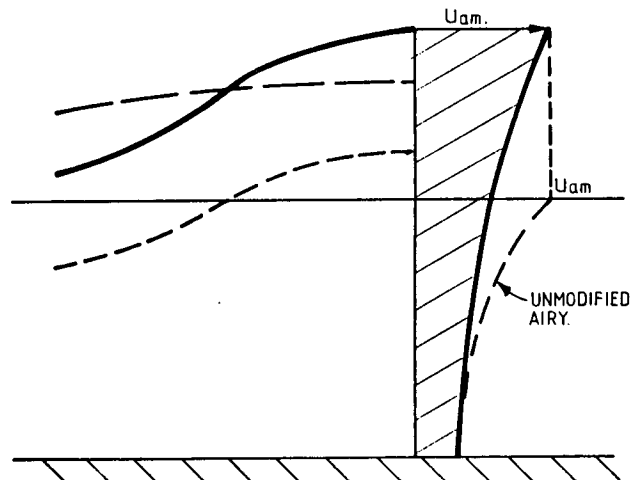
WATER SURFACE AND WAVELETS.



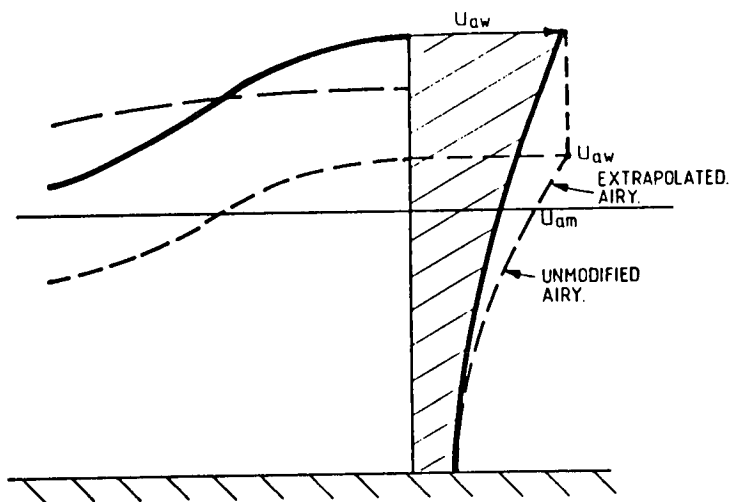
METHOD 1) AIRY THEORY APPLIED WITHOUT FINITE WAVE HEIGHT MODIFICATION.



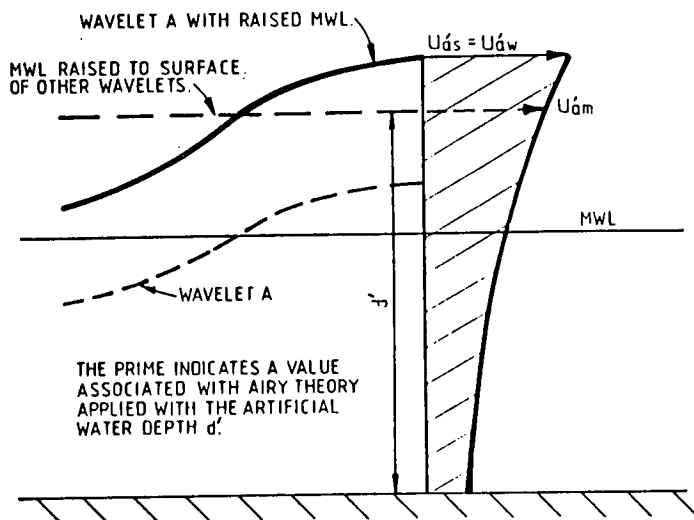
METHOD 2) AIRY THEORY HYPERBOLIC FUNCTIONS EXTRAPOLATED TO WATER SURFACE.



METHOD 3) AIRY THEORY MWL VELOCITY APPLIED AT SURFACE. PROFILE STRETCHED TO FIT



METHOD 4) AIRY THEORY HYPERBOLIC FUNCTIONS EXTRAPOLATED TO SURFACE OF WAVELET ALONE. THIS VELOCITY APPLIED AT THE WATER SURFACE. PROFILE STRETCHED TO FIT.



METHOD 5) MWL RAISED TO SURFACE OF OTHER WAVELETS. AIRY THEORY HYPERBOLIC FUNCTIONS EXTRAPOLATED TO SURFACE OF WAVELET ALONE, WHICH IS ALSO THE WATER SURFACE.

NOTES 1. THESE DIAGRAMS SHOW THE MODIFICATIONS TO 1 WAVELET 'A'. EACH WAVELET IS MODIFIED IN A SIMILAR MANNER.

NOTES 2. THE MODIFICATIONS ARE SHOWN FOR THE WATER SURFACE ABOVE MWL BUT APPLY ALSO FOR WATER SURFACE BELOW MWL.

Figure 2.2.1 Some modifications to Airy wavelets, used in random wave theory, to allow for finite wave heights

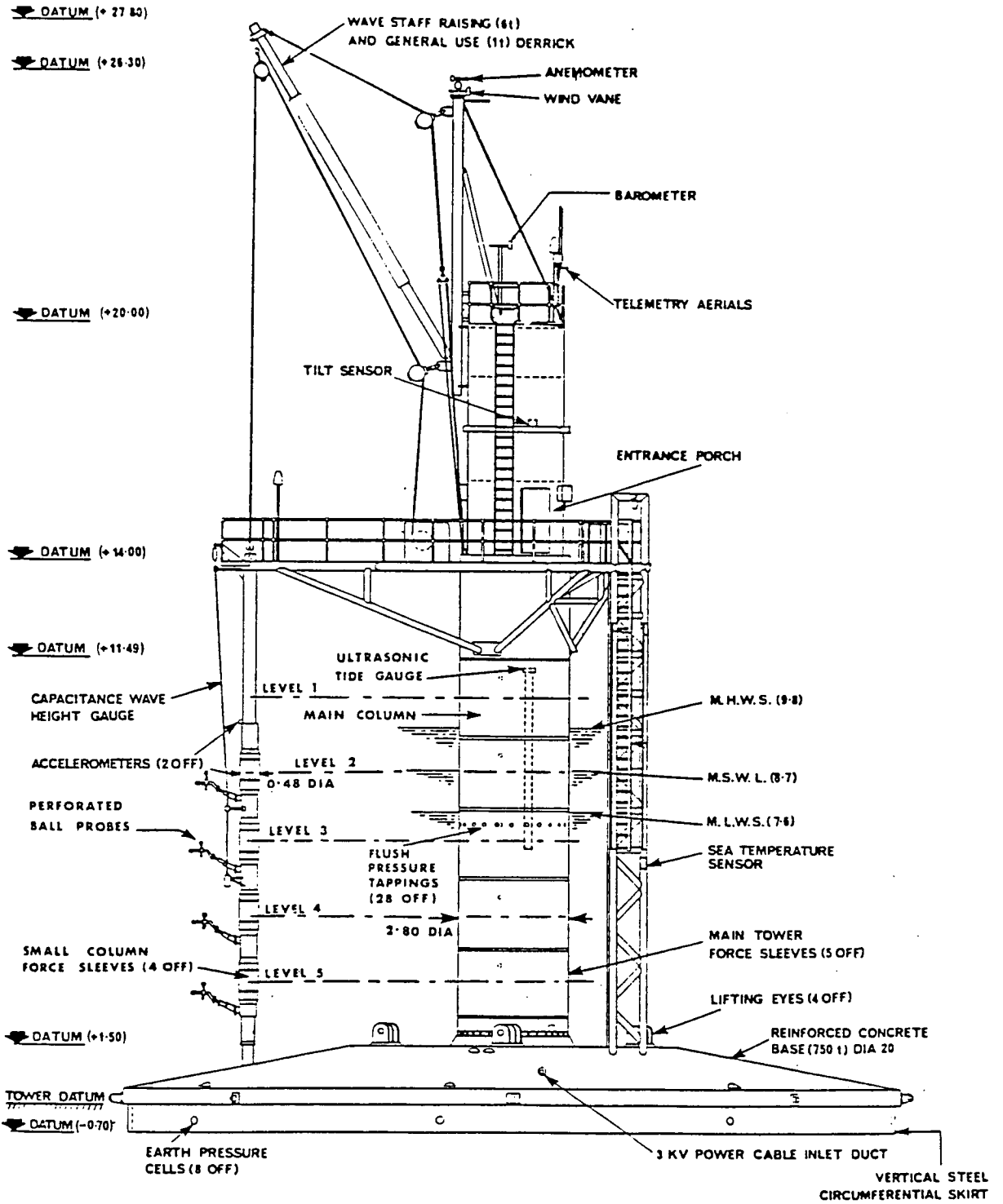


Figure 2.2.2. BMT Christchurch Bay tower

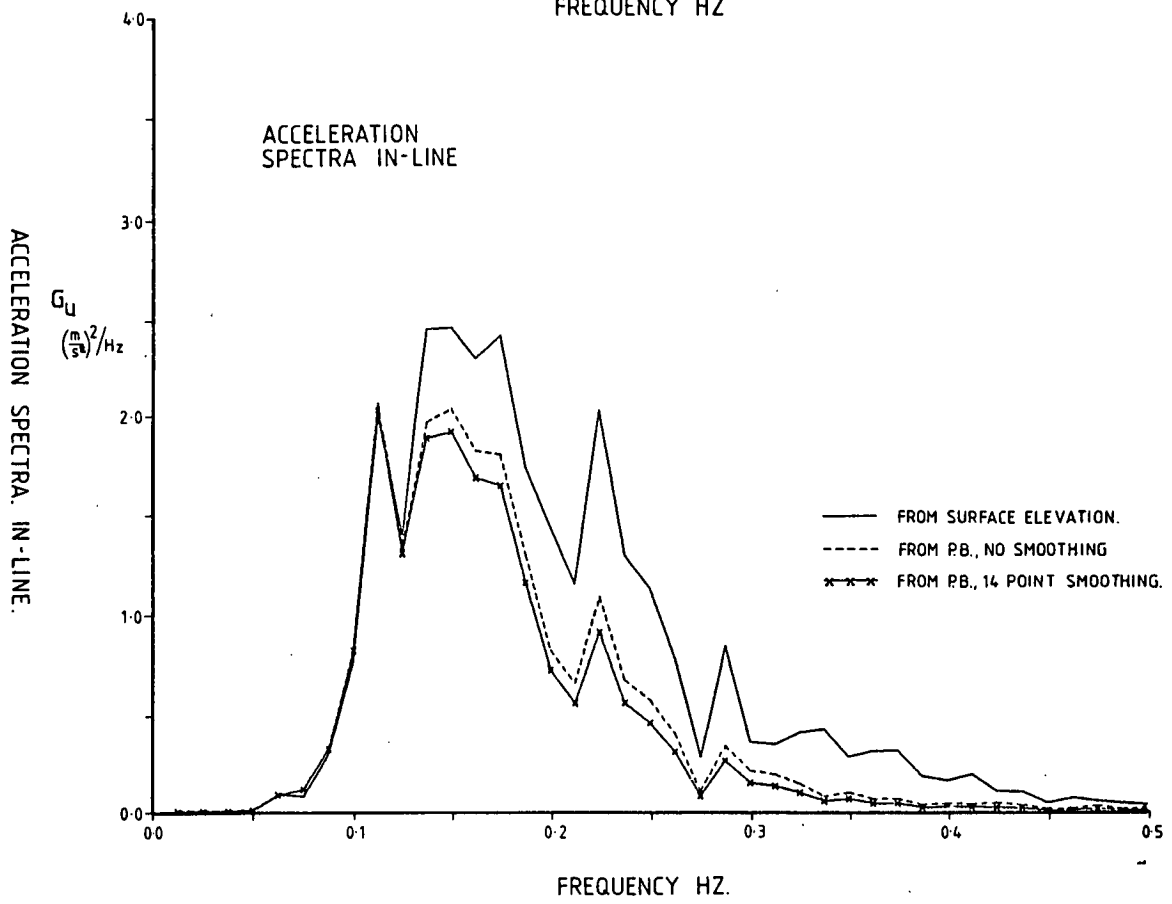
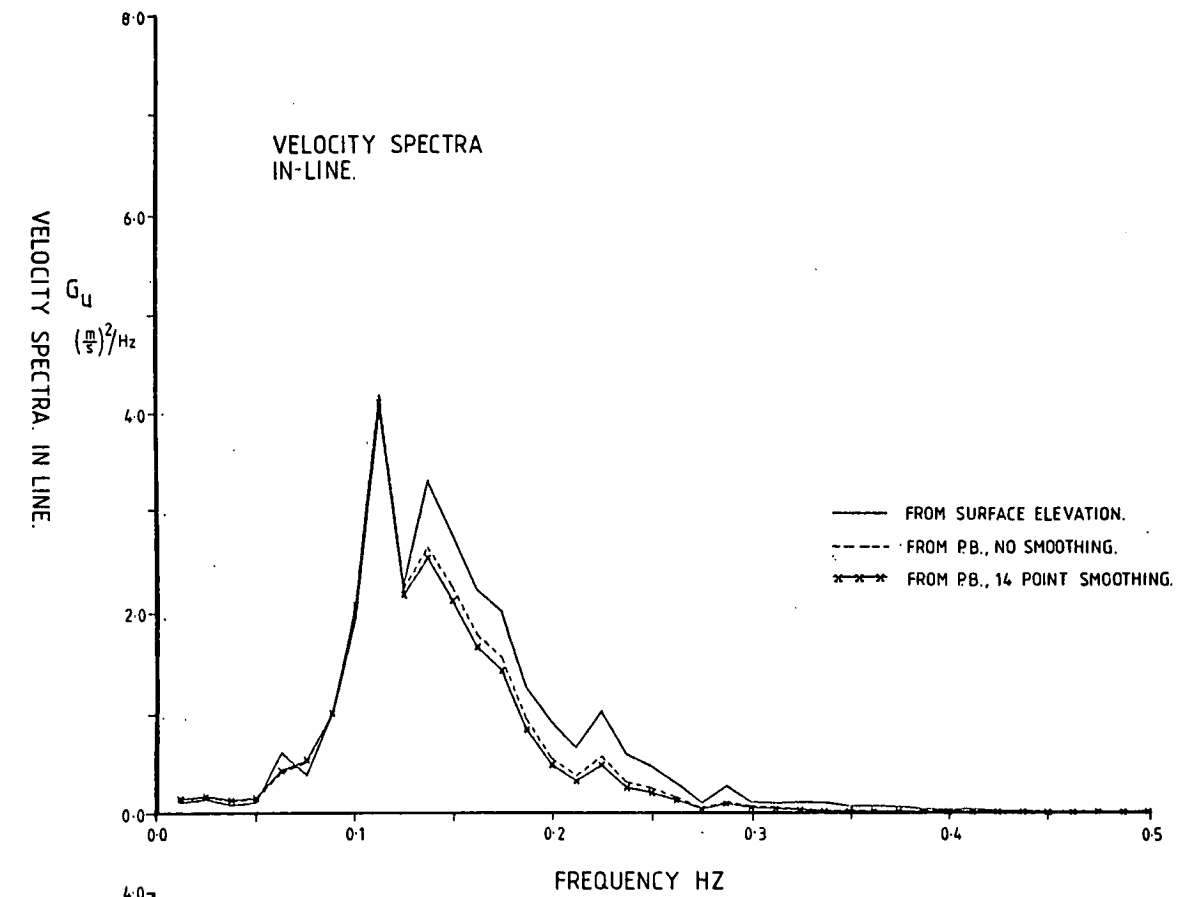
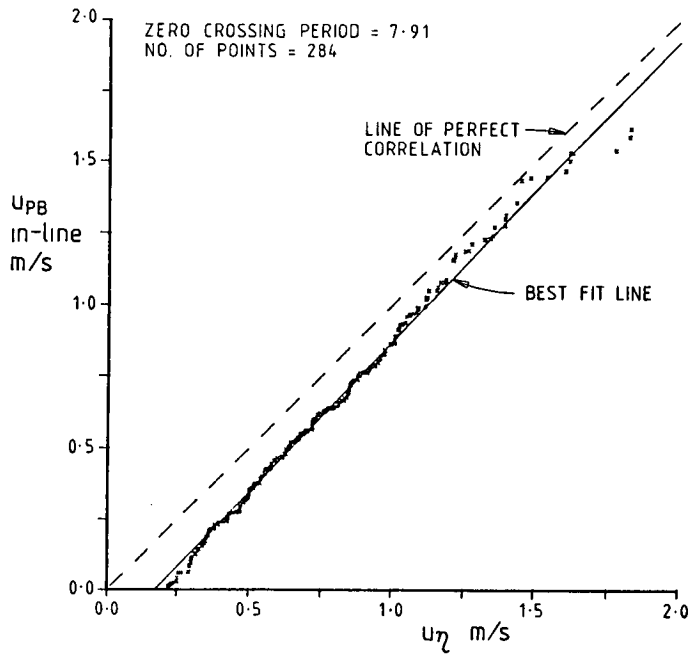
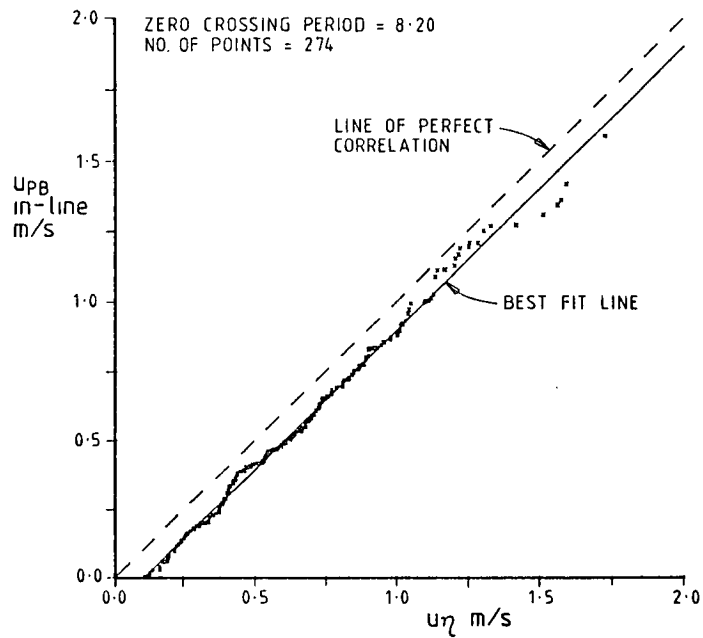


Figure 2.2.3. Predicted and measured velocity and acceleration spectra from Christchurch Bay (Bishop, 1984)

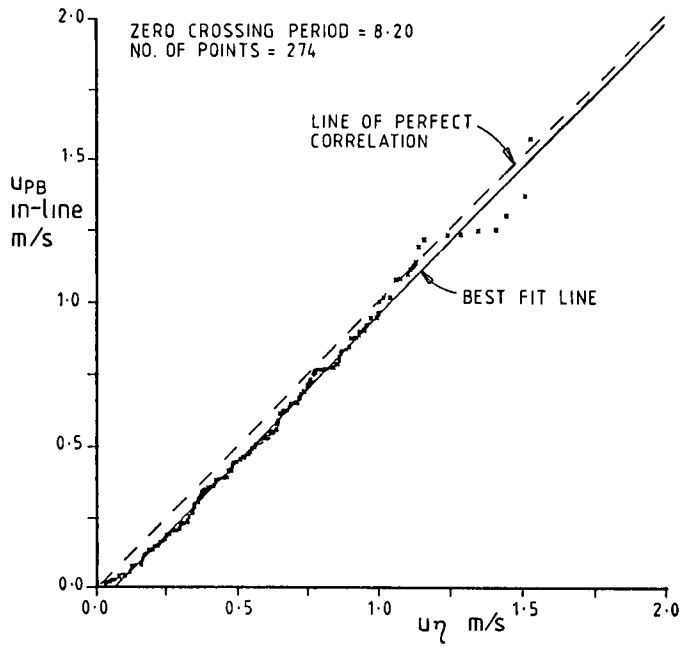


Comparison of in-line particle velocity from perforated ball (PB) and from surface elevation (η) at Level 3

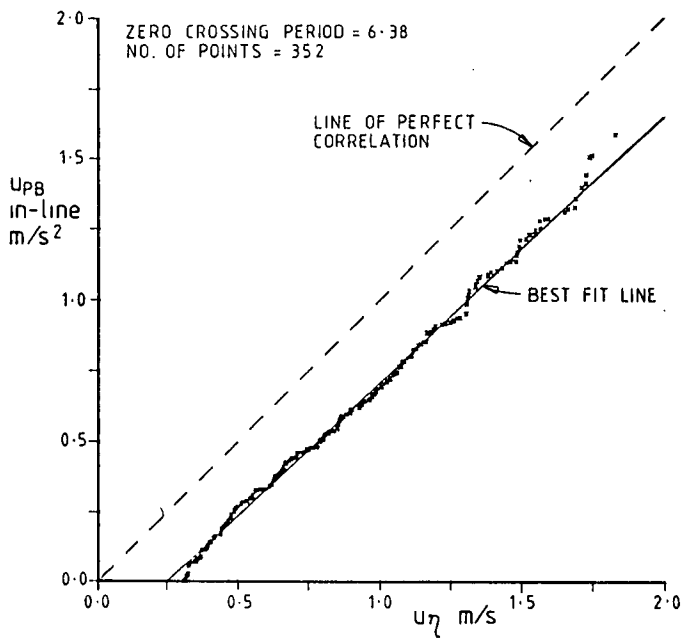


Comparison of in-line particle velocity from perforated ball (PB) and from surface elevation (η) at Level 4

Figure 2.2.4. Christchurch Bay Tower peak velocity and accelerations



Comparison of in-line particle velocity from perforated ball (PB) and from surface elevation (η) at Level 5



Comparison of in-line particle acceleration from perforated ball (PB) and from surface elevation (η) at Level 3

Figure 2.2.4. Christchurch Bay Tower peak velocity and accelerations

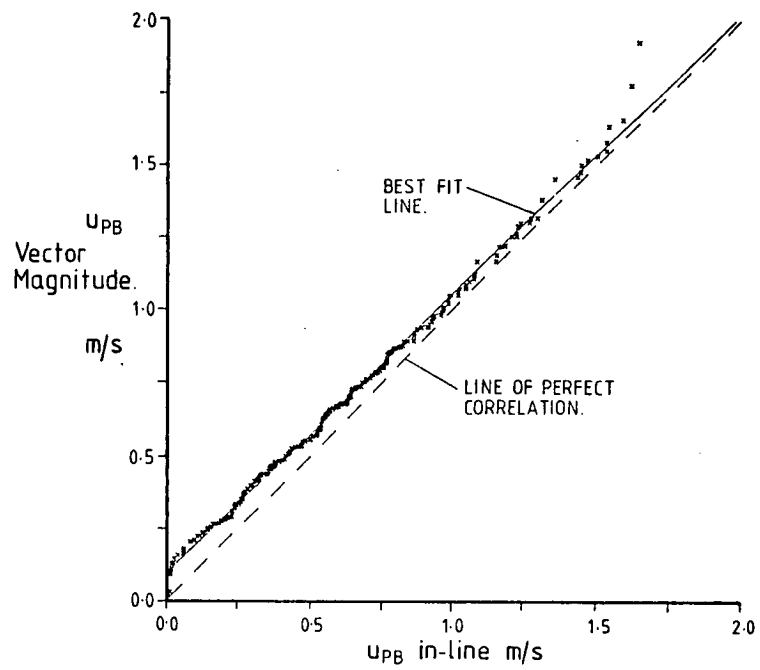


Figure 2.2.5. Comparison of vector magnitude and in line particle velocity. Christchurch Bay results at level 3 (Bishop, 1984)

b. Exxon Ocean Test Structure (OTS)

The Exxon Ocean Test Structure (Figure 2.2.6) has been used to check the prediction of random wave theory. Pawsey and Dello Stritto (1983) have compared time histories of velocity using unidirectional linear random wave theory (ULRWT) based on unmodified Airy theory (method 2) and with the modifications (methods 3 to 5) given above: see Table 2.2.1. All the comparisons were good. The modified Airy Theory fitted the observed data better than the unmodified Airy theory.

Table 2.2.1: Effect of various modifications to the Airy Theory basis of ULRWT predicted/measured velocity (averaged over 3 elevations below MWL) (Pawsey and Dello Stritto, 1983)

Method of using Airy Theory in ULRWT	Reference in 2.2.3a.	Predicted/measured velocity	Standard deviation
Airy hyperbolic functions extrapolated to instantaneous surface	2	1.11	0.158
Airy MWL values summed at surface	3	1.04	0.123
Airy surface values	4	1.02	0.118
Each wave component rides on the other waves components	5	0.96	0.122

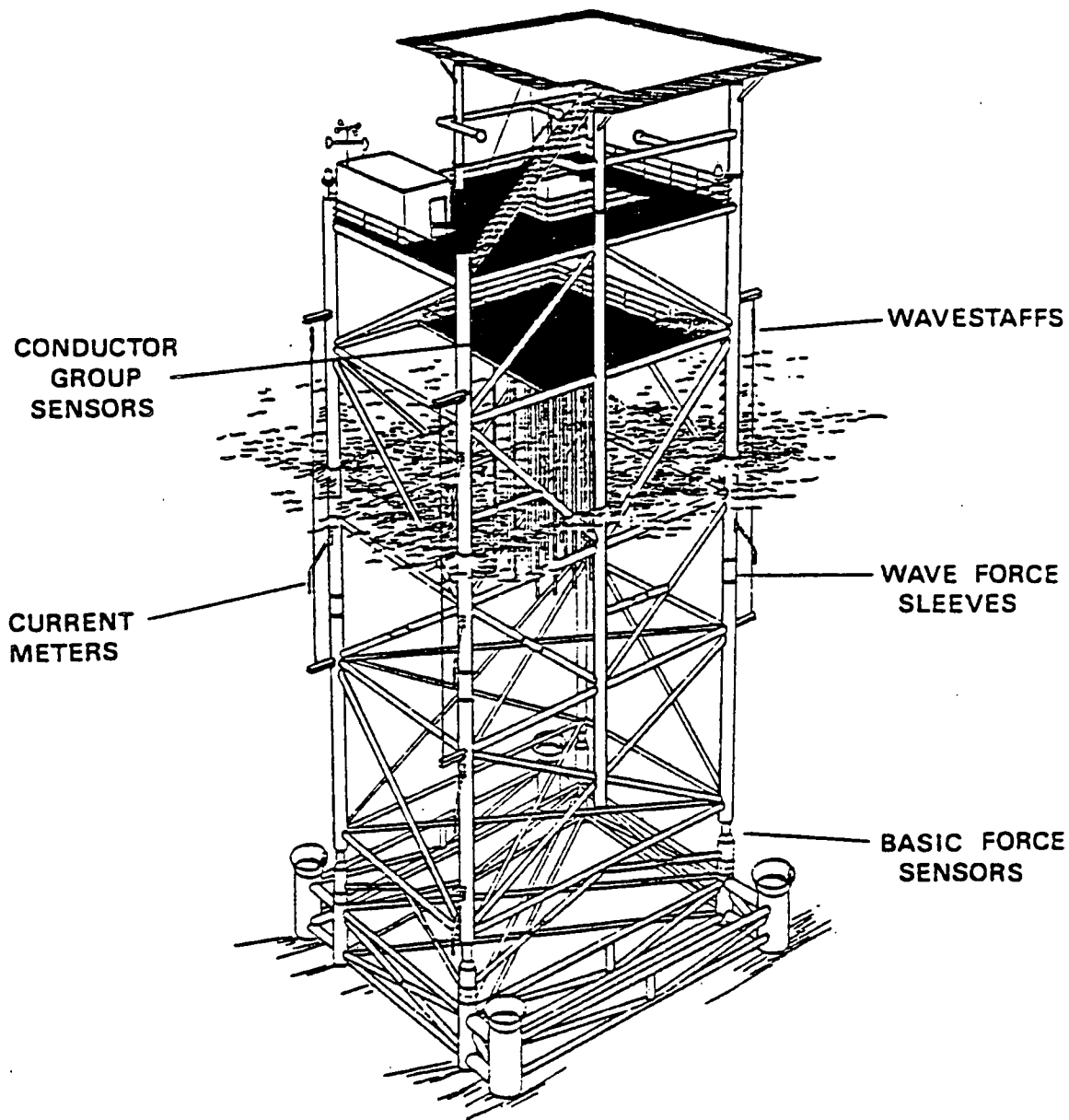


Figure 2.2.6. The Exxon Ocean Test Structure

All the methods showed a tendency to underestimate the measured velocities at the lower levels: see Table 2.2.2.

When directions were assigned to the wavelets used to represent the measured spectrum (on the basis of minimising water surface elevation errors at the four wave staffs) a still better average fit to the measured data was obtained: see Table 2.2.3.

Dean, Lo and Johansson (1979) also used OTS results to check unidirectional linear random wave theory (using modified Airy theory method (4)). They were mainly concerned with comparison of forces. However, they show that the forces calculated from ULRWT were approximately equal to those from Stokes 5 at the +1.5m level. Also the Stokes 5 wave overpredicted velocities at this level by an average 5%. Therefore the ULRWT may also be assumed to overpredict by about 5% at the +1.5m level. This is similar to the 4% over prediction at the -4.6m level given in Table 2.2.2.

Table 2.2.2 - Predicted/measured velocity at the various current meter levels, using ULRWT method 4 (Pawsey and Dello Stritto, 1983)

Level below MWL	Reference in 2.2.3a.	Predicted/ measured velocity	Standard deviation
-4.6m	4	1.04	0.121
-10.7m	4	1.01	0.093
-15.2m	4	0.94	0.071

Table 2.2.3 - Effect of directional spreading on predicted/measured velocity (averaged over 3 elevations and based on a different data set to Table 2.2.1) (Pawsey and Dello Stritto, 1983)

Directionality	Reference in 2.2.3a.	Predicted/ measured velocity	Standard deviation
Unidirectional LWRT	3	1.030	0.133
LRWT with directional spread	3	0.995	0.128

c. Buccaneer platform measurements

Forristall, Ward, Cardone and Borgman (1978) compared velocities, measured at the Buccaneer platform in the Gulf of Mexico, with directional linear random wave theory. They obtained velocity spectra which agreed to within 10% of the measured spectra over the range of frequencies which are significant. This 10% agreement of the spectra should result in a 5% agreement of velocity because the spectra is in terms of velocity squared.

The calculated velocity spectrum tends to be an underestimate at the lower frequencies and an overestimate at the higher frequencies. This is similar to the result obtained from Christchurch Bay. However, in this case directional spreading has been taken into account so the high frequency overestimate cannot be assumed to be caused by directional spreading.

Forristall et al suggest that the differences may be caused by non-linear phase locking between harmonics.

d. Forties Field Experiment

The measured water surface elevation spectra were transformed into velocity spectra using unidirectional LRWT and compared with measured velocity spectra at various levels (Atkins, 1979). Some problems occurred in interpreting the results of the velocity meters. They had been calibrated in steady flow but in the real flow the vertically mounted meters measured 0.7 times the horizontal velocity of the horizontal meters. Also the meters stalled at low velocity during the wave cycles.

The horizontal meters provided the best fit with the velocity spectra peaks as predicted from the water surface elevation. They showed that LRWT underestimated the measured spectra at low frequencies which is consistent with the results of Forristall et al (1978) and Bishop (1984). LRWT also underestimated the measured spectra at high frequencies but this is thought (Atkins, 1979) to be caused by high frequencies generated during meter stalling.

e. Comparison of linear random wave theory with experiments in the sea: conclusion

The experimental results show that linear random wave theory performs well both when used to determine the spectra of particle velocities and peak values of velocity from a measured water surface elevation spectrum. The best results are obtained when

directional spreading is taken into account. The low frequency part of the velocity spectrum may be subject to underestimation and the high frequency part to overestimation. Several researchers have suggested that this may be caused by non-linear effects.

2.2.5 Comparison of regular wave theory with experiments in the sea

a. Ocean Test Structure

Individual waves were identified (Dean Lo and Johansson, 1979) from the water surface elevation time history. Velocities calculated using Stokes 5 theory were compared with measured values under the wave crest and wave trough. Below the splash zone the mean velocity (current) was subtracted before the comparison was made but in the splash zone no adjustment for current was made.

The results are given by level, as averages for various storm periods, in Figure 2.2.7. Unweighted averages of these results are given in Table 2.2.4.

Table 2.2.4 - Stokes 5/measured velocity. Average results for several storms
(Dean et al 1979)

Current under elevation above MSL (m)	Predicted/measured velocity		Note
	Under crest	Under trough	
+1.5	1.07	-	1
-4.6	1.35	1.11	2
-10.7	1.38	1.21	2
-15.2	1.27	1.14	2

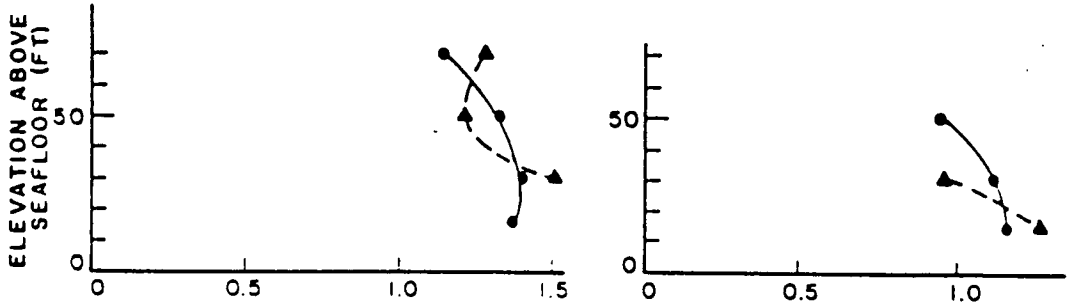
1 Not adjusted for current

2 Adjusted for current

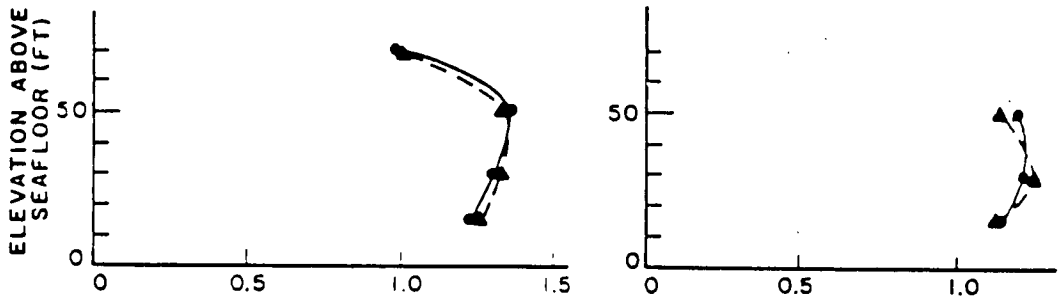
—●— SE PILING
 -▲- NW PILING

CREST VELOCITIES

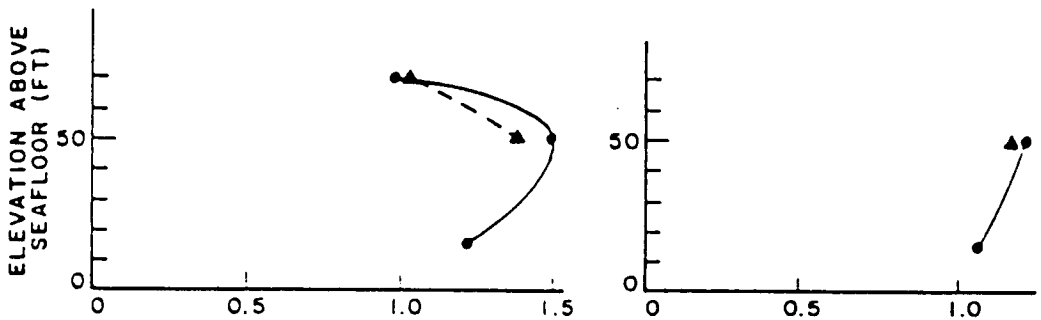
TROUGH VELOCITIES



(a) AVERAGE RATIOS - WINTER 76-77 DATA



(b) AVERAGE RATIOS - HURRICANE ANITA DATA



(c) AVERAGE RATIOS - WINTER 77-78 DATA

Figure 2.2.7. Ocean test structure results: Average ratios of Stokes to measured in-line velocities under crest and trough, Dean, Lo & Johansson (1979)

b. Buccaneer platform measurements

Velocities, measured at the Buccaneer platform, were compared with the predictions of Stokes 5 and a surface profile matching stream function theory (Forristall, Ward, Cardone and Borgman, 1978). Both methods overpredicted the particle velocities under the wave crest. The Stokes 5 results, which are slightly worse than the surface profile matching theory, are shown in Figure 2.2.8. The results for the highest meter at -4m show Stokes 5 to overestimate the measured velocities under the crest by about 40%.

c. Eugene Island measurements

Ohmart and Gratz (1978) measured particle velocities in the Gulf of Mexico at the Eugene Island jacket. The water depth was 54m and the measurements were taken at 1.5m and 6.1m below mean water level.

The measurements were compared with Airy theory and Stokes 5, which modelled the wave from the measured wave height and period, and surface profile matching stream function theory. It was concluded that there was some tendency for all the theories to overpredict horizontal velocities for the higher waves and to underpredict for the lower waves. Four examples are given in the paper: for wave heights of 7.5m and 5.3m at the two levels. They show an overestimate of velocity of up to 20%. Accelerations were in one case underestimated by 20%.

d. Comparison of regular wave theory with experiments in the sea: conclusion

Below MWL, and below the wave crest, the three experiments show significant overestimation of particle velocities. Above MWL only the OTS results are available. They show only a small overestimation at +1.5m. However, the effect of current has not been taken into account at +1.5m and this could be the cause of the better fit to the measured data.

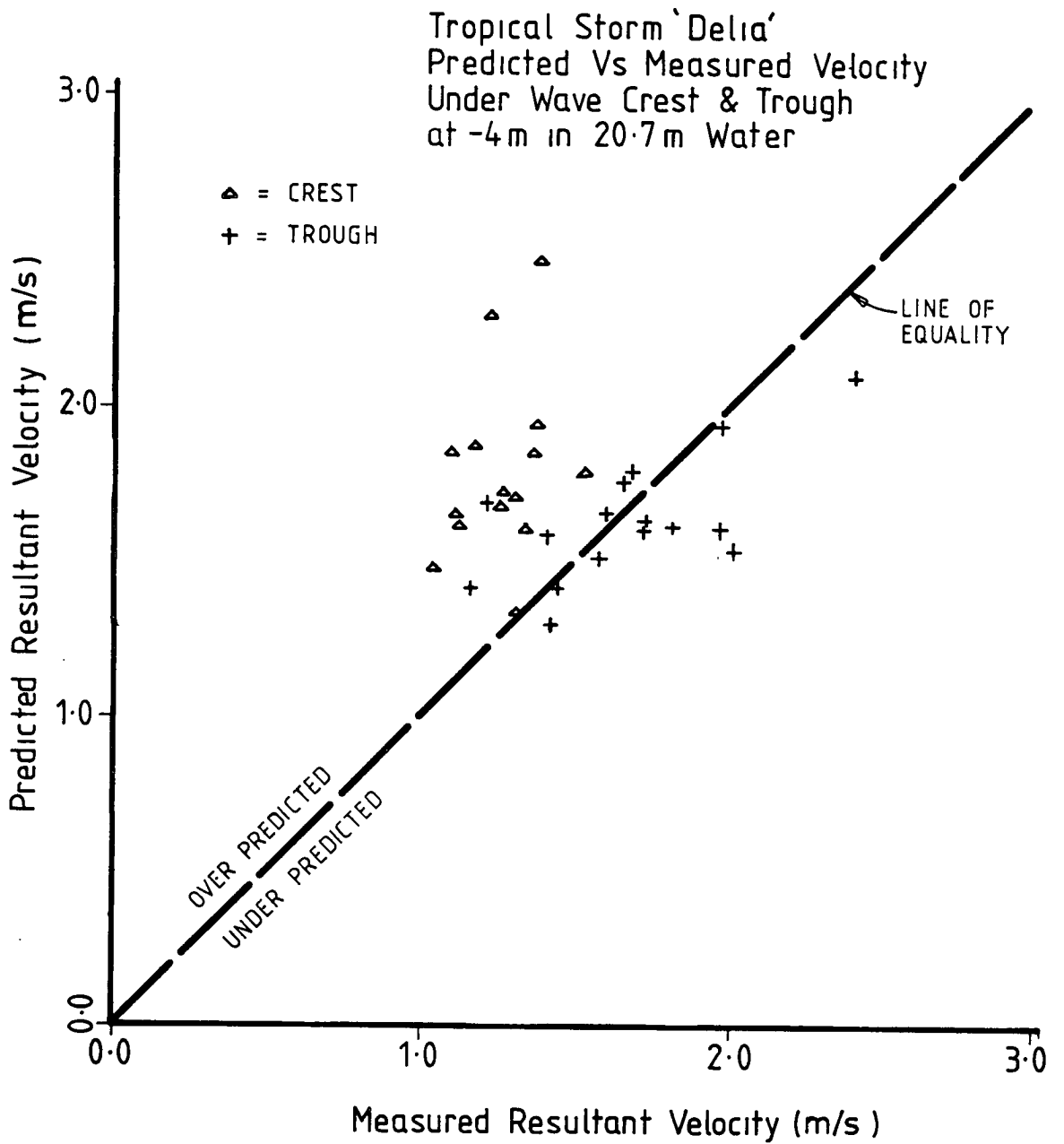


Figure 2.2.8. Comparison between Stokes 5 and maximum velocities in sea waves (Forristall et al, 1978)

2.2.6. Comparison of regular wave and random wave theories

a. Comparison based on measurements in the sea

Both the OTS and Buccaneer experiments show that regular wave theories significantly overestimate the measured particle velocities but that random wave theories, especially if directional spreading is taken into account can provide a good estimate of the measured velocities.

b. Theoretical comparison

Standing (Appendix D) performed a comparison of the extreme velocities and accelerations predicted by linear regular waves, of steepness 1/12 and 1/18, and unidirectional linear random wave theory (Section 2.2.3a, method 1). For a specific sea state and with no current the 1/18 regular wave gave conservative estimates of kinematics from the sea bed at 150m below MWL to 35m below MWL. The 1/12 regular wave gave conservative estimates of the kinematics from 50m to 15m below MWL. Neither regular wave was conservative relative to unidirectional random wave theory from 15m below MWL to MWL.

Holmes, Tickell and Burrows (1978) provide some indirect evidence which confirms Standing's conclusion that regular waves will tend to underestimate the kinematics at the wave surface when compared to the results of unidirectional random wave theory. They calculated the long-term probability distribution of drag and inertia loading:

- 1) in method (1) random waves (allowing for drag loading proportional to velocity squared)
- 2) using a deterministic approach (see 4.4) with the higher waves having a steepness of 1/10.7
- 3) using a deterministic approach with the higher waves having a steepness of 1/19.8.

(Other methods were also used which are not of interest here)

They found that, in 150m water depth, both regular waves underestimated the 1 year return value of wave loading at MWL. The next position at which calculations were performed was 7.5m below MWL. Here the steeper wave gave a conservative assessment of the loading on 0.5, 1.0 and 2.0m diameter cylinders but was unconservative for a 5m diameter cylinder. The shallow wave was always unconservative at 7m below MWL. At 22m below MWL both wave steepnesses gave a conservative assessment of the loading

on all cylinder sizes.

These studies suggest that, for members near the water surface, very steep regular waves may be required to obtain the particle kinematics predicted by unidirectional linear random wave theory. Further work is needed to determine whether these high kinematics only exist because directional spreading has not been taken into account. Also the high particle kinematics are caused by the high frequency components of the water surface elevation spectrum. These may not cause significant loading on a structure built up from several members.

2.2.7 Random waves: conclusion

From the experimental work that has been performed it is clear that linear random wave theories lead to a better prediction of particle kinematics than regular wave theories. Theories which allow for directional spreading within any sea state provide the best fit between measured water surface elevations data and particle kinematics. These theories are difficult to use in practice because there is a lack of data defining the spreading characteristics of seas. The Metocean document (1987) provides a spreading function but it corresponds approximately to an unidirectional sea.

Theoretical comparisons between unidirectional random wave theory and regular wave theory applied with a wide range of wave periods suggests that regular wave theory, used in this way, is conservative at depth but unconservative near the surface.

This conclusion is different to that obtained experimentally and warrants further research. The difference may be caused by wave spreading effects which, because they are most significant at the higher wave frequencies, would tend to reduce the kinematics most at the water surface. The conclusion may also be invalid for loading on a structure composed of several members in different plan positions.

2.3 WAVE - CURRENT INTERACTION

2.3.1 Introduction

A wave of given period travelling in conjunction with a current has wavelength and particle kinematics that are dependent on the current velocity.

If the current varies then the wave height and length will change. If a wave propagates into an area of different current velocity and the wave is not parallel to the current then the wave direction will also change. These effects are similar to, and may occur at the same time as wave refraction and shoaling from changes in water depth. Iver, Jonnson and Wang (1980) discuss the combined effects.

2.3.2 Effect of a uniform current (a steady current that is constant through the water depth)

The combination of a uniform current with any of the wave theories described in Section 2.1.2 is straightforward because the assumption of irrotationality and the boundary conditions are such that they still apply exactly providing the axis system for the wave theory is moving at the current velocity.

If therefore a wave is specified in terms of its height and length the wave particle kinematics may be calculated for zero current and the combined velocities exactly determined by vector addition. It must be noted however that the wave period is affected by the current. The wave is effectively travelling on the current and if the current has a positive component in the direction of wave travel then more crests will pass a fixed structure in a given time than if there is no current. The 'encounter period' of the waves is therefore reduced.

If alternatively, the wave is specified in terms of height and the encounter period with a stationary observer, then the vector addition approach is still acceptable but it is theoretically necessary to select a wave length $L = T (c + u_c)$.

where:

L = wave length

c = wave celerity (with no current)

u_c = current velocity resolved in the direction of wave propagation

T = wave period relative to a stationary observer

The method described is applicable to regular waves and each component in a model of a random sea (Hedges (1978), Hedges et al (1979), Hedges (1983), Hedges (1987) and Forristall, Ward, Cardone and Borgmann (1978).

Unfortunately because wave data and current data are collected independently, the wave period data does not define the wavelengths of the measured waves. Also it is difficult to decide whether measured periods should be treated as defining wave length or encounter period when a current is added for analysis purposes.

When using the wave theory selection diagram the value of T used in the parameters H/gT^2 and d/gT^2 should theoretically be the period relative to the current, i.e. L/c and not $L/(c+u_c)$.

The modification to wavelength by wave current interaction is discussed in more detail in Appendices E and F. It is also shown that peak MWL values of velocities and accelerations will be overestimated, typically by 5 and 10% if the wavelength modification, by a current of about 1 m/sec, is ignored.

Having established the wave particle kinematics, the current velocities should be added vectorially. For this case of a uniform current the same current velocity should be added to the wave particle velocities at all levels, from the instantaneous surface to the seabed. The modification of a current profile by a wave is discussed in 2.3.3.

2.3.3 Effect of a steady current which varies with depth

There are several reasons why the current may vary with depth, for example, the current can increase considerably near the surface because of the effect of wind.

The combination of a wave with a steady but depth varying current is not straightforward because a depth varying current implies a vorticity or rotation in the flow whereas irrotational flow is one of the basic assumptions of most wave theories.

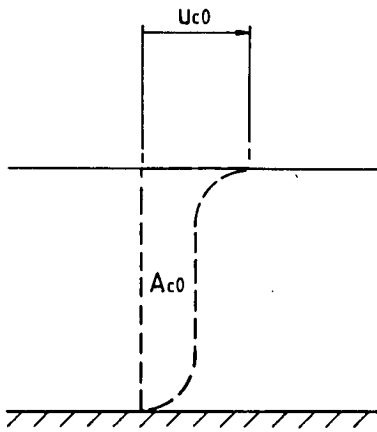
Biesel (1950) obtained a solution for small amplitude waves and a shear current varying linearly with depth. For the case of a uniform current this solution is equivalent to the method described in 2.2.

Ismail (1983) describes an experiment which shows the mutual effects of wave and current for following and opposing currents. He found that the wave particle kinematics were affected by the presence of the current but that Biesel's (1950) solution provide a good match to the measured velocities. He also notes a change in the mean current which he suggests is caused by the waves.

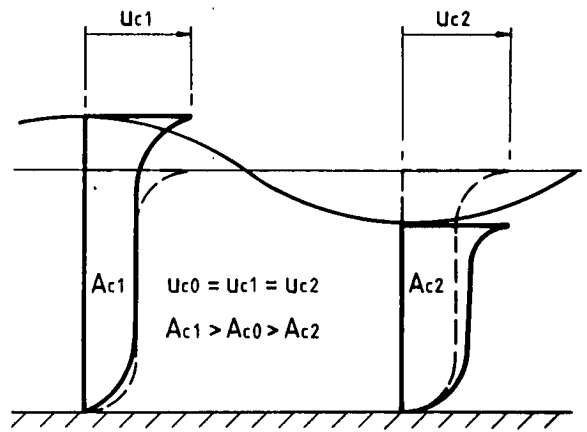
Dalrymple (1974 a,b) extended Dean's (1965) stream function theory to include a current which has a linear variation or a bi-linear variation with depth (i.e. a continuous profile made up of two joined linear variations). He found the wavelength modification to be in the same proportion as that predicted by the small amplitude theory (although the absolute values of wave length predicted by the two theories for no current may be different).

It should be noted that certain commonly used methods of adjusting the current profile in waves are physically incorrect. In particular the so called 'mass continuity' method reduces the current velocity under the wave crest and increases the current velocity in the wave trough. This is based on the assumption that the wave surface and seabed form a tunnel through which the current flows. This assumption is unconservative. Three simple and commonly used approximate methods of combining wave and current are shown in Figure 2.3.1. Method 1: current profile stretching is the most accurate of the three methods (Watson 1986). Also note that for the case of a uniform current Figure 2.3.1 methods 1 and 3 are consistent with the first paragraph of 2.3.2 whereas method 2 is not consistent with the known result for the uniform current case.

The wavelength of a wave travelling in a depth varying current will be modified in a similar manner to that described in 2.3.2 for a uniform current. As an approximation a mean current may be calculated for the purposes of wavelength modification. The mean should be weighted towards the value of current at the surface. The actual current profile should be vectorially added to the velocities obtained from the wave after the wavelength has been modified. Guidance on the effects of wind-current interaction is given in the Metocean (1987) Section 3.4. The nature of the near surface wind driven current, in the presence of waves, is still uncertain.



Current Profile with no Waves



Method 1 - Current Profile Stretching

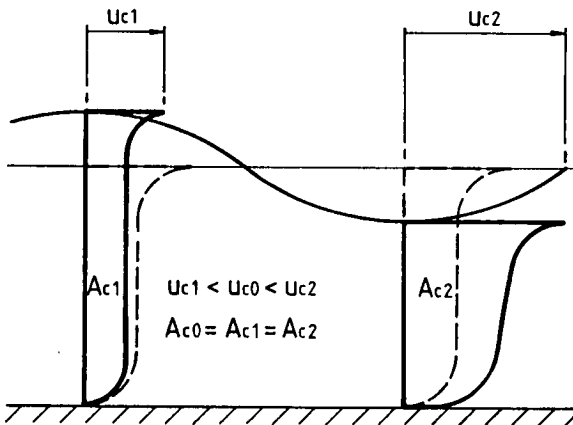
Profile is stretched or compressed vertically but the current velocity at any proportion of the instantaneous depth $d + \eta$ is constant.

This is the most accurate simple method of modifying the current profile to allow for waves.

Key

--- current profile without wave

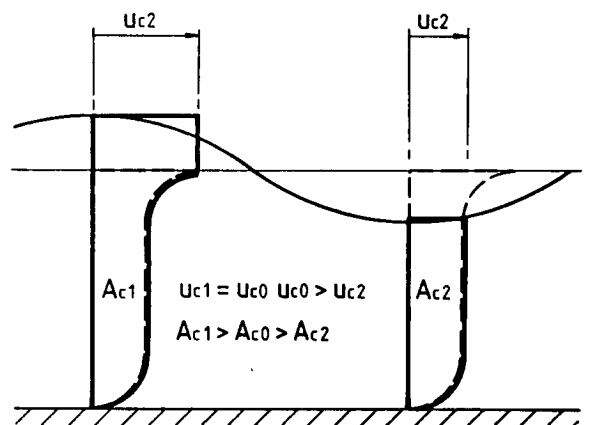
— current profile in the wave



Method 2 - Mass Continuity with Profile Stretching

The profile is stretched or compressed vertically but the current is adjusted so that the mass flow rate of the current is a constant; ie. the area of the current profile diagram is kept constant.

This method will underestimate the loading under the wave crest.



Method 3 - Cut-Off at Surface with Uniform Current Addition

When the instantaneous water level is below still water level the current profile with no wave is cut back to the instantaneous water level.

When the instantaneous water level is above still water level the current profile is extended upwards with a uniform current equal to the still water level surface value.

This method will overestimate the fluid loading under the wave crest.

Figure 2.3.1. Various methods of combining a current profile with the variation in instantaneous water depth due to wave action

2.3.4 Effect of unsteady and non uniform currents

If the current is not steady with time or not uniform with horizontal distance then the properties of a wave travelling on the current and the properties of the current itself will be changed by the interaction that occurs.

In this section the term unsteady is used to refer to variation with time and or distance. Unsteady currents produce changes of height and length of waves propagating on them. Additionally, if the current is not parallel with the wave direction then an unsteady current will change the direction of the waves.

The phenomena has been studied by Longuet-Higgins and Stewart (1961): see (Figure 2.3.2), Whitham (1965, 1967, 1974) and Phillips (1977). Skovgaard and Jonsson (1976) have considered the combined effects of current and refraction caused by changes of water depth. Herbich and Hales (1972) present the results of an experiment where the properties of waves travelling on unsteady currents were measured.

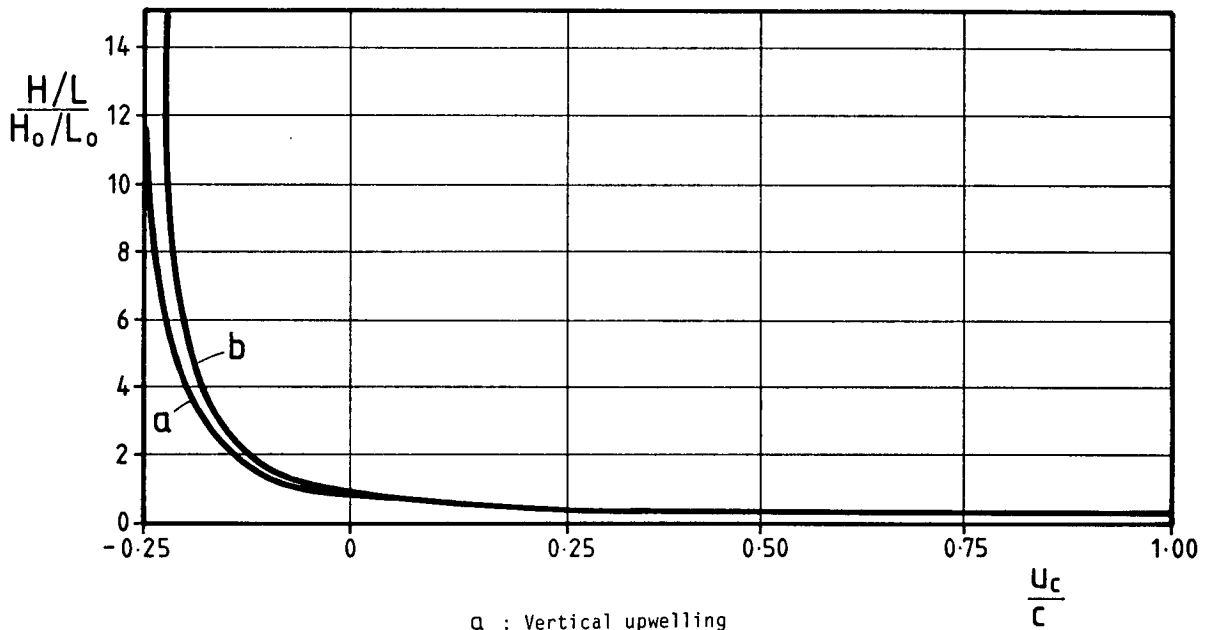
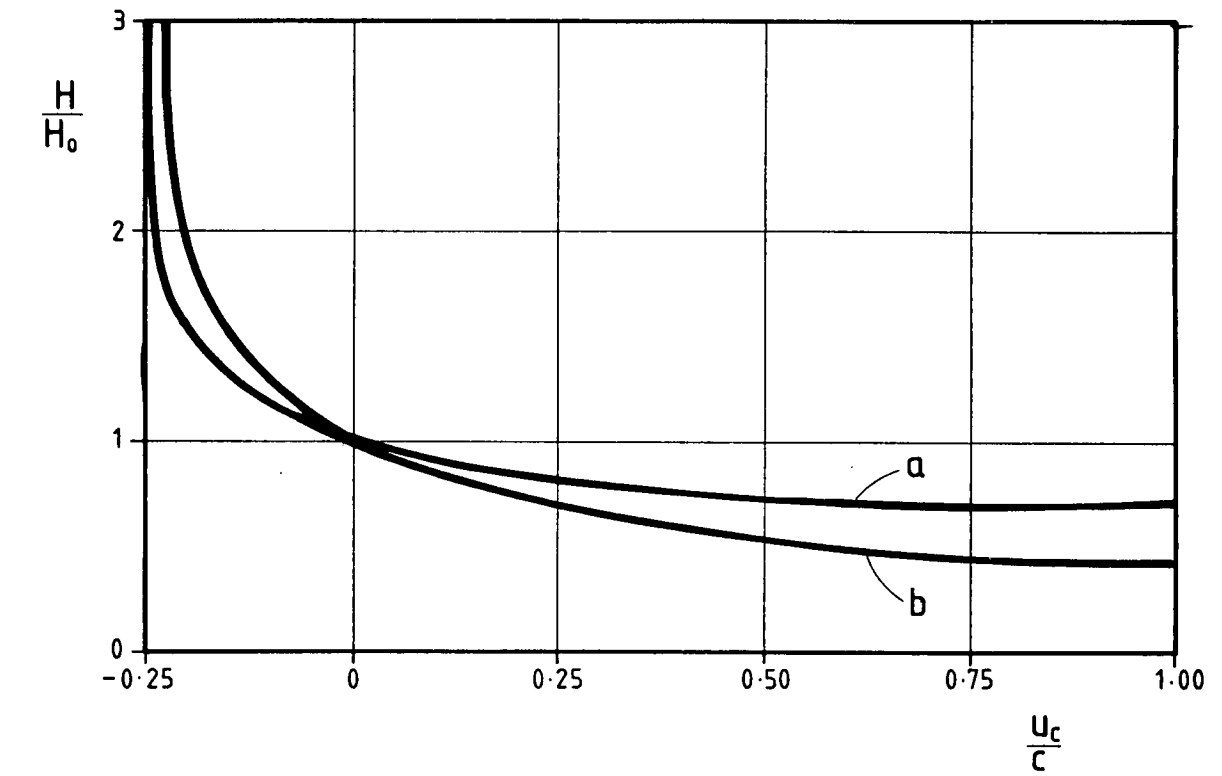
2.3.5 Wave - current interaction: conclusion

a. Steady current

The effect of wave current interaction from steady currents may be taken into account by the vector addition of the wave particle velocities and the current velocity.

For a given wave period the wavelength is dependent on the current. In most cases the effect on wavelength will be small. For the calculation of loading near the surface it will usually be conservative to ignore any change in wavelength caused by a current running in the same direction as the wave.

It is necessary to modify the current profile according to the instantaneous value of water surface elevation. The recommended method is that of stretching the profile (see Figure 2.3.1, method 1).



a : Vertical upwelling
 b : Horizontal inflow
 H/H_0 : Relative change in wave height
 U_c : Current velocity
 C : Initial wave celerity

Figure 2.3.2. Variation of wave height with current and initial celerity
 Longuet-Higgins & Stewart (1961)

b. Unsteady current

If the current on which the wave is propagating changes then the wave height, length and possibly direction will also change.

2.4 BREAKING WAVES

2.4.1 Introduction

The horizontal velocity of the water particles in a wave crest is normally less than the celerity (the horizontal velocity of the crest shape). For a given wavelength the celerity only varies slightly with wave height. However, the velocity of the water particles increases approximately in proportion to the height of the wave. Therefore, for any given wave there is a limiting height above which the water particles in the crest have a horizontal velocity greater than the celerity. Water is then ejected from the wave crest and the wave is said to break.

The measurement and analysis of breaking waves is difficult; Cokelet (1977), in an extensively referenced review article, points out that after more than one hundred years of study there are still unanswered questions about the phenomena.

Regular waves have a limiting height of approximately the lesser of 0.78 times the water depth (d) or 0.14 times the wavelength (L). Solitary waves have a limiting height of about $0.83d$.

There are several causes of breaking waves:-

- Shoaling: A wave moving from deep water into intermediate or shallow water decreases in length and after a small decrease in height it increases in wave height. (Iversen, 1953). This increase in height may eventually lead to wave breaking.
- Wind-Wave interactions: Wind may increase the wave height sufficiently for it to break. Wind may also shear the crest forwards and cause breaking.
- Wave-Wave interaction: Breaking may occur as a wave overtakes another wave or as waves from different directions interfere.

- **Current-Wave interaction:** A wave meeting an opposing current, or moving from an area of opposing current to another area of stronger opposing current, will increase in height and decrease in length. A sufficiently strong current will break the wave.

2.4.2 Waves breaking in shoaling water

Three types of breaking wave may occur in shoaling water as the water depth decreases and the wave height increases. Figure 2.4.1 (from Patrick and Wiegel, 1955) shows the combinations of seabed slope and deepwater wave steepness which lead to the different types of breaking wave.

The deep water wave steepness is the steepness that the wave either had in deep water or would have if it moved into deep water. If the shallow water steepness only is known then the deep water steepness can be obtained approximately from Figure 2.4.2 which is based on linear wave shoaling theory (Sarpkaya and Isaacsson, 1981) and a gradually varying water depth.

Galvin (1972) characterised the breaker type by the dimensionless ratio:-

$$B_r = H_o / (L_o m^2)$$

where:

H_o = wave height in deep water

L_o = wave length in deep water

m = seabed slope (dz/dx)

And:

- $B_r > 5$ - spilling breaker
- $5 > B_r > 0.1$ - plunging breaker
- $0.1 > B_r$ - surging breaker

Galvin's (1972) equation does not correspond to Patrick and Wiegel's (1955) dividing lines on Figure 2.4.2. This is probably because the transition from one type of breaking wave to another is not distinct. The similarity of spilling and plunging breakers is described by Basco (1985). Figure 2.4.3 shows the sequence of events in a plunging breaker. Figure 2.4.4 shows the characteristics of the spilling and plunging breakers at the stage 6 of Figure 2.4.3. It may be seen that the difference is primarily the relative size of the plunger vortex. In the spilling wave the plunger vortex is confined to the region of

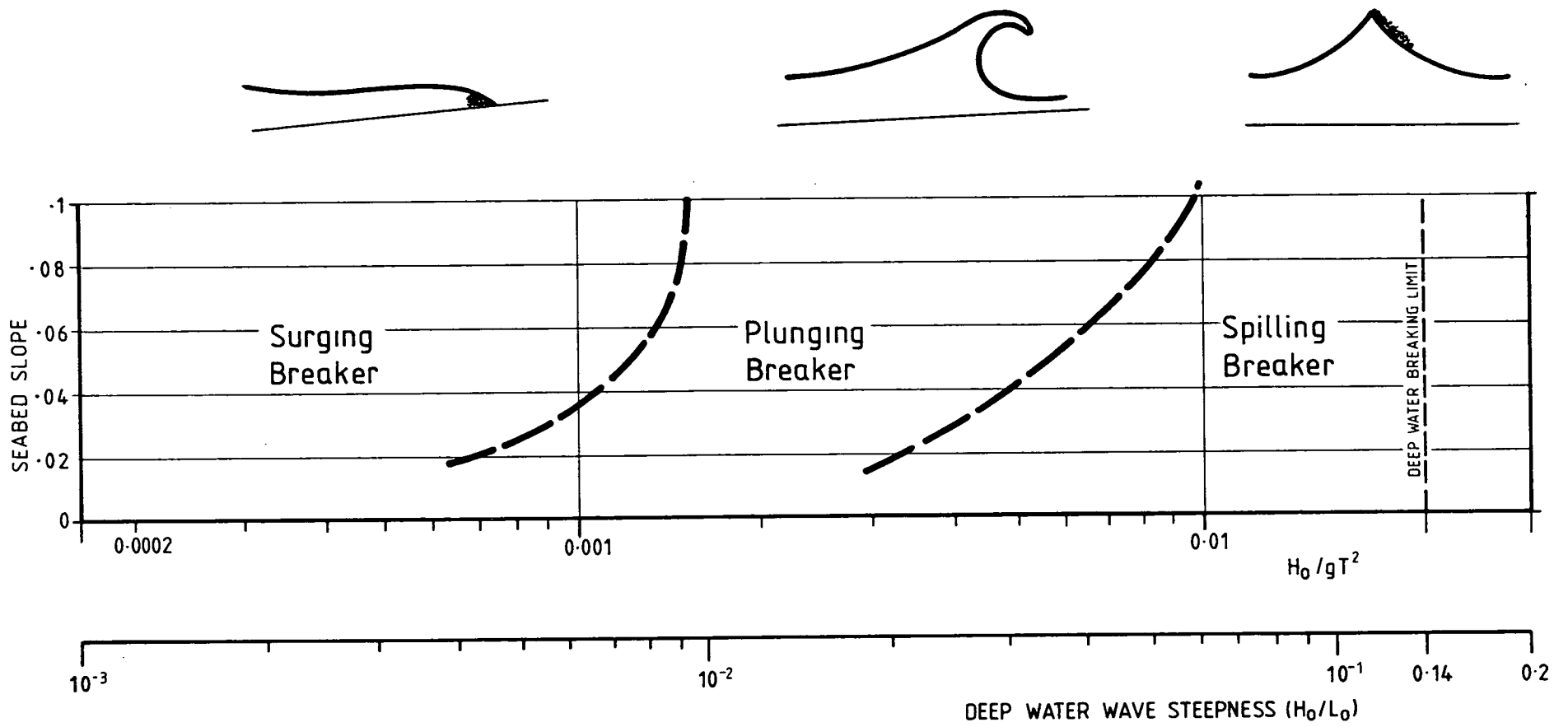
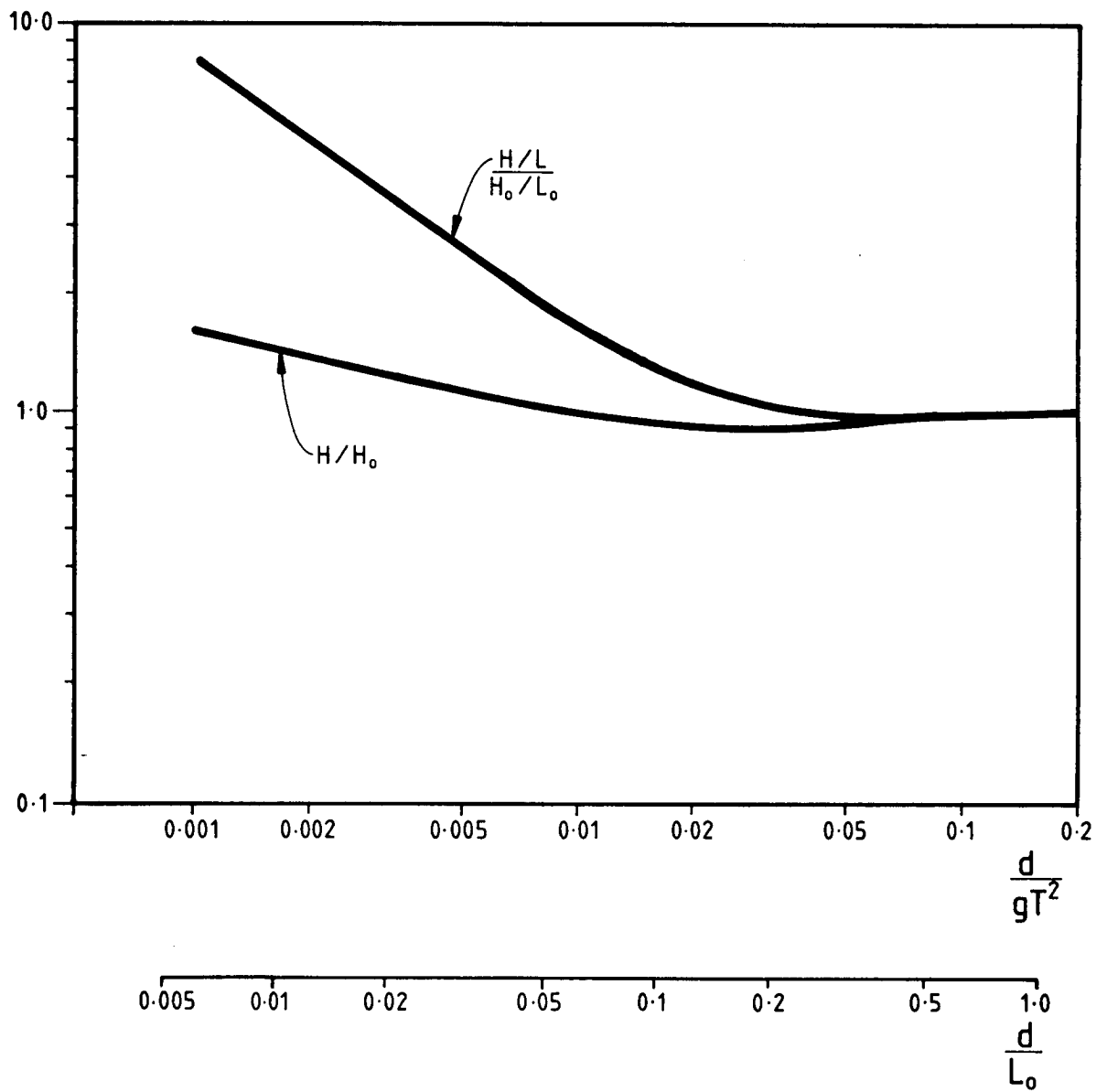


Figure 2.4.1. Type of breaking wave related to wave steepness and sea bed slope (Patrick & Wiggel, 1955)



H_0/L_0 : Deepwater Steepness
 H/L : Steepness at Given d/gT^2

Figure 2.4.2. Deepwater wave steepness and increase in wave height caused by shoaling
 (Based on Sarpkaya and Isaacson, 1981)

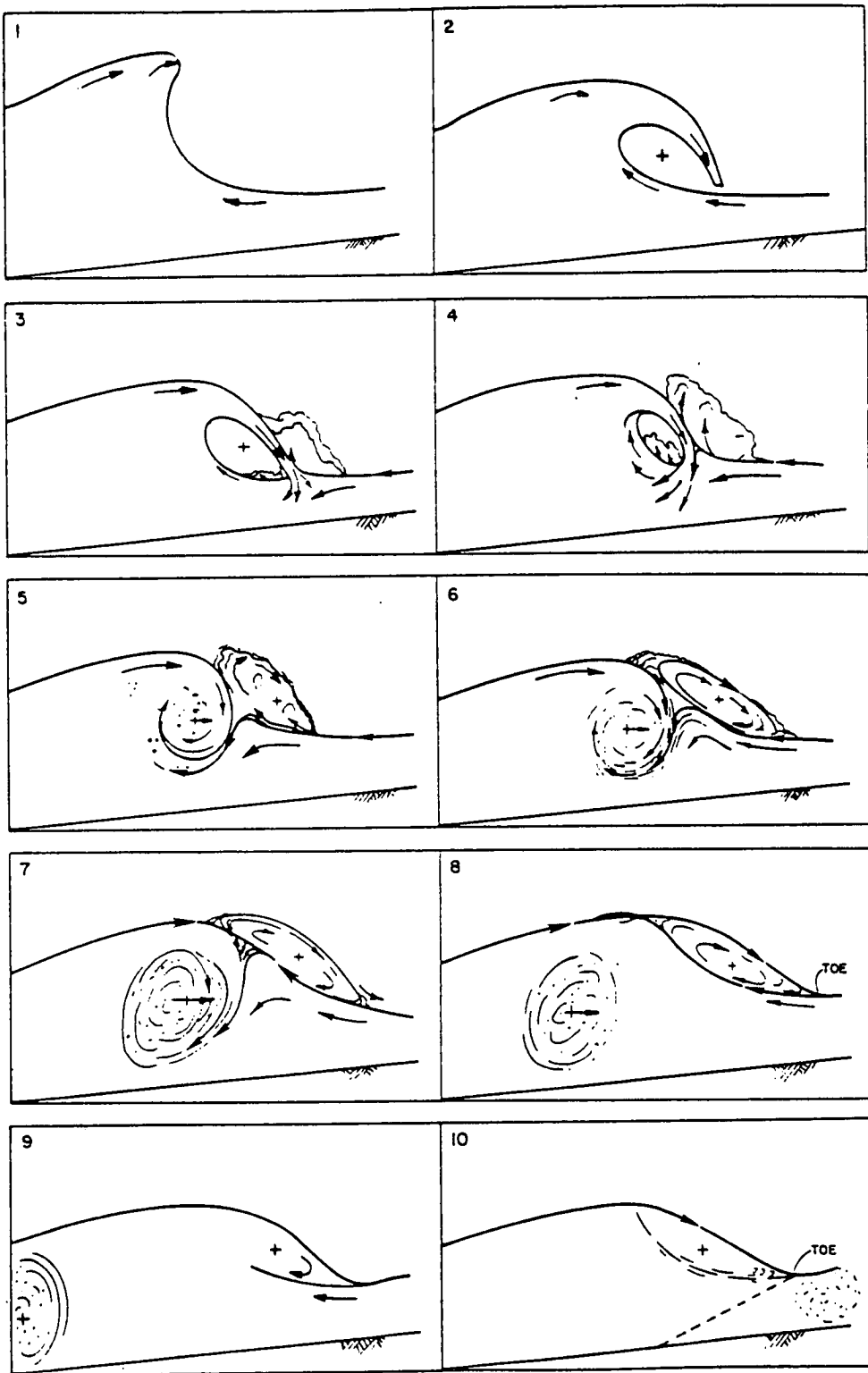
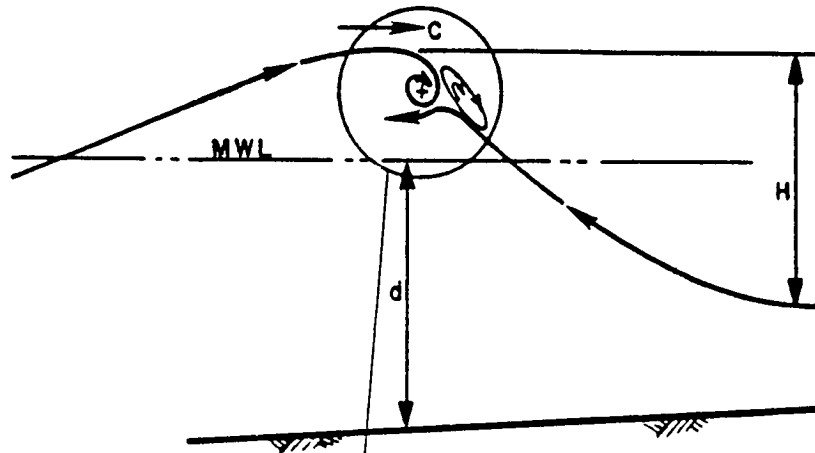


Figure 2.4.3. Sequence of events in a plunging breaker (Basco, 1985)

a) Spilling



b) Plunging

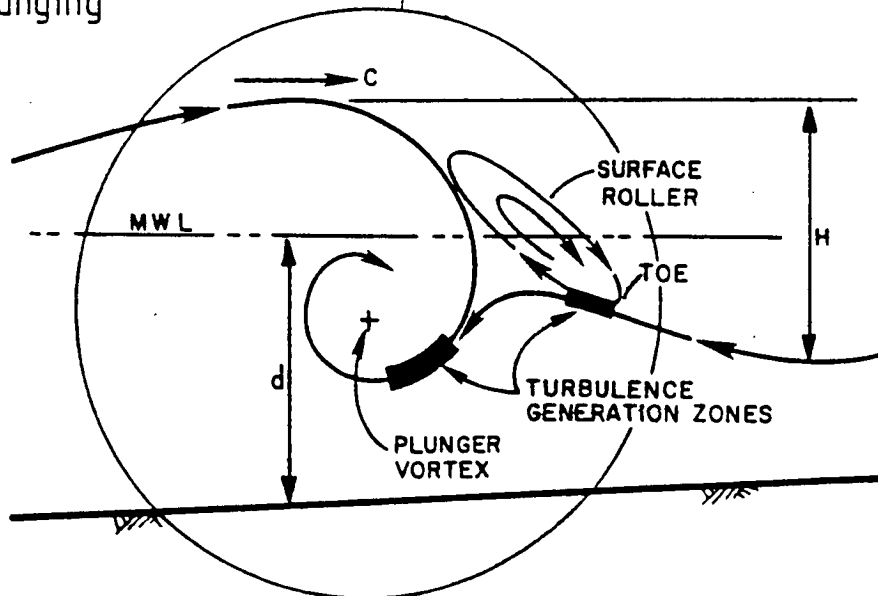


Figure 2.4.4. Similarity of fluid motion in spilling (top) and plunging (bottom) breakers (Basco 1985)

the wave crest. In the plunging wave the vortex size is similar to the wave height.

The surging breaker is a breaking wave in combination with wave reflection from a beach which is relatively steep compared with the wave. This type of breaker is not usually important for offshore structures. The foam in this wave is caused primarily by the vorticity induced by the roughness of the seabed and the horizontal velocities do not necessarily exceed the celerity.

Iversen (1953) has presented data showing the wave height at breaking under shoaling conditions (Figure 2.4.5). The wave heights can be considerably higher than the regular wave limiting values. In Figure 2.4.7 Iversen's data is plotted with Patrick and Wiegel's (1955) division into different breaking wave types; the transition from spilling to plunging is seen to occur approximately when the wave height is 1.1 times the regular wave limiting value of $0.78d$. This seems to be consistent with the descriptions, discussed above, of spilling and plunging breakers given by Basco (1985).

Figure 2.4.7 describes the types of breaking wave which may occur with a given slope, water depth and deep water wave steepness. It does not define the deep water wave height that will lead to breaking at a given location. This deep water height may be obtained by combining data presented by Goda (1970) and Iversen (1953) as described in Appendix G. By using the resulting Figure 2.4.6, the value of deep water wave height and steepness may be obtained that will cause a wave to break at a given water depth and seabed slope. Environmental data should then be consulted to select combinations of deep water wave height and steepness which are likely to occur. The selected values of deepwater steepness may then be used in Figure 2.4.7 to determine the heights at breaking. The period of the wave at breaking will be the same as the deepwater wave.

2.4.3 Wave breaking caused by wind

Wiegel (1964), reviewing the work of a number of researchers, explains that the turbulence in a wind speed of 1.5 to 3 m/sec will immediately generate small waves on a calm water surface. The wind then acts on the rough surface and in a number of ways, including inviscid flow, viscous friction and viscous drag, transfers energy to the water and builds up both a current and the wave. Providing the wind continues to act on the wave and the wind speed is high enough, the wave will continue to increase in height.

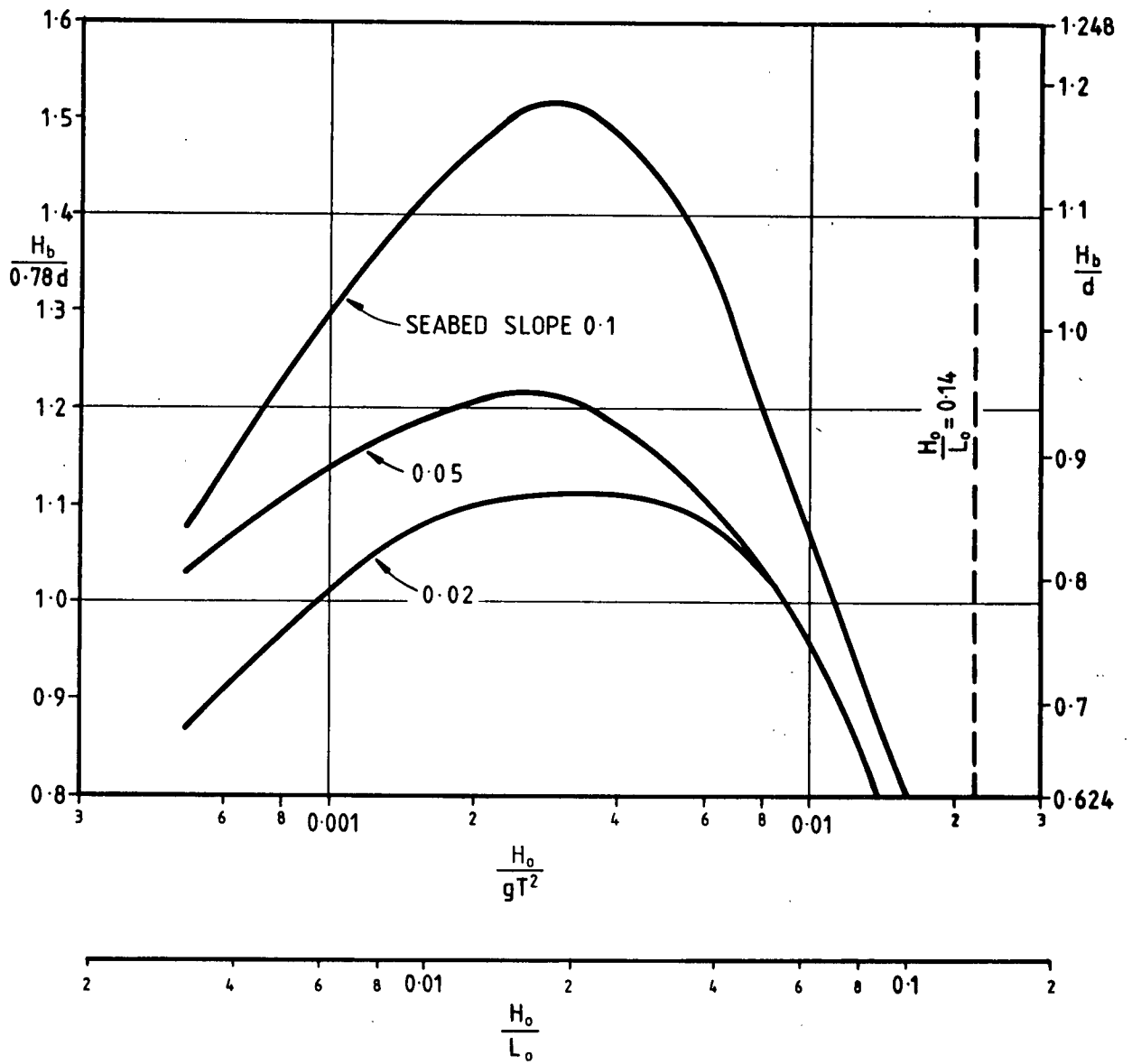
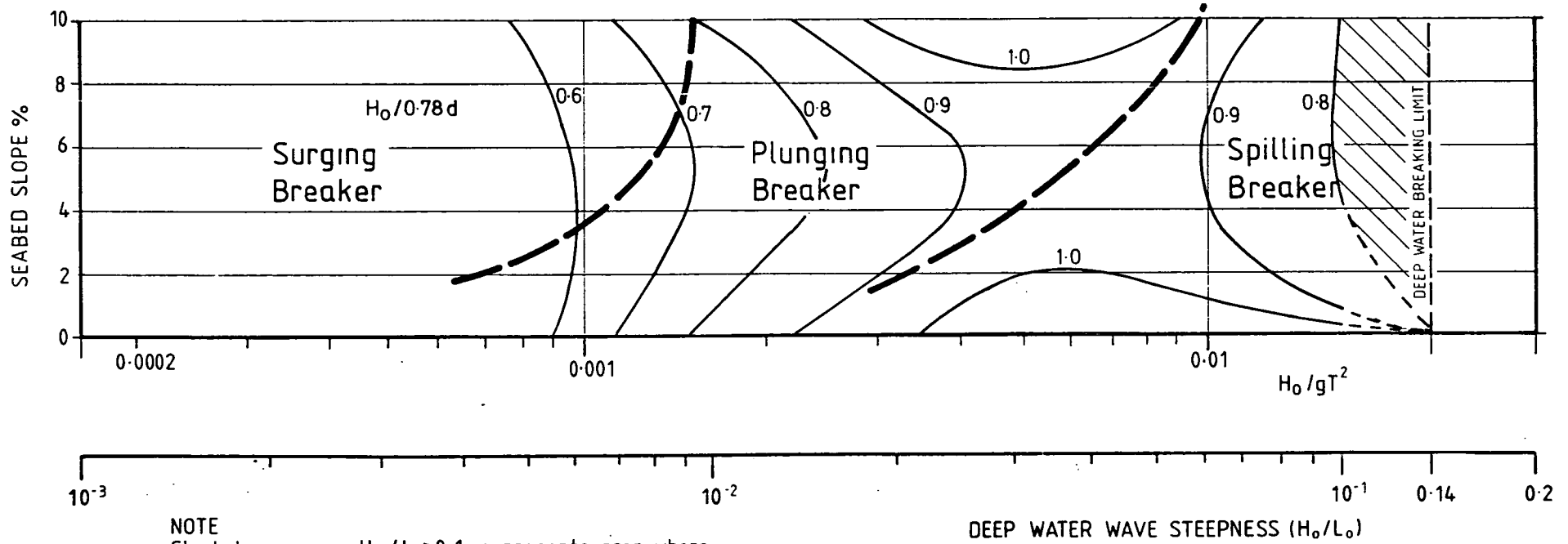
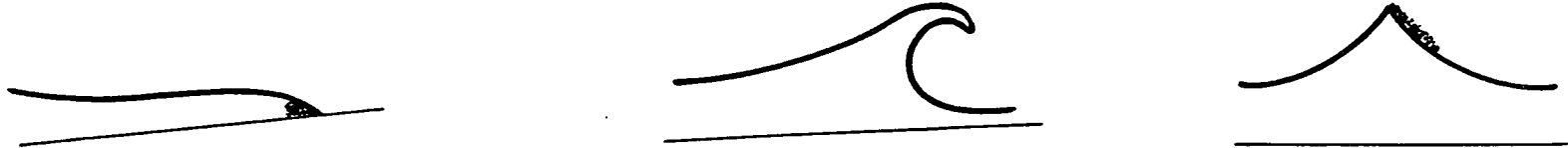


Figure 2.4.5. Increase in wave height under shoaling conditions over limiting height of regular waves (Iversen, 1953)



NOTE
 Shaded region, i.e. $H_0/L_0 > 0.1$, represents area where
 precise data is not available.

Figure 2.4.6. Deep water wave height and steepness that will break at a given water depth and sea bed slope
 (After Iversen, 1953 and Goda, 1970)

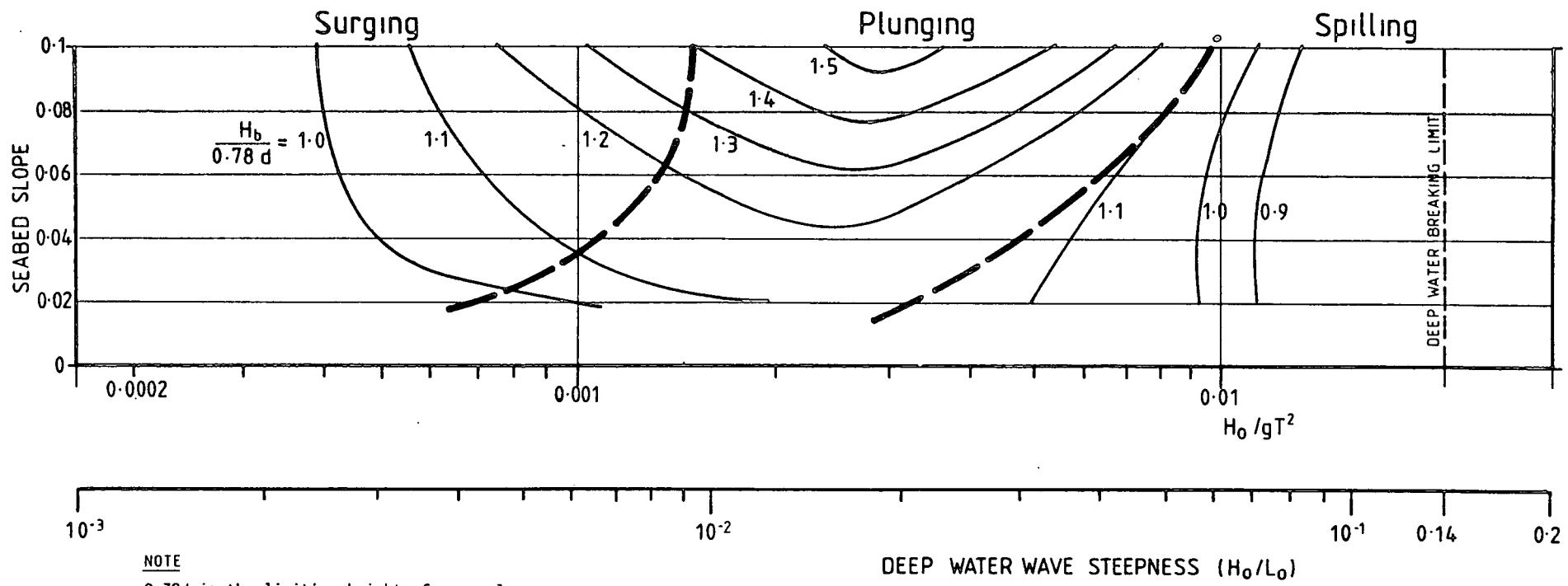
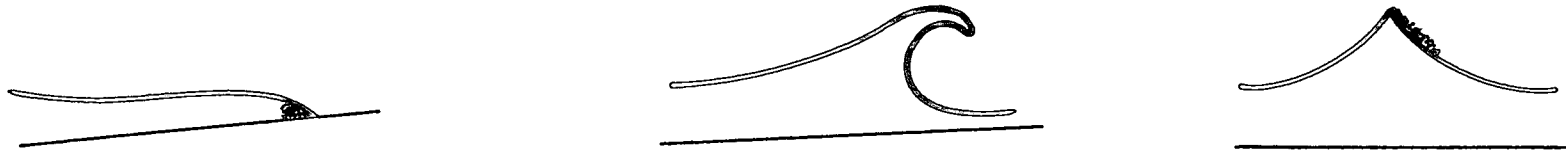


Figure 2.4.7. Increase in wave height over limiting height regular waves (Iversen, 1953) related to breaking wave type, wave steepness and sea bed slope (Patrick and Wiegel, 1955)

Breaking will probably occur before the wave reaches the limiting regular wave height because (a) the wind will tend to blow the top of the wave forward and (b) wave-wave interactions, described in 2.4.4, may occur.

2.4.4 Wave breaking caused by wave-wave interaction

Wave celerity in deep water is approximately proportional to wave period T . (For a small amplitude deep water wave $c = gT/2\pi$). Therefore a wave may be overtaken by a longer period wave. In shallow water the celerity of a solitary wave is $1.29 (g(d + H))^{0.5}$ therefore a wave may be overtaken by a higher wave. In either case the wave particle motions combine and a high wave is produced as the crests come together. If the horizontal particle velocities in the combined crest exceed the velocity of the crest shape then the combined wave will break.

Kjeldsen and Myrhaug (1979) generated breaking waves in the laboratory by wave-wave interaction and obtained two types of breaker:-

- A plunging breaker
- A deep water bore (shown in Figure 2.4.8)

Kjeldsen and Myrhaug do not report the occurrence of spilling waves from wave-wave interaction. Since spilling waves and plunging waves are similar, except that the breaking of the spilling wave is confined to the upper crest, we would anticipate that spilling breakers could also result from wave-wave interaction.

No data was found describing the particle velocities in bore breakers or the precise conditions under which they occur.

The case of regular waves of the same period and height travelling in different directions has been considered analytically by le Mehaute (1986). He concludes that breaking wave heights and internal velocities may all be greater for the resulting short crested breaking waves. Le Mehaute has only considered the breaking criterion of particle velocity exceeding celerity. It is possible that other criteria may be important for short crested waves.

2.4.5 Wave breaking caused by currents

When a wave travels from an area of no current into an area where there is an opposing current the wave steepens and may break. The effect of a current on wave height and wave steepness is shown in Figure 2.3.2 (Longuet-Higgins and Stewart, 1961).

2.4.6 Plunging wave after breaking

Svendsen (1984) has described the behaviour of a particular plunging breaker after the plunge had occurred. The wave continued with the original celerity and a 30% to 40% reduction in amplitude. However, the wave then carried a volume of water, in a surface 'roller', which had a volume of approximately $0.9 H^2$ and a forward velocity equal to the celerity of the wave.

2.4.7 Breaking wave kinematics

The kinematics of breaking waves are difficult to measure and there is only limited data available on their particle velocities and accelerations. However, laser doppler anemometry techniques, which are capable of measuring the velocities, are now being used, e.g. Stive (1980) and Easson and Greated (1984). Mathematical techniques have also been developed, e.g. Longuet-Higgins and Cokelet (1976), Vinje and Brevig (1980) and New, McIver and Peregrine (1985).

Cokelet (1979) presents analytical results for the velocity and acceleration in some deep water breakers.

A small breaker which was close to a spilling breaker in proportion had, at the point of breaking, a crest velocity of approximately the celerity (c) and accelerations under the crest which although not accurately determined were of the order of $0.5g$. These values are consistent with a limiting height regular wave. As breaking progressed the crest turned into a plunging spout and the maximum velocity increased to $1.09c$ and the acceleration to about $0.9g$.

Results are also presented for a breaking wave which was 22.5% steeper than the wave described above. The velocities and accelerations are generally higher in this steeper wave. It is difficult to compare the results in a precise way but the general increase is probably about 30%. As the plunging spout forms velocities in the spout reach 1.3c. Accelerations behind the front face of the wave, below the spout reached 1.6g. The work of New et al (1985) confirms the area of very high accelerations below the spout.

Note that the values quoted above should not be taken as typical for all plunging breakers. Higher values of velocity have been obtained in model tests, e.g. Van Dorn and Pagan (1975) measured velocities of 1.6c.

Stive (1980) measured velocities in spilling breakers and compared the maximum and minimum values at various levels below MWL with the predictions of Airy and Cnoidal theory. He found that Airy theory gave a reasonable prediction but that Cnoidal theory overestimated the measured velocities. Unfortunately the equipment used was not capable of measuring the velocities above MWL. However, the calculations performed in Appendix B show that linear wave theory may only predict velocities of about half the celerity at the breaking limit therefore linear wave theory is not satisfactory for the breaking wave above MWL.

Measurements by Easson and Greated (1984) show crest velocities in spilling breakers of about the wave celerity. They have compared a limited number of their measurements with the results of analyses using the Longuet-Higgins and Cokelet (1976) programme. Horizontal velocities were found to compare well. Larger vertical velocities were found in the experimental work.

Griffiths, Easson and Greated (1987) present particle kinematics for a number of breaking waves. These waves, which would be predicted by Figure 2.4.7 to have spilling characteristics, were found to have crest velocities of about the celerity. Comparisons were made with various wave theories but the agreement was found to be poor. In most cases the velocities in the upper crest were underestimated and the particle kinematics for the lower half of the wave crest and from MWL to the seabed were overestimated by the wave theories. We have briefly compared the crest velocities found by Griffiths et al with those predicted by stream function theory. The theory predicts breaking to occur at a higher wave height. For this higher wave height the predicted crest velocities are a little greater than the experimental values. The different trend with depth between the experimental results and the wave theories is qualitatively similar to that presented for regular waves by Standing (1981) (See Section 2.1.4). We speculate

that this tendency in the breaking wave and regular wave results may be caused by currents in the wave flume.

2.4.8 Breaking waves: conclusion

Breaking waves may result from shoaling, or the interaction of a wave with other waves, current or wind. Breaking waves caused by shoaling are the most important type for offshore structure design.

The type of breaking wave that may occur at a given site depends on the water depth: d , seabed slope: m , and the height: H_0 and length: L_0 that the wave had in deep water.

For a given seabed slope Figure 2.4.6 defines the various combinations of d , H_0 and L_0 that will lead to a breaking wave.

The environmental data should be used to determine which combinations of d , H_0 and L_0 to consider further. These values may then be used in conjunction with Figure 2.4.7 to determine the type of breaking wave (spilling, plunging or surging) and the height of the wave at breaking: H_b .

If the breaking wave type is a spilling breaker it may be analysed as a limiting height regular wave, see 2.1.

If the breaking wave type is a plunging breaker then it will be necessary to obtain advice from hydrodynamic specialists because very little data is available on the velocities and accelerations in these types of wave. A tentative estimate of the kinematics in a plunging breaker may be made with reference to Appendix G.2.

It is unlikely that surging breakers would be of importance for offshore structure design.

The statistics of breaking waves are discussed in Section 3.5.8.

2.5 REFERENCES

References in 2.1

Bretschneider CL, 1960, A Theory for Waves of Finite Height, Proc 7th Conf, Coastal Eng, The Hague.

Chaplin JR and Anastasiou K, 1980, Some implications of Recent Advances in Wave Theories. Proc 17th Int Conf Coastal Eng, Sydney.

Chaplin JR, 1980, Developments of Stream Function Theory, Coastal Eng. Vol. 3 pp 179-205.

Cokelet ED, 1977, Steep Gravity Waves in Water of Arbitrary Uniform Depth, Phil Trans Roy Soc, Ser A, Vol 286, pp 183-230.

Dalrymple RA, 1986, Nonuniqueness in Stream Function Wave Theory, J Waterway Port and Coastal Eng Div, ASCE, Vol 112, No 2, pp 333-337.

Dean RG, 1965, Stream-Function Representation of Nonlinear Ocean Waves, J Geophys Res, Vol 70, pp 4651-4572.

Dean RG, 1970, Relative Validities of Water Wave Theories. J Waterways Harbours and Coastal Eng Div, ASCE, Vol 96, No 1, pp 105-119.

Dean RG, 1974, Evaluation and Development of Water Wave Theories for Engineering Application, Volumes 1 and 2, US Army Coastal Eng Res Center, Fort Belvoir, va 22060.

Ebbesmeyer CC, 1974, Fifth Order Stokes Waves Profiles, J Waterways Harbours and Coastal Eng Div ASCE, Vol 100, No 3, pp 264-265.

Fenton JD, 1979, A High-Order Cnoidal Wave Theory, JFM, Vol 94, pp 129-161.

Fenton JD, 1985, A Fifth Order Stokes Theory for Steady Waves, J Waterways Port Coastal and Ocean Eng Div, ASCE, Vol 111, No 2, pp216-234.

Goda Y, 1964, Wave Forces on a Vertical Circular Cylinder; Experiments and Proposed Method of Wave Force Computation, Port and Harbour Res Inst, Ministry of Transport, Japan.

- Iwagaki Y and Sakai T, 1970, Horizontal Water Particles Velocity of Finite Amplitude Waves, Proc 12th Coastal Eng Conf, ASCE, Chap 19, pp 309-325.
- Keller JB, 1948, The Solitary Wave and Periodic Waves in Shallow Water, Commun Appl Math, Vol 1, pp 323-338.
- Keulegan GH and Patterson GW, 1940, Mathematical Theory of Irrotational Translation Waves, J Res Nat Bureau Standards, Vol 24, pp 47-101.
- Korteweg DJ and De Vries G, 1895, On the Change of Form of Long Waves Advancing in a Rectangular Canal, and on a New Type of Long Stationary Waves, Phil Mag, 5th Series, Vol 39, pp 422-443.
- Laitone EV, 1961, The Second Approximation to Cnoidal and Solitary Waves, JFM, Vol 9, pp 430-444.
- Lambrakos KF and Branon HR, 1974, Wave Force Calculations for Stokes and Non-Stokes Waves, OTC, Houston.
- Le MeHaute B, 1976, An Introduction to Hydrodynamics and Water Waves, Springer-Verlag, Dusseldorf.
- Le Mehaute B, Divoky D and Lin A, 1968, Shallow Water Waves: A Comparison of Theories and Experiments, Proc 11th Coastal Eng Conf, pp 87-107 London.
- Longuet-Higgins MS, 1973, On the Form of the Highest Progressive and Standing Waves in Deep Water, Proc Roy Soc, Ser A, Vol 331, pp 445-456.
- Longuet-Higgins MS and Fox MJH, 1977, Theory of the Almost Highest Wave : the inner solution. J Fluid Mech, Vol 80, Part 4, pp 721-741.
- Longuet-Higgins MS and Fox MJH, 1978, Theory of the Almost Highest Wave : Part 2. Matching and Analytic Extension, J Fluid Mech, Vol 85, Part 4, pp 769-786.
- Longuet-Higgins MS, 1985, Accelerations in steep gravity waves, J Phys Ocean, Vol 15, pp 1570-1579.

Nishimura H, Isoke M and Honkawa H, 1977, Higher Order Solutions of the Stokes and Cnoidal Waves, J Fac Eng Univ Tokyo, Series B, Vol 24, pp 267-293.

Sarpkaya T and Isaacson M, 1981, Mechanics of Wave Forces on Offshore Structures, Van Nostrand Reinhold.

Schwartz LW, 1974, Computer Extension and Analytic Continuation of Stokes' Expansion for Gravity Waves, JFM, Vol 62, pp 553-578.

Skjelbreia L, Hendrickson JS, 1960, Fifth Order Gravity Wave Theory, Proc 7th Coastal Eng Conf, pp 184-196, The Hague.

Standing RG, 1981, Wave Loading on Offshore Structures : A Review, NMI Report R102, 0T-R-8113.

Wheeler JD, 1970, Method for Calculating Forces Produced by Irregular Waves. J Petroleum Technology, March.

References in 2.2

Atkins, 1979, Wave Force Investigation at Forties Field Platform FB, Final Report of Results, WS Atkins Consultants, Epsom.

Bishop JR, 1980, A New Coefficient for Total Wave Force, NMI Report 1977, R 77.

Bishop JR, Tickell RG and Gallagher KA, 1980, The UK Christchurch Bay Project - a Review of Results, OTC 3796, Houston (also NMI Report 87).

Bishop JR, 1984, Wave Force Investigation at the Second Christchurch Bay Tower, NMI Report 0T-0-82100.

Dean RG, Lo JM and Johansson PI, 1979, Rare Wave Kinematics vs Design Practice, Civil Engineering in the Oceans IV, pp 1030-1049, San Francisco.

Forristall GZ, Ward EG, Cardone VJ, Borgman LE, 1978, The Directional Spectra and Kinematics of Surface Gravity Waves in Tropical Storm Delia, J Phys Oceanog Vol 8, pp 888-909.

Holmes P, Tickell RG and Burrows R, 1978, Prediction of Long Term Wave Loading on Offshore Structures, Liverpool Univ Reports OT 7823 and 7824 for OSFLAG Project 5.

Metocean, 1987, Meteorological and Oceanographic Design Parameters, Proposed Revision to Offshore Installations : Guidance on Design and Construction Part II Section 2, D En, UK.

Ohmart RD and Gratz RL, 1978, A Comparison of Measured and Predicted Ocean Wave Kinematics. OTC 3276, P 1947 Houston.

Pawsey SF and Dello Stritto FJ, 1983, Improved Wave Kinematics from Wave Staff Arrays, OTC Paper No. 4587, p 69 Houston.

References in 2.3

Biesel F, 1950, Etude Theoretique de La Houle en Eau Courante, La Houille Blanche, Vol 5A, pp 279-285.

Dalrymple RA, 1974a, A Finite Amplitude Wave on a Linear Shear Current, J Geophys Res Vol 79, pp 4498-4504.

Dalrymple RA, 1974b, Models for Nonlinear Water Waves in Shear Currents, OTC 2114, pp 843-856, Houston.

Dean RG, 1965, Stream-Function Representation of Non-linear Ocean Waves, J Geophys Res, Vol. 70, pp 4651-4572.

Forristall GZ, Ward EG, Cardone VJ, and Borgmann LE, 1978, The Directional Spectra and Kinematics of Surface Gravity Waves in Tropical Storm Delia, J Phys Oceanog Vol 8, pp 888-909.

Hedges TS, 1978, Some Effects of Currents on Measurement and Analysis of Waves. Proc Inst Civil Eng, Vol 65, pp 685-692

Hedges TS, Burrows R and Mason WG, 1979, Wave-Current Interaction and It's Effect on Fluid Loading, Res Rpt MCE/3/79, Dept of Civil Eng, University of Liverpool.

Hedges TS, 1983, Effects of Currents on Wave Drag and Inertia Loads, Proc Coastal Structures Conf 83, ASCE, March, p 461.

- Hedges TS, 1987, Combination of Waves and Currents : An Introduction, Proc Inst Civ Eng, Part 1, 82, June, pp 567-585.
- Herbich JB and Hales L, 1972, The Effect of Tidal Inlet Currents on the Characteristic and Energy Propagation of Ocean Waves, OTC 1618, Houston
- Ismail NM, 1983, Effects of Wave-Current Interaction on the Design of Marine Structures, OTC 4615, pp 307-316, Houston.
- Iver G, Jonnson IG and Wang JD, 1980, Current-Depth Refraction of Water Waves. Ocean Eng, Vol. 7, pp 153-171.
- Longuet-Higgins MS and Stewart RW, 1961, The Changes in Amplitude of Short Gravity Waves on Steady Non-Uniform Currents, JFM, Vol 10, pp 529-549.
- Metocean, 1987, Meteorological and Oceanographic Design Parameters, Proposed Revision to Offshore Installations : Guidance on Design and Construction Part II Section 2, D En, UK.
- Phillips OM, 1977, The Dynamics of the Upper Ocean, 2nd ed, Cambridge University Press.
- Skovgaard O and Jonsson IJ, 1976, Current Depth Refraction Using Finite Elements, Proc 15th Coastal Eng Conf, Vol 1, pp 721-737 Honolulu.
- Watson CJH, 1986, Wave Propagation on a Rotational Current, Background Document to the Revision of Metocean Data Section of Dept of Energy Guidance Notes, MATSU.
- Whitham GB, 1965, Nonlinear Dispersive Waves, Proc Roy Soc, Ser A, Vol 283, pp 238-261.
- Whitham GB, 1967, Nonlinear Dispersion of Water Waves, JFM, Vol 27, pp 399-412.
- Whitham GB, 1974, Linear and Nonlinear Waves, Wiley, New York.

References in 2.4

- Basco DR, 1985, A Qualitative Description of Wave Breaking, J Waterways Harbours and Coastal Eng Div, ASCE, Vol 111, No 2, pp 171-188.

- Cokelet ED, 1977, *Breaking Waves*, Nature Vol 267, 30th June, pp 769-774.
- Cokelet ED, 1979, *Breaking Waves - the Plunging Jet and Interior Flow Field*, *Mechanics of Wave Induced Forces on Cylinders*, Ed T Shaw, Pitman, London, pp 379-392.
- Easson WJ and Greated CA, 1984, *Breaking Wave Forces and Velocity Fields*, *Coastal Eng*, 8, pp 233-241.
- Galvin CJ, 1972, *Waves on Beaches* (ed Meyer RE), Academic, pp 413-456 New York.
- Griffiths MW, Easson WJ and Greated CA, 1987, *A Comparative Study of Water Particle Kinematics in Breaking Waves*, To be published.
- Goda Y, 1970, *A Synthesis of Breaker Indices*, *Trans Jap Soc Civ Eng*, Vol 2, pp 227-230.
- Iversen HW, 1953, *Waves and Breakers in Shoaling Water*, *Proc 3rd Conf Coastal Eng*, Berkeley California, The Engineering Foundation Council on Wave Research, pp 1-12.
- Kjeldsen SP and Myrhaug D, 1979, *Breaking Waves in Deep Water and Resulting Wave Forces*, OTC 3646, Houston.
- Le Mehaute B, 1986, *On the Highest Periodic Short - Crested Wave*, *J Waterway Port and Coastal Eng Div*, ASCE, Vol 112, No. 2, pp 320-330.
- Longuet-Higgins MS and Stewart RW, 1961, *The Changes in Amplitude of Short Gravity Waves on Steady Non-Uniform Currents*, *JFM*, Vol 10, pp 529-549.
- Longuet-Higgins MS and Cokelet ED, 1976, *The Deformation of Steep Surface Waves on Water; 1. A Numerical Method of Computation*, *Proc Roy Soc A*, 350, pp 1-26 London.
- New AL, McIver P, Peregrine DH, 1985, *Computations of Overturning Waves*, *J Fluid Mech*, Vol 150, pp 233-251.
- Patrick DA, Wiegel RL, 1955, *Amphibian Tractors in the Surface*, *Proc First conf on Ships and Waves*, The Engineering Foundation Council on Wave Research and the American Society of Naval Architects and Marine Engineers, pp 397-422.
- Sarpkaya T, and Isaacson M, 1981, *Mechanics of Wave Forces on Offshore Structures*, Van Nostrand Reinhold.

Stive MJF, 1980, Velocity and Pressure Field of Spilling Breakers, 7th Coastal Eng Conf Sydney.

Svendsen IA, 1984, Wave Heights and Set-Up in a Surf Zone, Coastal Engineering, Vol 8, pp 303-329.

Van Dorn WG and Pagan SP, 1975, Scripps Inst of Ocean, Adv Ocean Eng, Lab Report AOEC 71.

Vinje T and Brevig P, 1980, Numerical Simulation of Breaking Waves, 3rd Int Conf on Finite Elements in Water Resources, University of Missouri.

Wiegel RL, 1964, Oceanographical Engineering, Prentice-Hall International.

3. FLUID LOADING

3.1 INTRODUCTION

3.1.1 General

For most fluid loading calculations it is necessary to first calculate the 'incident' fluid particle kinematics, i.e. those that would occur if the structure was not in place. In other cases the interaction of the fluid and the structure is calculated from first principles. This is the case in diffraction theory where wave theory is effectively included in the calculation. This section (3.1) briefly describes the types of fluid loading that are of importance for offshore structures. The remainder of section 3 considers in greater detail the calculation of loading and the selection of suitable parameters.

3.1.2 Vortex formation, drag and lift forces

The viscosity of water results in a shearing of the flow along the boundary with a member. This applies a direct, though for most structures negligible, shear force on the surface of the member. More importantly the shearing imparts a rotation to the flow leading to the formation of vortices. These become detached from the member and are carried downstream as a 'vortex street' in the wake of the member. The energy dissipated in the vortices results in a reduction of pressure which produces a drag force in the direction of the flow. Any lack of symmetry in the flow also produces a lift force at right angles to the flow.

Even when the incident flow is steady the drag and lift forces vary with time as vortices are shed. It is convenient to consider the fluctuating forces to have a time average steady value on which is superimposed a fluctuating force with a zero mean.

In waves the behaviour of the vortices is complicated by the oscillation of the incident flow. In shallow water the flow may be essentially oscillating in a horizontal plane. In some cases the vortices may not be shed before the flow reverses. In other cases vortices will be shed and then they may be swept back over the member as the flow reverses.

In oscillating flow the behaviour is independent of whether the member is horizontal or vertical although the angle the member makes with the flow will affect the vortex shedding pattern.

In deep water the flow describes approximately circular orbits. A horizontal member, orientated with its axis parallel to the wave crests, will then produce a vortex shedding pattern that is very different from a vertical member.

The forces induced by vortex shedding are usually assumed to be proportional to velocity squared and are given by empirical equations of common form:-

Time average drag force	$0.5C_d\rho LD U^2$
Fluctuating drag force	$0.5C'_d\rho LD U^2$
Time average lift force	$0.5C_l\rho LD U^2$
Fluctuating lift force	$0.5C'_l\rho LD U^2$

where:

ρ = fluid density

L = member length

D = member diameter

U = flow velocity resolved normal to the member.

C_d , C'_d , C_l , C'_l are coefficients which will depend on the member geometry and the incident flow.

The first equation for time average drag force is also the drag term in Morison's Equation which is widely used for the calculation of fluid forces on offshore structures. Section 3.2 'Morison Drag and Inertia Loading' contains a detailed description of the time average drag force, the choice of values for C_d and some comments on C_l .

The fluctuating forces are discussed in Section 3.3 'Vortex Shedding Induced Loading'.

3.1.3 Inertia forces

A member in a uniformly accelerating flow is subject to an inertia force which may be calculated from potential flow theory, see for example Sarpkaya and Isaacson (1981). It is convenient to consider the force as having two components :-

1 The Froude Krylov component of the inertia force

An accelerating fluid contains a pressure gradient equal to $\rho\dot{U}$ where ρ is the fluid density and \dot{U} is the fluid acceleration. If the presence of a member in an accelerating fluid did not affect the pressure distribution then the force on a member of volume V would be $\rho V\dot{U}$ (cf. buoyancy where the pressure gradient is ρg and the buoyancy force is ρVg). The force $\rho V\dot{U}$ is sometimes called the Froude Krylov Force.

2 The added mass component of the inertia force

The presence of a member in the flow does affect the pressure distribution and an additional force $C_a \rho V\dot{U}$ also occurs. This force is similar to the force that an accelerating member would have to exert on an initially stationary fluid. An 'added mass' of fluid having C_a times the volume of the member may be thought of as trapped by the member hence the coefficient C_a is known as the added mass coefficient.

1 and 2 are combined in the 'Inertia Term' of Morison's Equation as:

$$(1 + C_a)\rho V\dot{U} = C_m \rho V\dot{U}$$

where C_m is known as the inertia coefficient, $C_m = 1 + C_a$.

Note - added mass coefficients are commonly also given the symbol C_m .

The selection of values for C_m is discussed in 3.2.

3.1.4 Diffraction loading

When a body has a diameter or width of more than about one fifth of a wavelength, the incident waves are modified or diffracted by the presence of the body and force calculations should then take this into account. In this regime loading may be calculated using a wave theory with additional boundary conditions corresponding to the surfaces of the structure. This is usually performed using Airy (linear) Theory and the resulting analysis, known as a linear diffraction analysis is described further in Section 3.4.

On single members wave diffraction generally leads to lower wave loading than would be estimated from uniformly accelerating flow. In physical terms, the particle accelerations of the undisturbed incident wave are, at any given time, only at a maximum over one portion of the structure. However, when the interaction between several members is analysed, diffraction theory may result in higher calculated loading than the inertia coefficient approach. When diffraction is important, the fluid particle displacements usually become sufficiently small relative to the member size for the effects of vortex shedding to be minimal or localised. Nevertheless, in certain situations vortex effects remain an important consideration. Near corners they may cause sea bed scouring and the shed vortices may buffet nearby minor structures.

A local modification to the water surface occurs around members which penetrate the surface. This is a second order effect which is referred to in section 3.2.8h.

3.1.5 Wave slam, slap and impulsive buoyancy

Wave slam results from the sudden immersion of a member in water during the passage of a wave. In addition to buoyancy, drag and inertia forces a transient peak load occurs, due to the impact of the water with the member. The member may respond dynamically and this may increase the effect of the slam force.

Wave slap occurs when a breaking wave meets a member. It may induce very high local pressures on the member.

The change in buoyancy of a structure, as the water level changes with the passing of a wave, can be a significant design load for both horizontal and inclined members. Even when there is provision for free flooding, a member may not be able to flood and empty during a wave cycle. Normal hydrostatics are applicable for computing the static response to these loads, but in some cases, particularly for horizontal members, the

change in buoyancy may produce a dynamic response.

Wave slam and slap are the subject of Section 3.5.

3.1.6 Hydrostatic and hydrodynamic pressure

The pressure at any point beneath the surface consists of the hydrostatic pressure (corresponding to the depth of submergence beneath the mean water level), plus a dynamic component associated with passing waves. The magnitude and phase of the dynamic component may be derived from an appropriate wave theory.

However, the pressure which acts on submerged members is not simply the ambient pressure in the undisturbed flow because it is modified by the changes to the flow, brought about by the presence of the body, which cause the drag and inertia or diffraction forces.

The calculation of pressure loading is discussed in Section 3.6.

3.1.7 Loading regimes

Wave frequency loads on members in waves may be categorised as drag, inertia, diffraction or reflection. The relative importance of these in a particular case will depend on the type and size of the member, the nature of the wave and the depth of the member.

The distinction between drag, inertia and diffraction forces and their relative significance will determine the method to be used in the prediction of wave loads on offshore structures. It is therefore necessary to consider the various loading regimes in more detail.

The relative importance of drag force and inertia force is dependent on wave height and depth of immersion. The drag force is dominant on small diameter members with large wave height. Currents increase the importance of the drag force. As the member size increases relative to the wave height the inertia force becomes dominant. The inertia force also becomes relatively more important as the depth of the member below the water surface increases.

Diffraction becomes important for a single member when its diameter (D) is greater than $1/5$ of the wavelength. However, for multiple members, diffraction effects associated with interference may also be important at smaller D/L ratios.

3.2 DRAG AND INERTIA LOADING ON CIRCULAR CYLINDERS

3.2.1 Morison's equation

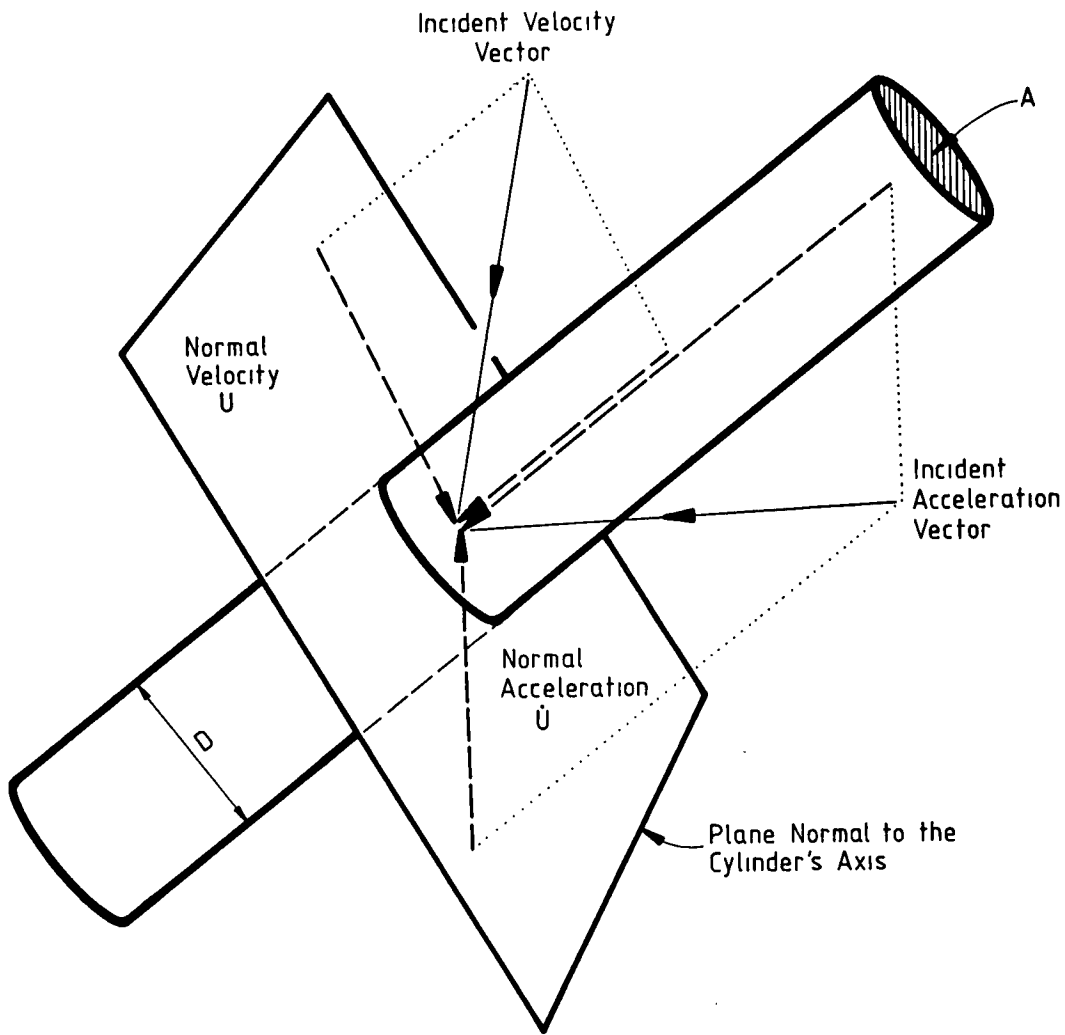
The wave loading formula known as Morison's Equation is usually applied to members which have cross section dimensions less than about one fifth of the wavelength.

The equation (O'Brien and Morison, 1952) reads:-

$$F = 0.5 C_d \rho D |U|U + C_m \rho A \dot{U}$$

where:	(see also Figure 3.2.1)	Typical units
F	is the force/unit length of member	N/m
C_d	is the drag coefficient	-
C_m	is the inertia coefficient	-
ρ	is the density of water	kg/m ³
D	is the member diameter or width perpendicular to the flow inclusive of marine growth (see figure 3.2.6)	m
A	is the member cross sectional area inclusive of marine growth	m ²
U	is the velocity vector of the incident flow resolved normal to the member	m/sec
\dot{U}	is the acceleration vector of the incident flow resolved normal to the member. \dot{U} should include both temporal and convective accelerations (Isaacson 1979)	m/sec ²

The selection of values for C_d and C_m and the general use of the equation is discussed in the remainder of Section 3.2.



A - Cross-Sectional Area of Member and Enclosed Space

D - Diameter or Width of Member

U - Velocity Normal to Member

\dot{U} - Acceleration Normal to Member

Subscripts:

w wave only

c current only

otherwise wave + current

m maximum value through the wave cycle

Figure 3.2.1 Definition of symbols for member loading

3.2.2 Flow conditions

a. General

The values of C_d and C_m required for Morison's equation are dependent on the characteristics of the incident flow and the shape, size and roughness of the loaded member.

In steady flow there is no inertia force and Reynolds number (R_e) and surface roughness (k) determine C_d .

In waves the orbit size of the fluid particles, the orientation of the member, the current, the random nature of the sea and the random re-encounter of the cylinder with its own wake (and possibly the wakes of other members) give rise to a considerable scatter in measured C_d and C_m values and make the selection of appropriate values difficult.

Should locked-on vortex shedding occur (see Section 3.3) C_d values may be larger than those discussed in 3.2. Adjacent members may also modify the flow and change C_d and C_m (see Section 3.7).

b. Reynolds number

Reynolds Number is a non-dimensional parameter which relates the fluid mass times acceleration forces to the viscous forces from shearing of the fluid:

$$R_e = \frac{U_m D}{\nu}$$

where

U_m = maximum velocity of water particles (wave + current) during a wave cycle. For the calculation of U_m the flow is assumed undisturbed by the member. In principle U_m may be the total velocity or the velocity resolved normal to the cylinder. In practice the total velocity is the most useful.
(see 3.2.4 c)

Typical
Units

m/sec

D	=	member diameter or a characteristic width	m
μ	=	fluid viscosity	Ns/m ²
ρ	=	fluid density	kg/m ³
ν	=	kinematic viscosity = μ/ρ	m ² /sec

Representative values for sea water and comparative values for air are given in the following table. U is in m/sec and D is in metres:-

Table 3.2.1 - Data for the Calculation of R_e

	Sea water (0°C)	Sea water (4°C)	Sea water (8°C)	Air (0°C)
ρ (kg/m ³)	1028.0	1027.7	1027.2	1.3
μ (Ns/m ²)	1.879×10^{-3}	1.654×10^{-3}	1.470×10^{-3}	17×10^{-6}
ν (m ² /s)	1.828×10^{-6}	1.609×10^{-6}	1.431×10^{-6}	13×10^{-6}
R_e	547×10^3 UD	622×10^3 UD	699×10^3 UD	77×10^3 UD

The significance of Reynolds number for cylinders in steady flow is shown in Figures 3.2.7 and 3.2.8. The R_e value of the flow is seen to have a large effect on the drag coefficient. In wave flow Figure 3.2.11 shows that R_e is still an important parameter. However, for R_e greater than about 2×10^5 the flow regime is said to be post supercritical and the drag coefficient becomes less sensitive to R_e . For most wave loading on offshore structures the R_e will be in this post-supercritical range.

c. Ellipticity

In long crested regular waves, with no current, the water particles move in approximately elliptical orbits, as shown in Figure 2.1.2. The ellipticity of the orbit is defined as:-

Ellipticity = E = Height of orbit/length of orbit

$E = 1$ for circular orbital flow

$E = 0$ for (planar) oscillating flow

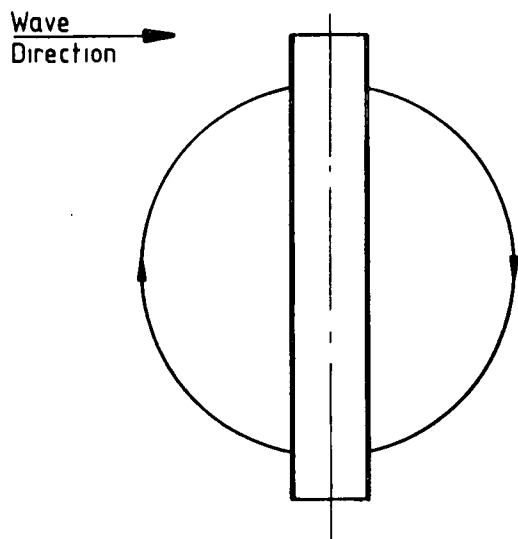
In reality orbits tend to be more complex because:-

- i) finite height regular waves have orbits which are neither perfectly elliptical nor fully closed
- ii) current effects the orbit shape as discussed below
- iii) random seas result in the addition of several orbit shapes so that the water particles follow three dimensional paths.

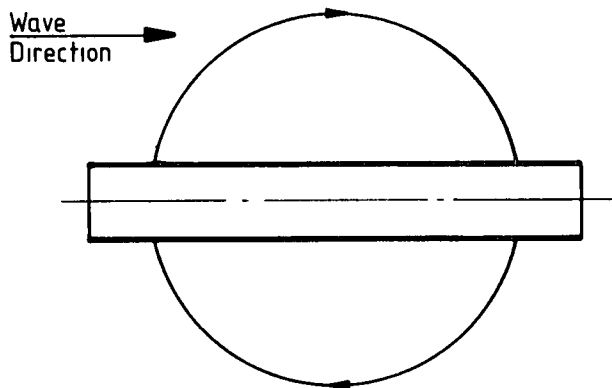
d. Keulegan Carpenter number

For the simple case of an elliptical orbit the undisturbed flow relative to a member is dependent on whether the member is in or out of the plane of the orbit. Figure 3.2.2 shows a vertical member in a circular orbit plane. Inclined and horizontal members may be in or out of the orbit plane as shown in Figures 3.2.2 b) and c). Laboratory measurements frequently show different values of C_d and C_m for members in and out of the orbit plane. The ratio of the size of the orbit to the diameter of the member also affects C_d and C_m . This ratio is proportional to the Keulegan Carpenter (1958) number:

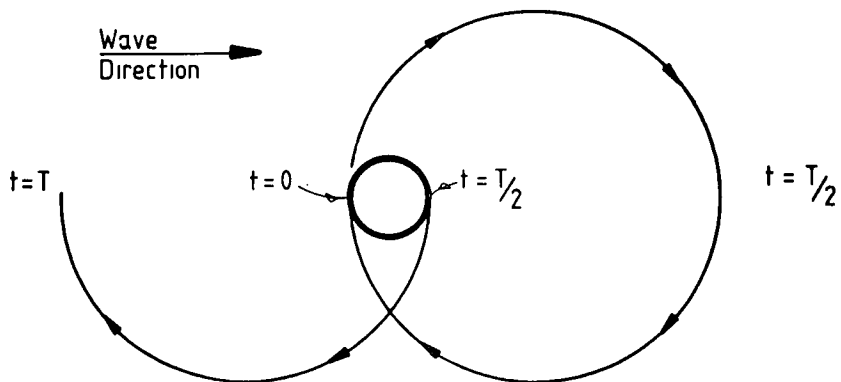
$$K_c = \frac{U_{wm} T}{D} = \frac{\pi b}{D}$$



a) UNDISTURBED PARTICAL PATHS IN ORBITAL FLOW VERTICAL CYLINDER, NO CURRENT



b) UNDISTURBED PARTICLE PATHS IN ORBITAL FLOW HORIZONTAL CYLINDER PARALLEL WITH WAVE DIRECTION



c) UNDISTURBED PARTICLE PATHS IN ORBITAL FLOW HORIZONTAL CYLINDER PERPENDICULAR TO WAVE DIRECTION

Figure 3.2.2. Undisturbed particle paths in orbital flow

Where:	Typical units
U_{wm} = maximum wave particle velocity, resolved normal to the cylinder during cycle, see Figure 3.2.1	m/sec
T = wave period	sec
D = dimension of structure (e.g. member diameter)	m
b = diameter of orbit	m

In conjunction with C_d and C_m , K_c also indicates the relative importance of drag and inertia forces:

$$\frac{F_d}{F_i} = \frac{K_c}{\pi^2} \frac{C_d}{C_m}$$

Where:

F_d/F_i = ratio of drag force/inertia force

C_d = drag coefficient

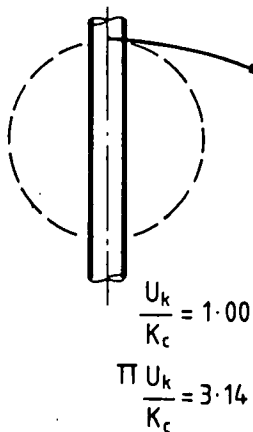
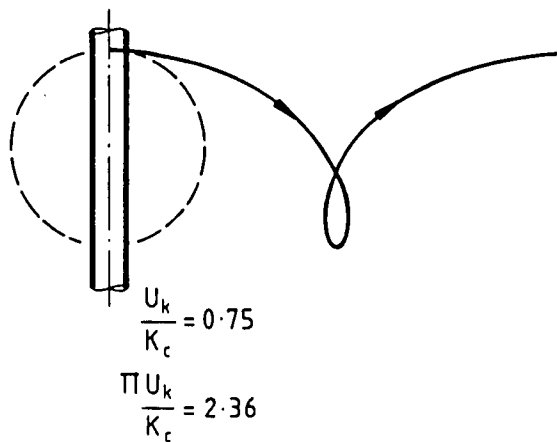
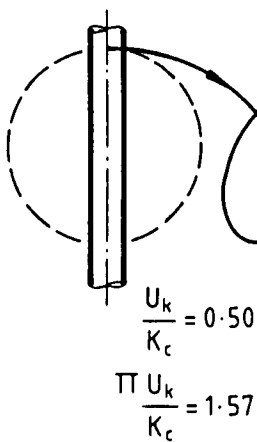
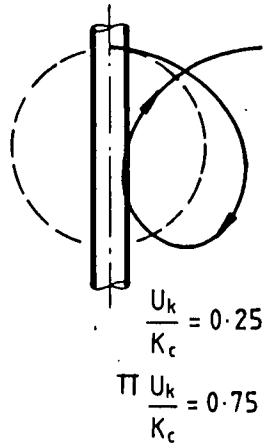
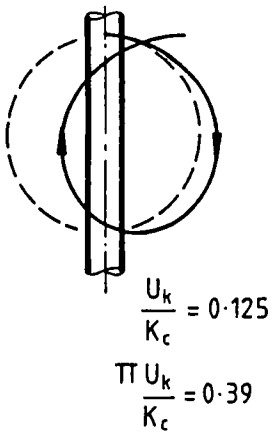
C_m = inertia coefficient

Bishop (1980) has defined an equivalent parameter K_c^* for random waves where the above definitions are not applicable.

e. Current

Current affects the values of C_d and C_m , especially at low values of K_c . The direction of the current relative to the orbit plane and the member is important, as shown in Figures 3.2.3 and 3.2.4 for members in the orbit plane.

Wave &
Current
Direction →



$$\frac{U_k}{K_c} = \frac{\text{CURRENT VELOCITY}}{\text{MAX WAVE PARTICLE VELOCITY}} = \frac{U_c}{U_{wm}}$$

$$K_c = \frac{U_{wm} T}{D}$$

$$\pi \frac{U_k}{K_c} = \frac{\text{CURRENT MOVEMENT / WAVE CYCLE}}{\text{ORBIT DIAMETER}}$$

$$U_k = \frac{U_c T}{D}$$

Figure 3.2.3 Undisturbed particle paths in orbital flow, with current parallel to the wave

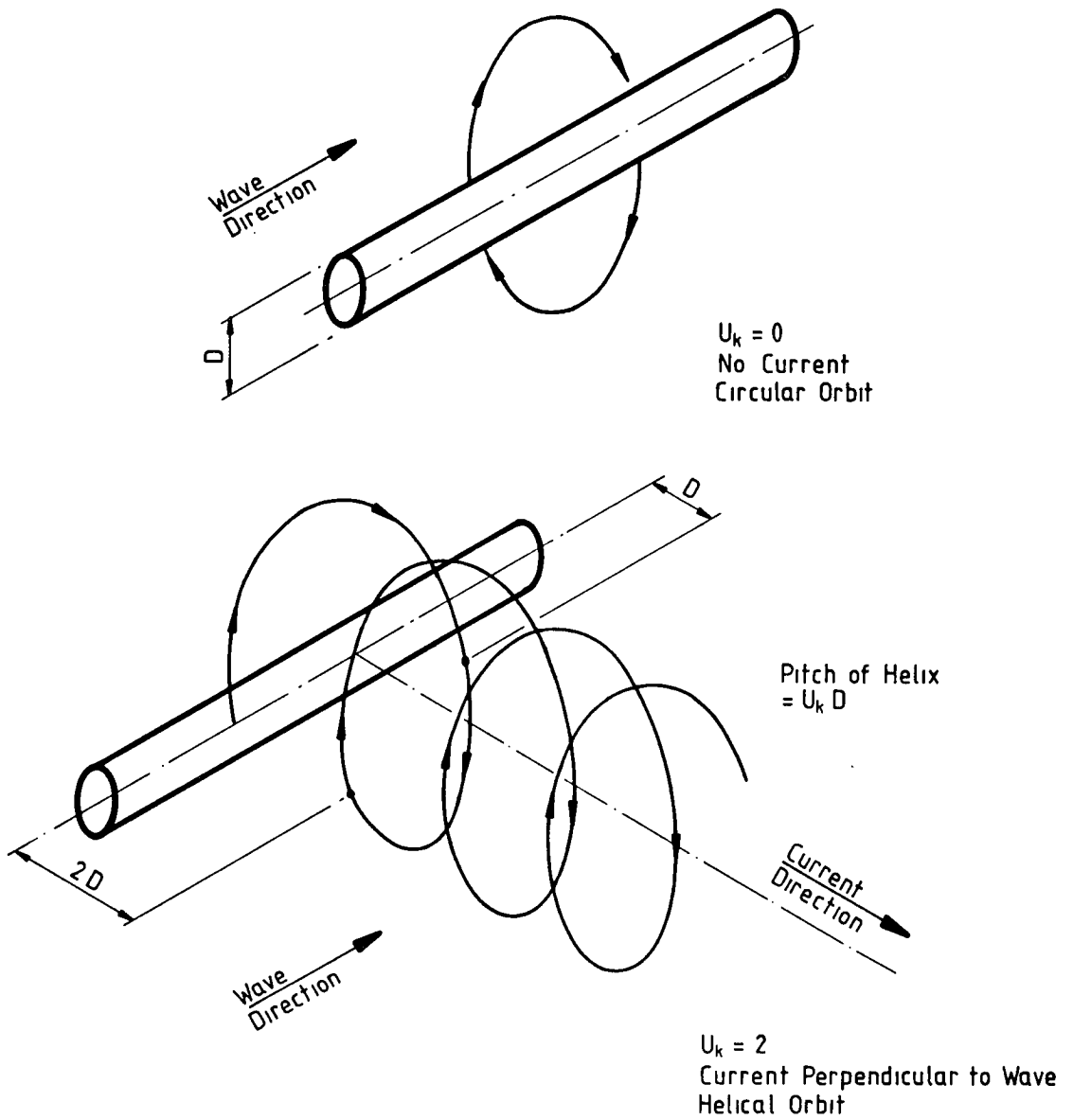


Figure 3.2.4. Undisturbed particle paths in orbital flow with current perpendicular to the waves

It is convenient with current in the presence of waves to calculate a non-dimensional current: U_k :

$$U_k = \frac{U_c T}{D}$$

Where:

U_c is the current velocity resolved normal to the cylinder T,D are as defined in Section 3.2.2 d.

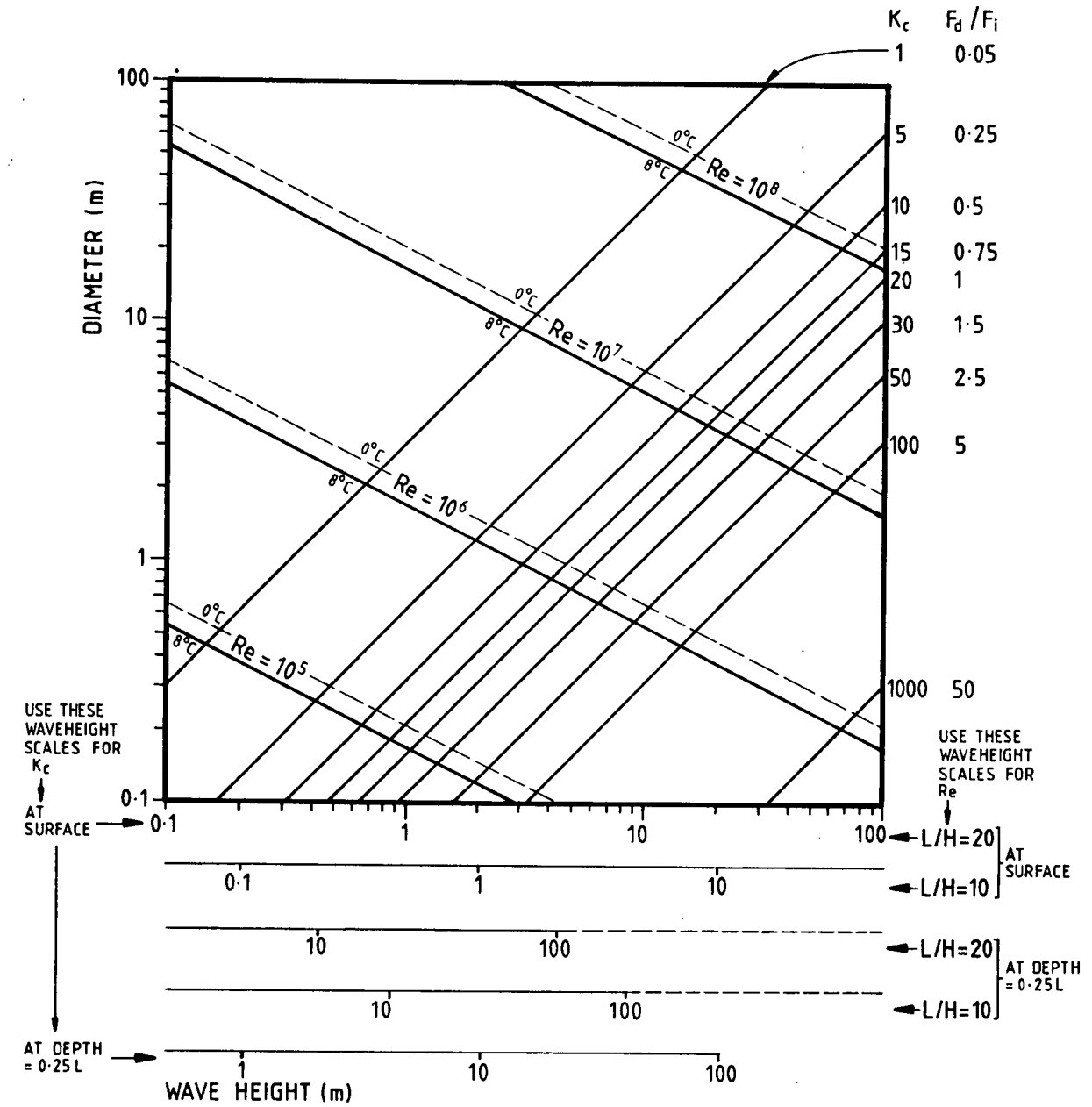
Typical values for R_θ and K_c in waves may be determined from Figure 3.2.5. The ratio of drag force to inertia force is given for a cylinder with $C_d = 1.0$ and $C_m = 2.0$.

Actual values of drag and inertia coefficient would, most conveniently, be obtained in laboratory experiments. However figure 3.2.5 shows that in order to obtain R_θ values greater than about 2×10^5 , which are necessary if the experimental flow is to be similar to the flow around the actual structure, it is necessary to use quite large cylinders in large waves. For example, in order to obtain $K_c = 30$ and post-supercritical conditions the minimum requirement would be a 0.25m cylinder in 2.5m, deep water, waves. In order to avoid using such large wave heights, and to simplify the problem, various researchers have carried out tests in simulated wave flows where the water oscillates in a U shaped tunnel or where the cylinder itself is made to move.

f. Total force coefficients

In order to compare the wave loading resulting from different C_d and C_m pairs it is convenient to use a single total force coefficient which, for a given member and wave, is proportional to the total drag and inertia force acting on the member.

$$C_f = \frac{((C_d K_c / \pi)^2 + C_m^2)^{0.5}}{((K_c / \pi)^2 + 1)^{0.5}}$$



- F_d / F_i = Drag Force/Inertia Force
- L/H = Wave Length/Wave Height = 10 or 20
- C_d = Drag Coefficient = 1
- C_m = Inertia Coefficient = 2
- Re = Reynolds Number = $U_{wm}D/\nu$
- K_c = Keulegan-Carpenter Number = $U_{wm}T/D$
- U_{wm} = $\pi H / T e^{2\pi z/L}$
- T = $(2\pi L/g)^{1/2}$

NOTES

- 1) Zero current is assumed.
- 2) The member is assumed to be perpendicular to the wave
 $U_m = U_{wm} = U_{wm}$
- 3) Effect of temperature on Re is shown for 0° and 8°C.

METHOD OF USE

Select horizontal scale according to whether Kc or Re is wanted and for required depth of member and wave steepness. The wave height then defines a vertical line and the cylinder diameter a horizontal line. The intersection point allows Kc or Re to be determined from the contours.

Figure 3.2.5. Reynolds number, Keulegan Carpenter number and ratio of drag force to inertia force for deepwater waves

This coefficient has the value of C_m at low K_c when C_m is dominant and C_d at high K_c when C_d is dominant. It is dependent on the flow conditions as represented by the Keulegan Carpenter number K_c described above. This coefficient is very similar to the total force coefficient C_f^* defined by Bishop (1980) for the case of random waves.

The coefficient C_f does not allow for the presence of a current. When the effect of a current is to be taken into account the following force coefficient has been used instead:-

$$C_{ft} = \frac{(C_d K_c / \pi^2) (U_k / K_c + \cos \theta)^2 + C_m \sin \theta}{(K_c / \pi^2) (U_k / K_c + \cos \theta)^2 + \sin \theta}$$

Where C_{ft} is evaluated at the value of phase angle θ : $0 < \theta < 2\pi$ corresponding to the maximum value of the numerator of the expression.

Both C_f and C_{ft} are approximations to the equal drag and inertia coefficients that would cause the same fluid loading as the actual C_d, C_m pair.

However, C_f and C_{ft} are based on different assumptions and do not generally have the same values for the case of no current. C_f assumes a square root sum of squares addition of the drag and inertia loading whereas C_{ft} more closely follows the time history of the loading on a single member. We would anticipate C_f to be the best indicator for a structure with several members attracting wave loading but C_{ft} to be a better indicator for the loading on a single vertical member.

3.2.3 Marine growth and surface roughness

Offshore structures are roughened by corrosion and colonised by marine growth. Roughness and marine growth substantially increase the forces exerted by waves and currents.

This increase is caused by:-

- a) increased dimensions of the member, which should be taken into account by the use of larger D and A values in Morison's equation

- b) increased surface roughness caused by, for instance, rust, barnacles and mussels
- c) entrainment of water, e.g. by kelp.

Surface roughness is defined here in terms of k/D as shown in Figure 3.2.6. Some researchers define D as the diameter of the cylinder excluding the marine growth and others include all the marine growth.

Values of surface roughness may be approximately 0.1mm for poorly painted, galvanised or very lightly rusted surfaces and about 25mm for hard marine growth such as barnacles and mussels. For cylinder diameters in the range 0.5m to 5m the relative roughness k/D could therefore be in the range 1/50,000 to 1/20 although the range of practical interest is probably 1/1000 to 1/20. Soft marine growth may be compact, e.g. sea anemones, or long, e.g. kelp. Very little research has been performed on the effect that soft marine growth has on hydrodynamic loading. In practice marine growth does not grow evenly on members of offshore structures. This also affects loading. Wolfram and Theophanatos (1985) describe some relevant characteristics of marine growth.

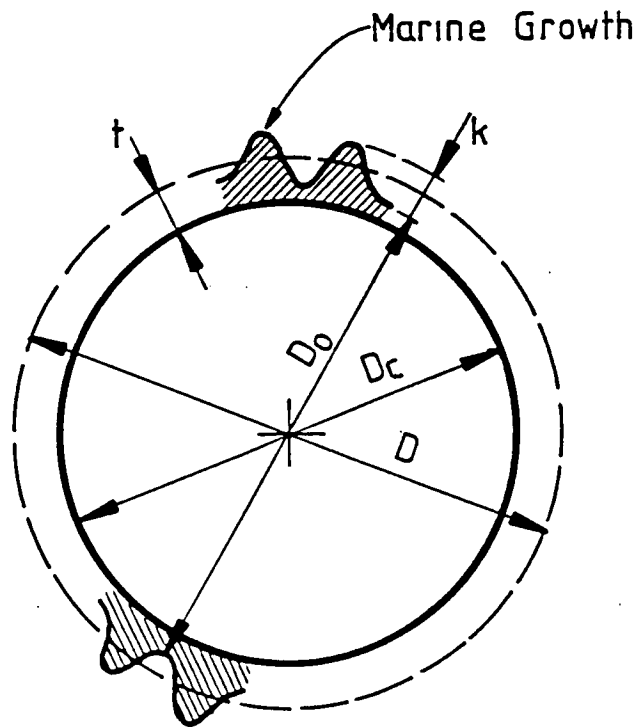
Surface roughness also changes the Reynolds number at which the transition from subcritical, through critical to supercritical flow occurs. The effect is shown in Figure 3.2.8 for steady flow and in Figures 3.2.15 and 3.2.16 for oscillating flow.

3.2.4 Steady flow

a. Smooth cylinders

The drag coefficient of a long smooth cylinder for steady flow has been determined using wind tunnels, by many researchers, e.g. Delany and Sorensen (1953). Figure 3.2.7 shows the dependence of C_d on Reynolds number and, in conjunction with Table 3.2.2, shows the various flow types which are characteristic of various ranges of Reynolds number (R_e).

The value of R_e corresponding to the minimum value of C_d reduces (ESDU, 1981) if there is any turbulence in the incident flow or any surface roughness because the boundary layer becomes turbulent at a lower velocity. For design purposes it is therefore difficult to benefit from the lowest C_d values in the critical range of R_e .



D_c = cylinder diameter
 $D_o = D_c - k + 2t$
 D = mean diameter of cylinder and marine growth
 t = mean marine growth thickness
 k = mean roughness height
 $A = \pi D^2/4$ = mean cross sectional area
 A and D are used in Morison's equation in this report

Figure 3.2.6 Marine roughness definition

Table 3.2.2 – The characteristics of steady flow past a smooth cylinder at various Reynolds number

Reynolds number range	Flow velocity for 1m diameter smooth cylinder at 8°C	Flow characteristic
<u>Subcritical flow</u>		
1. 0.5	3mm/hour	'Streamlined' flow around the cylinder with no vortices formed. The drag force is mainly 'skin friction' and is proportional to the flow velocity
2. 2-30	10-150mm/hour	Two vortices form in the 'wake' behind the cylinder but they are not shed downstream. At the higher flow velocities they oscillate from side to side
3. 40-2x10 ⁵	200mm/hour – 0.3m/sec	Vortices are shed alternately from each side of the cylinder at a frequency which is dependent on the flow velocity. The drag force is becoming proportional to velocity squared as it is now dominated by the reduced pressure in the wake
<u>Critical flow</u>		
4. 3x10 ⁵	0.43m/sec at 8°C (0.55 m/sec at 0°C)	The flow in the boundary layer around the front of the cylinder has been laminar but at this stage it becomes turbulent. This has the effect of reducing the width of the wake and reducing the drag force on the cylinder. Vortices are now shed randomly and not at a particular frequency
<u>Supercritical flow</u>		
5. 4x10 ⁵ -4x10 ⁶	0.6-6m/sec	The width of the wake and the drag coefficient increase slightly
<u>Post-supercritical flow</u>		
6. >4x10 ⁶	6m/sec at 8°C (7m/sec at 0°C)	The width of the wake and drag coefficient remain constant. The drag force is now proportional to velocity squared. Regular vortex shedding is re-established

Note: The flow is modified by turbulence in the incident flow and by surface roughness

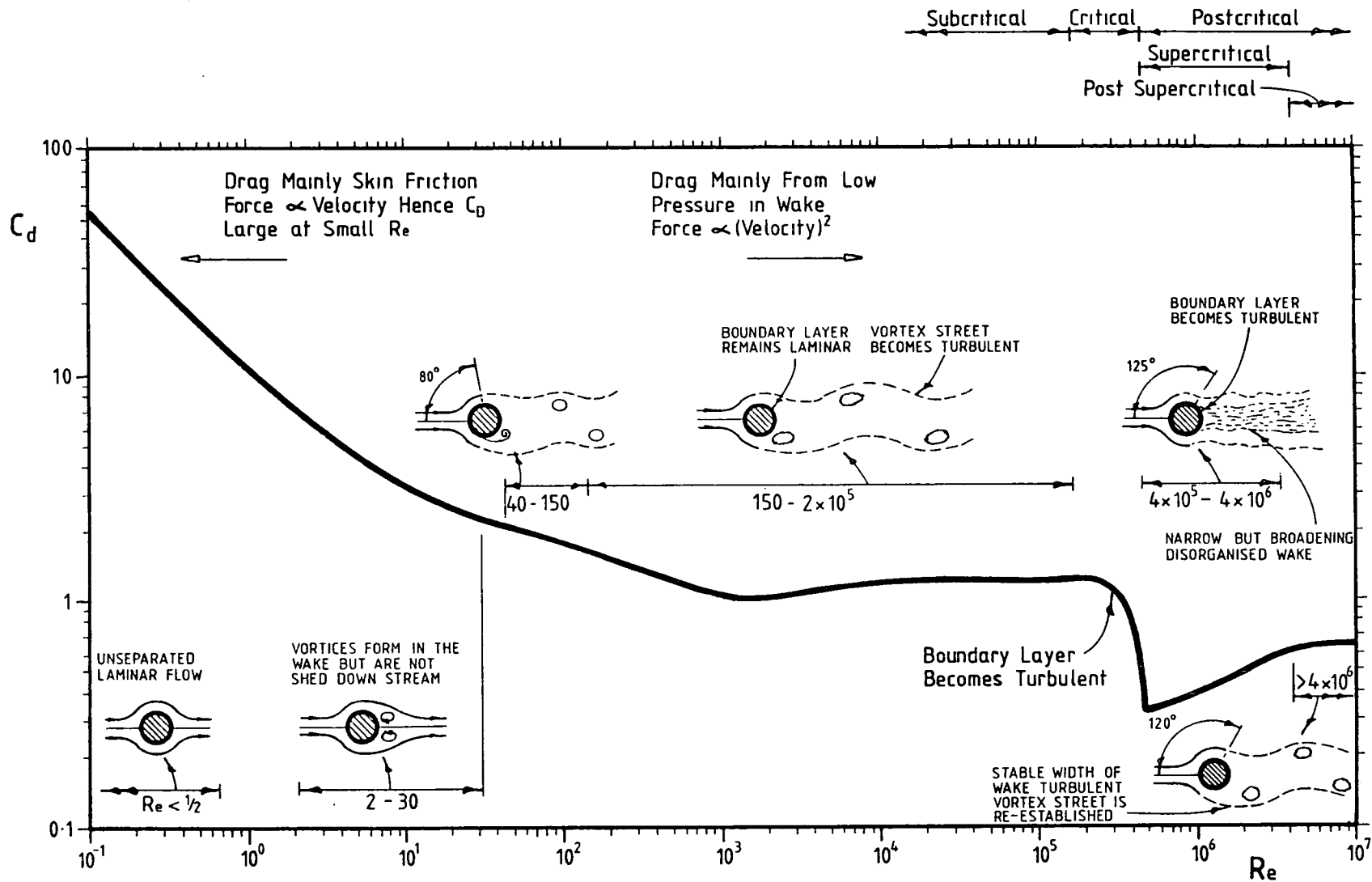


Figure 3.2.7. The effect of Reynolds number on flow characteristics and drag coefficients for a smooth cylinder in steady flow

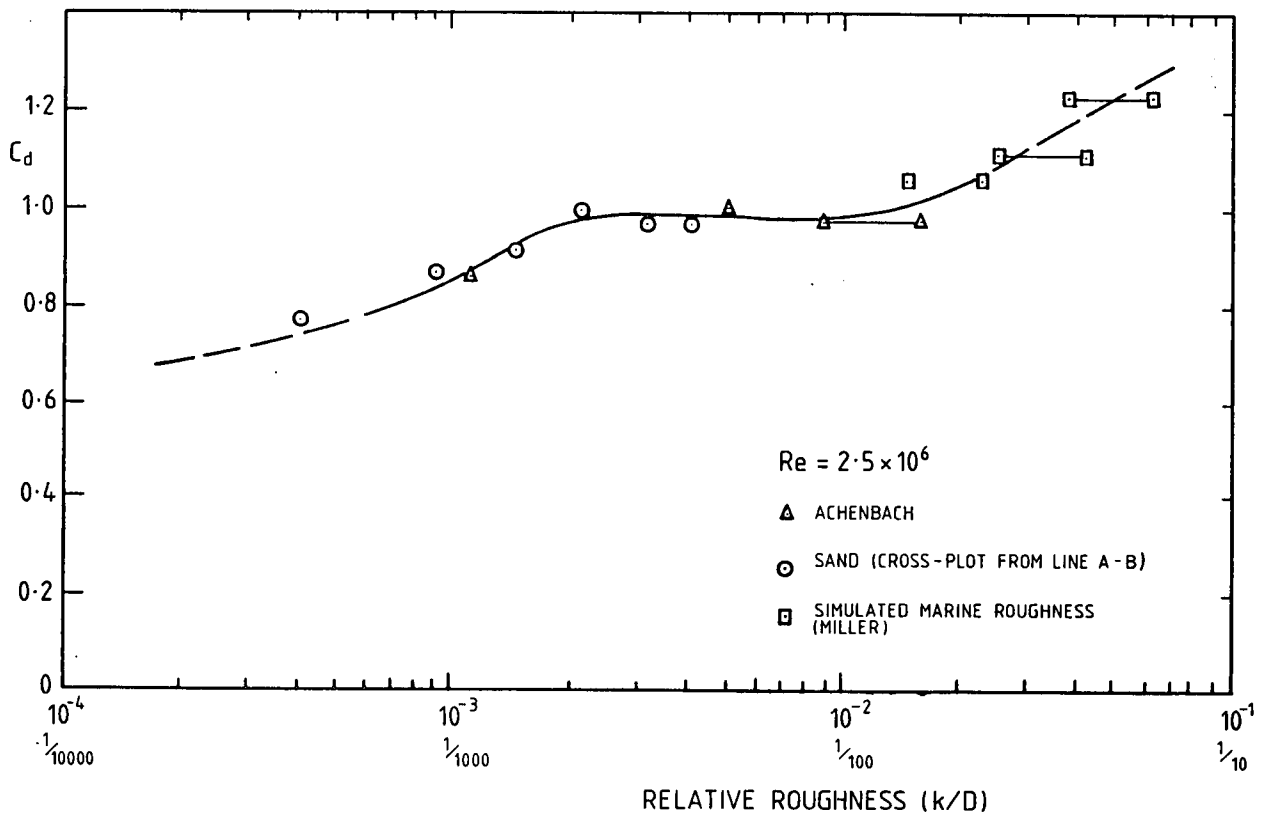
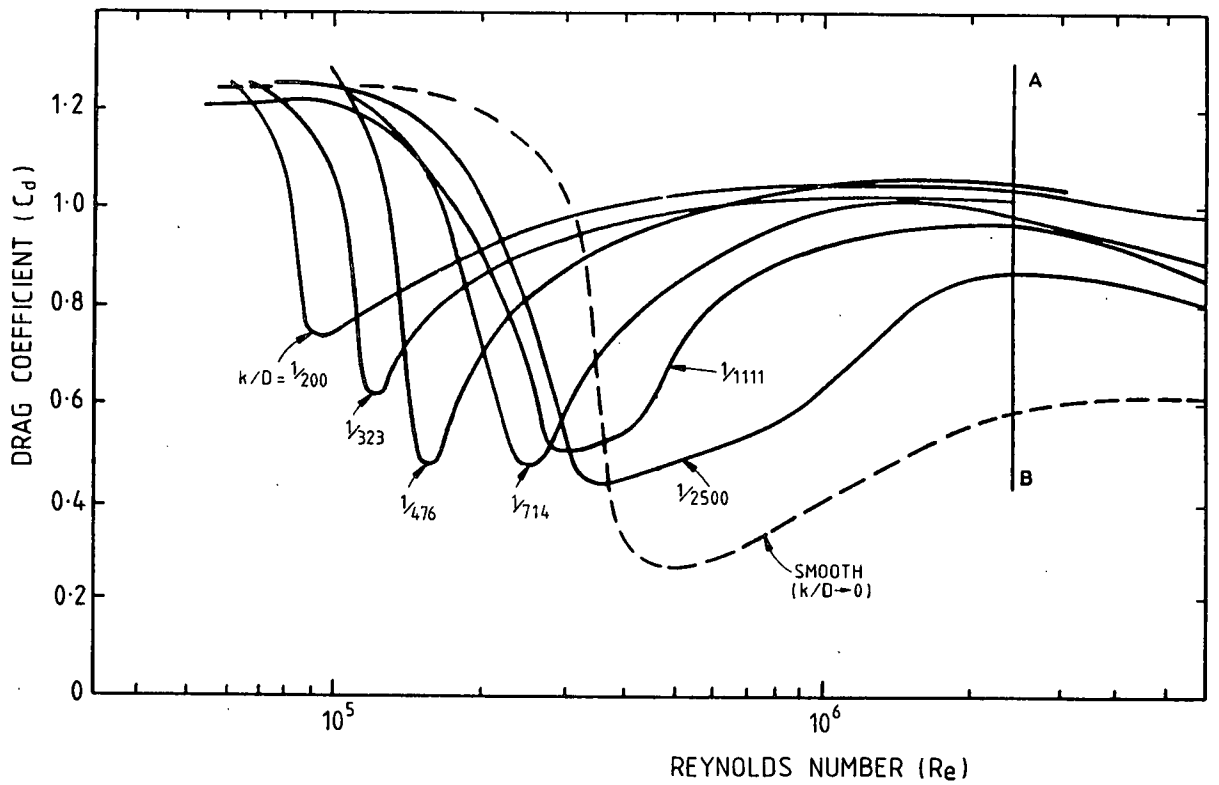


Figure 3.2.8. The influence of roughness height and Reynolds number on the drag coefficient for steady flow (Miller, 1976)

b. Rough cylinders

Roughness increases C_d as shown in Figure 3.2.8, from tests in wind tunnels (Miller, 1976). Miller uses the roughness parameter k/D_o (see Figure 3.2.6). Similar results have been obtained by Achenbach (1971) and Guven et al (1975) and by Lloyds Register of Shipping (see Appendix P). Miller also compared the drag on a barnacle encrusted cylinder (with flexible growths removed) and the drag with an artificial roughness (pearl barley) of similar k/D_m . Similar C_d values were obtained. For the post critical flow conditions and roughnesses likely to be found on offshore structures Miller's steady flow C_d value is in the range 0.85 to 1.25.

Wolfram and Theophanatos (1985) measured C_d values of cylinders, with various types of marine growth using instrumented cylinders floating to the surface under the effect of their own buoyancy. After an initial acceleration approximately steady post critical flow conditions are achieved. These results were originally presented in terms of D_c , are shown in Table 3.2.3 after adjusting, both the roughness parameter and C_d to be consistent with D , the mean equivalent diameter including marine growth as given by Wolfram and Theophanatos. C_d values of about 1.3 were obtained for both mussels and kelp. C_d values of about 1.0 were obtained for sea squirts, anemones and for cylinders with a mixture of barnacles, soft seaweed and very small mussels. The irregularity of the roughness does not allow the k or D to be defined very precisely.

The findings of various pieces of research on the effects of surface roughness are compared in Section 3.2.10 h and are plotted in figure 3.2.55.

c. Inclination

The effect of cylinder inclination to a steady flow has been investigated for example, by Bursnall & Loftin (1951), Chiu (1966), Hanson (1966), Novak (1975) and Norton, Heideman and Mallard (1981).

These investigations have generally confirmed the crossflow or independence principle (Hoerner, 1965). This states that the normal pressure force is independent of any component of the incident velocity which is parallel to the axis of the member. However, the transition from subcritical to post-supercritical flow is more closely related to the Reynolds number of the total incident flow velocity than the Reynolds number of

Table 3.2.3 - Values of C_d for steady flow and C_m for accelerating flow, Wolfram and Theophanatos, 1985

Nature of marine growth	Details	D_o	D	k	k/D	k/D	C_d	C_m
Clean, smooth		200	200	-	-	-	-	2.08
Clean, smooth		400	400	-	-	-	0.49	2.14
Clean, roughened		200	200	0.4	.002	1/500	0.83	2.22
Clean, roughened		400	400	0.4	.001	1/1000	0.78	2.17
0.5m long kelp - 100% cover	Effective diameter found by wrapping	400	500	-	-	-	1.34	2.27
1.0m long kelp - 100% cover	the kelp around the cylinders	400	520	-	-	-	1.30	2.26
Single layer of mussels - 100% cover	Mussels glued in place	400	455	27	.059	1/17	1.05	2.02
Multiple layers of mussels - 100% cover	Natural covering of 1-6 layers of mussels	200	285	42	.147	1/7	1.30	1.74
Multiple layers of mussels - 50% cover	Reduced cover was obtained by removing	200	242	42	.173	1/6	1.39	2.09
Multiple layers of mussels - 25% cover	mussels	200	221	42	.179	1/5	1.41	2.28
Sea anemones and squirts	Sea anemones and sea squirts covered	315	365	40	.127	1/8	0.94	1.87
- top and bottom covered	70% of cylinder. Average size 30-50mm.	315	365	40	.127	1/8	1.17	1.80
- sides covered	Remainder covered by barnacles and soft fouling							
Naturally grown fouling								
- leading edge covered	Barnacles, soft seaweed and clumps of	315	339	24	.071	1/14	0.96	1.87
- trailing edge covered	small mussels.	315	339	24	.071	1/14	1.03	1.85
Naturally grown fouling	Barnacles 24mm high							
- leading edge covered		400	424	24	.057	1/18	1.04	1.95
- trailing edge covered		400	424	24	.057	1/18	0.87	1.94

Notes:

1. The C_d and C_m values are based on the mean diameter D whereas in the original paper the values were based on D_c
2. The C_m value given above is the inertia coefficient. In the original paper C_m is the added mass coefficient

the component resolved normal to the cylinder. Also the low value of C_d in the critical flow region, see Figure 3.2.7, increases with inclination until at about 45° the C_d value changes directly from about 1.2 to 0.6 (Bursnall and Loftin, 1951).

3.2.5 Accelerating flow

The inertia force on a cylinder in an inviscid, irrotational, accelerating flow may be calculated from potential flow theory. This results in a C_m of 2.0.

Sarpkaya and Garrison (1963) measured the forces on a cylinder in a flow accelerated uniformly from zero velocity. C_d and C_m were found to be close to 0 and 2.0 as the flow started to accelerate. After the fluid had displaced by about 3 cylinder diameters the drag and inertia coefficients had (fluctuating) values of about 1.25.

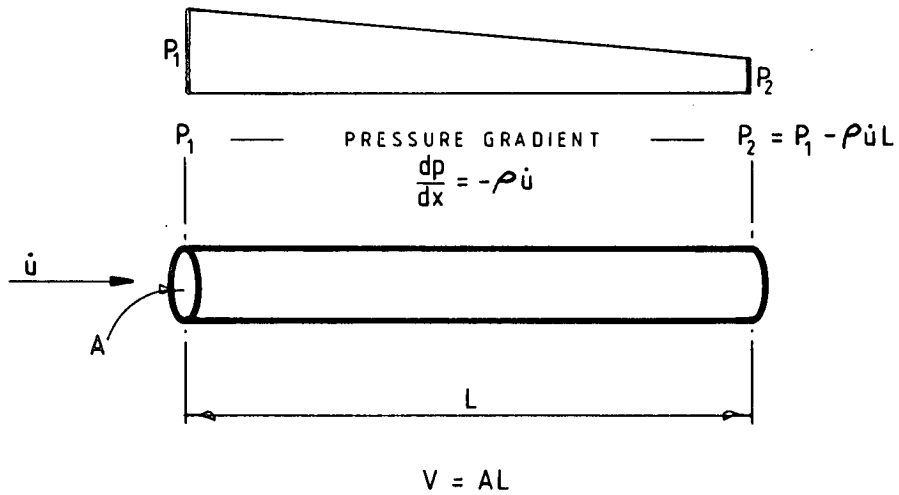
Wolfram and Theophanatos (1985) also estimated C_a (and hence $C_m = 1 + C_a$) (see Section 3.1.3) from the experiments with cylinders described in Section 3.2.4. C_m values corresponding to the initial acceleration are given in Table 3.2.3.

Most types of marine growth resulted in slightly lower C_m values than a smooth cylinder. The kelp value was based on an equivalent cylinder area obtained by wrapping the kelp around the cylinder and measuring the circumference.

The effect of inclination on the inertia force in uniformly accelerating flow is most easily understood by separating the force into the Froude Krylov and added mass components (see Section 3.1.3).

The total Froude Krylov Force $\rho V \dot{U}$ behaves very much like a buoyancy force which acts in the direction of the fluid acceleration. It is independent of the orientation of the member. However, the pressure acting on any part of the member is dependent on the orientation of the member as shown by Figure 3.2.9. For a general orientation of the member the acceleration may be resolved parallel and transverse to the member and the pressures from the two components added.

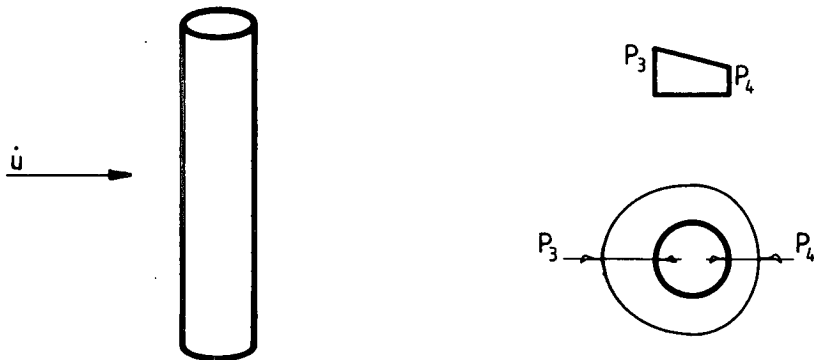
The independence principle (see Section 3.2.4) therefore applies to the transverse Froude Krylov force on the member. However there is also a Froude Krylov force in the axial direction. This axial force is not usually taken into account in jacket design, but exists



Total Froude Krylov force on the member is the difference between the forces acting on the ends : the radial Froude Krylov pressures balance and cause no contribution to the total force :

$$F = P A - (P - \rho \dot{u} L) A = \rho \dot{u} L A = \rho \dot{u} V$$

a) AXIAL ACCELERATION



The total Froude Krylov force is again $\rho \dot{u} V$ although this is now the resultant of a varying pressure applied around the curved face of the cylinder. The forces on the ends of the cylinder are equal and opposite.

b) TRANSVERSE ACCELERATION

Figure 3.2.9. Froude Krylov forces acting on a cylinder from axial and transverse components of acceleration

for a brace member framing into chords, as well as for the case of the isolated member. The effect of ignoring the force is estimated, for a simple example structure, in Appendix I. The error was found to be small: 11% of the inertia force. It is therefore just reasonable to ignore this force.

The added mass forces can also be considered in the parallel and transverse to member directions. However, the added mass parallel to a member is small and may usually be ignored. The added mass force therefore obeys the independence principle as it is proportional to the transverse acceleration.

3.2.6 Planar oscillating flow

a. Smooth cylinders

The simplest type of wave flow, though only found near the sea bed in shallow water waves, is planar oscillating flow. This flow has been generated by Sarpkaya (1976 a,b) in the large U shaped tunnels shown in Figure 3.2.10. Using this apparatus it is possible to study drag and inertia forces at a wide range of R_e and K_c .

The independence principle (see Section 3.2.4) suggests that the flow parallel to the axis of a cylinder does not influence the loading normal to the member. This would suggest that the oscillating flow results should also be applicable to vertical cylinders in regular waves with elliptical orbits. However, experimental work, described in the following sections, has shown that until K_c reaches about 300 the oscillating flow measurements lead to higher forces than have been measured on structures in waves (Heideman and Sarpkaya, 1985). This may be caused by the re-encounter with the cylinders own wake which occurs repeatedly in Sarpkaya's tunnel but occurs less frequently in real seas because of the effects of currents and random waves.

The C_d and C_m results for smooth cylinders are shown in Figures 3.2.11 to 3.2.14. At R_e values less than 10^5 , lower than are relevant to offshore structures, the drag coefficient C_d is higher than the steady flow value and the inertia coefficient C_m lower than the potential flow value of 2. In the range of R_e and K_c that is most important for drag loading (R_e greater than 10^5 , K_c greater than 20) the value of C_d is between 0.6 and 0.7. This is similar to the post-supercritical steady flow value of 0.68. The inertia loading is most important at lower values of K_c . Figure 3.2.11 shows a C_m value of about 1.75 for $K_c = 20$ and R_e greater than 10^5 . C_m values for lower K_c at high R_e are not available from the experiments. However extrapolation of the

APPROXIMATE DIMENSIONS OF TUNNELS (METRES)				
TUNNEL	L	H	w	h
1	9.1	4.9	0.9	0.9
2	10.7	6.7	0.9	1.4

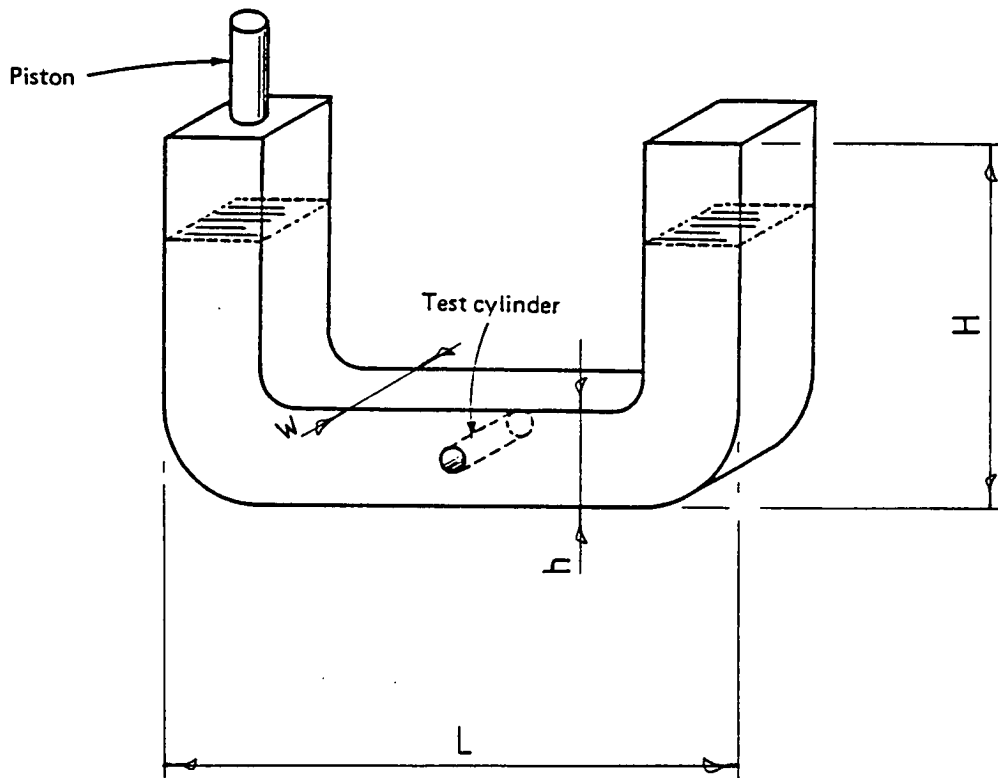


Figure 3.2.10. Diagram of the oscillating flow U tunnels used by Sarpkaya (1976a)

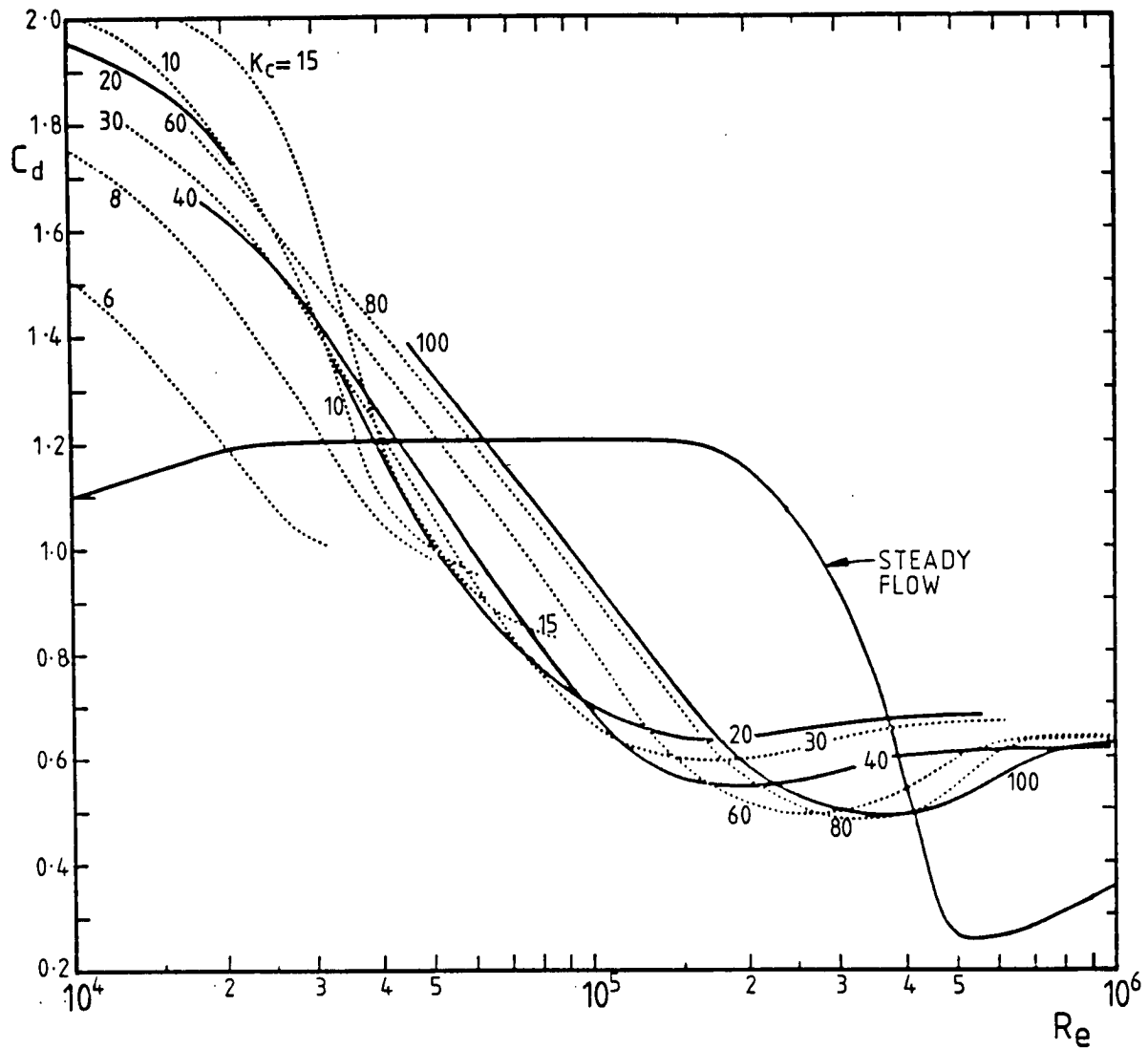


Figure 3.2.11. Smooth cylinder C_d versus Re for various values of Re in oscillating flow (Sarpkaya 1976a)

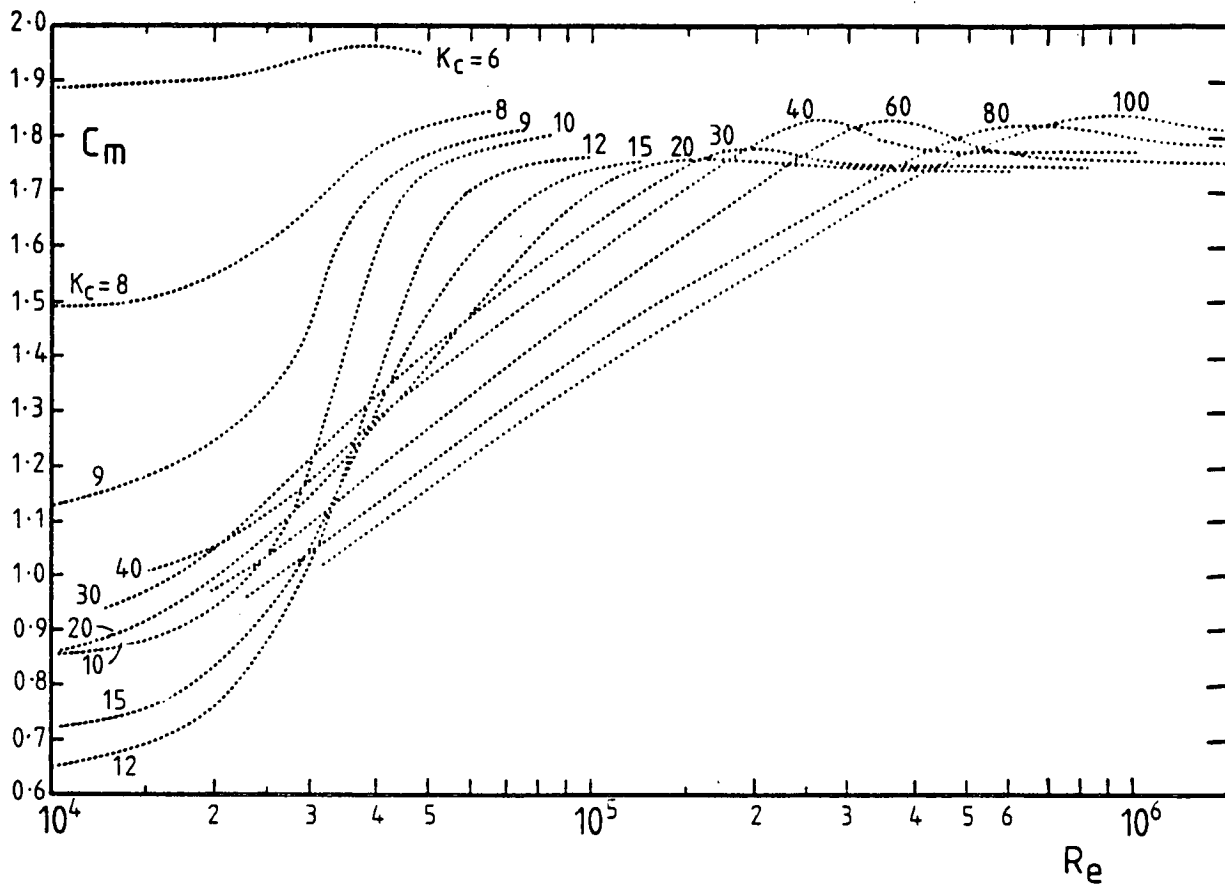


Figure 3.2.12. Smooth cylinder C_m versus Re for various values of K_c in oscillating flow (Sarpkaya 1976a)

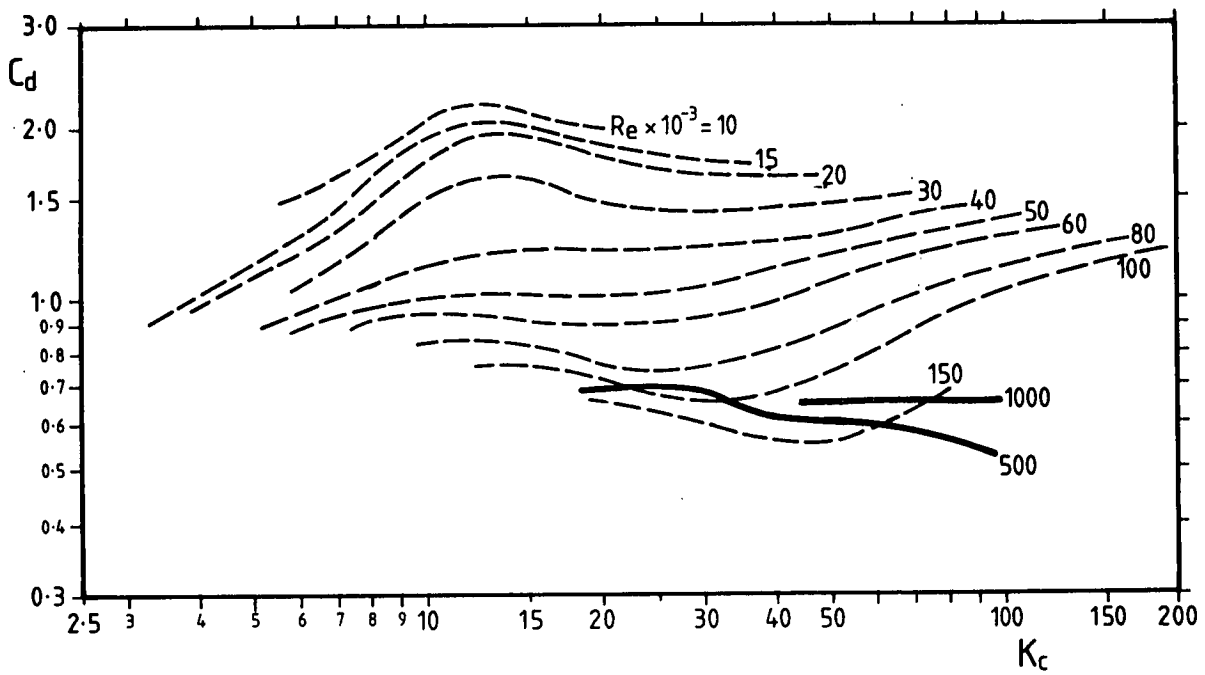


Figure 3.2.13. Smooth cylinder C_d versus K_c for various values of Re in oscillating flow (Sarpkaya, 1976a)

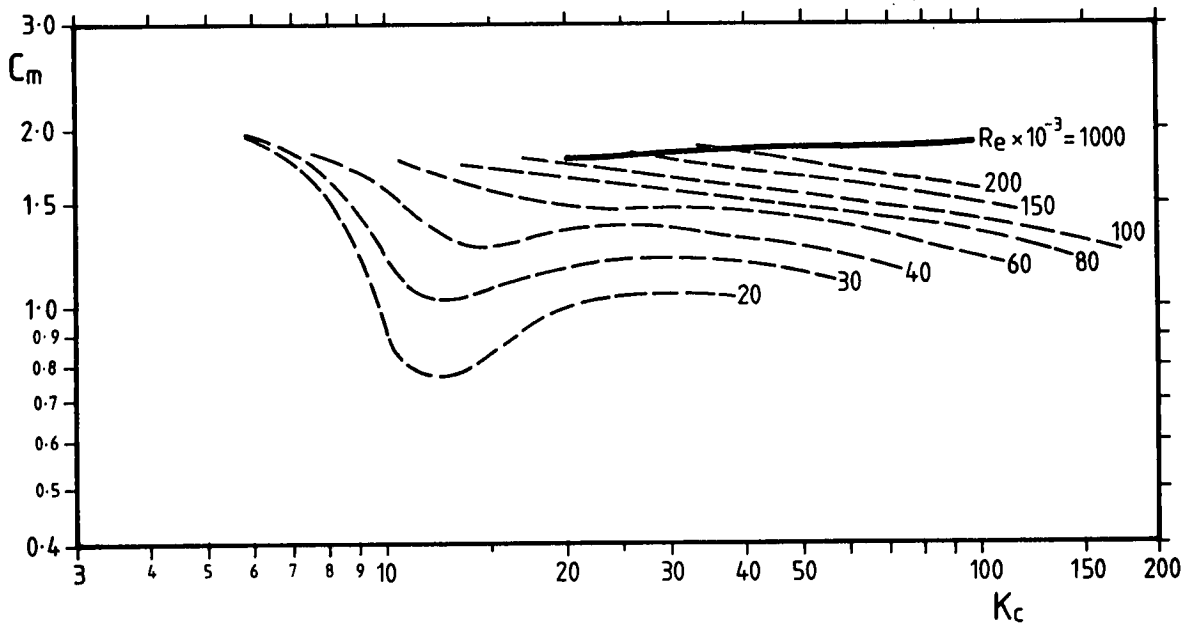


Figure 3.2.14. Smooth cylinder C_m versus K_c for various values of Re in oscillating flow (Sarpkaya, 1976a)

results in Figures 3.2.12 and 3.2.14 suggest that C_m may be in the range 1.75 to 2.0 for these conditions. Further comparison of the steady flow results, with Sarpkaya's (1976a) oscillating flow results, shows that the lowest C_d values in the critical flow regime occur at an R_e of about 2×10^5 in oscillating flow but at the higher R_e of about 5×10^5 in steady flow.

b. Rough cylinders

To examine the effect of roughness in oscillating flow Sarpkaya (1976a, b) carried out a series of experiments with sand-roughened cylinders in the tunnel. His C_d and C_m results are shown in Figures 3.2.15 and 3.2.16 for $K_c = 20$ and $K_c = 100$ as a function of R_e . Each curve on each plot corresponds to a particular relative roughness. The variation of C_d , C_m and C_f with K_c for post critical flow conditions is shown in Figures 3.2.17 to 3.2.19.

Qualitatively, the effect of hard roughness on the oscillating flow C_d value is similar to the effect on the steady flow C_d value: a small amount of roughness significantly increases C_d in post critical flow conditions. However the smooth cylinder, post - supercritical C_d values are similar in steady flow and oscillating flow but the rough cylinder C_d values are significantly higher in oscillating flow than in steady flow as shown by Table 3.2.4

c. Planar oscillating flow with current

The effect of a current parallel to and superimposed on planar oscillating flow has been simulated, by translating cylinders in oscillating flow, in the U tunnel apparatus (Sarpkaya and Storm, 1985). Some results, showing the variation of C_d and C_m with current and K_c , are shown in Figures 3.2.20 and 3.2.21. Note however that the data is mainly in the critical range of R_e and that the changes in C_d and C_m may be caused partly by the change in R_e when current is added.

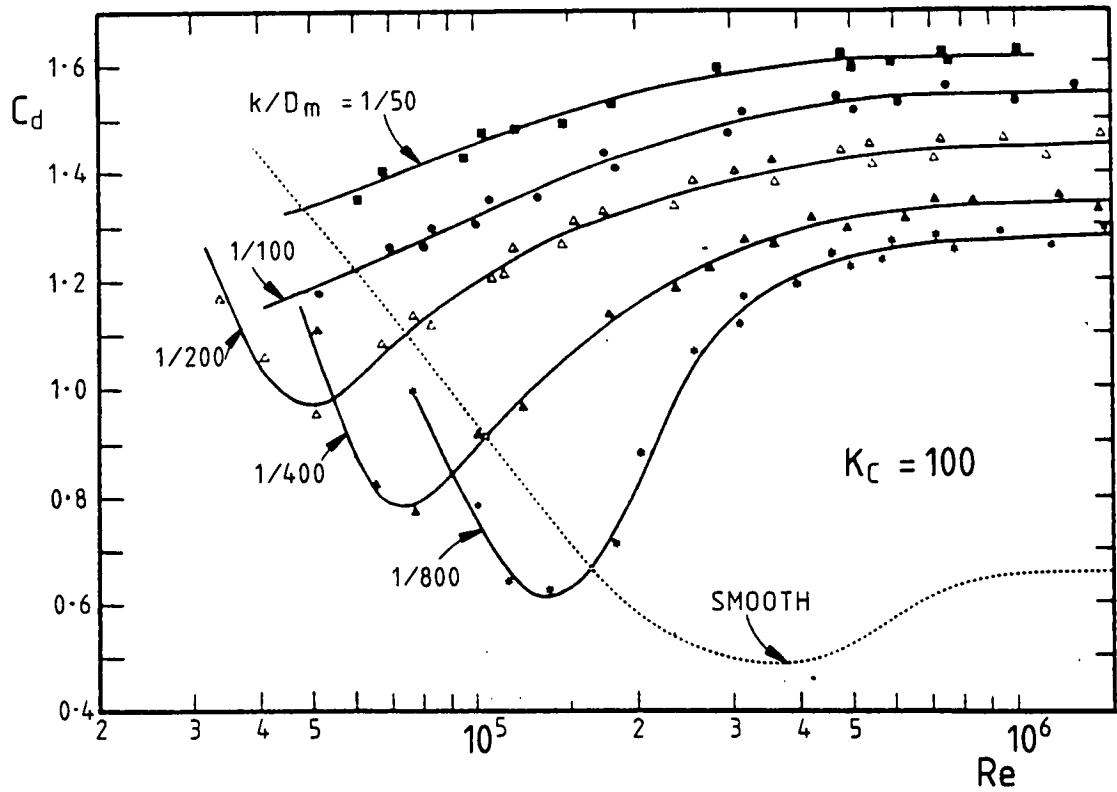
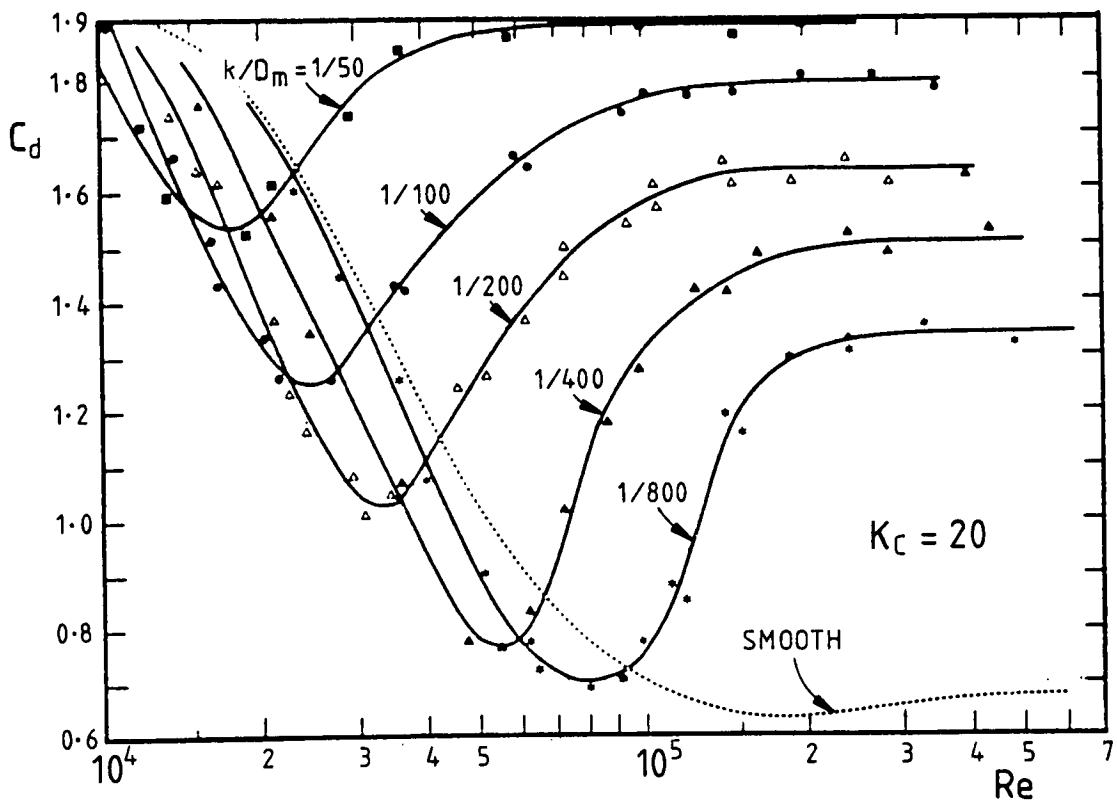


Figure 3.2.15. Rough cylinder C_d versus Re for $K_c = 20$ and $K_c = 100$ in oscillating flow (Sarpkaya, 1976a)

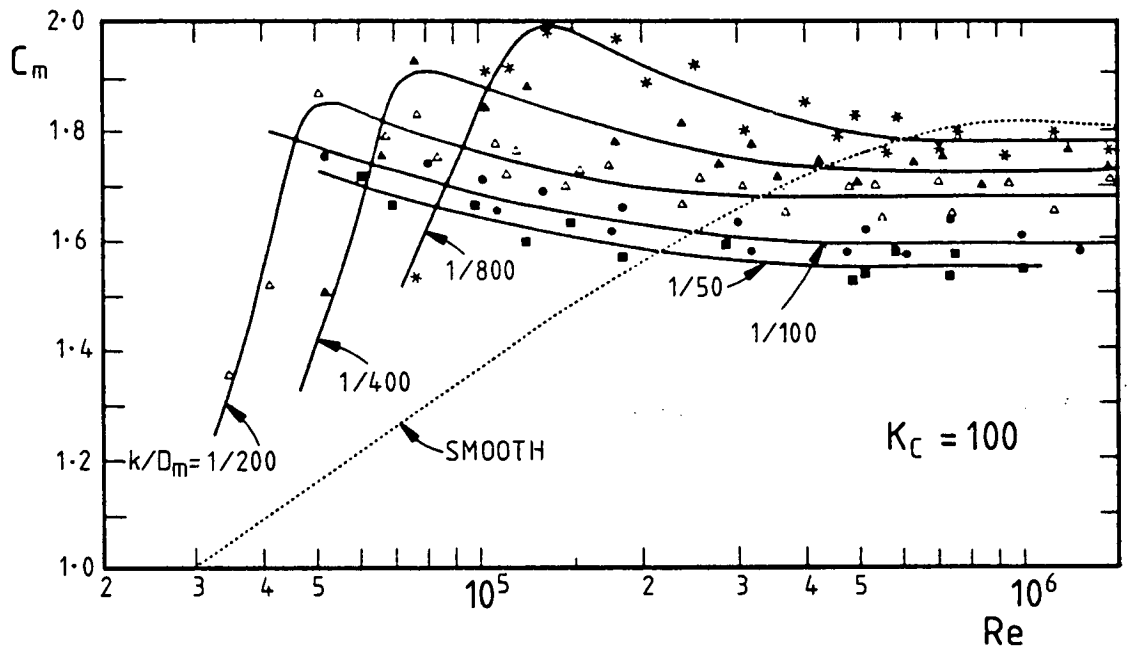
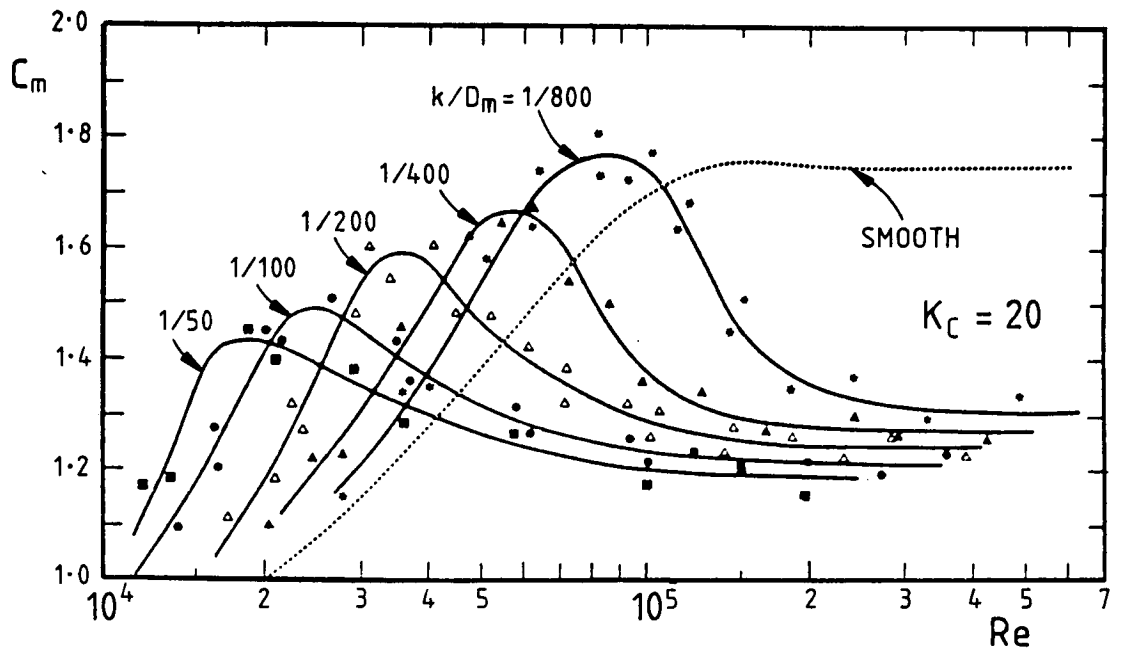


Figure 3.2.16. Rough cylinder C_m versus Re for $K_c = 20$ and $K_c = 100$ in oscillating flow (Sarpkaya, 1976b)

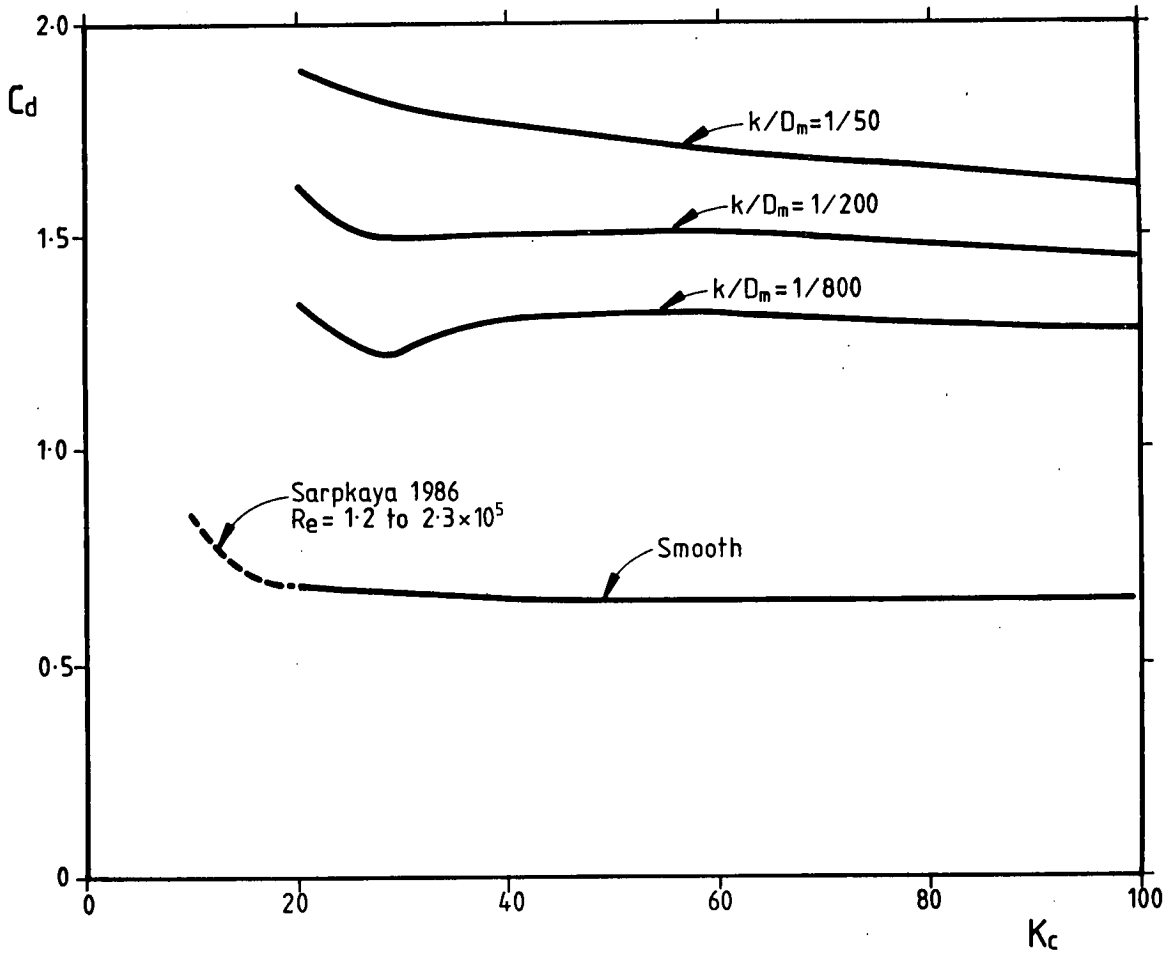


Figure 3.2.17. C_d versus K_c for post critical oscillating flow
 (Based on Sarpkaya 1976a,b)

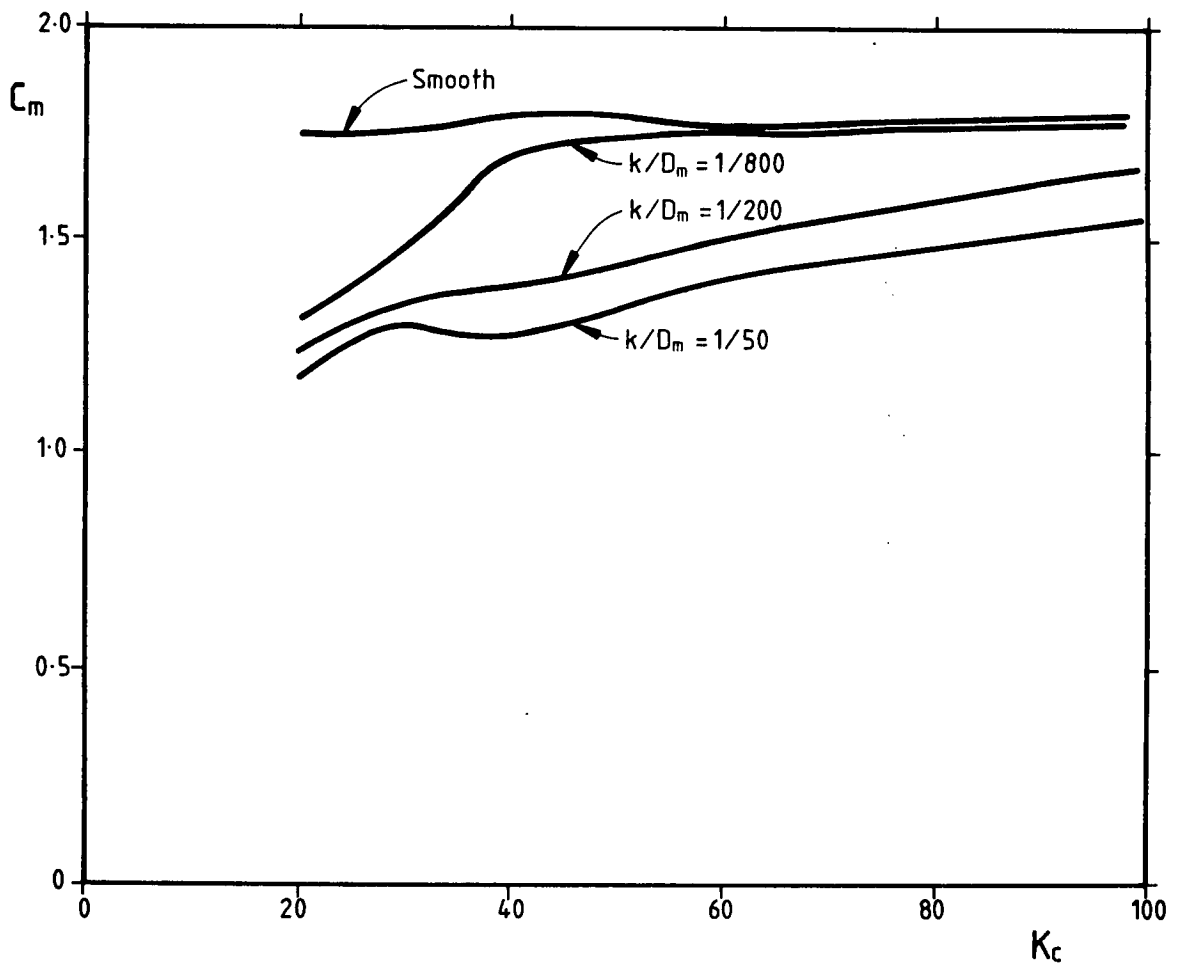


Figure 3.2.18. C_m versus K_c for post critical oscillating flow
 (Based on Sarpkaya 1976a,b)

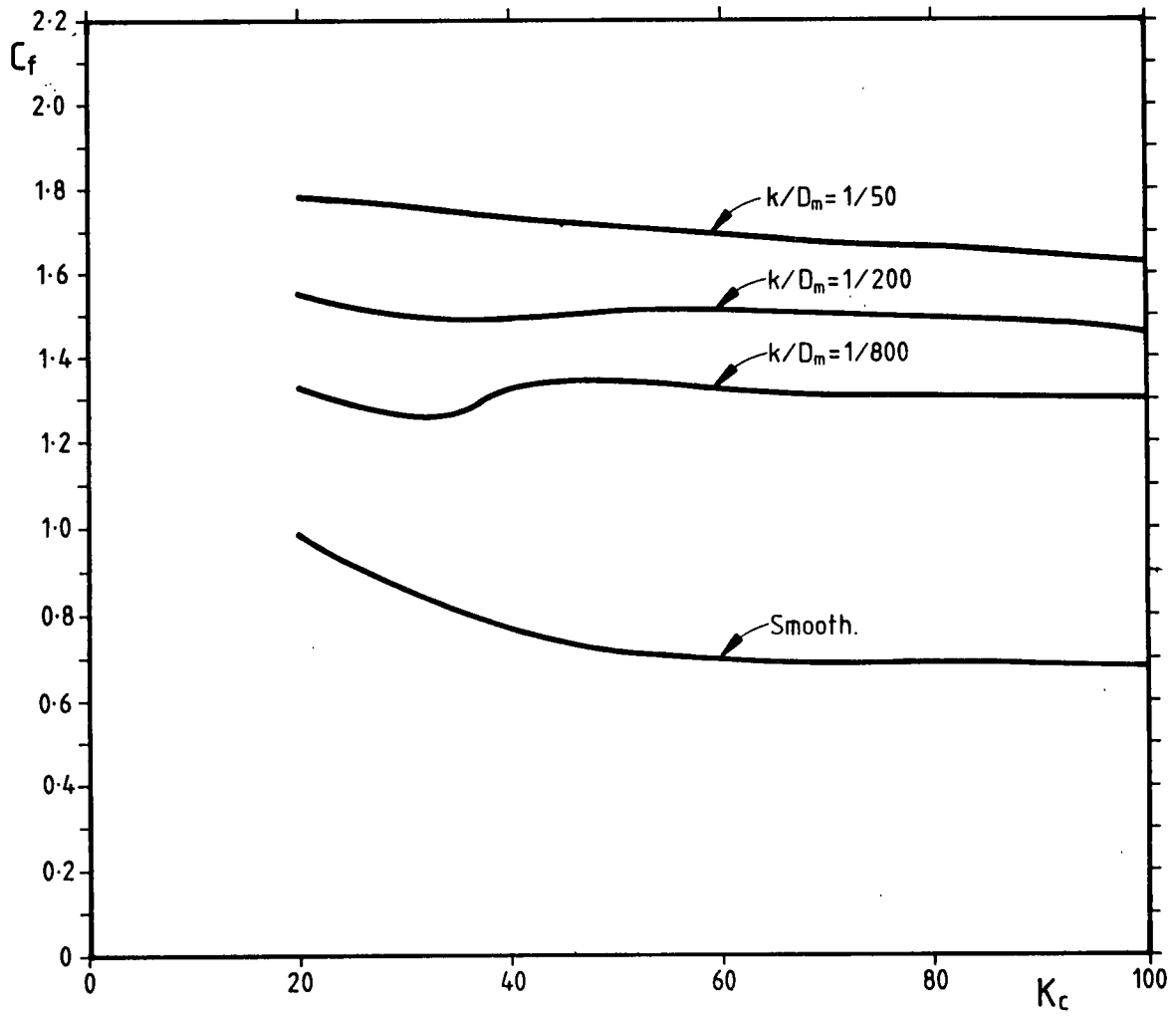


Figure 3.2.19. C_f versus K_c for post critical oscillation flow
 (Based on Sarpkaya 1976a,b)

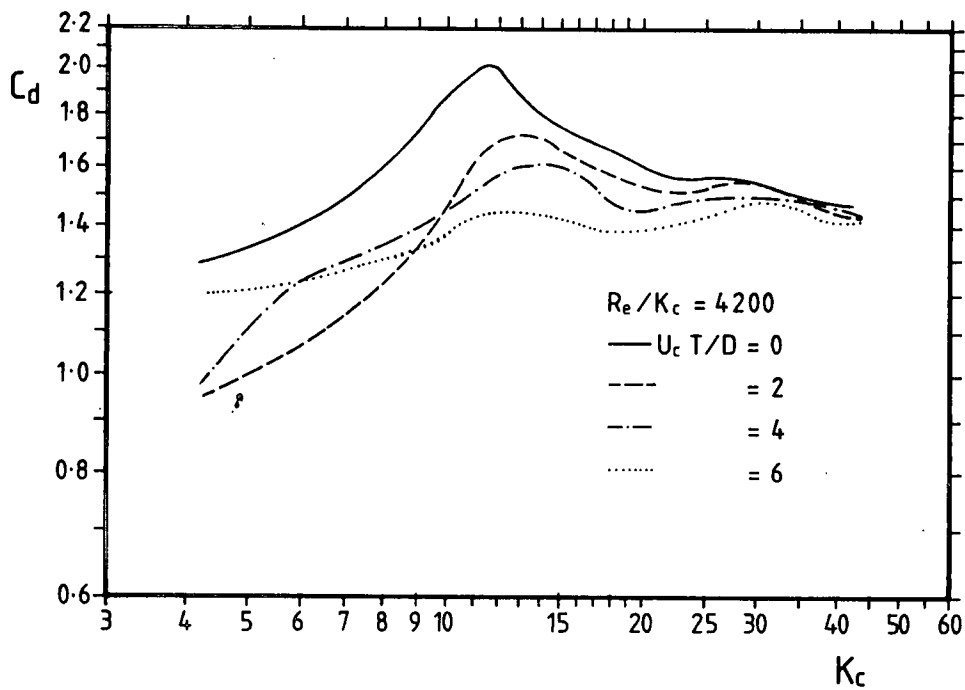


Figure 3.2.20. Rough cylinder C_d versus K_c for oscillating flow with current (Sarpkaya and Storm, 1985)

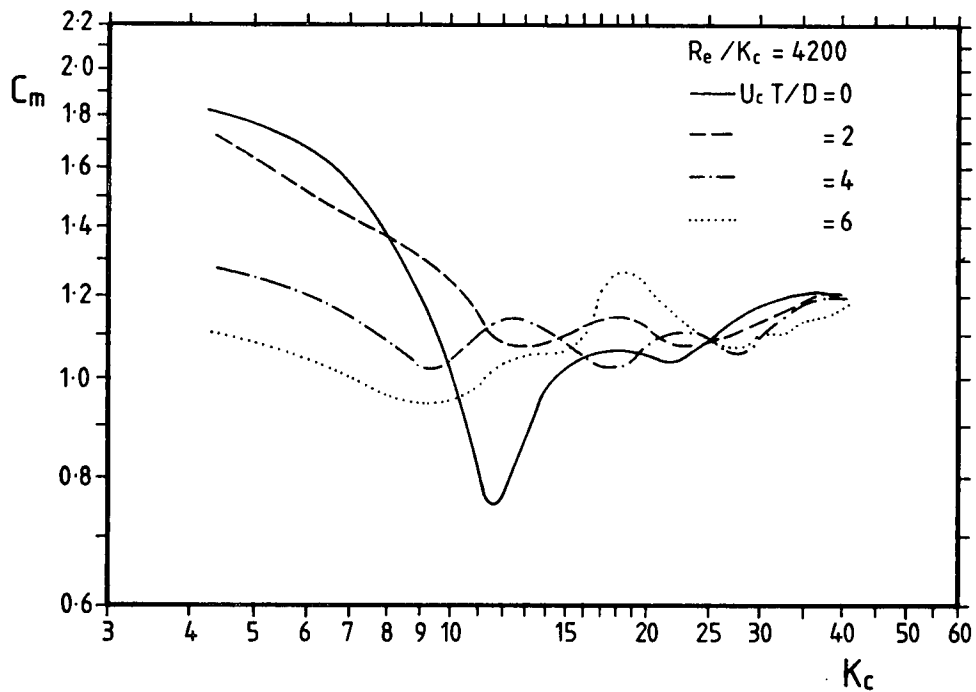


Figure 3.2.21. Rough cylinder C_m versus K_c for oscillating flow with current (Sarpkaya and Storm, 1985)

Table 3.2.4 - Comparison of C_d values in post-supercritical steady flow and oscillating flow

	steady flow C_d	Oscillating flow C_d	
	$R_e = 10^7$	$R_e = 10^6$ $K_c = 100$	$R_e = 3 \times 10^5$ $K_c = 20$
Smooth cylinder	0.68	0.65	0.68
Rough cylinder $k/D = 1/200$	1.00	1.45	1.62

Current reduced the value of C_d . For K_c greater than about 10 increasing K_c also reduces the value of C_d . Sarpkaya and Storm show that a value for C_d with current may be estimated from the C_d for no current at the effective K_c of $K_c + U_k$. (For definition of K_c and U_k see 3.2.2). In Appendix H comparison is made with an alternative method of estimating the effect of current on C_d .

C_m was also found to be dependent on current, particularly for K_c values of less than 20 where with no current C_m varies quite rapidly with K_c . As the current increases the C_m value becomes less dependent on K_c and tends to the C_m value corresponding to no current but high K_c .

d. Inclined cylinders in oscillating flow

The effect of cylinder inclination to oscillating flow ($R_e = 12,000$ to $160,000$ and $K_c = 3$ to 40) has been reported by Sarpkaya, Raines and Trytton (1982) and a correction was made by Garrison (1985). The independence principle was shown to work fairly well for inertia forces at the higher values of R_e and K_c considered.

3.2.7 Cylinders in Simulated waves

a. General

The difficulties of achieving high R_e in laboratory waves have led researchers to simulate wave flow by orbiting cylinders in initially stationary flow. The flow around a cylinder orbiting in a stationary fluid is similar to the orbital flow of a wave about a horizontal cylinder. However, the inertia force acting on the orbiting cylinder is only the added mass force, described in 3.1. The Froude-Krylov force, which is associated with the acceleration of the flow, does not occur. This force can however be estimated and the inertia coefficient adjusted.

b. Holmes and Chaplin

Chaplin (1985b) (also Chaplin 1981, 1985a and Holmes and Chaplin, 1978) performed experiments in which a smooth cylinder was driven around an elliptical path in a tank of water. The ellipticity: E of the path was varied from 0 (planar oscillating flow) to 1 (circular orbital flow corresponding to a horizontal cylinder parallel to the crest of a deep water wave). K_c values were in the range 6 to 20 and R_e 7×10^4 to 2.2×10^5 .

For planar oscillatory flow values of C_d and C_m were similar to those obtained by Sarpkaya in his U tunnel, see Figures 3.2.22 and 3.2.23.

As the ellipticity of the flow was increased C_m was found to decrease, typically from about 1.8 at $E=0$ to about 1.0 or less at $E=0.9$. Chaplin has shown that this is consistent with a lift force, caused by the circulation of the flow relative to the cylinder, acting in the opposite direction to the inertia force. C_d also decreased as E increased but this was probably caused by the stirring effect of the cylinder rotating in the fluid.

c. Grass, Simons and Cavanagh

Grass, Simons and Cavanagh (1984) have also performed experiments in which a cylinder is oscillated or driven in an elliptical path in a tank of water. They obtained subcritical R_e of 2×10^3 to 2×10^4 and K_c between 10 and 30. They also found that C_d and C_m reduced as the ellipticity of the flow increased. They noted Chaplin's suggestion that this was caused by a potential flow lift force but make an alternative suggestion that

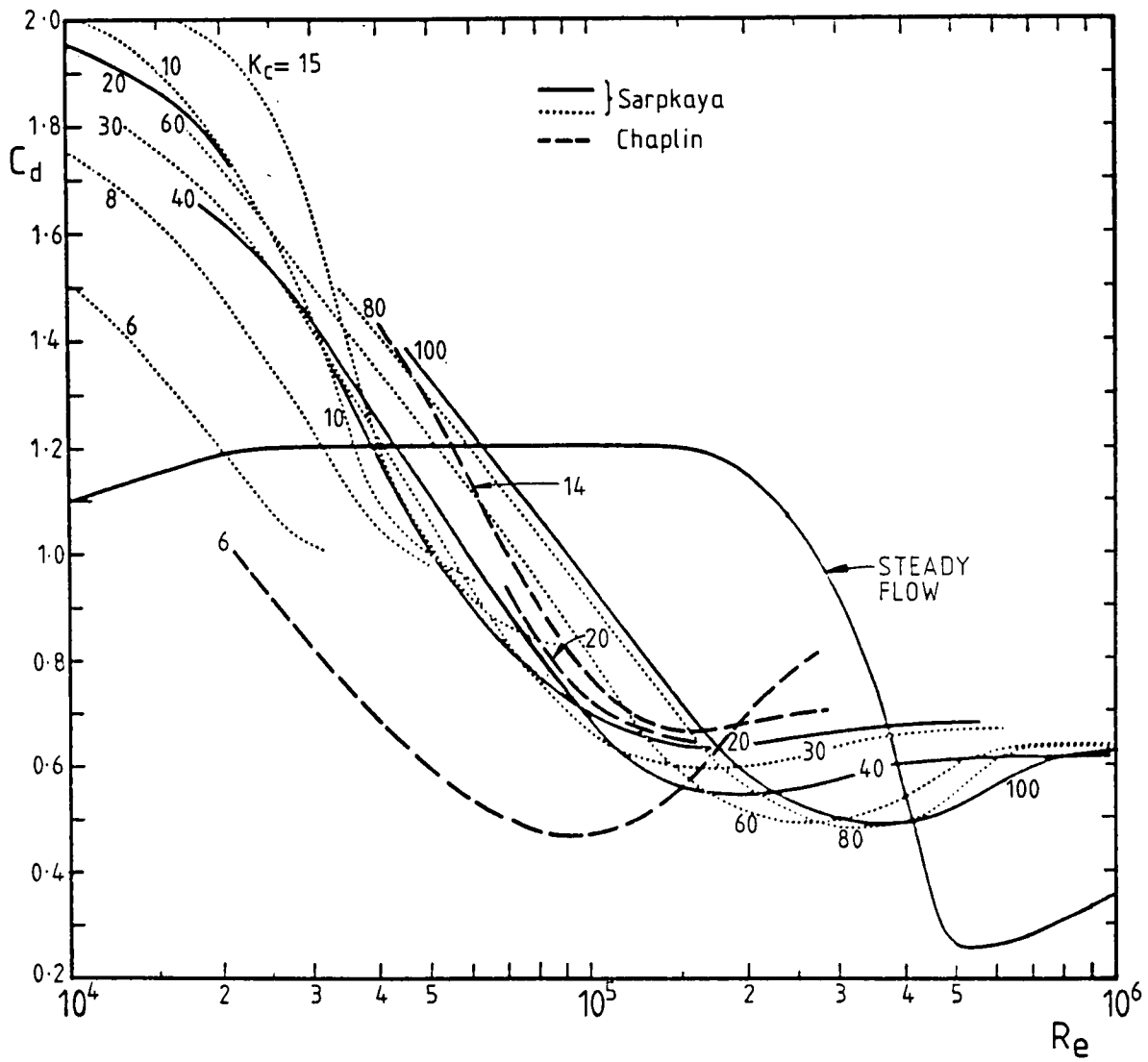


Figure 3.2.22. Smooth cylinder C_d versus Re for various values of K_C in oscillating flow (Sarpkaya, 1976a and Chaplin, 1985)

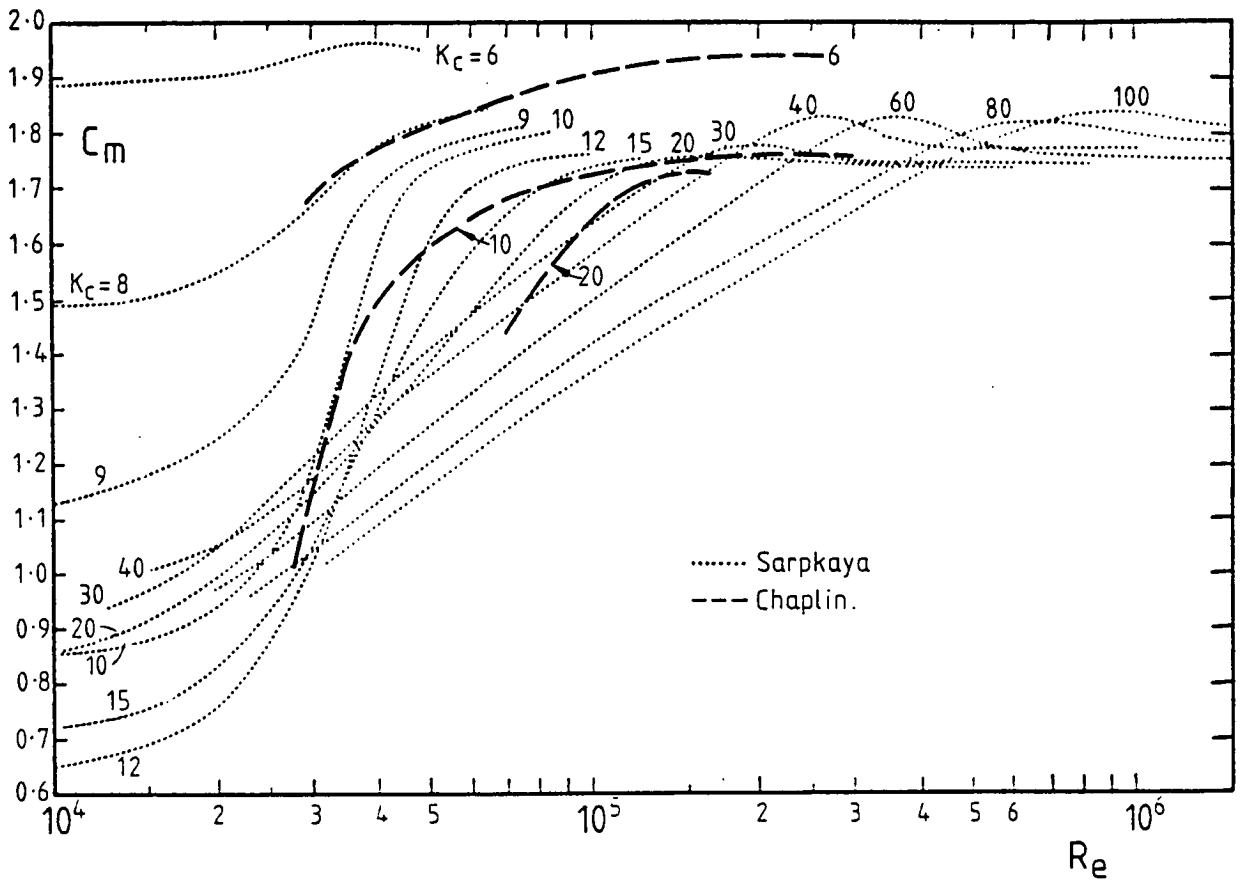


Figure 3.2.23. Smooth cylinder C_m versus Re for various values of K_c in oscillating flow. (Sarpkaya 1976a and Chaplin, 1985)

it is caused by the drag force being imperfectly in phase with the velocity of the cylinder, and cancelling part of the inertia force.

3.2.8 Laboratory waves

a. General

As already discussed it is difficult to achieve the post-supercritical Reynolds numbers for laboratory wave flows because of the size of cylinders and waves that are needed. This section contains the results of experiments which are not all in post-supercritical flows therefore some caution is needed in extrapolating those results to offshore structures. Nevertheless Bearman et al (1985), Gaston and Ohmart (1979) and Teng and Nath (1985) have achieved post-supercritical flows under laboratory conditions.

b. Bearman, Chaplin, Graham, Kostense, Hall and Klopman

Bearman et al (1985) conducted experiments in the large Delta flume at the Delft Hydraulics Laboratory. The cylinder was 0.5m in diameter and had a painted finish. Vertical and horizontal cylinders were studied in regular and irregular waves. R_g was in the range 1.46×10^5 to 5.05×10^5 and K_c ranged from 4 to 20. C_d and C_m were determined for regular waves. These are shown for the vertical cylinder in Figure 3.2.24, and for the horizontal cylinder in Figure 3.2.25. Bearman et al suggest that the increased scatter in the horizontal cylinder results is caused by lift forces as vortices are shed. The effect of ellipticity was studied to determine if the effect, found by Holmes and Chaplin (1978), of circulation lift forces could be identified. No effect was discernible in the measured data and it is suggested that this could be caused by slight currents and irregularities in the waves preventing re-encounter of the cylinder and its wake.

Total force coefficients were determined for both random and regular waves. These were plotted against K_c . There was good agreement between the total force coefficients for the two types of waves. The C_f values for regular waves are shown in Figures 3.2.26 and 3.2.27.

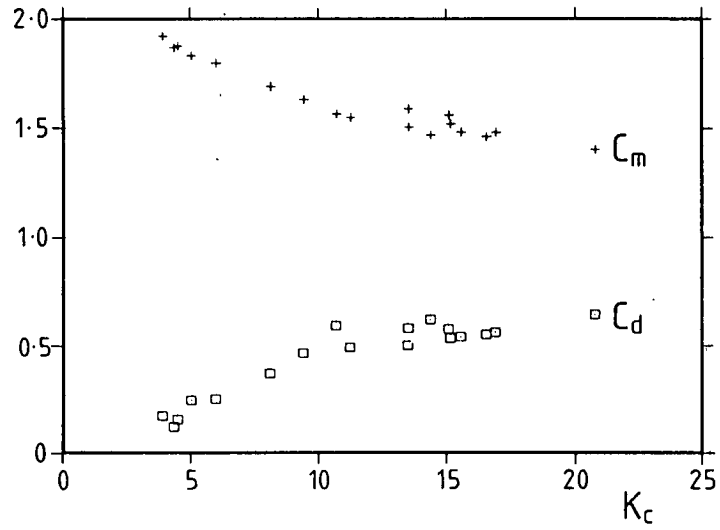


Figure 3.2.24. Smooth vertical cylinders C_d & C_m versus K_c post critical flow in waves (Bearman et al, 1985)

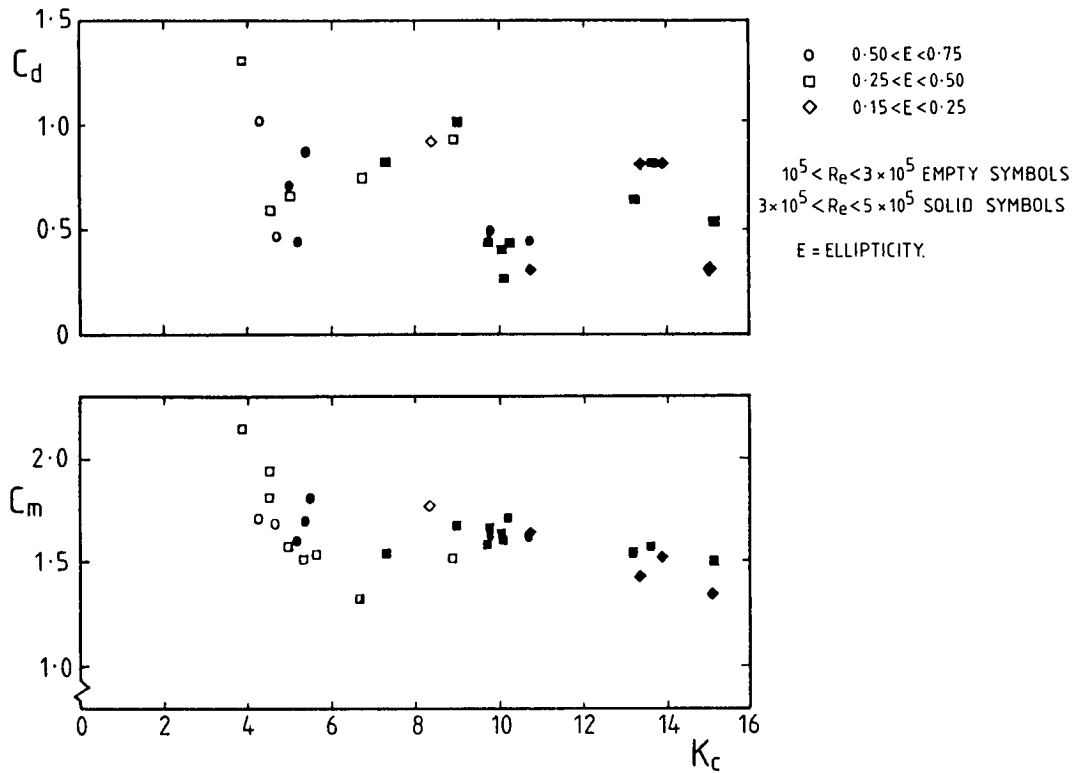


Figure 3.2.25. Smooth horizontal cylinder C_d and C_m versus K_c , post critical flow in waves (Bearman et al, 1985)

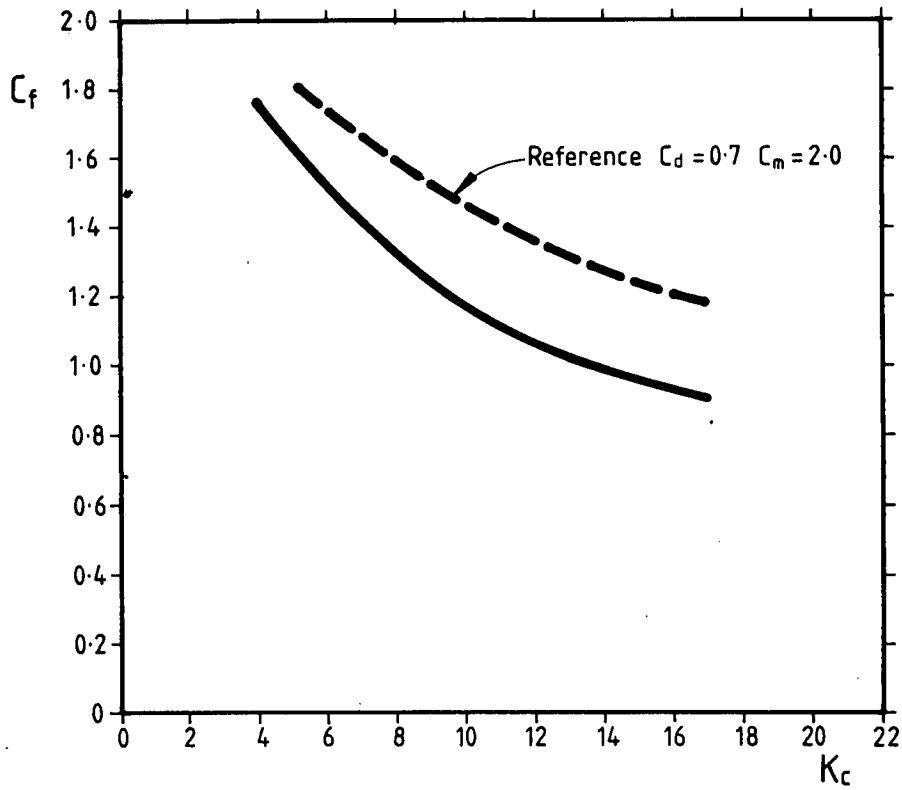


Figure 3.2.26. Smooth vertical cylinder C_f versus K_c , post critical flow in waves (Bearman et al, 1985)

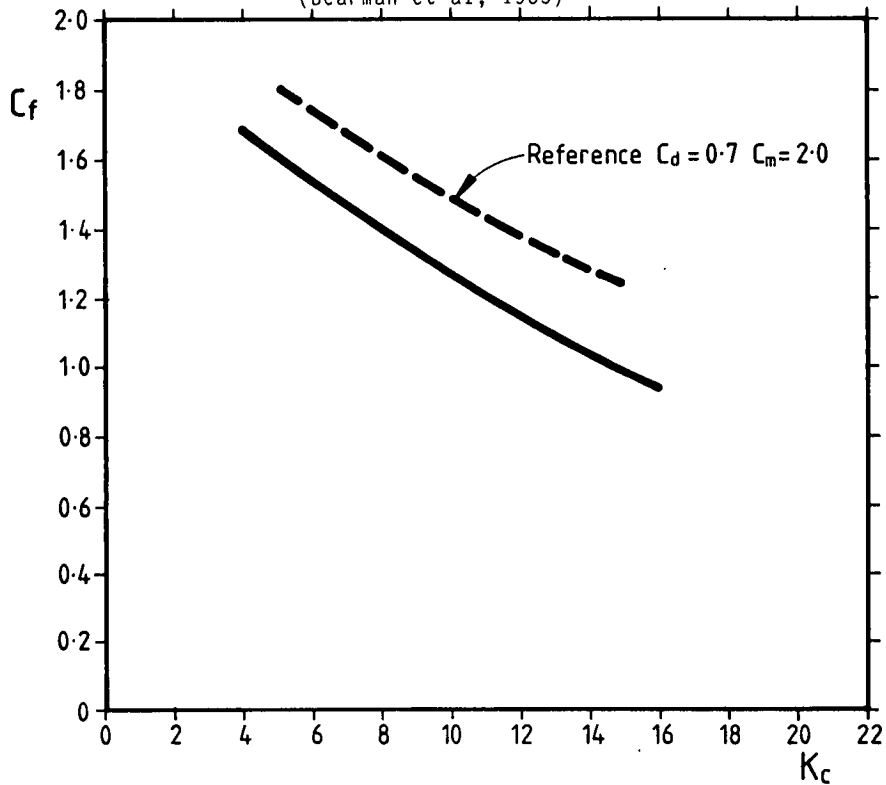


Figure 3.2.27. Smooth horizontal cylinder C_f versus K_c post critical flow in waves (Bearman Et Al, 1985)

c. Gaston and Ohmart

Gaston and Ohmart (1979) measured the total wave force and overturning moment on a smooth and roughened 4.3m long by 0.305m diameter vertical cylinder in a wave tank. Drag and inertia coefficient were determined (Table 3.2.5) using the measured in-line moment and particle kinematics. The wave height was 1.2m. The K_c at MWL would therefore have been about 12.5. Reynolds numbers, based on the rms water particle velocity at MWL, were from 2×10^5 to 3×10^5 . The change from the smooth to the rough surface $k/D = 1/99$ increased the drag coefficient by 70%. Further increase in surface roughness had a smaller effect. C_m decreased with roughness.

Table 3.2.5 - Values of C_d and C_m for rough vertical cylinders

k/D	C_d	C_m	C_f
0	0.77	1.81	1.27
1/99	1.30	1.76	1.49
1/34	1.35	1.81	1.54
1/25	1.34	1.80	1.54

$Re = 2 \times 10^5$ to 3×10^5 , $K_c = 12$ (Gaston and Ohmart, 1979)

Note: Original paper gives k/D , C_d and C_m based on the smooth cylinder diameter: D_c . The above results have been estimated allowing for the mean rough cylinder diameter: D (see Figure 3.2.6).

d. Pearcey, Singh, Cash and Matten

Pearcey (1979) and Pearcey et al (1985) measured C_d and C_m values for rough and smooth vertical and horizontal cylinders. The Re range was 2×10^4 to 9×10^4 and the K_c range 2 to 14. The flow conditions are almost certainly not post-supercritical, (Pearcey et al, 1986). However, the results may be relevant to cylinders at some depth see Figure 3.2.5).

The equipment used is shown in Figure 3.2.28 and the C_d and C_m values for the various cases are given in Figures 3.2.29 to 3.2.34.

The results show low values of C_m for horizontal cylinders which is consistent with Holmes and Chaplin (1978).

e. Teng and Nath

Teng and Nath (1985) obtained drag coefficients for smooth and rough horizontal cylinders. The results are shown in Figures 3.2.35 and 3.2.36. C_m was found to be approximately 1.0 for both the smooth and rough cylinders. The C_d values increased by about 80% with roughness.

Teng and Nath also towed smooth and rough horizontal cylinders through waves. They observed that the drag coefficient tended to the steady flow value as the towing velocity increased to that of the wave particle velocity.

f. Cotter and Chakrabarti

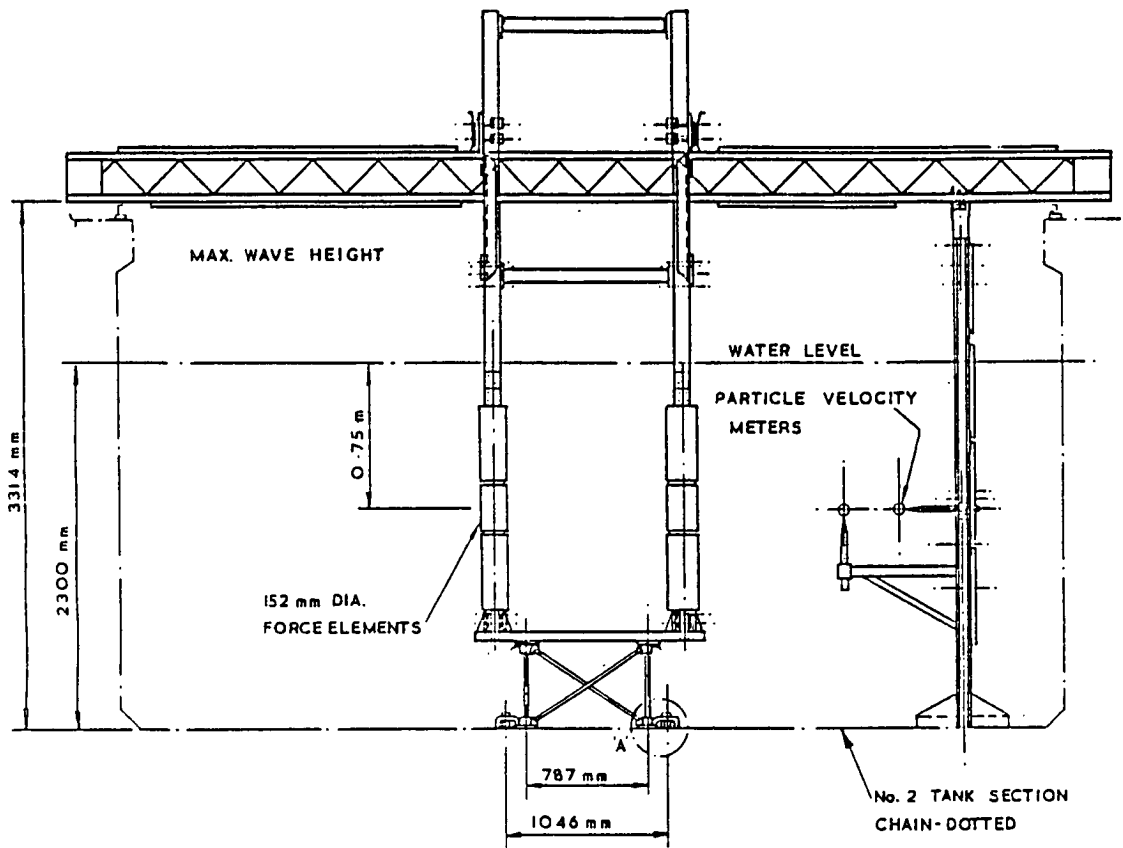
Cotter and Chakrabarti (1984), in laboratory waves, measured the transverse load on a cylinder at various angles to the vertical but in the orbit plane of waves. R_e values were up to 10^5 and K_c values were up to 30. It was concluded that the independence principle seemed to be valid.

g. Bullock

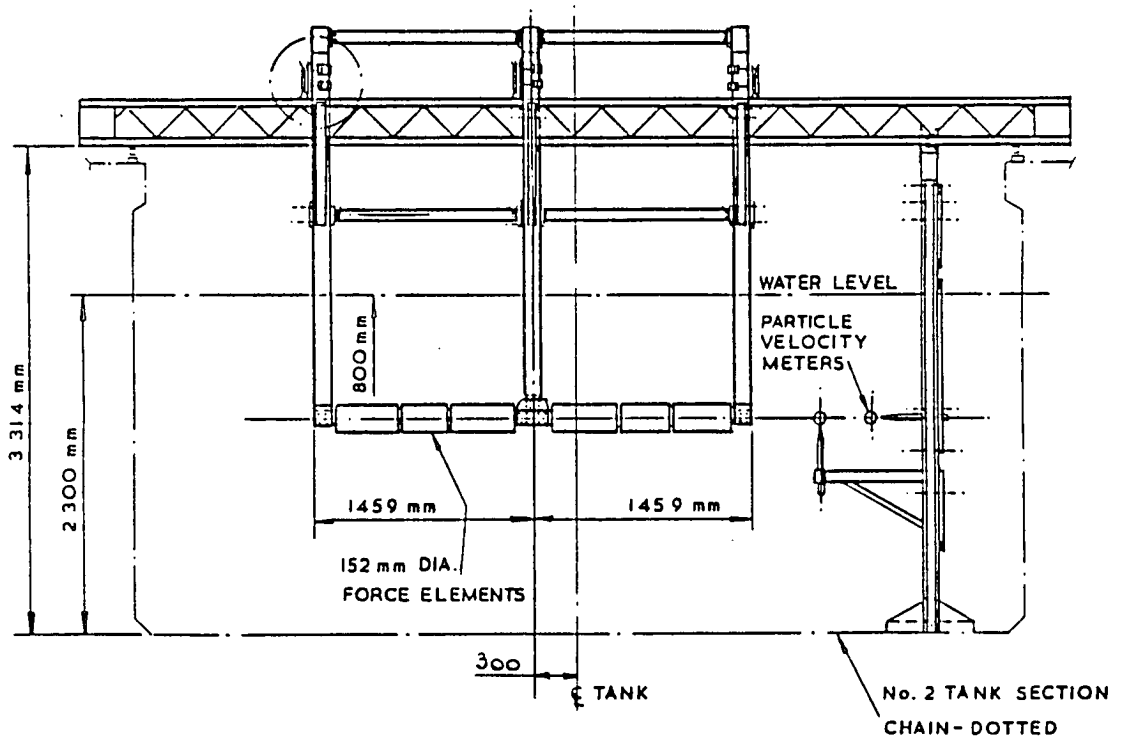
Bullock (1983) measured C_d and C_m values for a cylinder at five orientations relative to waves of various ellipticities. The range of R_e was from 1.6×10^3 to 7.5×10^3 which is subcritical and therefore of limited interest for offshore structure design and analysis. The effects of cylinder orientation and ellipticity of the flow are both shown to be large with increased ellipticity usually reducing both C_d and C_m .

h. Torum

Torum (1985) investigated the wave forces in the near surface region following field measurements reported by Dean et al (1981) which showed a surface effect. This is explained by the Bernoulli effect giving a run up on the waveward side of the cylinder of approximately $U^2/2g$ and a similar drop of water level on the down wave side of the cylinder.

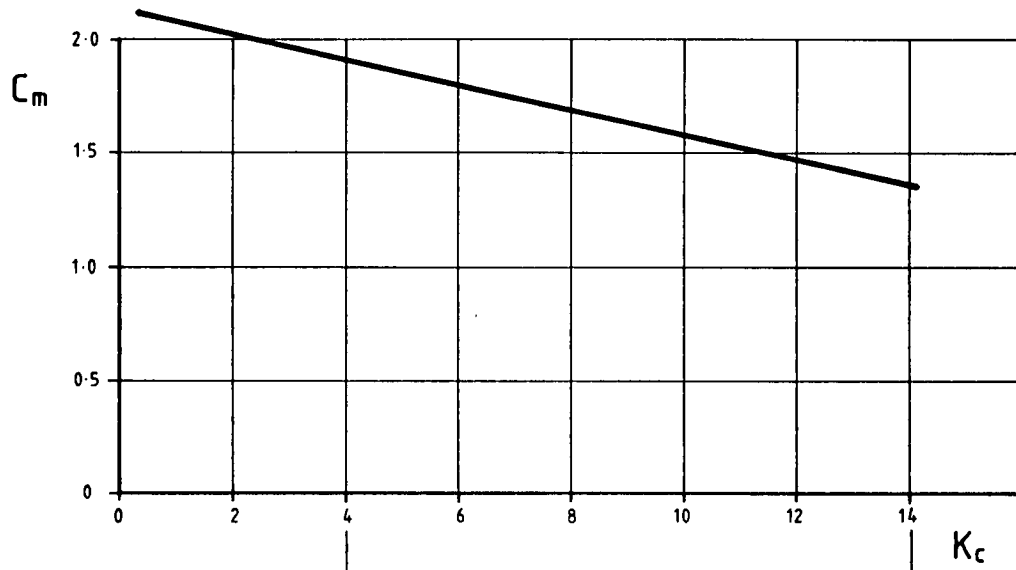
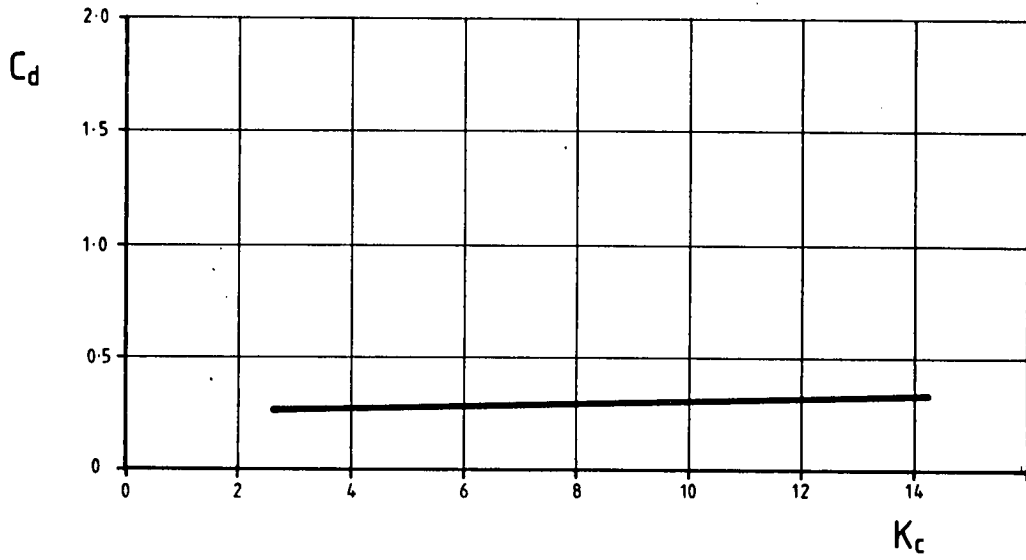


ARRANGEMENT OF VERTICAL CYLINDERS



ARRANGEMENT OF HORIZONTAL CYLINDERS

Figure 3.2.28. Equipment used by Percy et al (1985)



$\frac{\text{Drag Force}}{\text{Inertia Force}}$	-----	0.05		0.34
Orbit Ellipticity	-----	1.0		0.6

Figure 3.2.29. Smooth vertical cylinder C_d and C_m in waves
 R_e 2×10^4 to 9×10^4
(Pearcey et al, 1985)

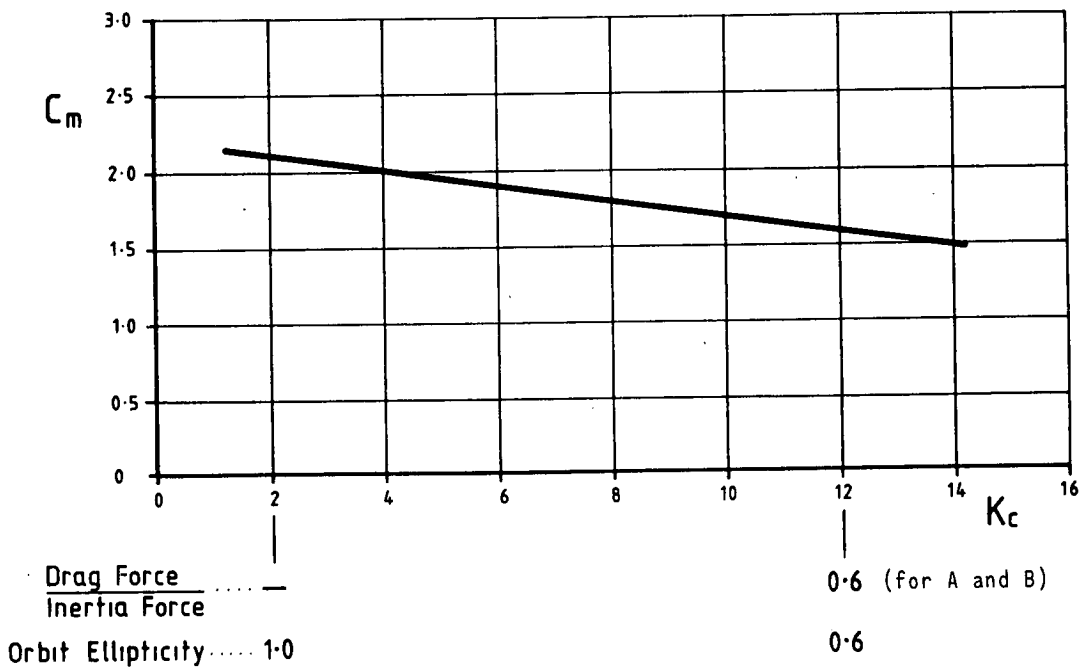
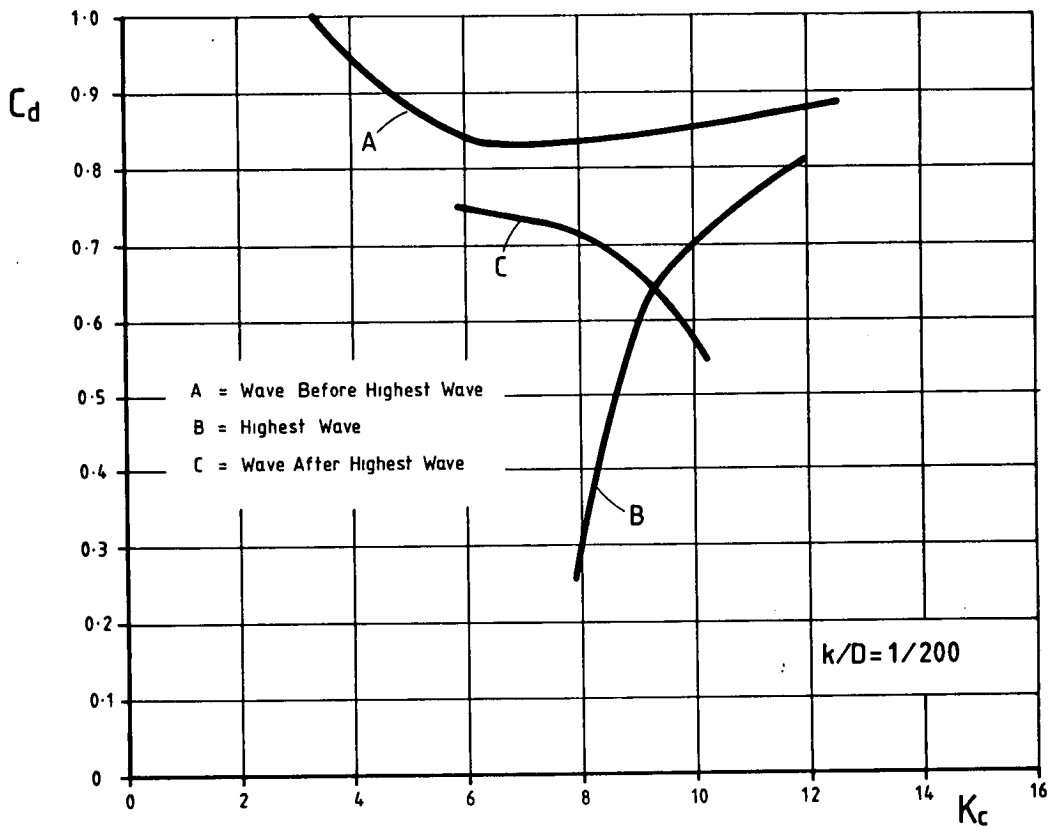


Figure 3.2.30. C_d and C_m for a rough vertical cylinder in waves
 R_e 2×10^4 to 9×10^4 (Pearcey et al, 1985)

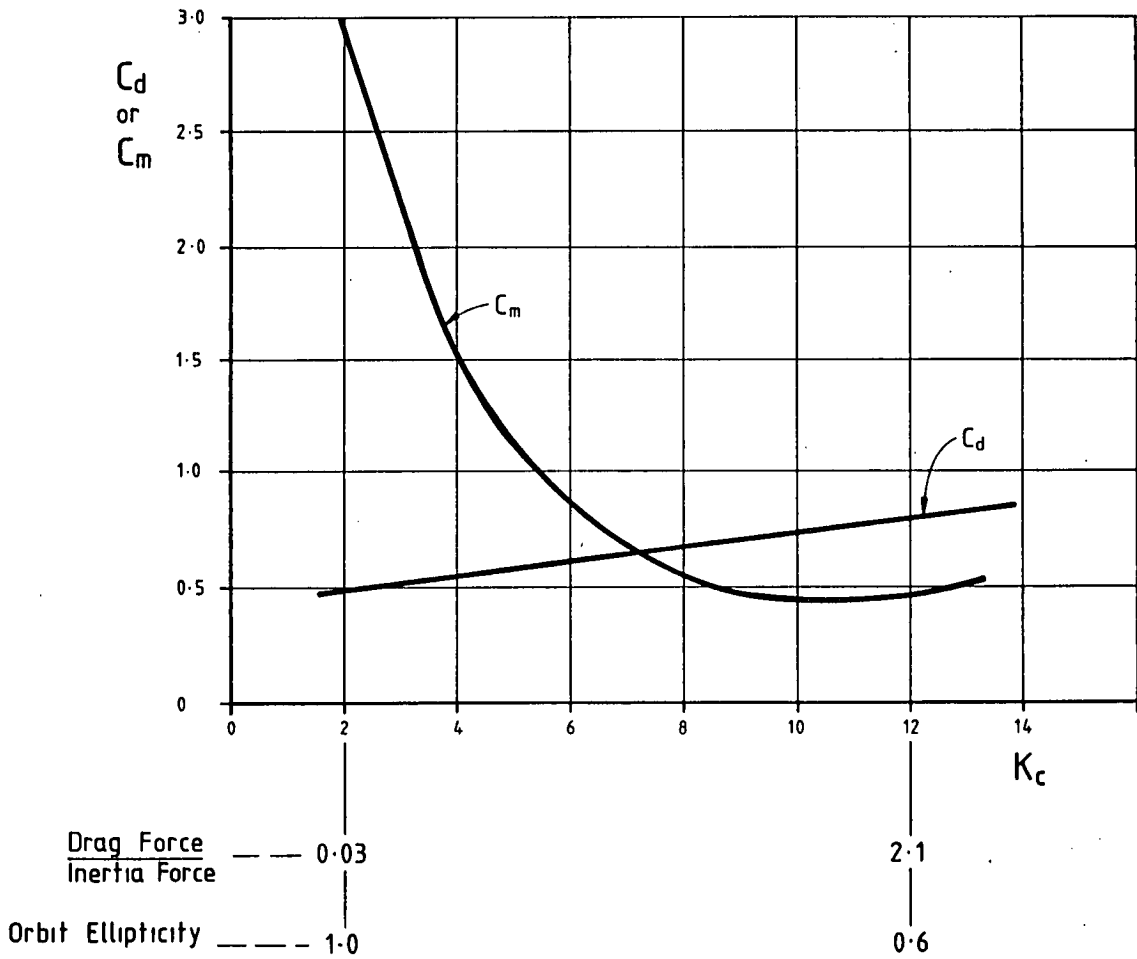


Figure 3.2.31. Smooth horizontal cylinder C_d and C_m for vertical force in waves at Re of 2×10^4 to 9×10^4 (Pearcey et al, 1985)

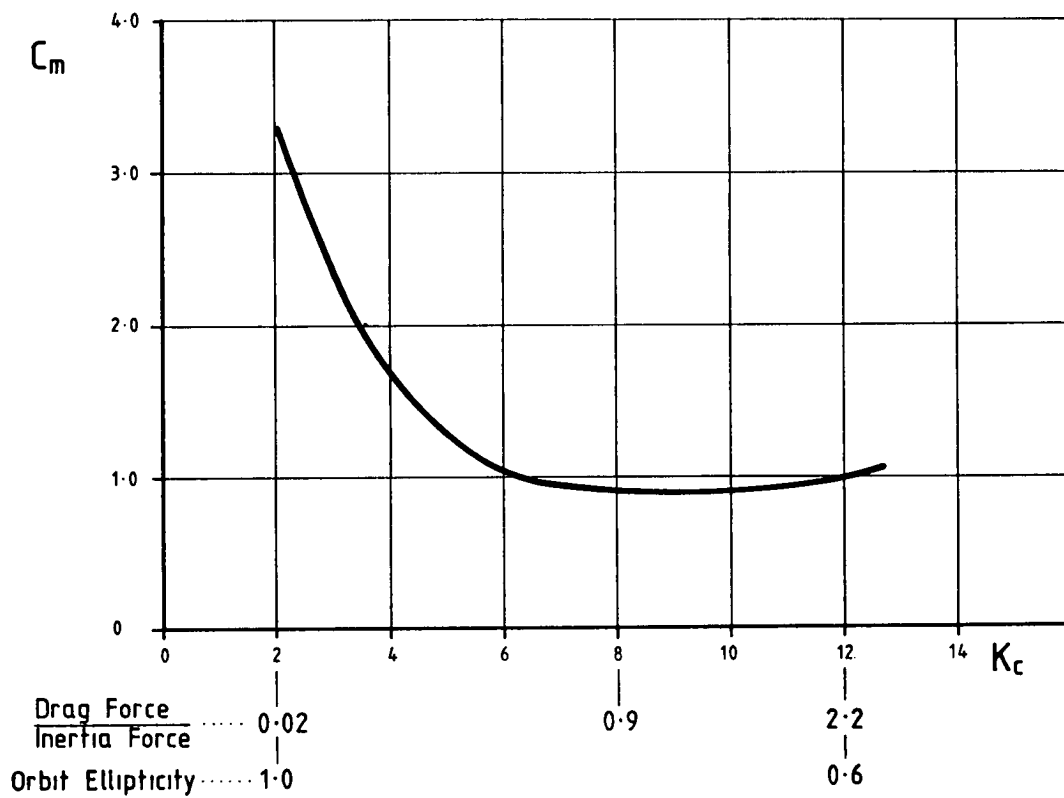
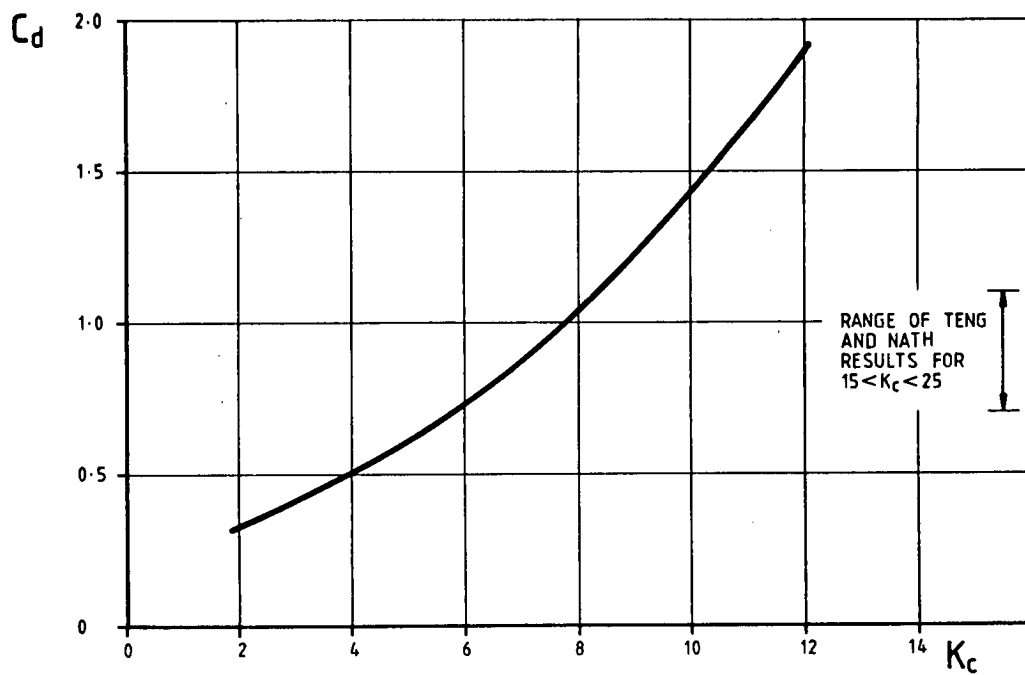


Figure 3.2.32. Rough horizontal cylinders C_d and C_m for vertical forces in waves at Re of 2×10^4 to 9×10^4 (Pearcey et al, 1985)

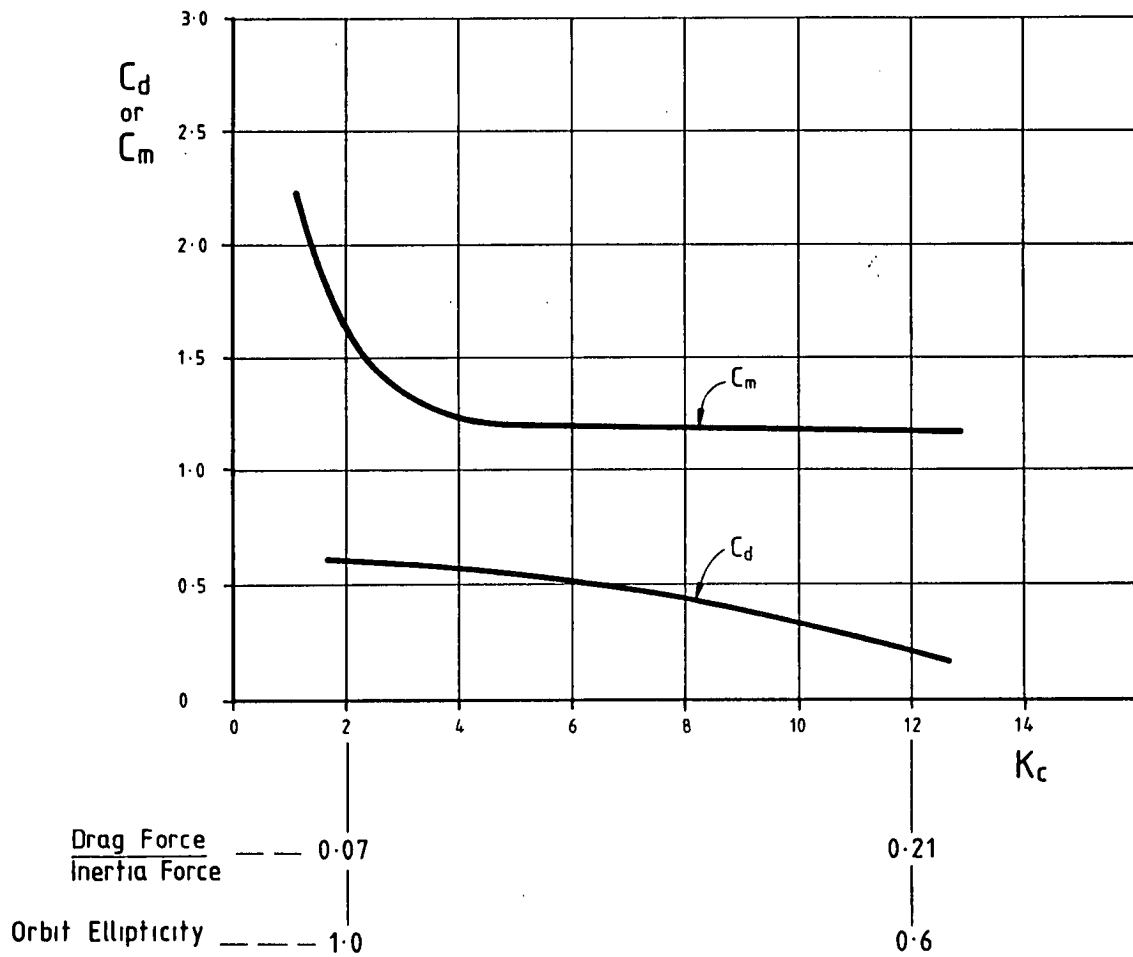


Figure 3.2.33. Smooth horizontal cylinder C_d and C_m for horizontal force in waves at R_e of 2×10^4 to 9×10^4 (Pearcey et al, 1985)

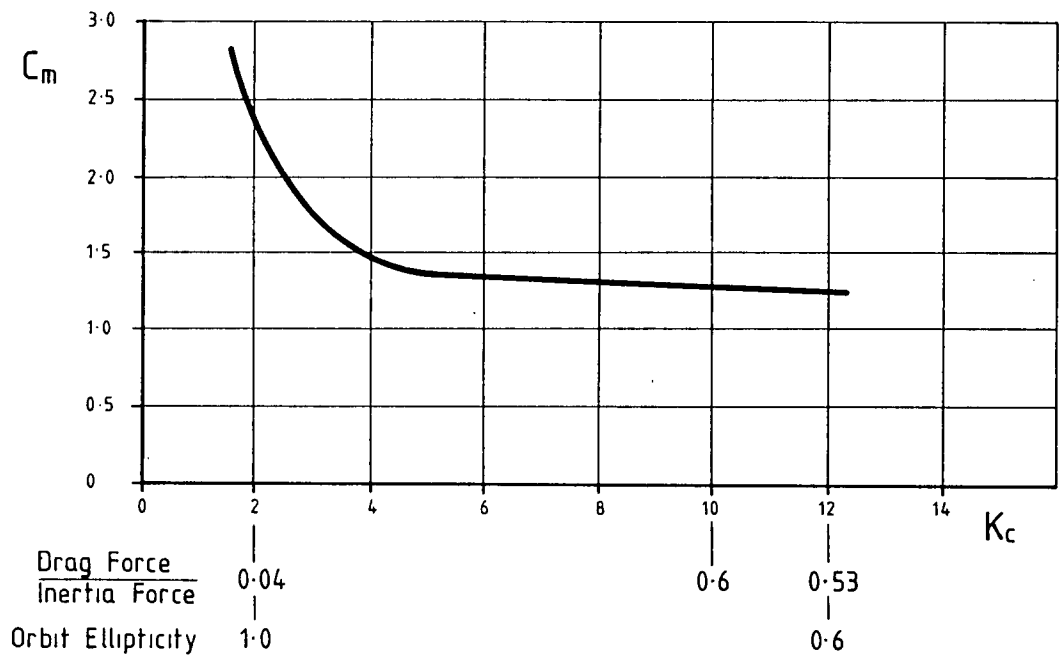
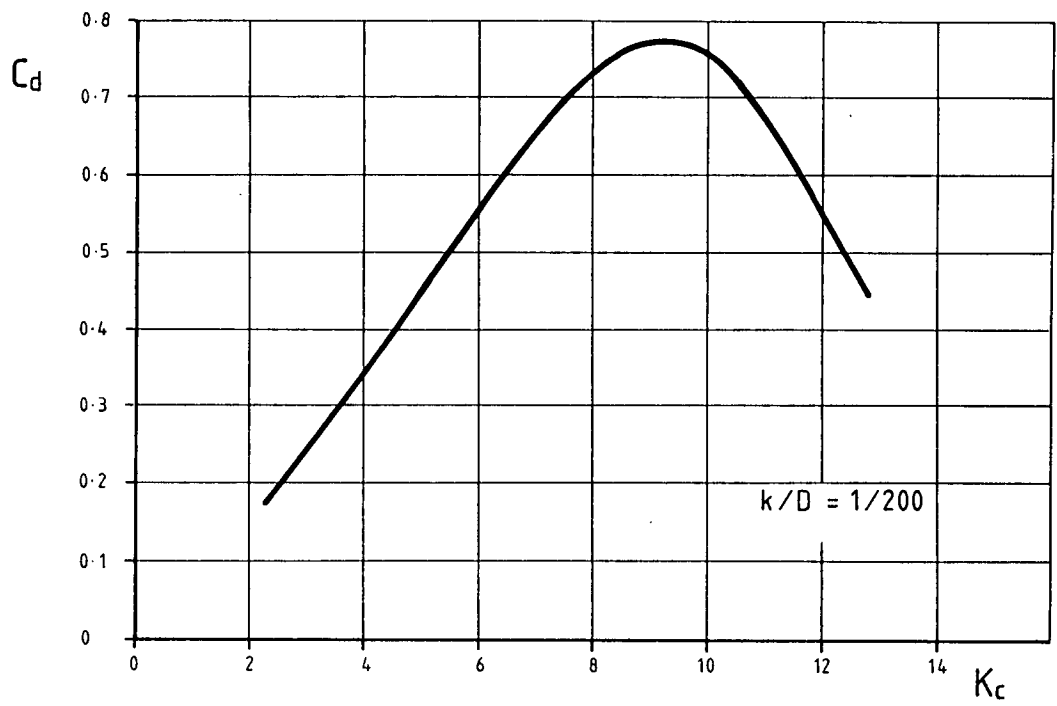


Figure 3.2.34 Rough horizontal cylinders C_d and C_m for horizontal forces in waves at R_e of 2×10^4 to 9×10^4 (Pearcy et al, 1985)

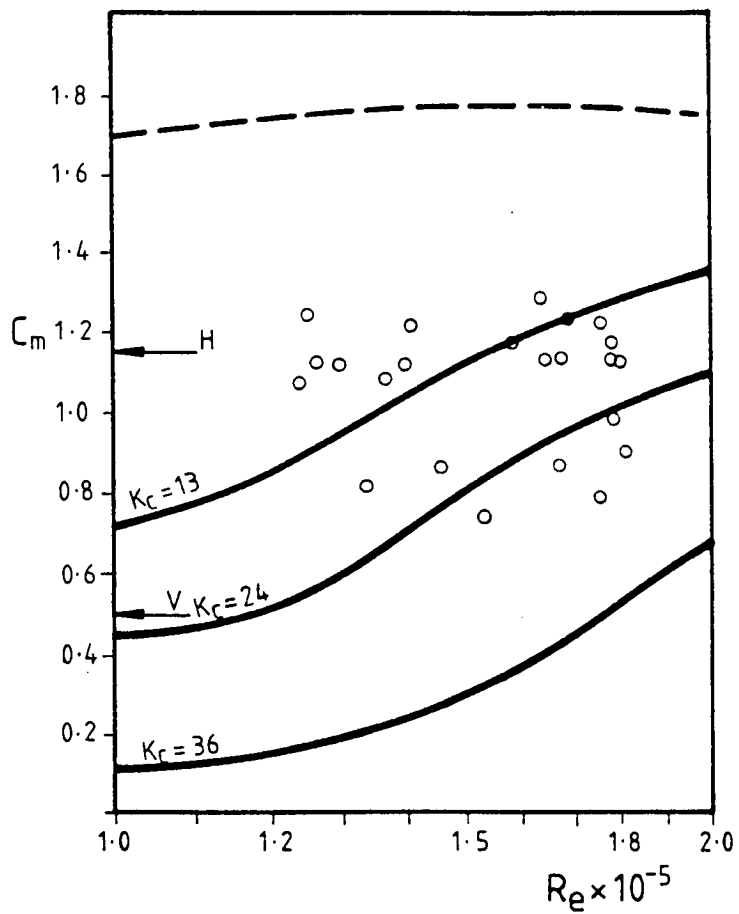
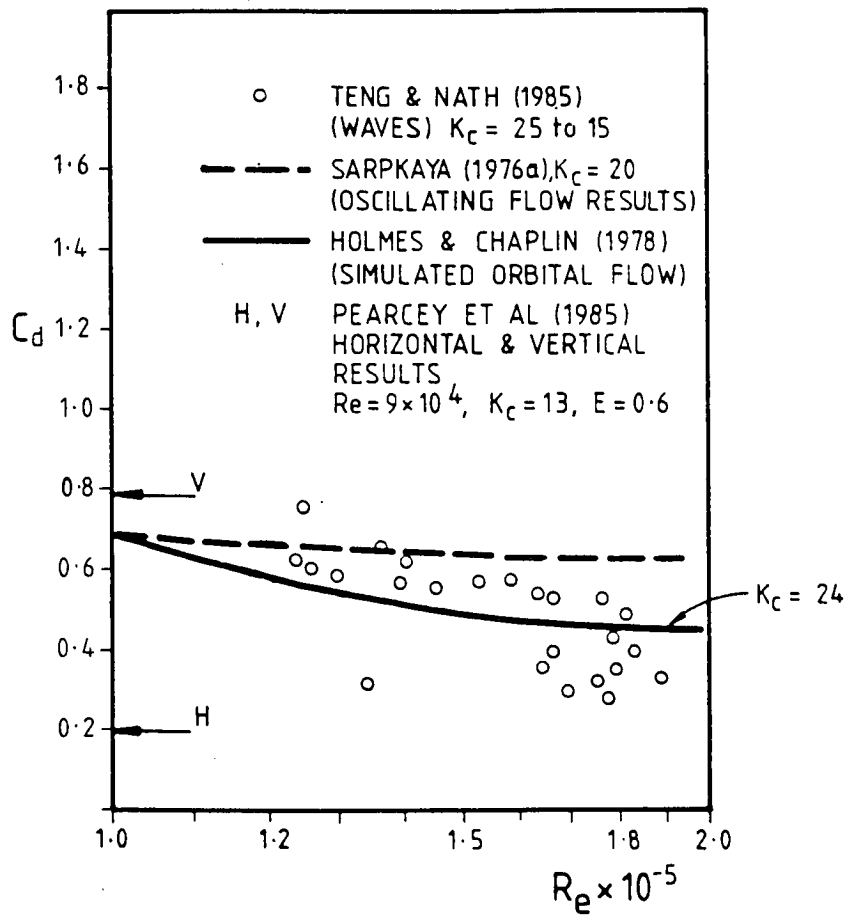


Figure 3.2.35 Smooth horizontal cylinder C_d and C_m values in waves for $25 > K > 15$ (Teng and Nath, 1985)

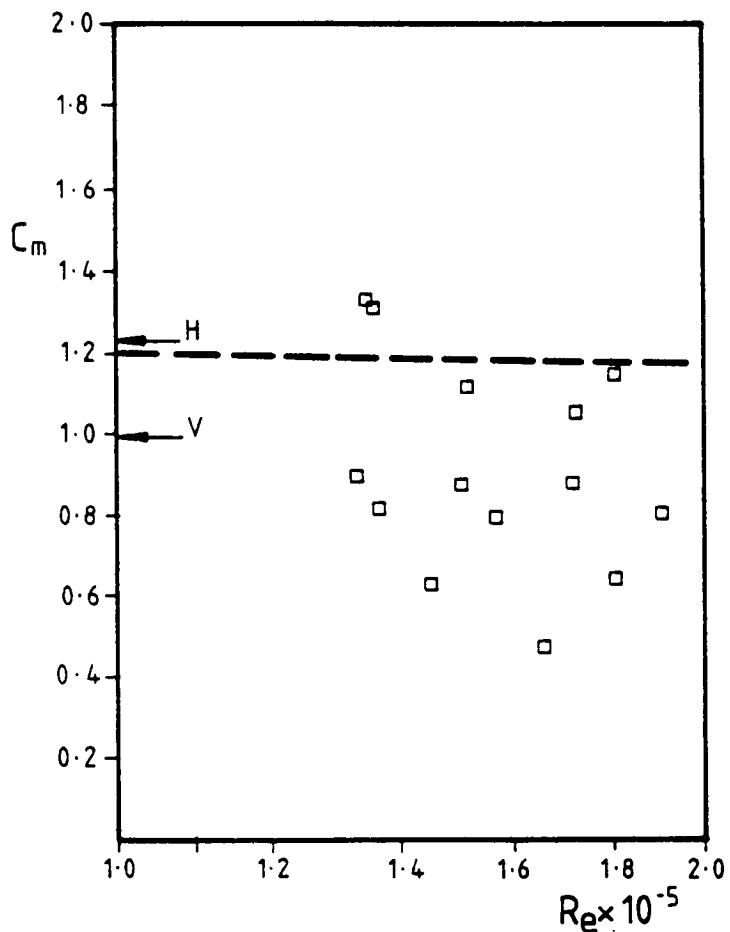
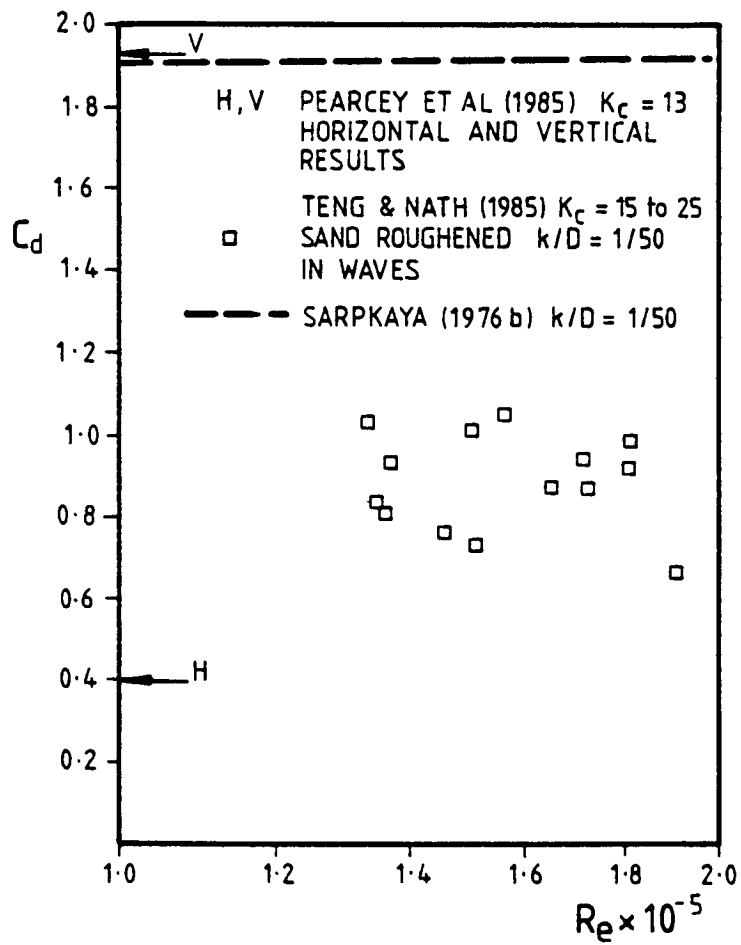


Figure 3.2.36. Sand roughened horizontal cylinder C_d and C_m values in waves (Teng and Nath, 1985)

3.2.9 Sea waves

a. General

Several experiments have been performed in the sea. These experiments often also produced particle kinematics data as described in Section 2.2.

b. The Christchurch Bay experiment

This experiment, conducted in the sea off Southern England, has generated a large amount of data at high R_e and over a range of K_c (see Section 2.2.4).

Most of the loading data is for clean vertical cylinders but some data has also been obtained for clean horizontal cylinders and for kelp fouled cylinders, both vertical and horizontal. Figure 3.2.37 gives C_d and C_m values for all these cases. Figure 3.2.38 gives C_f^* values for the clean vertical cylinders and Figure 3.2.39 gives C_f^* values for the clean and kelp fouled cylinders over the range of K_c for which results are available.

For smooth vertical cylinders Bishop (1984) concludes in his summary report:

1. Extensive wave force measurements for clean vertical cylinders in real sea conditions have led to confident results for mean force coefficients, based on reliable measurements of the wave particle kinematics. The results are shown to be applicable to North Sea structures.
2. The mean force coefficients, C_m and C_d at the depth station nearest to the sea surface are:-
 - at high Keulegan Carpenter numbers ($K_c > 30$) $C_m = 1.8$, $C_d = 0.66$
 - at intermediate Keulegan Carpenter numbers ($30 > K_c > 5$) C_m and C_d both increase as K_c reduces
 - at low Keulegan Carpenter numbers ($K_c < 5$) $C_m = 2.0$
(The value of C_d is unimportant at $K_c < 5$)

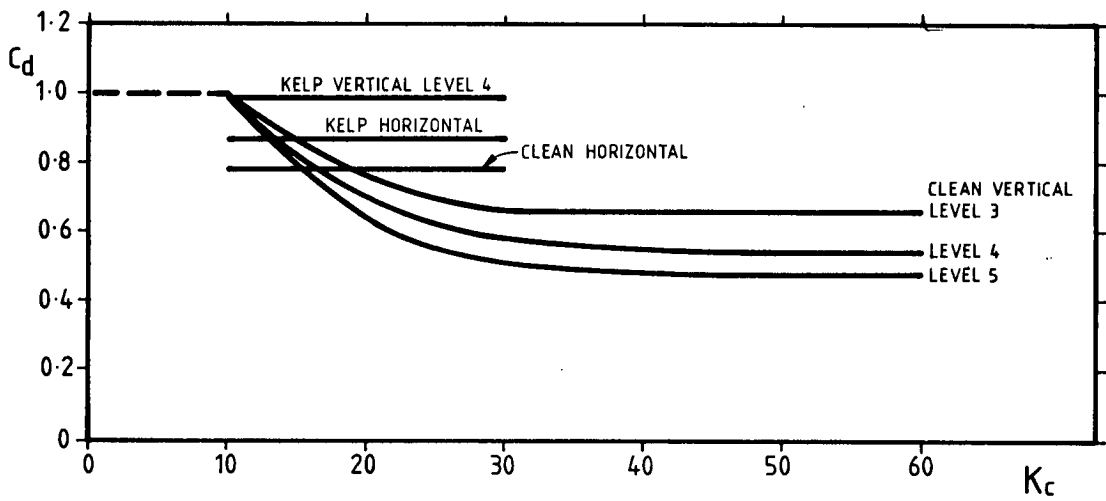
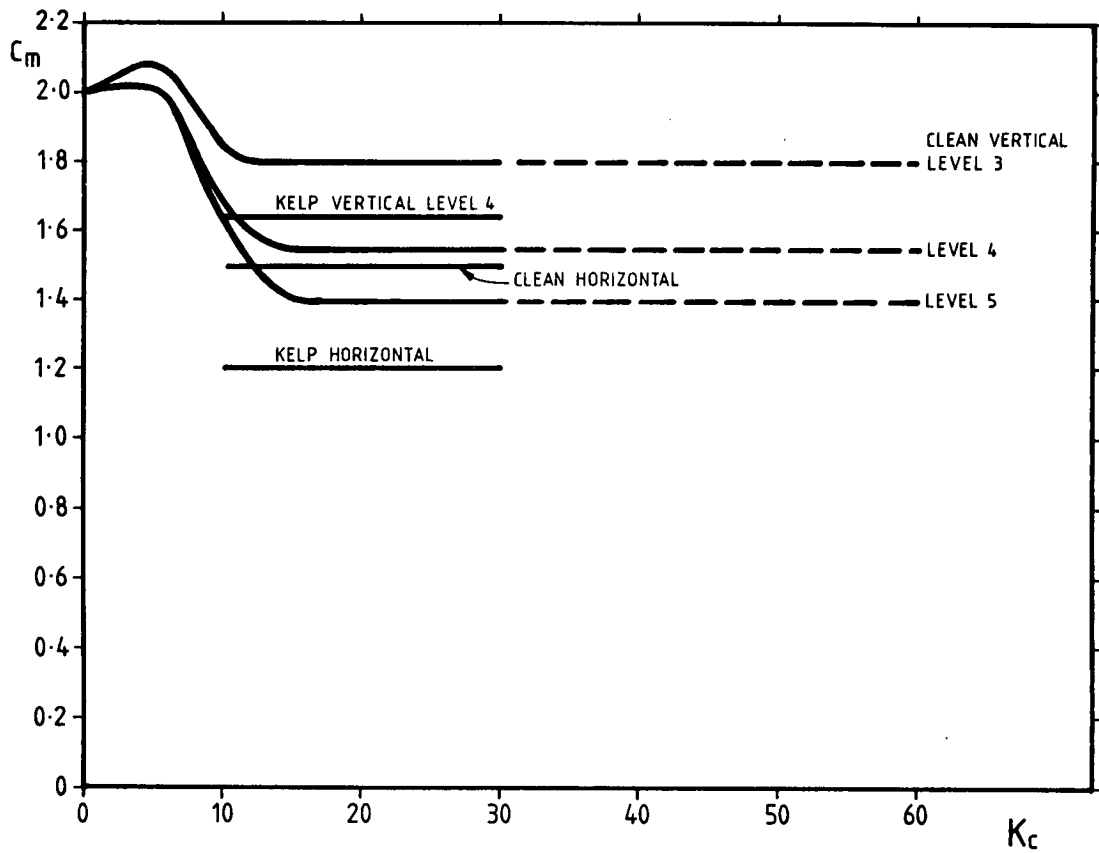


Figure 3.2.37. Mean C_d and C_m values at the Christchurch Bay Tower (Bishop, 1984, 1987)

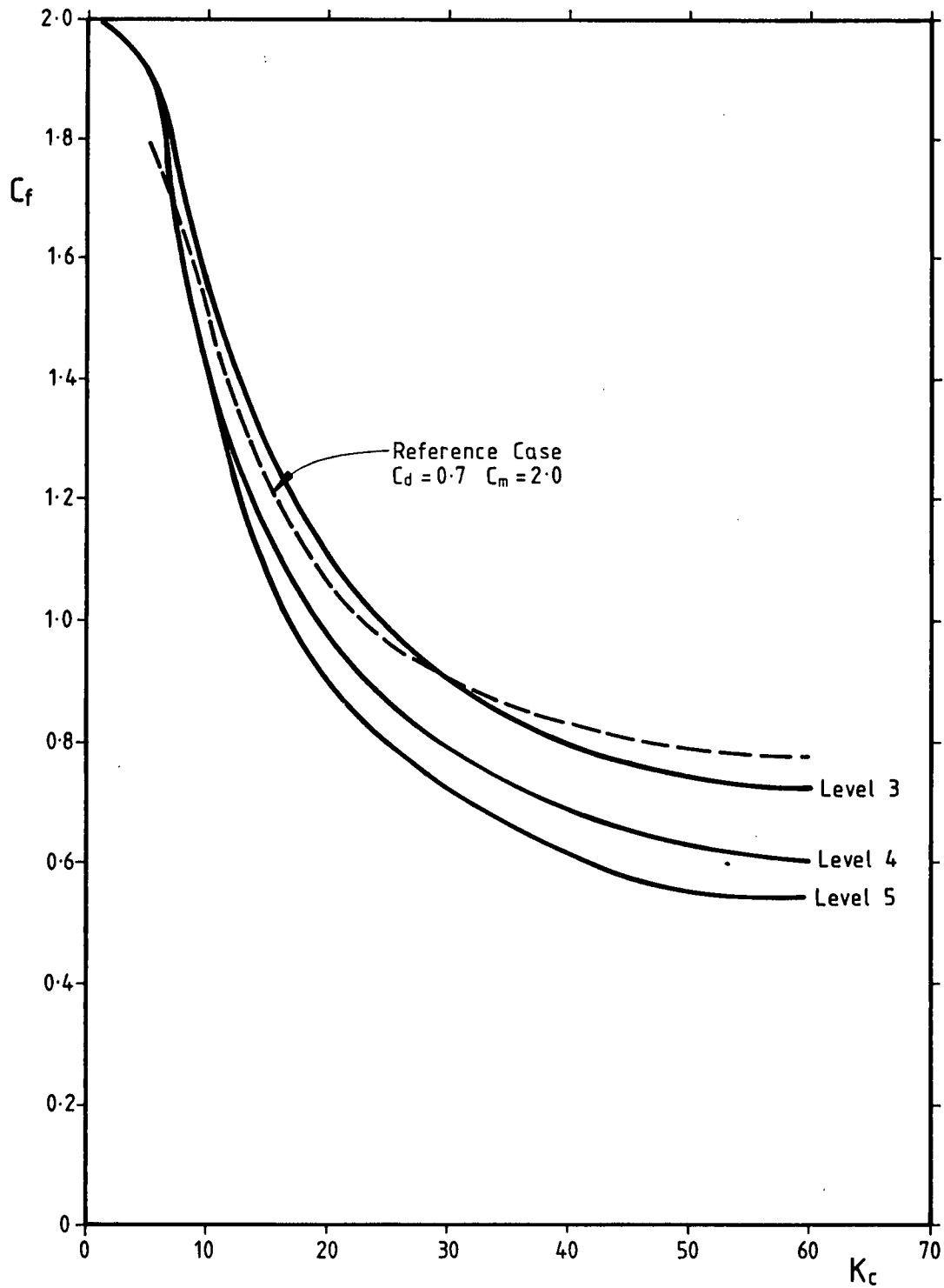


Figure 3.2.38. Clean vertical cylinder mean C_f^* values for 3 levels at the Christchurch Bay Tower (Bishop, 1984)

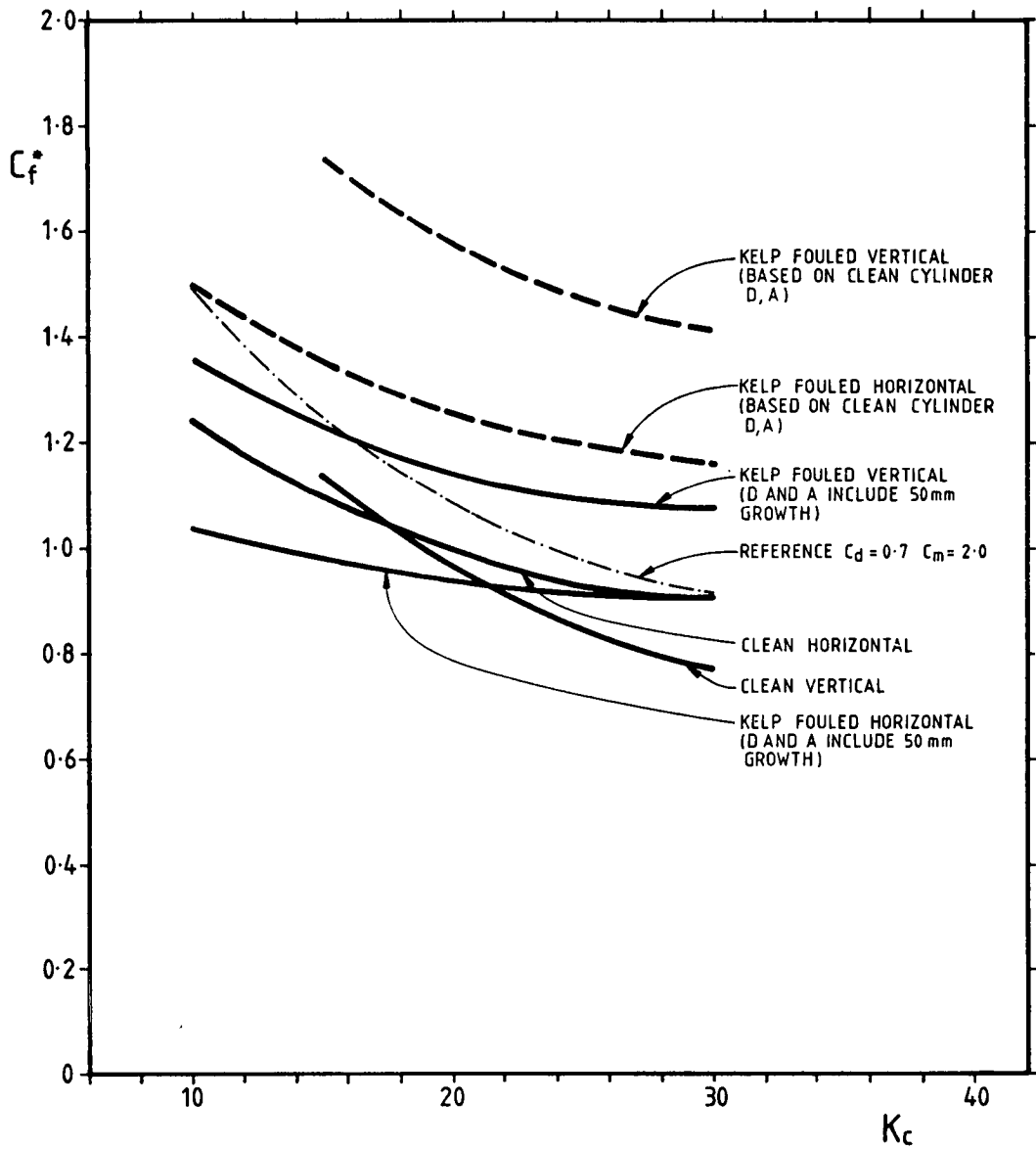


Figure 3.2.39. C_f^* values for clean and kelp fouled vertical and horizontal cylinders (Bishop, 1984, 1987)

3. At lower depth stations the force coefficients show some progressive reduction with depth. However, for design purposes, it is safer to use values applicable to the upper depth station quoted above.
4. The total force coefficients have been found to be invariant with Reynolds number over the range of conditions tested ($2 \times 10^5 < R_e < 2 \times 10^6$ approximately). It follows that the results may be applied with confidence to North Sea structures.
5. Analysis of peak values of wave forces for individual waves has shown that they are generally well-predicted when using the long-term mean force coefficients in conjunction with the measured particle kinematics. The mid-range values (which are important in fatigue calculations) are well predicted at all Keulegan Carpenter numbers. However, the upper-range values (which are important in extreme load calculations) are susceptible to some underprediction at high Keulegan Carpenter numbers and this should be recognised in the prediction of extreme loads.
6. Force spectra are generally well predicted when using the long-term mean force coefficients in conjunction with the measured particle kinematics. This is particularly so when considering the largest force component, in line with the wave direction. Spectra for the smaller transverse force are less well predicted and this is evidence of the increased influence of vortex shedding at the higher Keulegan Carpenter numbers. Overall however, the transverse force spectrum is dominated by transverse wave components in the multi-directional sea and this makes the significance of vortex shedding less than it would be with uni-directional waves.
7. Borgman's linearisation of the drag term in the force spectrum can lead to significant under-prediction of the drag force spectrum. In this work, the under-prediction was typically some 25% at the spectral peak, with larger differences at lower frequencies.
8. The measured particle motion data, in terms of velocity and acceleration, have been used to evaluate linear random wave theory, in conjunction with the measured surface elevation. Generally, the velocity prediction is good, but there is some over-prediction at higher frequencies and some under-prediction at the lower frequencies. The cause of the low frequency under-prediction is probably the effect

of depth-limited waves, but the present results have only explored this to a limited degree.

With particle acceleration, linear random wave theory gives a more marked over-prediction at the higher frequencies.

9. When force predictions are based on surface elevations the deficiencies of wave theory, as outlined above, follow through to force predictions that are less satisfactory than those based on the measured particle kinematics. The major effect is over-prediction of inertia forces due to the over-prediction of particle acceleration.

Results for kelp fouled cylinders have also been obtained from the Christchurch Bay Experiment, Bishop (1987). These have been determined over the range $K_c = 15$ to $K_c = 30$. Values are given in Table 3.2.6. Note that these values have been calculated using the clean cylinder diameter and area.

Table 3.2.6 - C_d and C_m for kelp fouled cylinders at $K_c = 15$ to 30 Christchurch Bay Experiment (Bishop 1987)

	C_d	C_m
Vertical cylinder	1.20	2.40
Horizontal cylinder	1.05	1.75

In practice an allowance is usually made for marine growth increasing the cylinder diameter and area. We assume an equivalent thickness of marine growth to be 50mm. The clean cylinder diameter was 490mm and C_d and C_m values consistent with the 590mm effective diameter are shown in Table 3.2.7. (This effective thickness is similar to that given by Wolfram and Theophanatos in Table 3.2.3).

Table 3.2.7 - C_d and C_m for kelp fouled cylinders at $K_c = 15$ to 30 using an effective D and A. Based on the results of Bishop (1987)

	C_d	C_m
Vertical cylinder	1.0	1.66
Horizontal cylinder	0.87	1.20

c. The Ocean Test Structure experiment

This experiment was performed in the Gulf of Mexico (see Section 2.2.4). It determined C_d and C_m values in waves for clean and marine fouled (barnacles, $k/D = 1/35$) vertical cylinders. Values have been calculated using both spectral methods (Borgman and Yfantis, 1979) and by two wave by wave methods (Heideman, Olsen and Johansson, 1979).

Both estimates show a large scatter. The spectral estimates were typically C_d : 0.6 to 0.8 and C_m : 1.4. The highest reported spectral estimates for C_d and C_m were 1.75 and 1.65. The wave by wave analysis results (calculated by two methods) are shown in Figures 3.2.40 and 3.2.41. The corresponding inertia coefficients could not be related to K_c and are shown in Table 3.2.8. Total force coefficients are given in Figure 3.2.42.

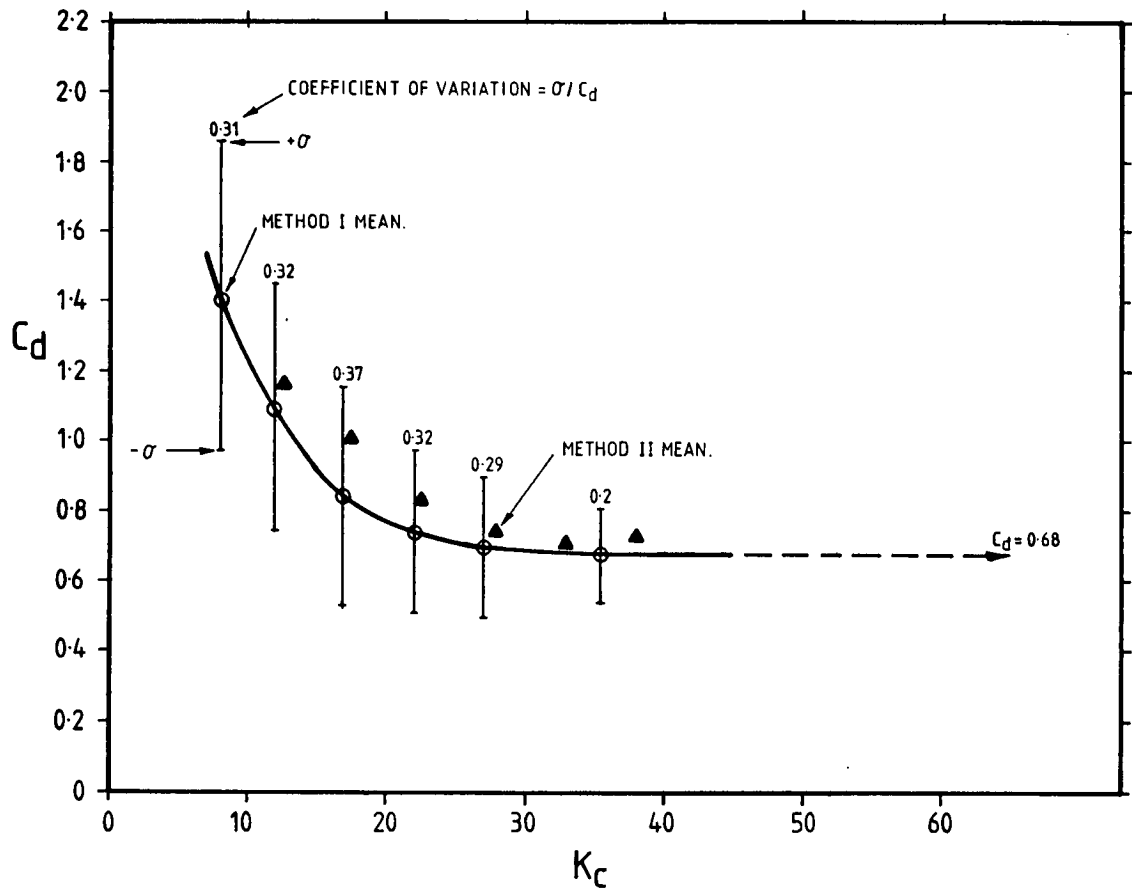


Figure 3.2.40. Clean vertical cylinder and coefficient of variation of C_d values. Ocean Test Structure (Heideman et al, 1979)

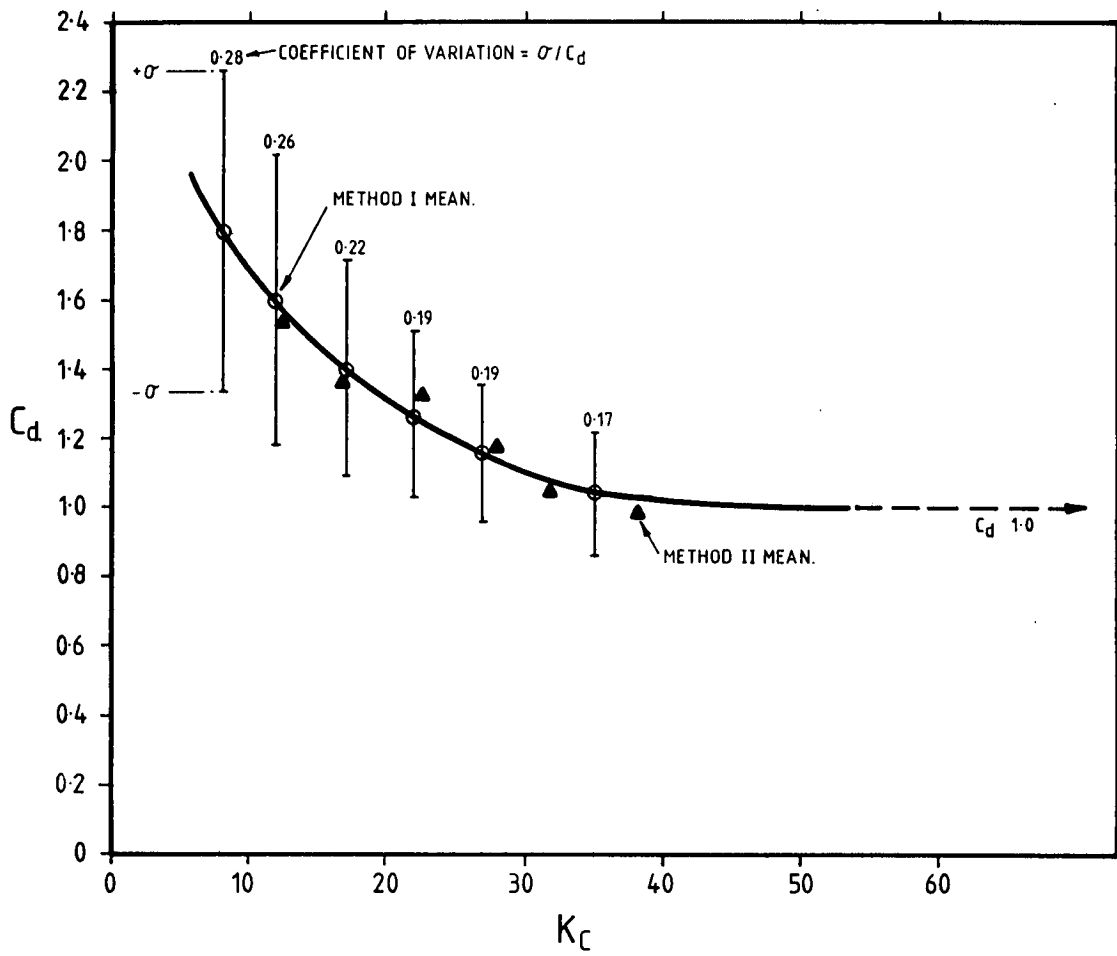
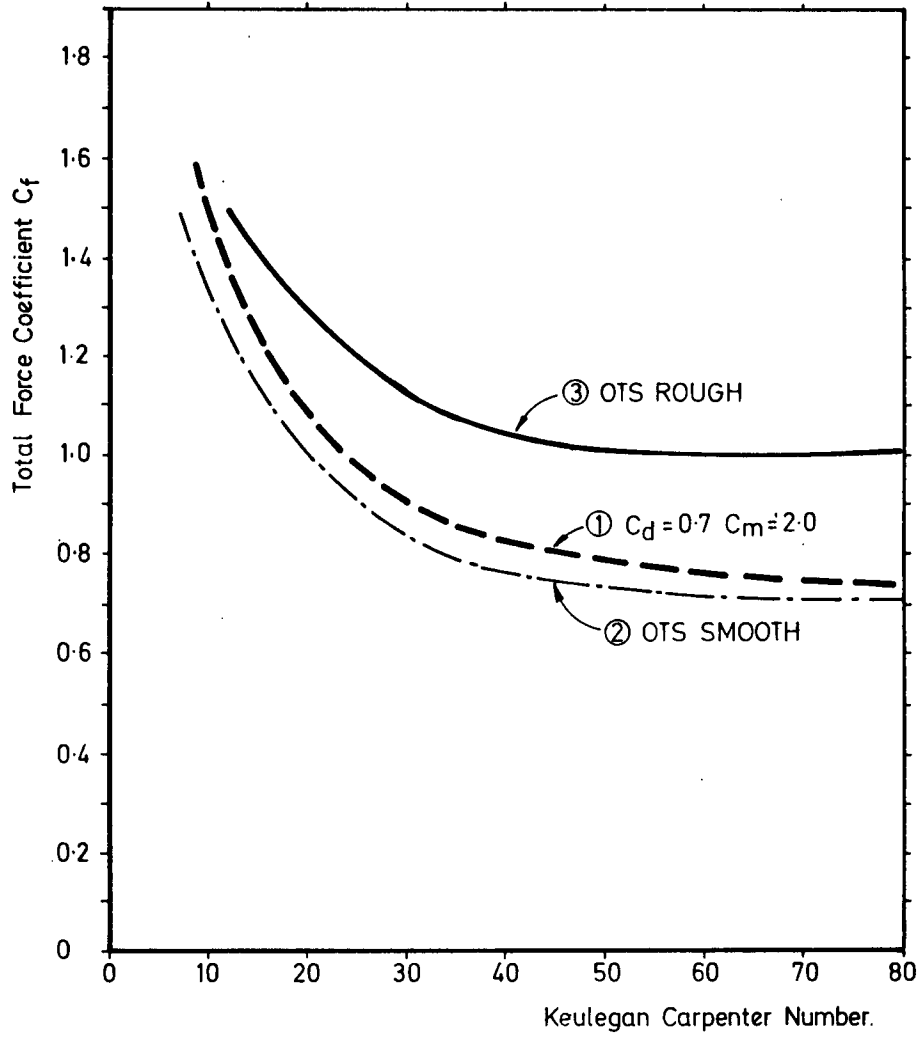


Figure 3.2.41. Rough vertical cylinder mean and coefficient of variation of C_d values. Ocean Test Structure (Heideman et al, 1979)



- ① $C_d = 0.7$ $C_m = 2.0$
- ② OTS Smooth Cylinder Results.
- ③ OTS Rough Cylinder Results.

Figure 3.2.42. Comparison of total force coefficients

Table 3.2.8 - C_m from the OTS experiment (Heideman et al, 1979)

Cylinder condition	Method 1		Method 2	
	C_m	standard deviation	C_m	standard deviation
Clean	1.51	0.31	1.65	0.28
Fouled	1.25	0.34	1.43	0.35

The measurements taken on the OTS structure were in the presence of currents. Sarpkaya and Cakal (1983) analysed some of the data to determine the effect of current running parallel with the wave direction. Their results, shown in Figures 3.2.43a and b and analysed further in Appendix H show that increasing current reduces C_d but, for K_c greater than 10, has little effect on C_m . These results are qualitatively similar to those, obtained by Sarpkaya and Storm (1985), for planar oscillating flow (see Section 3.2.6 and Figures 3.2.20 and 3.2.21). Pearcey (1986) suggested that the reason for the decrease in C_d is that the wake is being convected away from the cylinder.

At K_c greater than about 30 the effect of current on C_d was small in the oscillating flow tests. This also seems to be the case for the R_e/K_c of 25,000 but not necessarily for the $R_e/K_c = 20,000$. However, we speculate that the effect of currents does reduce as K_c increases because, as discussed by Heideman et al (1979), in a random sea at high K_c the wake will be convected away from the cylinder, in much the same way as by a current. Any component of the current running perpendicular to the wave direction may also be expected have an effect on C_d .

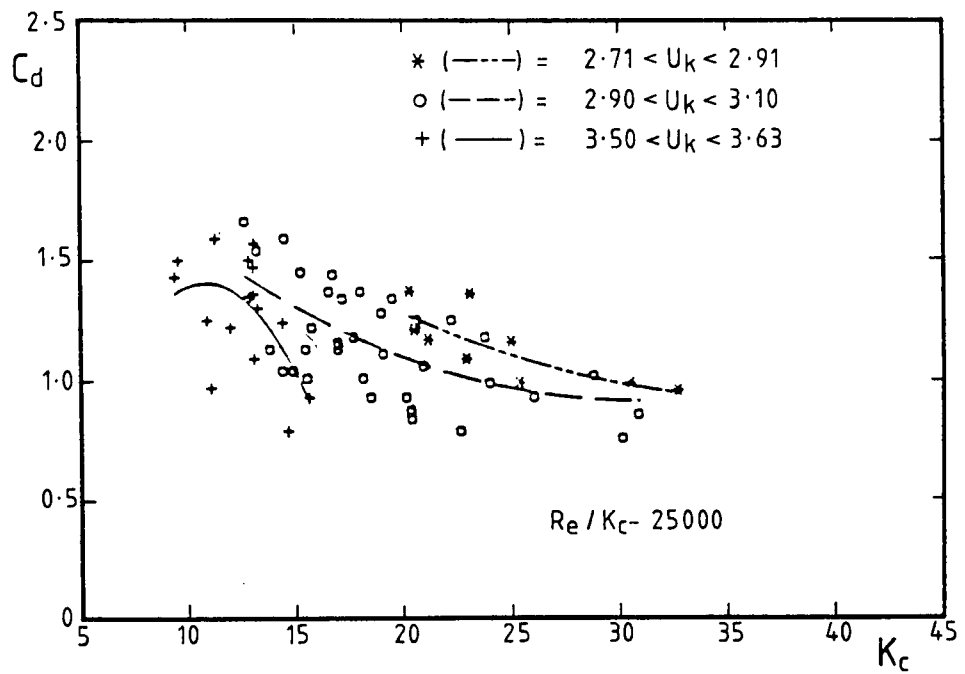
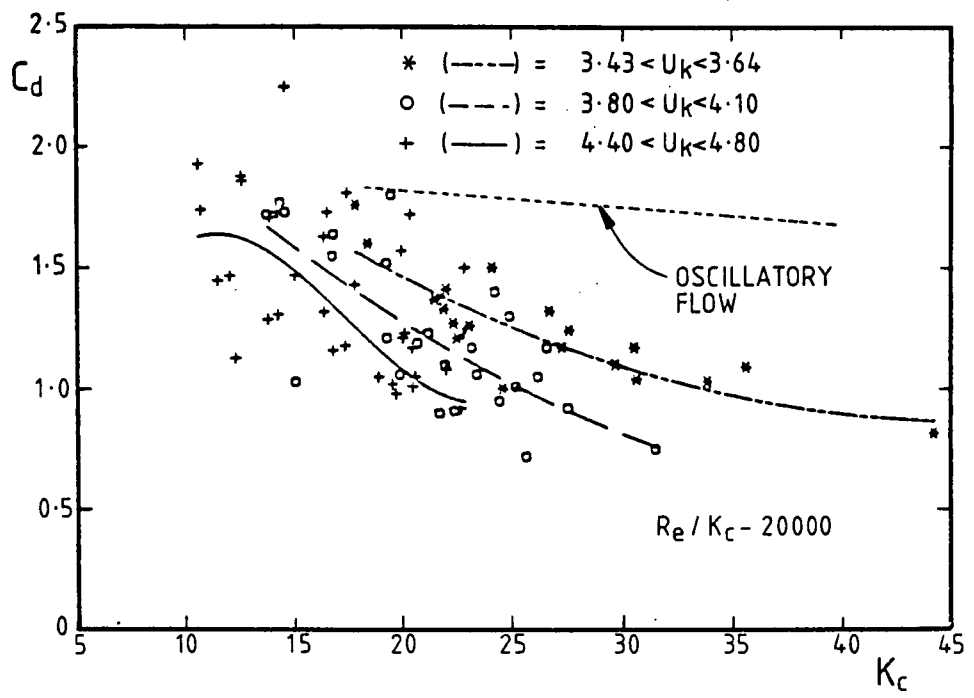


Figure 3.2.43a. Vertical cylinder relative current effect on C_d .
 Ocean Test Structure
 (Sarpkaya and Cakal, 1983)

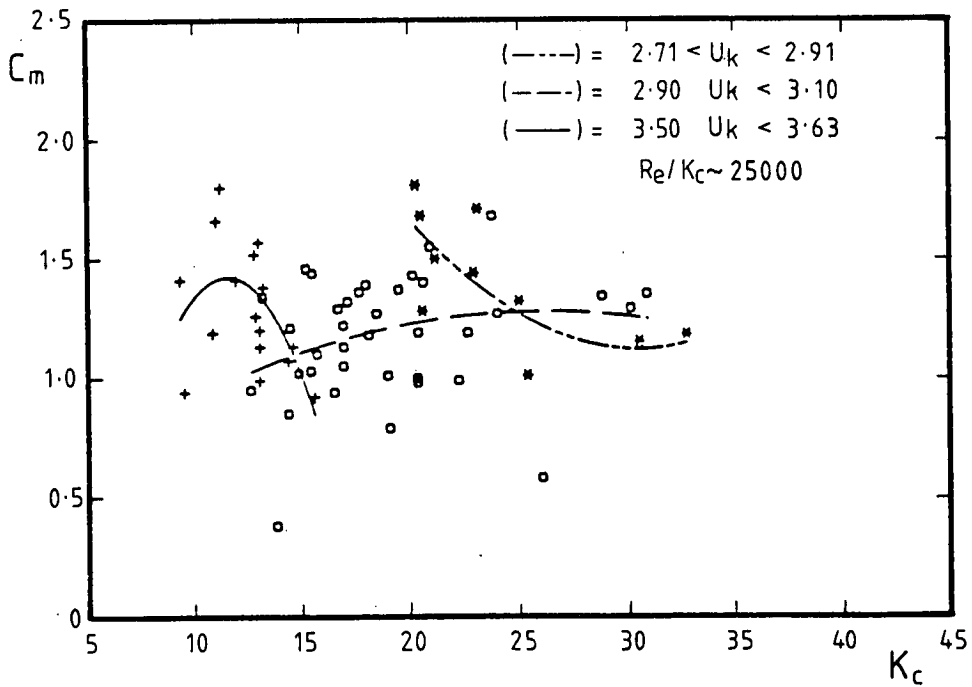
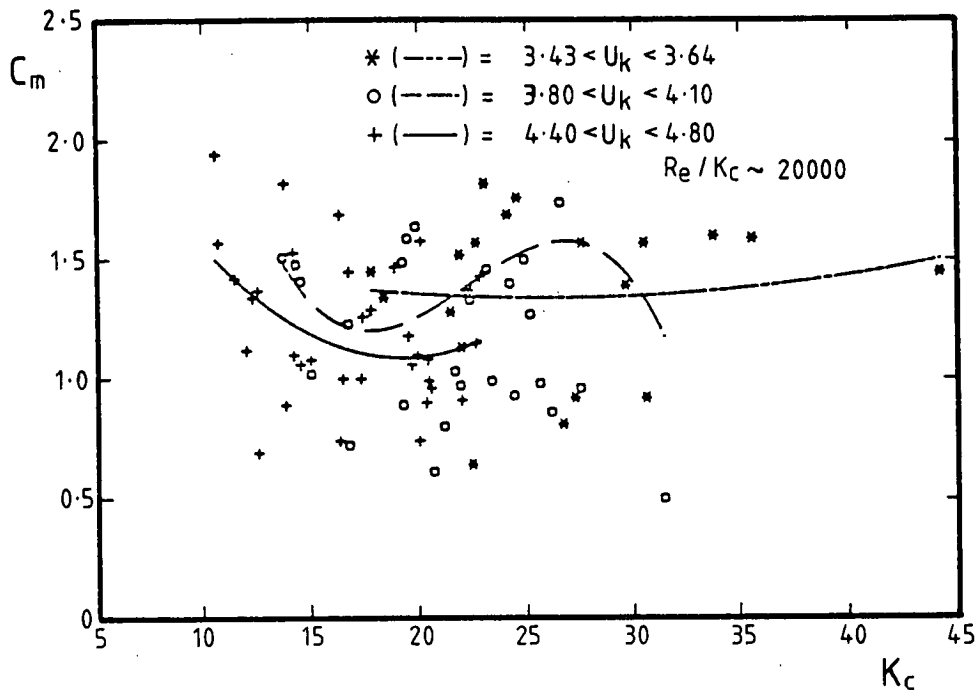


Figure 3.2.43b. Vertical cylinder relative current effect on C_m . Ocean Test Structure (Sarpkaya and Cakal, 1983)

d. The Forties Field experiment

The Forties Field Experiment (Atkins, 1979) produced estimates of C_d and C_m using the equipment shown in Figure 3.2.44. K_c was in the range 5 to 15 and R_e ranged from 3×10^5 to 6×10^5 . The results, based on the horizontal velocity meters at -7.5m and the wave force sleeves at -8.5m, are shown in Figures 3.2.45a and b. The force sleeves were coated with an antifouling compound which would have resulted in some surface roughness. The C_d and C_m values were found to be correlated with R_e and K_c . The C_d and C_m values were calculated from the peaks in total force on the basis of an average phase lag between the times of maximum force and maximum velocity. At the time of writing there is some controversy over the results produced by this form of analysis. Bishop (private communication) argues that the method is not satisfactory in the presence of currents. Starsmore (1981), who has obtained similar results from analysing Christchurch Bay data, argues that the effects of current are small and that the method explains some of the scatter found in the OTS experiment.

e. The Eugene Island experiment

Ohmart and Gratz (1979) analysed data from a wave force transducer and current meters fitted to the Eugene Island Platform in the Gulf of Mexico. It is not known whether the wave force transducer was clean or fouled but the data was measured 9 months after installation of the structure.

Drag and inertia coefficients were estimated on the basis of minimising the sum of the squares of the error between measured and predicted force time histories. Coefficients were obtained for various subsets of the data as shown in Tables 3.2.9 and 3.2.10.

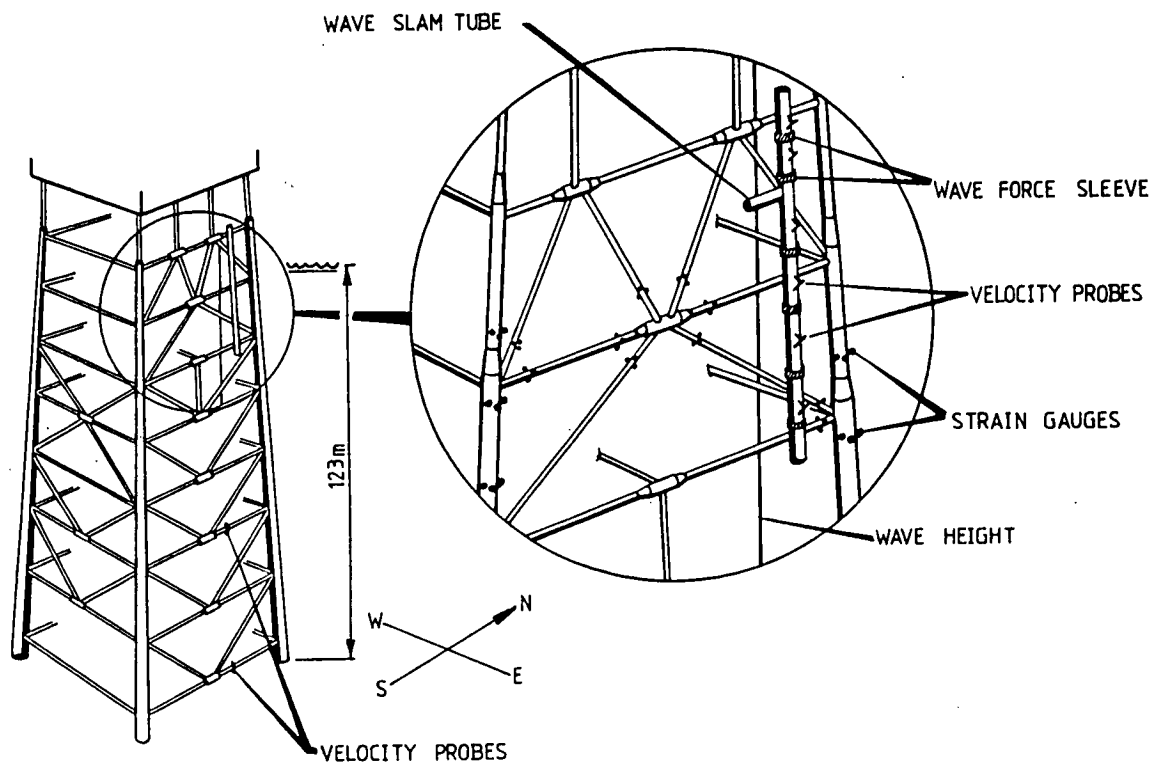


Figure 3.2.44. Instrumentation deployed on B.P. Forties Field Platform FB Jacket

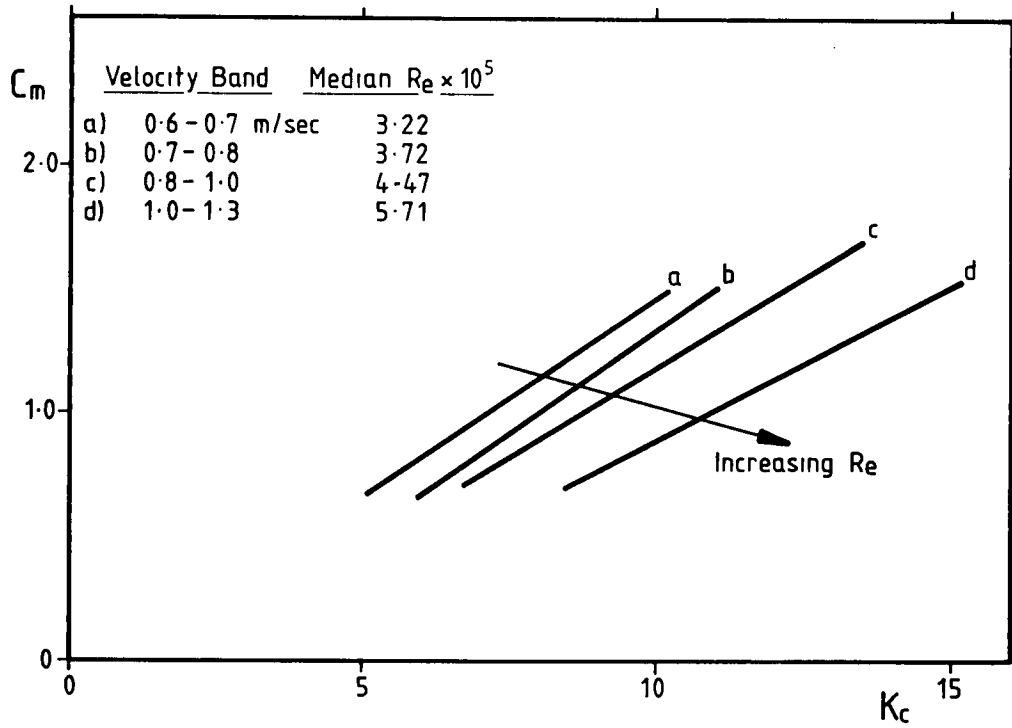
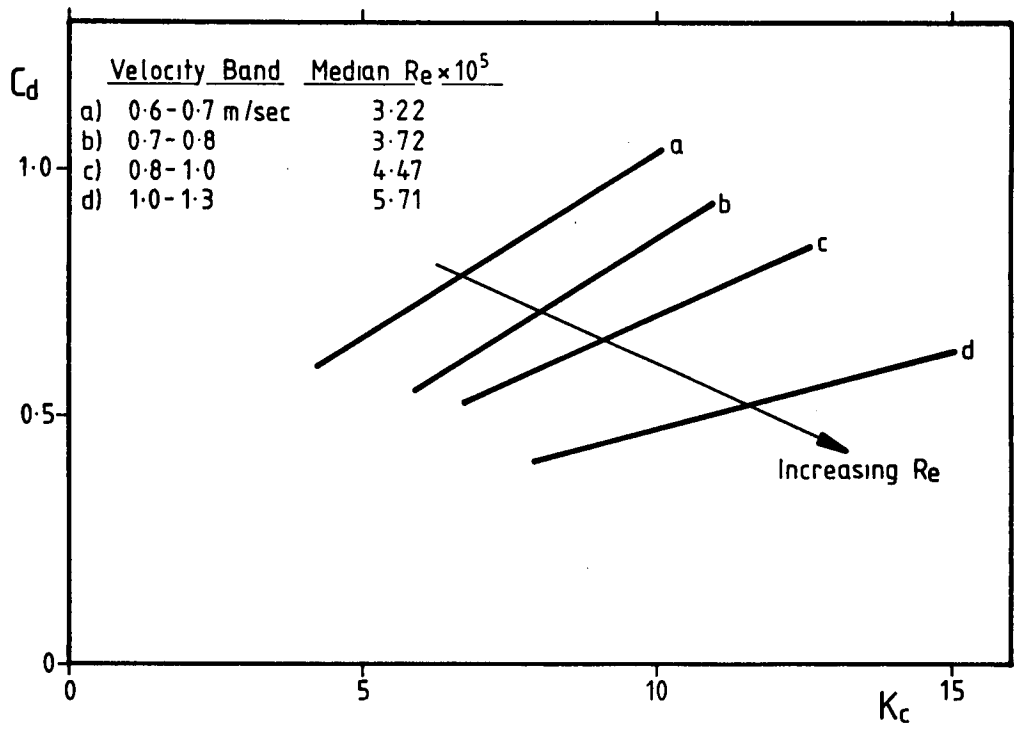


Figure 3.2.45. C_d and C_m values from Forties Field (Atkins, 1979)

Table 3.2.9 - C_d values for two ranges of R_e , Eugene Island Experiment
(Gaston and Ohmart, 1979)

Subset	C_d
$1 \times 10^6 < R_e < 3 \times 10^6$	0.70
$R_e > 3 \times 10^6$	0.86

Table 3.2.10 - C_m from Eugene Island experiment (Gaston and Ohmart, 1979)

Subset	C_m
All data	1.06
Data better conditioned for accurate determination of C_m	1.37

These C_d and C_m values were then used to predict the force peaks occurring in the time history. This resulted in an underestimate of the measured force as shown in Table 3.2.11.

Table 3.2.11 - Measured/predicted peak forces and coefficient of variation obtained by applying C_d and C_m , based on the loading time history, to the peaks of load, Eugene Island experiment (Gaston and Ohmart, 1979)

C_d for R_e $3-10 \times 10^5$	C_d for R_e $1-3 \times 10^6$	C_m	Measured / Predicted Peak Force		
			Median	Mean	Coefficient of variation
0.07	0.07	1.37	1.09	1.14	0.305
0.86	0.07	1.37	1.07	1.11	0.304

f) Pearcey: Tests in the sea

Pearcey et al (1985) reports a comparison of wave forces on a smooth and rough cylinder placed in the sea off a pier. The results are shown in Figure 3.2.46. The effect of hard roughness and seaweed is to increase the forces applied to the cylinder. Seaweed resulted in a 40% increase in loading. Hard roughness ($k/D = 1/200$) resulted in an 11% increase in the rms value of the load and a 40% increase in the maximum loads recorded in 10 minute samples.

3.2.10 Summary and discussion of C_d and C_m results for circular cylinders

a. Steady flow

The research based on steady flow has shown how the flow regime around a cylinder may be classified as subcritical, critical, supercritical or post-supercritical. The regime is primarily dependent on Reynolds number but is also affected by cylinder surface roughness and by turbulence in the incident flow. Most flows of significance for total loading on offshore structures are post-supercritical. C_d in steady flow is dependent on the flow regime and the surface roughness. For smooth cylinders in post-supercritical flow $C_d = 0.68$. For cylinders roughened by hard marine growth the roughness to diameter range is likely to be $k/d = 1/1000$

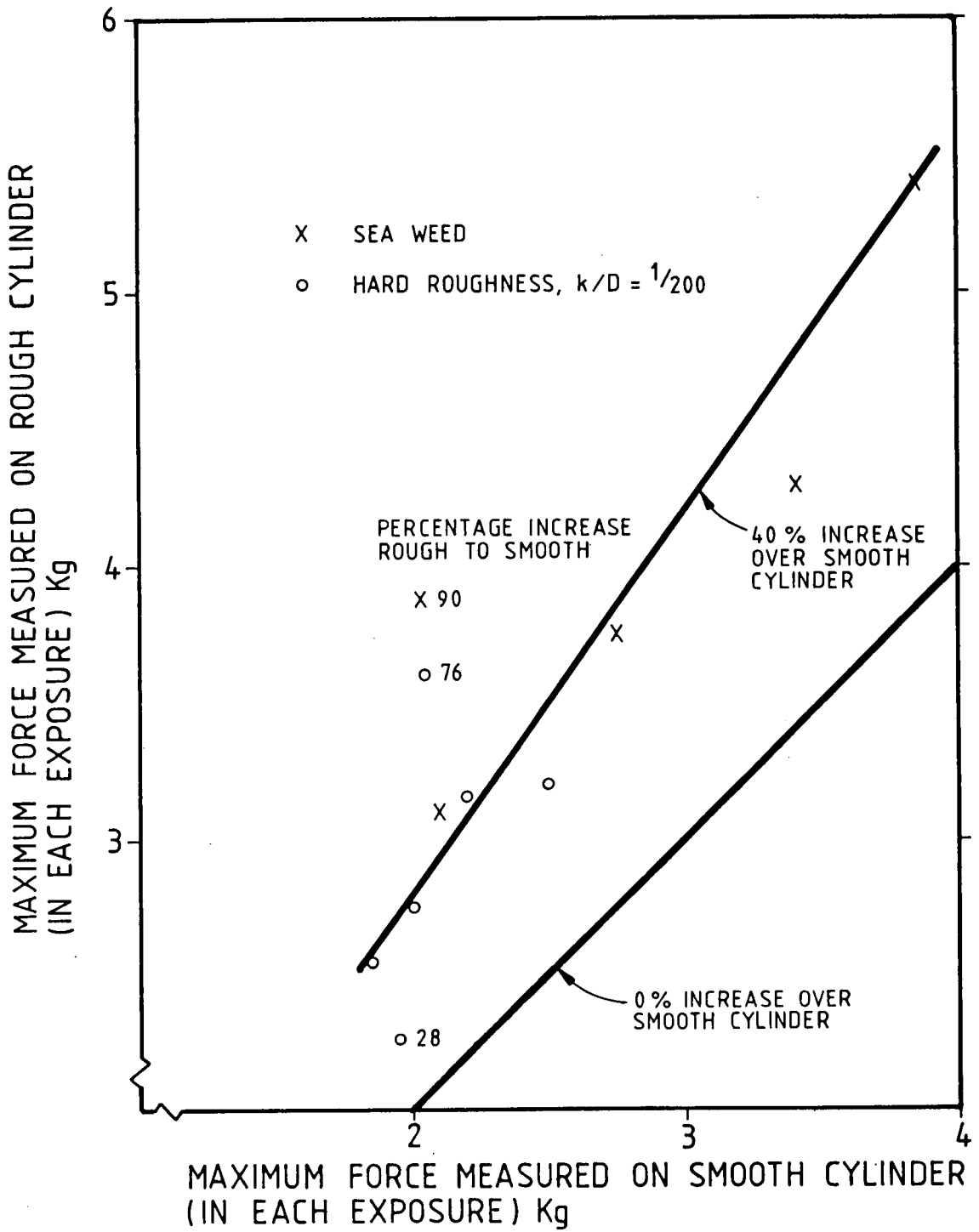


Figure 3.2.46a Forces measured on smooth and rough vertical cylinders in the sea (Pearcey, 1985)

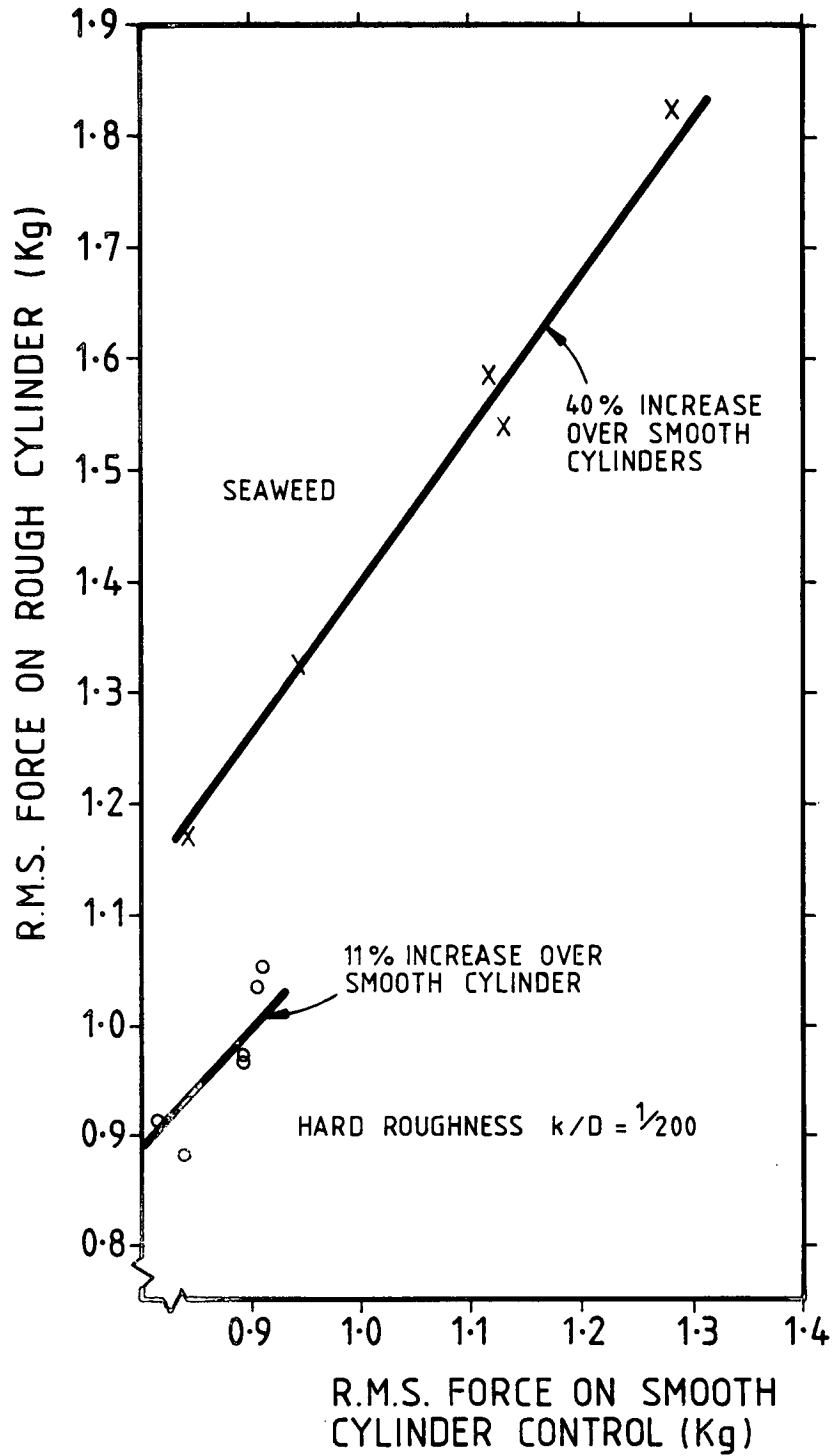


Figure 3.2.46b. Forces measured on smooth and rough vertical cylinders in the sea (Pearcey, 1985)

to 1/20 in which the steady flow C_d varies from 0.8 to 1.1. Soft compact marine growth (sea anemones' etc) and long kelp seaweed also increase C_d considerably. Values of $C_d = 1.2$ and 1.34 have been measured for the two types of fouling. (Wolfram and Theophanatos, 1985).

Work in steady flow has also established the independence principle which states that the normal pressure force is independent of any component of the incident velocity which is parallel to the axis of the member. However the experiments have shown that the location of the critical regime is most closely related to the R_e of the full incident flow velocity and not the resolved normal flow velocity (Bursnall and Loftin, 1951).

b. Accelerating flow

C_m may be calculated theoretically: for inviscid accelerating flow around a circular cylinder $C_m = 2.0$ and the independence principle applies to the normal force. However, if there is a component: \dot{U}_a of the fluid acceleration which is parallel to the axis of the member this will produce an additional, non Morison, force approximately equal to $\rho V \dot{U}_a$, where V is the volume of the member. This force is small and is not usually taken into account in jacket design and analysis.

C_m values in accelerating flow are similar to the theoretical value of 2 but may increase with marine growth to about 2.3 (Wolfram and Theophanatos, 1985). (However, values of C_m measured in waves are generally less than 2).

c. Planar oscillating flow

Sarpkaya (1976 a,b) has for this type of flow, determined the effect of R_e , K_c and roughness on C_d and C_m . The C_d value for a smooth cylinder in postcritical oscillating flow is approximately the steady flow value. However, the rough cylinder C_d values are much higher 1.7 to 1.9 at $k/D = 1/50$ for which the steady flow C_d would be 1.1. Studies of planar oscillating flow with current (Sarpkaya and Storm, 1985) show that C_d is reduced by the current towards the steady flow value. C_m values for rough cylinders in planar oscillating flow decrease with roughness.

C_d values determined in oscillating flow have been found to be much higher than the average C_d values in waves. This is probably caused by the repeated re-encounter of the cylinder by its own wake which occurs in the oscillating flow experiments but, because of the effects of small currents and random seas, only occurs at very low K_c in the real sea. At very high K_c the oscillating flow C_d values do become equal to the steady flow C_d values.

d. Simulated wave flow

Cylinders propelled around elliptical paths in, initially, still water simulate horizontal cylinders in waves. The results of these experiments have shown that as the ellipticity increases C_d and C_m reduce from the planar oscillating flow values. The reduction in C_d may be caused purely by the stirring action of the orbiting cylinder, which reduces the relative velocity of the cylinder and water. The reduction in C_m is probably caused by potential flow lift forces acting against the inertia force (Holmes and Chaplin, 1978) although Grass et al (1984) suggest that the reduction in C_m may be caused by the drag force being imperfectly in phase with the velocity and cancelling part of the inertia force.

e. Vertical cylinders in waves : post-supercritical flow

The mean results of the vertical cylinder experiments in waves are summarised in the following figures:-

- Figure 3.2.47 C_d for clean vertical cylinders
- Figure 3.2.48 C_d for rough vertical cylinders
- Figure 3.2.49 C_m for clean vertical cylinders
- Figure 3.2.50 C_m for rough vertical cylinders
- Figure 3.2.51 C_f for vertical cylinders

The various results for C_f , the total force coefficient show a generally similar trend with Keulegan Carpenter number. The Forties data appears to show a different trend. This is probably caused by the method of data analysis as discussed in 3.2.9d. In general the rough cylinders have a higher loading than the smooth cylinders and the difference is greatest at the higher values of K_c .

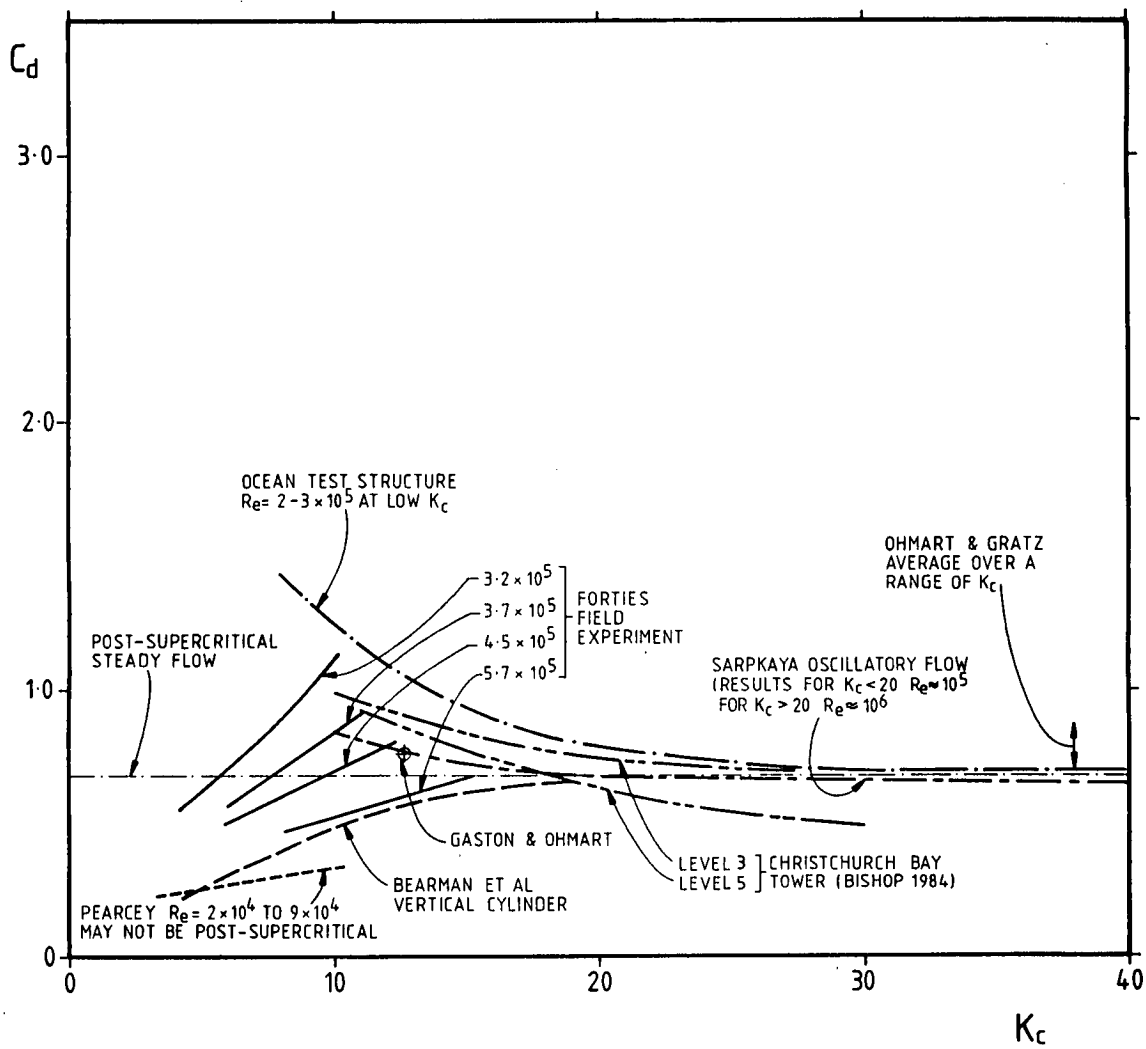


Figure 3.2.47. C_d for clean vertical cylinders in post-supercritical flow

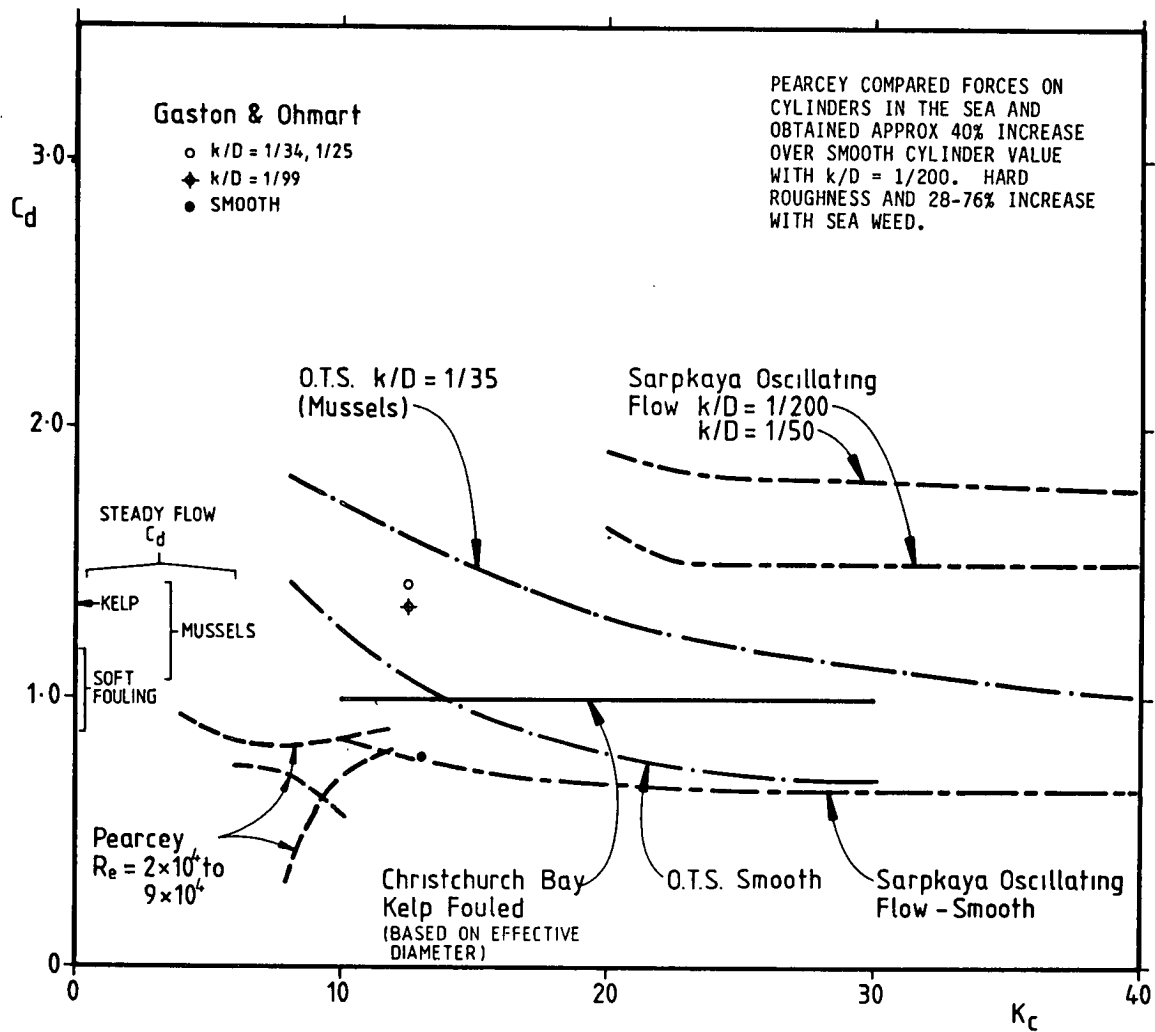


Figure 3.2.48. C_d for rough vertical cylinders in post-supercritical flow

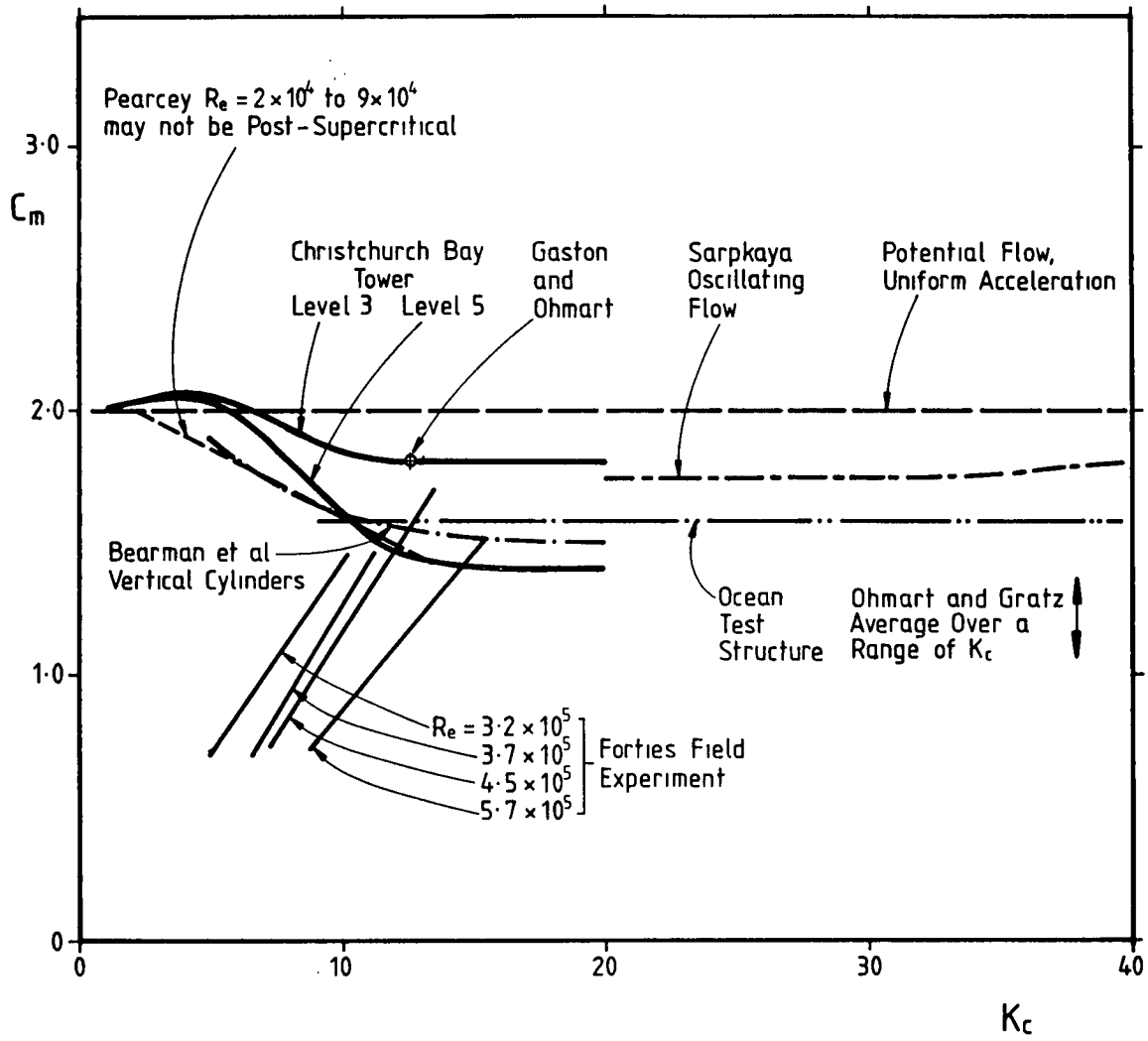


Figure 3.2.49. C_m for clean vertical cylinders in post-supercritical flow

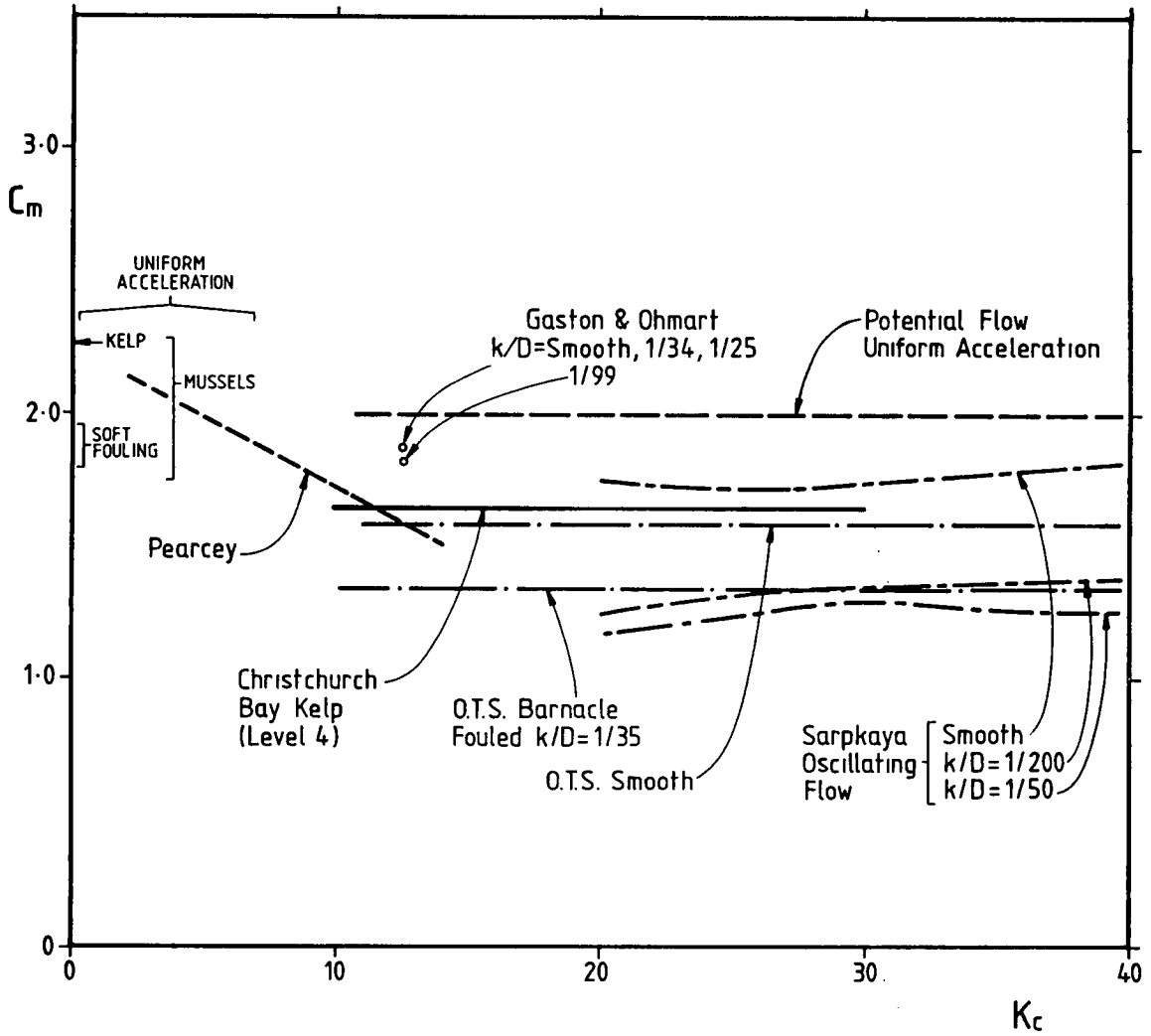


Figure 3.2.50. C_m for rough vertical cylinders in post-supercritical flow

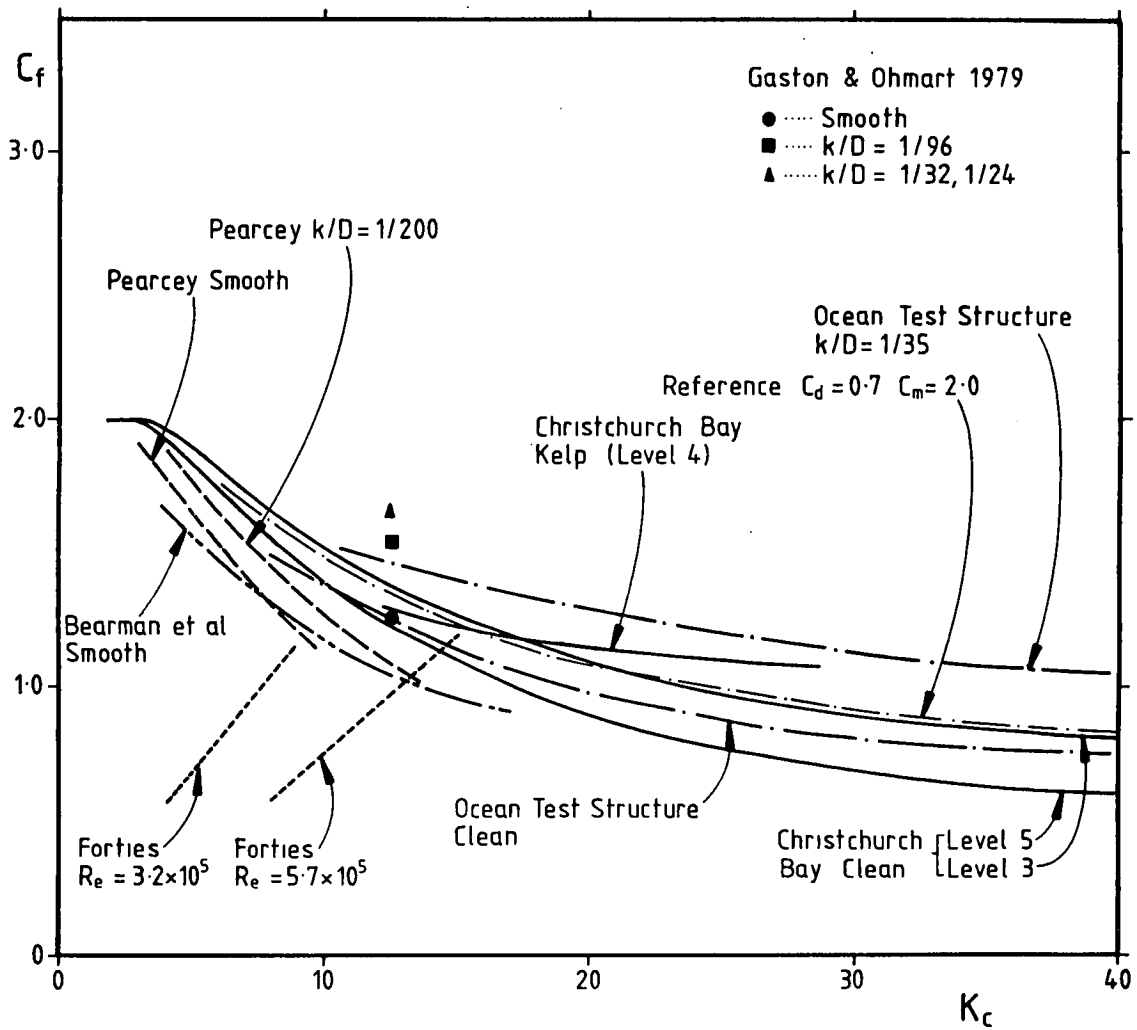


Figure 3.2.51. C_f for vertical cylinders

The OTS clean curve (Heideman et al, 1979) is very similar to the Christchurch Bay (Bishop, 1984) clean curves but the laboratory experiments by Pearcey et al (1985) and Bearman et al (1985) have produced slightly lower total force coefficients.

The Christchurch Bay results for C_f , C_d and C_m reduce with depth. The reason for this is not known but the difference is significant.

At small K_c the OTS results show a lower C_f than the Christchurch Bay results. This is associated with the lower C_m values determined at the OTS than at Christchurch Bay. Also at small K_c , Bearman's C_f is lower than both the OTS and Christchurch Bay values. This is associated with the very much lower C_d determined by Bearman. The reason why this C_d is much lower is not known although Sarpkaya (1986) has suggested that it might be caused by currents in the wave flume.

At high K_c the smooth and rough cylinder C_d values correspond to the steady flow values. These are much lower than the rough cylinder C_d values obtained by Sarpkaya (1976b). The reason for this is discussed in 3.2.10.c.

C_d and C_m for kelp fouled vertical cylinders have been determined at Christchurch Bay (Bishop, 1987). The results, after allowing for 50mm effective thickness of marine growth were $C_d = 1.0$, $C_m = 1.66$ for K_c in the range 10 to 30. These compare with $C_d = 0.81$ and $C_m = 1.55$ for a smooth cylinder at the same location and $K_c = 15$.

All the results for C_d and C_m measured in waves show considerable scatter. Various reasons have been put forward for this scatter; Heideman et al (1979) suggest that the randomness of the re-encounter of the wake with the cylinder itself, and with the velocity meters may cause the scatter. Sarpkaya and Cakal (1983) show that currents have an effect on C_d which explains some of the scatter. Starsmore (1981) suggests that some of the scatter may be caused by Reynolds number effects.

f. Horizontal cylinders in waves : post-supercritical flow

The mean results of the horizontal cylinder experiments in waves, and simulated waves are summarised in the following figures:-

Figure 3.2.52 C_d for horizontal cylinders

Figure 3.2.53 C_m for horizontal cylinders

Figure 3.2.54 C_f for horizontal cylinders

Teng and Nath's (1985) data suggests that the drag coefficient for horizontal cylinders corresponds approximately to the steady flow value. Holmes and Chaplin's (1978) smooth cylinder data is in the range 0.5 to 0.75. This shows a variation with K_c and R_θ but a steady flow coefficient of about 0.66 would match the data reasonably. Bearman et al (1985) show that C_d may be higher at K_c less than 10 but C_d is not important at these values of K_c . Pearcey's (1985) horizontal cylinder C_d is somewhat variable but again not important at the low K_c values.

The C_m values from Bearman et al and Holmes and Chaplin show a tendency to decrease as K_c increases. (Holmes and Chaplin explain this as being caused by lift forces counteracting the inertia force). The Christchurch Bay and Teng and Nath results do not show the same tendency. Also Bearman et al shows that their results are not sensitive to the ellipticity of the flow whereas increased ellipticity would be expected to reduce the lift forces.

Pearcey's results show large values of C_m at very low K_c which reduce very rapidly with increasing K_c . Pearcey's results for both the smooth and rough cylinder link well with the results of Teng and Nath.

The Christchurch Bay clean horizontal cylinder C_m of 1.5 is very similar to the vertical cylinder C_m values for the same level at Christchurch Bay and much larger than Teng and Nath's value of 1.0.

Overall there is no clear pattern to the horizontal cylinder C_m results. The highest values of C_m , obtained for smooth cylinders by Bearman et al and at Christchurch Bay by Bishop, are similar to the vertical cylinder results from the same experiments. The large reduction of inertia force that occurs in the smaller scale laboratory tests does not seem to occur in the larger scale experiments.

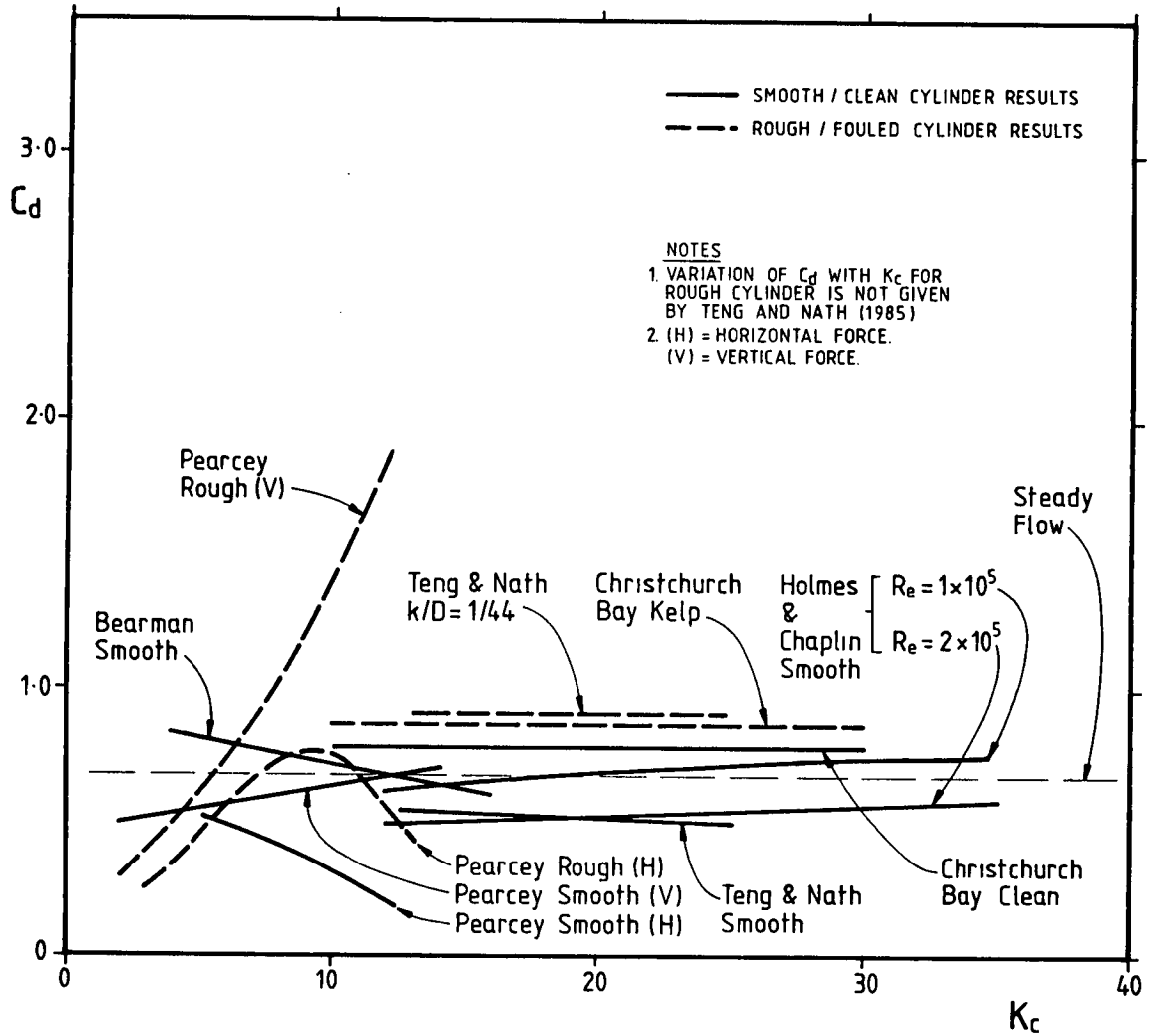


Figure 3.2.52. C_d for horizontal cylinders

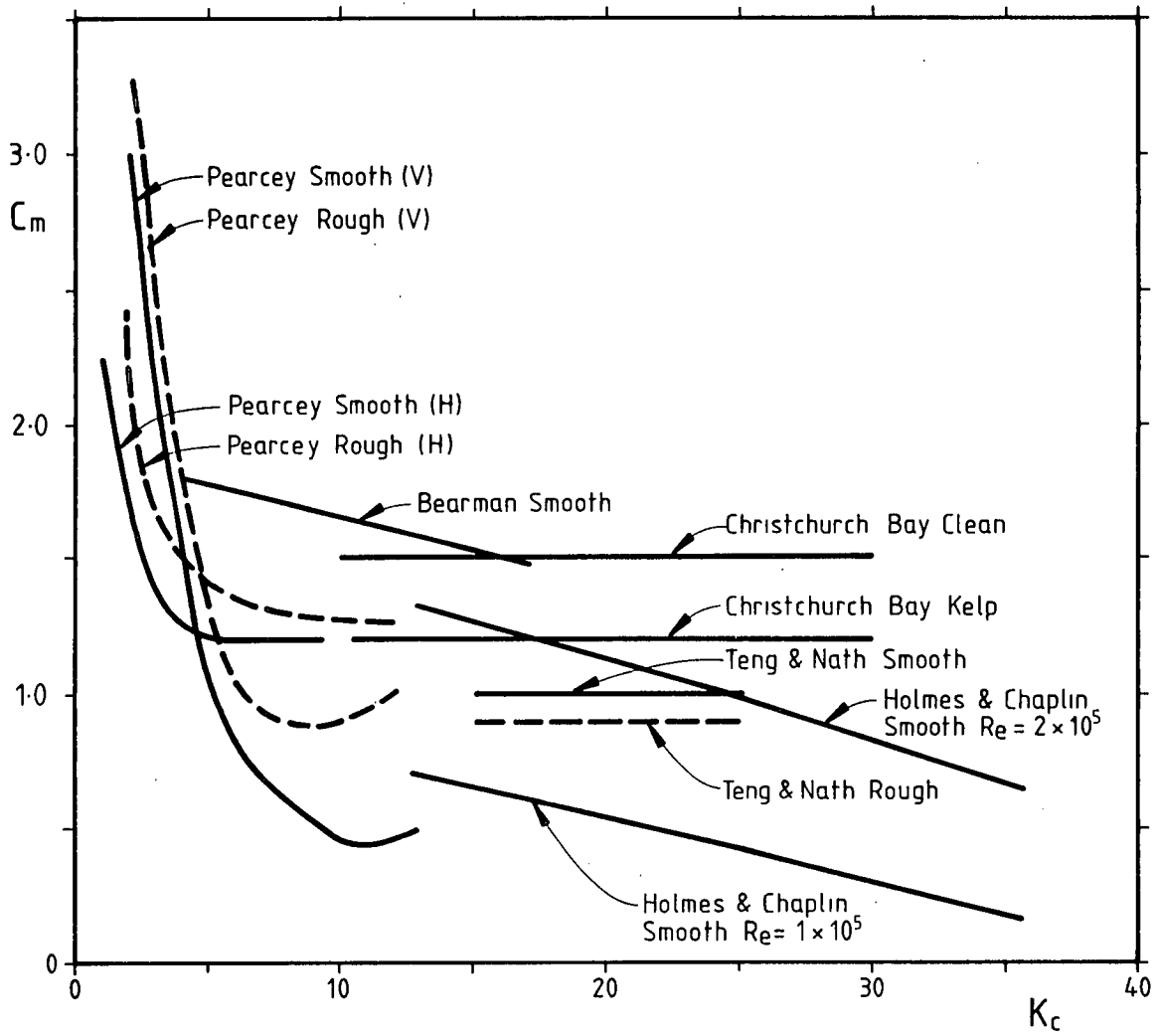


Figure 3.2.53 C_m for horizontal cylinders

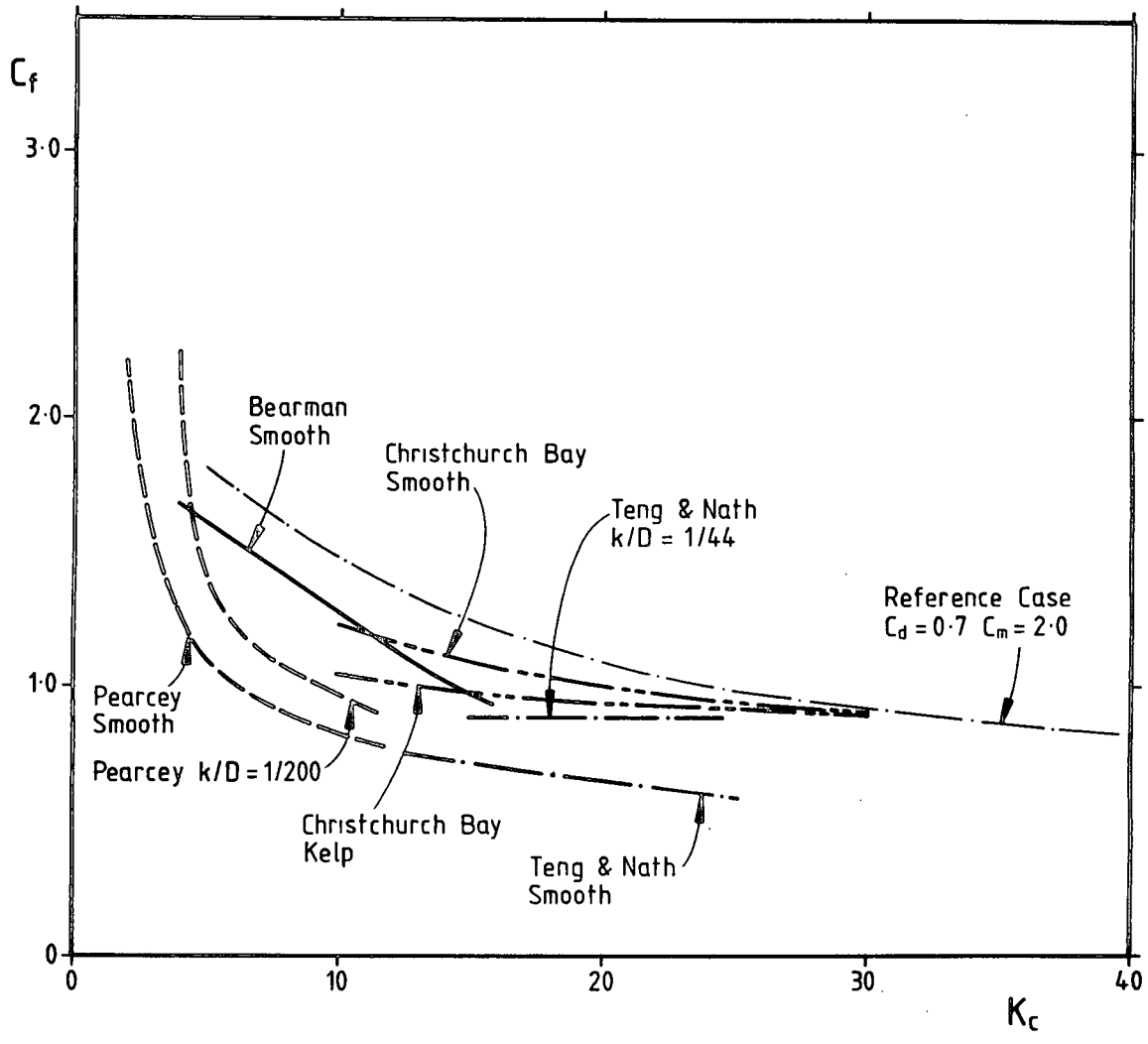


Figure 3.2.54. C_f for horizontal cylinders

The C_d values obtained for smooth and rough horizontal cylinders are similar to the steady flow C_d values.

Both the C_d and C_m values obtained at Christchurch Bay for the kelp fouled horizontal cylinder are lower than the values for the vertical cylinder. We speculate that this might be caused by the wave action around the vertical cylinder wafting the seaweed backwards and forwards whereas the seaweed will tend to be wound around the horizontal cylinder by the wave action.

g. Cylinders in waves with current : post-supercritical flow

C_d values are affected by the presence of currents as shown by Sarpkaya and Storm (1985) for oscillating flow, Sarpkaya and Cakal (1983) for vertical cylinders and Teng and Nath (1985) for horizontal cylinders. As the current increases, towards the maximum wave particle velocity, C_d tends to the steady flow value (see Appendix H). In oscillating flow Sarpkaya and Storm also find an effect of current on C_m . However in waves neither Sarpkaya and Cakal nor Teng and Nath found any significant relationship between C_m and current.

Since the Christchurch Bay and OTS C_d coefficients were measured in the presence of currents there is a possibility that higher average C_d and C_f values could occur at sites where the current velocities are smaller, relative to the wave particle velocities. Fortunately, the largest effect of current on C_d appears at low values of K_c where C_m is dominant and the currents required to produce the lower C_d values are not very large (see Appendix H) so the importance of the effect is reduced.

h. Effect of roughness and marine growth on C_d and C_m

In general, for the various types of flow, roughness causes an increase of C_d and a reduction in C_m .

Figure 3.2.55 shows the effect of surface roughness on C_d as determined in a large number of experiments. It is clear that the effect of roughness on C_d is dependent on the flow characteristics as well as on k/D . Oscillating flow results in much larger rough cylinder C_d values than either steady flow or wave flow. This is probably caused by the repeated wake re-encounter that occurs in oscillating flow conditions but is reduced in wave flow and does not occur in steady flow. Increasing K_c reduces the rough cylinder C_d both for oscillating flow and wave flow. This is again explainable in terms

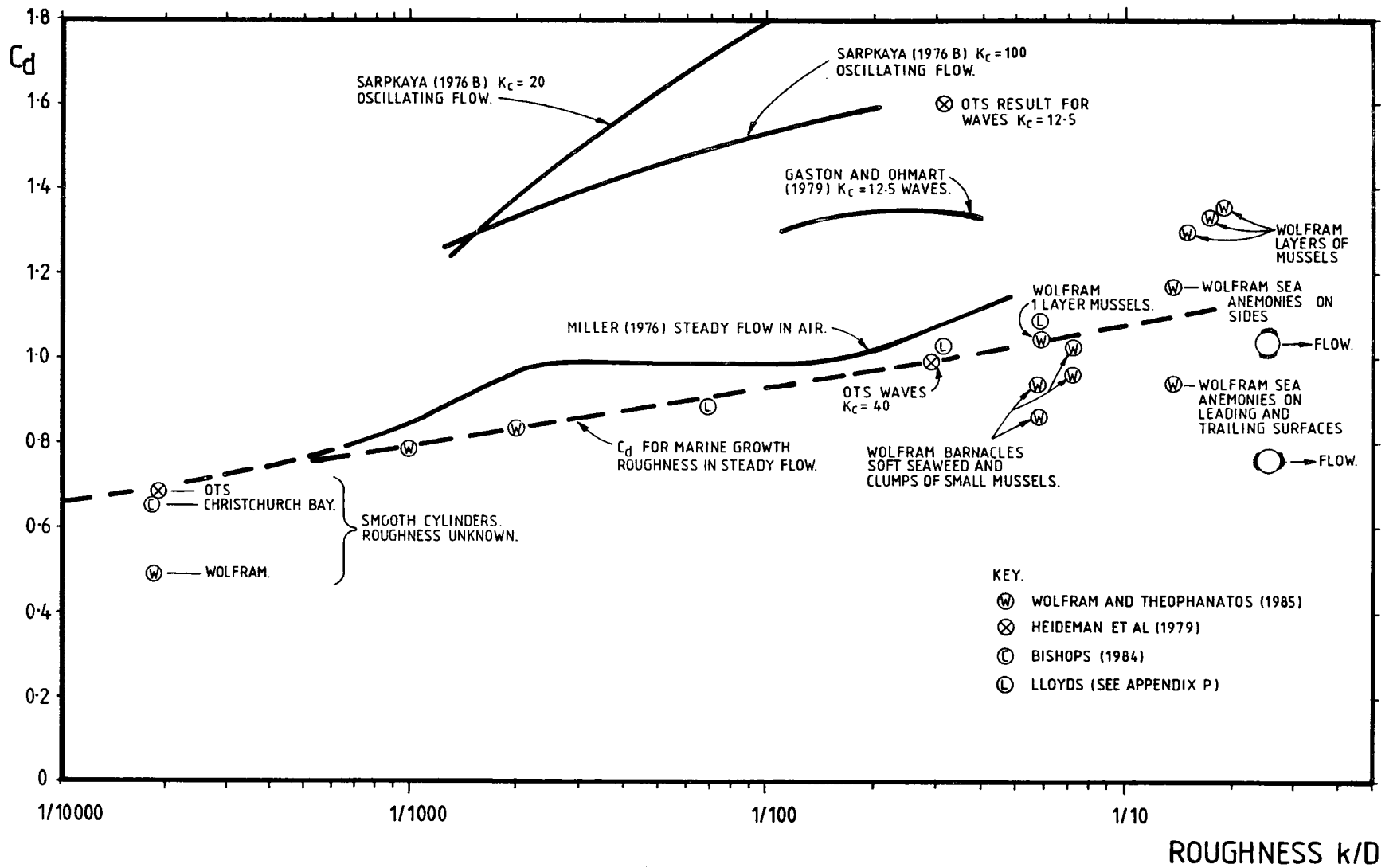


Figure 3.2.55. Effect of surface roughness on C_d

of reduced probability of wake re-encounter as the orbit size to member size ratio increases. Also the vorticity in the wake must decay with time and the re-encountered wake in a large orbit (large K_c) may be less strong than the wake in a small orbit.

The steady flow C_d values from Wolfram and Theophanatos (1985) are lower than the values from Miller (1976). This may be because the characteristics of marine growth give slightly lower coefficients than the artificially roughened cylinders that were the basis of most of Miller's results. It is clear from the results that the nature of the marine fouling considerably affects C_d and that the simple measure of k/D gives a good first indication of the effect. We have plotted a straight line relationship between C_d and $\log(k/D)$. This may underestimate C_d at k/D greater than 0.1.

The OTS rough cylinder C_d value at high K_c corresponds well with Wolfram's data. This suggests that C_d results for steady flow may be applied to high K_c wave flow.

C_m values (Figure 3.2.56) tend to reduce with roughness as shown by Sarpkaya's (1976b) results for oscillating flow and, to a limited extent, Wolfram's (1985) results for accelerating flow. Note, however the high k/D results are very sensitive to the assumed area in Morison's equation and at present it would be unwise to draw too firm a conclusion from the C_m values at high k/D .

At low K_c where C_m is most important we would expect the flow to be similar to the accelerating flow conditions of Wolfram and Theophanatos (1985).

i. Subcritical and critical flow

In steady subcritical flow, at R_θ from about 10^3 to 4×10^5 for a smooth cylinder, the value of C_d is about 1.2 (see Figure 3.2.7). For rough cylinders and turbulent incident flow the upper value of R_θ may reduce but the C_d value remains at 1.2.

In critical and supercritical steady flow C_d for a smooth cylinder drops to a value lower than both the subcritical and post supercritical value. Because of the uncertainty in the value of R_θ corresponding to these lower values of C_d it is preferable to use the post-supercritical value of C_d in the critical and supercritical range. The post-supercritical value is dependent on the surface roughness, see Figure 3.2.8.

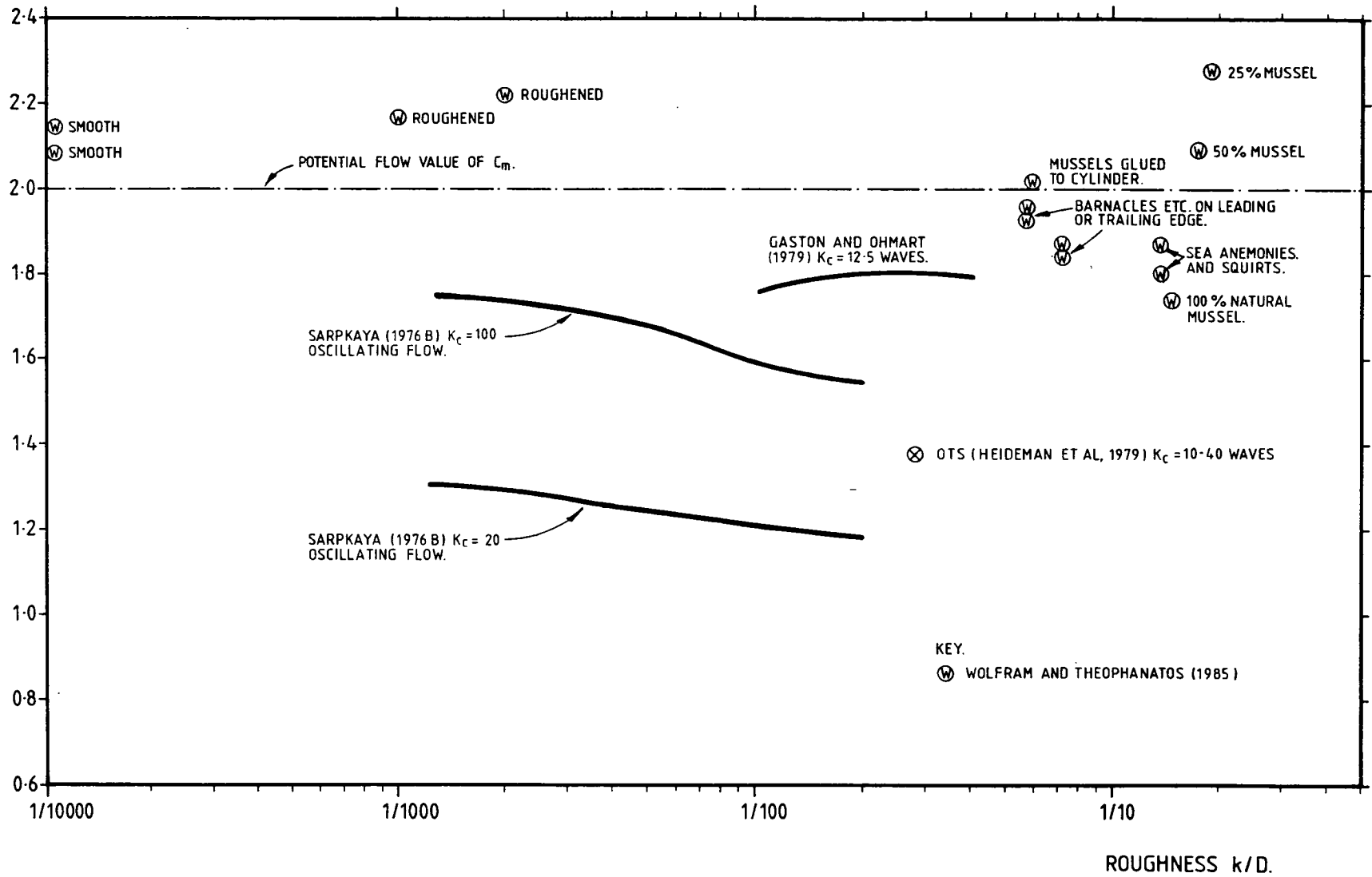


Figure 3.2.56. Effect of surface roughness on C_m

For subcritical wave flow a large number of experimental results are available, e.g. Bullock (1983), Chakrabarti (1982), Cotter and Chakrabarti (1984). These results show that the drag coefficient on cylinders in subcritical wave flow is dependent on K_c and member inclination. At K_c greater than 30, C_d is found to be about 1.2, for smooth and rough cylinders. At K_c of 10 to 20 higher values of C_d , typically 2.0 to 2.5, are often found and roughness may increase the C_d value.

C_m values in subcritical flow are typically approximately 1.0 to 1.5 at K_c greater than 20. C_m increases to between 2.0 and 2.5 as K_c approaches 0. C_m values do not seem to be affected by roughness.

Usually drag and inertia loading in subcritical wave flow is of little importance.

3.2.11 The Selection of C_d and C_m for Circular Cylinders in Waves and Current

a. General

These recommendations are in two parts. This first part gives estimates of C_d and C_m , for post critical flow, as variables dependent on roughness or marine growth, K_c and current. These values are deduced from the experimental data described previously. The second part again for post critical flow (Section 3.2.12) gives approximate values for C_d and C_m which are dependent on roughness or marine growth alone but which, to the accuracy with which we are able to predict fluid loading, produce the same loading on the structure over the whole range of K_c .

C_d and C_m values have been selected as pairs because different analysis techniques may result in different C_d and C_m for the same total force.

We have aimed to recommend sets of C_d and C_m values (for different roughnesses etc.) which show consistent trends between sets. This has meant that the recommended values do not necessarily correspond to any single experiment.

Current affects C_d and C_m . This is discussed in Appendix H. The conclusion, Section 3.2.11 g takes into account the effects of current.

On the basis of the discussion in 3.2.10f we have generally not made separate recommendations for horizontal and vertical cylinders. Although there are some indications of differences in their C_d and C_m values these differences are much smaller in the large scale experiments, at the Delft Flume and Christchurch Bay, than in the smaller scale laboratory experiments. However, when more research has been performed it would be appropriate to make specific recommendations for horizontal cylinders.

The exception to the above is kelp fouled cylinders where the C_d and C_m values are apparently lower for horizontal cylinders than vertical cylinders and this is taken into account in our recommendations.

The resulting coefficients are our best estimates of the likely mean C_d and C_m values. However, knowledge of fluid loading in waves is still evolving and further research is needed in order to understand better how the many variables affect fluid loading.

b. Clean cylinders

The Christchurch Bay C_d and C_m values are the most detailed available from measurements in the sea. They benefit from the two sizes of cylinder used for the experiments and correspond reasonably with the OTS values. It is unfortunate that the difference between the levels is still unexplained but the level 3 results were obtained nearest the surface and therefore should be the most significant for design purposes. These level 3 results are the basis of our recommendations. At high K_c the drag coefficient is 0.66 which is very close to the steady flow value. At $K_c = 10$, $C_d = 1.0$. For K_c less than 10 the value of C_d has not been determined by the Christchurch Bay experiment but has been set equal to 1. C_m has been determined to be consistent with $C_d = 1$. However, the loading is dominated by C_m in this region and the total force is only slightly sensitive to the value of C_d as shown approximately by the effect on the total force coefficient in Table 3.2.12. Therefore arbitrarily setting C_d equal to one in this range of K_c is acceptable.

The C_m value is close to 2 for low values of K_c and reduces to 1.8 for the higher values of K_c

Table 3.2.12 - Percentage change in total force for a 50% change in C_d at $K_c = 5$ and 7 (clean cylinder coefficients)

K_c	C_d	C_m	C_f	Percentage change
5	1.0	2.04	1.875	
5	1.5	2.04	1.942	+3.6%
7	1.0	1.91	1.637	
7	1.5	1.91	1.771	+8.2%

c. Rough cylinders

The most useful data for rough cylinders in waves has come from the Ocean Test Structure. This has shown that C_d increases to about 1.5 times the smooth cylinder value and C_m reduces to about 0.85 times the smooth cylinder value for a k/D of 1/35.

This C_d value for the rough cylinder at high K_c corresponds approximately with the steady flow rough cylinder drag coefficient. The smooth cylinder, high K_c , C_d values were also similar to the steady flow values. At large K_c we therefore assume that, for other values of k/D the marine growth steady flow C_d values from Figure 3.2.55 could be applied. This is a linear relationship between C_d and $\log(k/D)$.

For K_c greater than 12 the C_m value for a $k/D = 1/35$ cylinder was assumed to be equal to 0.85 times the clean cylinder value on the basis of the OTS results. Again values of C_m for other k/D have been obtained by assuming a linear relationship between C_m and the logarithm of k/D . For K_c less than 12 Pearcey's results suggest the rough C_m could be greater than the clean C_m . As K_c becomes small vortex effects should reduce because vortices do not have time to form. We anticipate that this will result in the inertia coefficient becoming independent of roughness and we have therefore brought all C_m values to the common value of 2.0 at $K_c = 0$.

d. Compact soft fouled cylinders

The only data available for soft fouling is that obtained by Wolfram and Theophanatos (1985). This shows C_d and C_m values for soft fouling to be similar to those that would be obtained for hard fouling with a similar roughness height.

e. Kelp fouled vertical cylinders

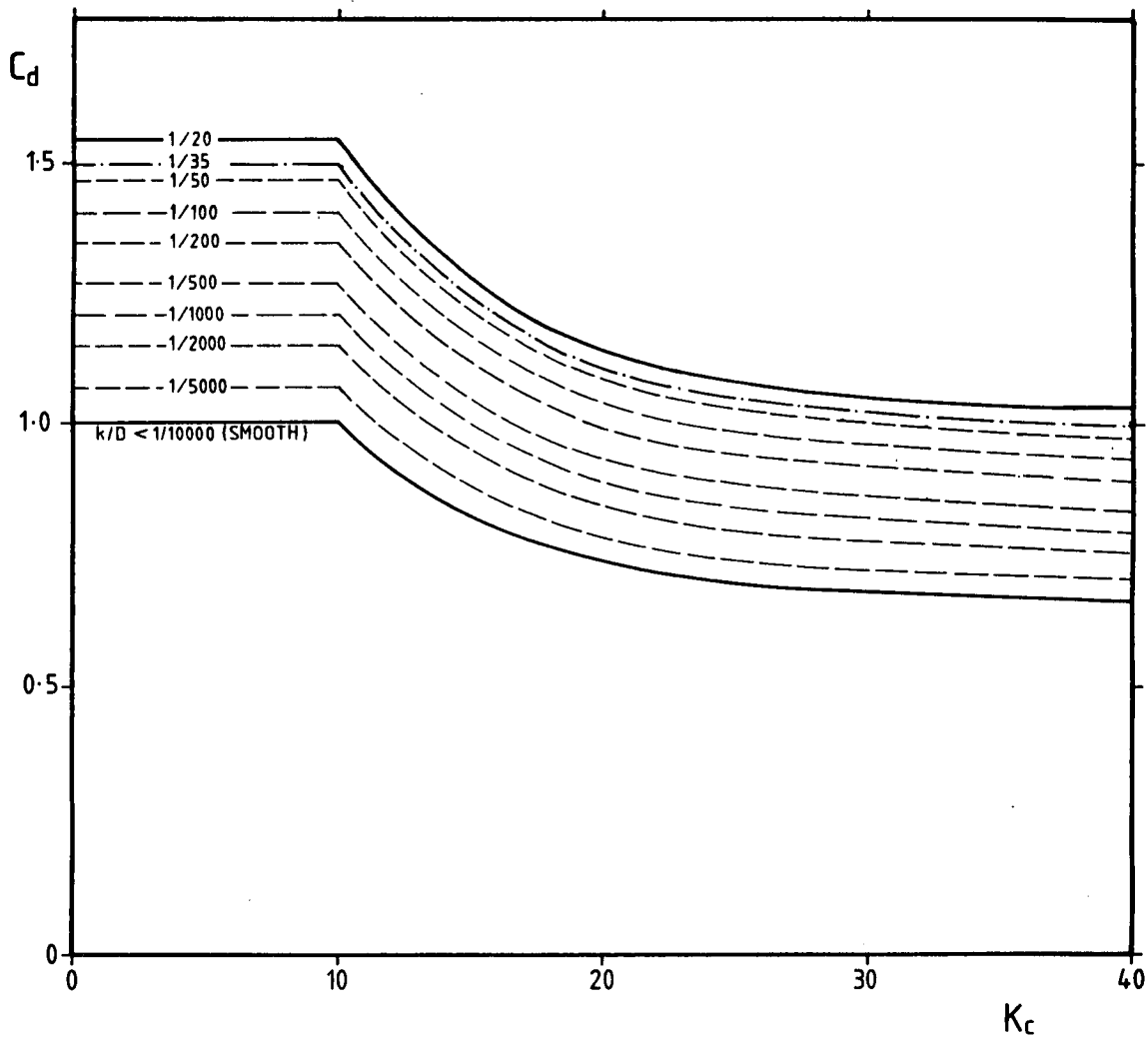
The Christchurch Bay experiment obtained $C_d = 1.0$, for a kelp fouled cylinder, with K_c in the range 10 to 30, at level 4. However at $K_c = 20$ the level 4 smooth cylinder C_d value was 7% less than the level 3 C_d value. The level 3 results have been used as the basis for the smooth and rough cylinder curves. Therefore, for consistency, the recommended kelp C_d value has been increased by 7% to 1.07. Wolfram and Theophanatos obtained C_d values of 1.30 and 1.34 for kelp fouled cylinders in steady flow. These C_d values may be higher than the Christchurch Bay values because of the different characteristics of the steady and wave flows around kelp fouled cylinders or there may be some difference in the nature of the kelp fouling. However, preference was given to the Christchurch Bay data since it was a test in waves. The C_m values for the kelp fouled vertical cylinder at Christchurch Bay level 4 are 1.66. Allowing again for the difference between the level 4 and level 3 clean cylinder results the kelp fouled C_m has been increased by 16% to 1.92. Wolfram and Theophanatos obtained C_m values of 2.26 and 2.27 in accelerating flow. This difference is similar to the difference in the drag coefficients. Again preference was given to the Christchurch Bay C_m data.

f. Kelp fouled horizontal cylinders

The recommended values of C_d and C_m have been taken directly from the Christchurch Bay experiment. C_d was found to be 0.87 and C_m 1.20 over the range of K_c from 10 to 30 (after allowing for an assumed 50mm thickness of marine growth).

g. Conclusion

Based on the discussion in 3.2.11 we have prepared Figures 3.2.57 and 3.2.58 as our best estimate of C_d and C_m values in waves with moderate currents. For current alone and post supercritical flow our best estimate of C_d is given by the dotted line in Figure 3.2.55. For wave plus current a gradual reduction from the wave C_d to the steady flow C_d could be made (see Appendix H). The steady flow C_d should be applicable when



- Notes
- 1) For kelp fouling C_d may be taken as 1.07 for vertical cylinders
0.87 for horizontal cylinders based on data for $15 < K_c < 30$
 - 2) In the presence of current C_d may be reduced as described in
3.2.11g
 - 3) Diagram based on logarithmic interpolation between $k/D = 1/35$
and $k/D = 1/10000$

Figure 3.2.57. Best estimate of C_d for cylinders in waves

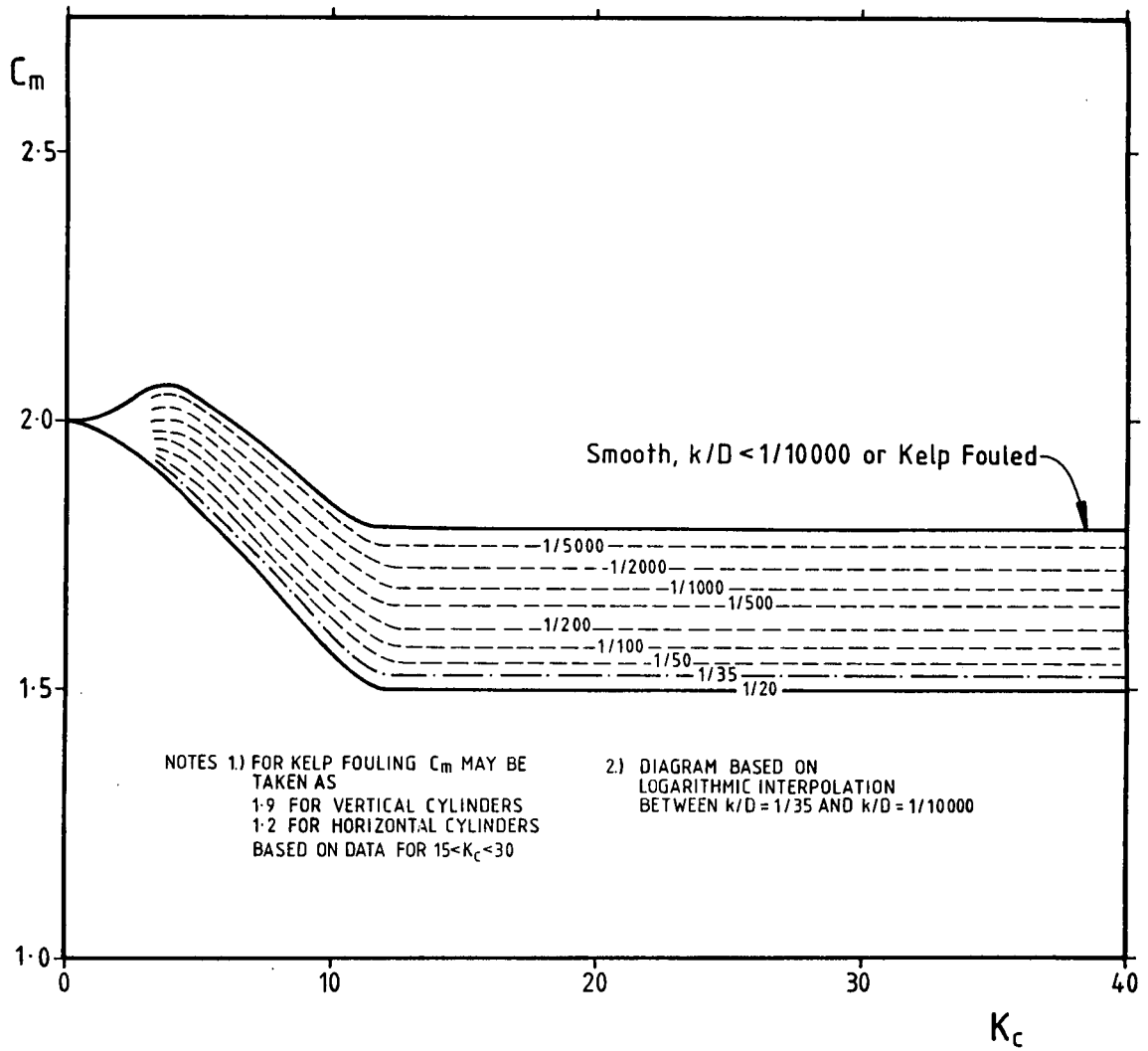


Figure 3.2.58. Best estimate of C_m for cylinders in waves

the current velocity exceeds the maximum wave particle velocity. Current probably has an effect on C_m but the effect is uncertain. We have therefore assumed that C_m is independent of current.

3.2.12 Approximate C_d and C_m values for circular cylinders in waves and currents

In Section 3.2.11 we presented our best estimates of the mean values of C_d and C_m . However, these best estimate values were dependent on Keulegan Carpenter number, roughness and ratio of wave particle velocity to current velocity. When we consider the high scatter in the measured C_d and C_m values this complicated selection of C_d and C_m does not seem justified. Instead we present C_d and C_m values which are dependent on roughness only but will produce, to a reasonable accuracy, the same loading on the structure as the best estimate C_d and C_m values. These approximate coefficients have been obtained, by trial and error, using the total force coefficients C_f for no current, and C_{ft} with current, as a basis of comparison.

The approximate coefficients are given in Figure 3.2.59. The total force coefficients determined using the approximate coefficients and the best estimates from 3.2.11 are compared in Figures 3.2.60 and 3.2.61. The approximate coefficients are seen to be satisfactory.

3.2.13 Drag, inertia and steady lift coefficients non-circular members

a. General

In waves little experimental work has been performed on shapes other than cylinders.

For flat plates, at low R_e , Keulegan and Carpenter (1958) give curves for C_m and C_d . Paape and Breusers (1967) considered the wave force on square pipes but did not derive C_d and C_m values. Wave forces on a sphere have been considered by O'Brien and Morison (1952). They did not recommend any average values and their results are only for R_e less than 10^4 . For spheres Grace and Casciano (1969), from a drag dominant experiment, recommended a value of $C_d = 0.65$ to 0.70 , with an assumed C_m value of 1.15 . The R_e range was 6×10^4 to 3×10^5 and the K_c range 8 to 60 . Sarpkaya (1975) gives C_d and C_m , as functions of K_c , for oscillatory flow around spheres at low R_e .

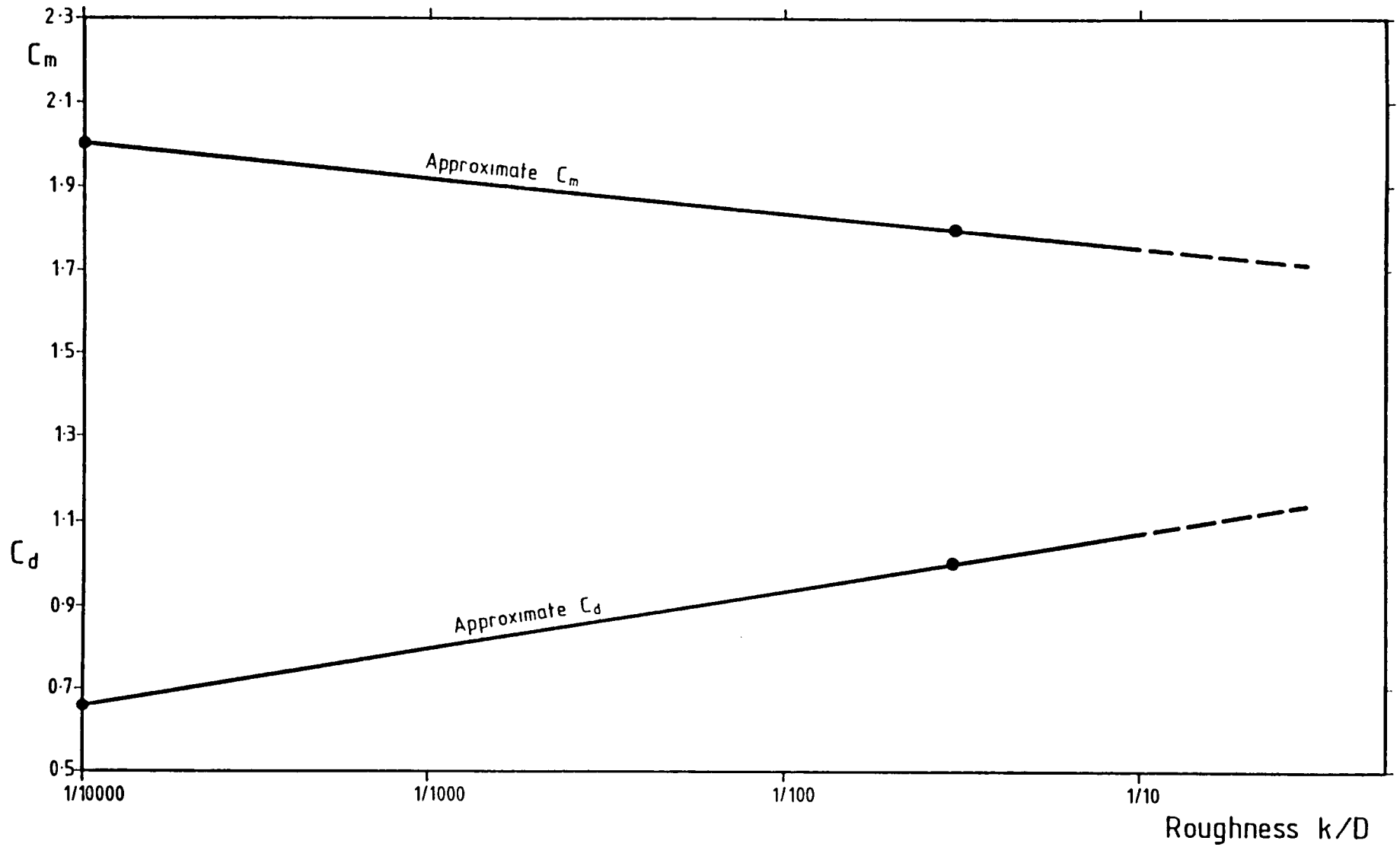
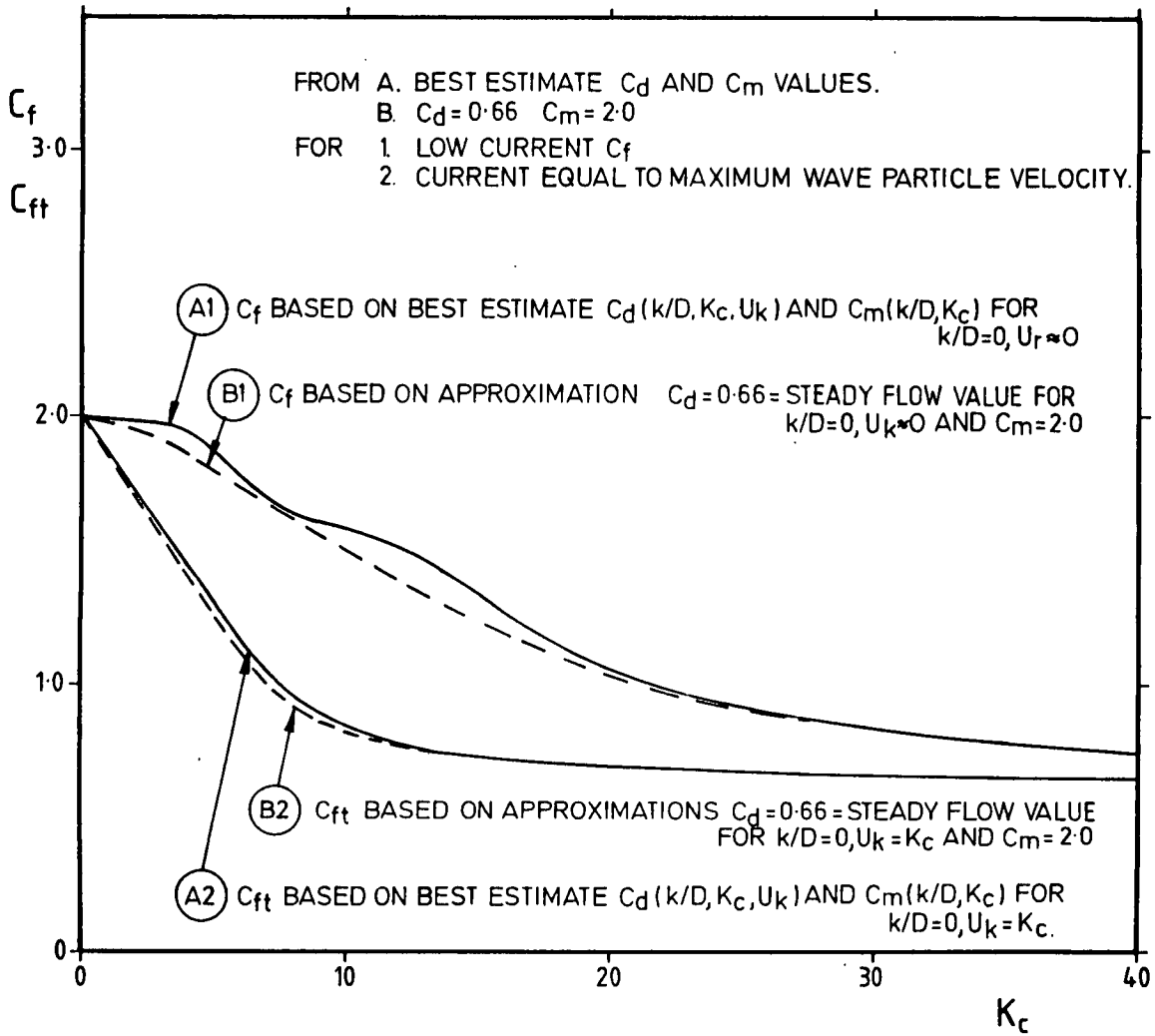


Figure 3.2.59. Approximate C_d and C_m values for all K_c and current in post-supercritical flow



NOTE:- FOR $U_k = K_c, C_d(k/D, K_c, U_k) = 0.66$

Figure 3.2.60. Comparison of total forces:simplified and best estimate smooth cylinders force coefficients

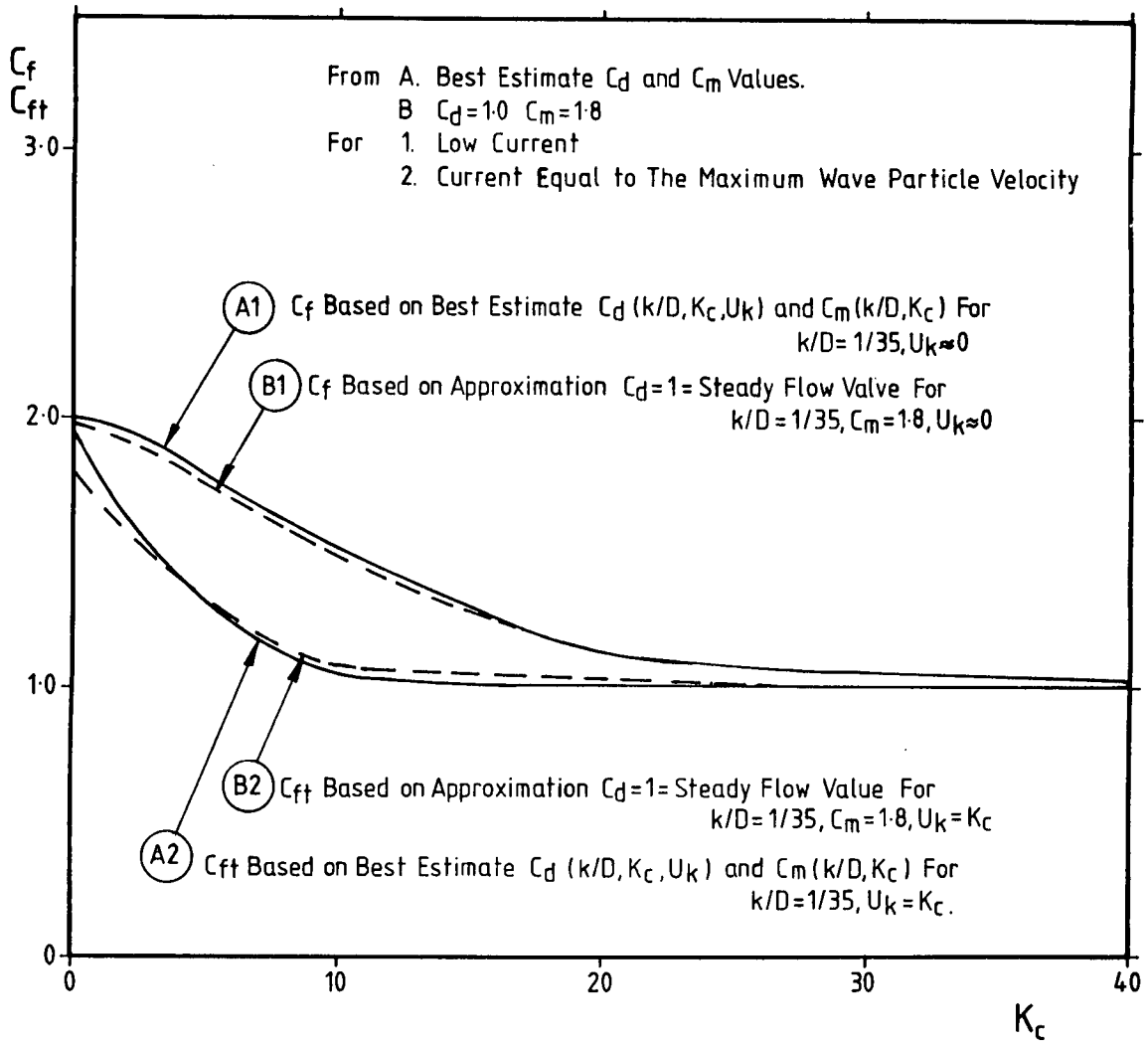


Figure 3.2.61. Comparison of total forces using simplified and best estimate rough cylinder force coefficients

For drag coefficients it is therefore necessary to rely on wind tunnel tests. Delany and Sorenson (1953) present C_d , for R_θ in the range 10^5 to 10^6 , for various 2-dimensional prismatic shapes.

Hoerner (1958), gives C_d value for many shapes at R_θ between 10^4 and 10^6 .

The Engineering Sciences Data Unit (London) has presented a considerable amount of information on prismatic sections and plates for various incident flow directions and Reynolds number. Of particular interest are their data items:-

- 70015 Fluid forces and moments on flat plates
- 71016 Fluid forces, pressures and moments on rectangular blocks
- 82007 Structural members mean fluid forces on members of various cross sections

b. Drag coefficients

Figures 3.2.62 to 3.2.64 present a limited number of results from the above references for post-supercritical steady flow. C_d values for sharp cornered shapes in steady flow are not sensitive to surface roughness. This is apparently because the flow separates from the shape at the sharp corner, independent of the surface roughness. For rectangular prisms with rounded edges we have recommended that the drag coefficients are increased with roughness in proportion to the increase for a circular cylinder. We do not have any test data to justify this recommendation but it would clearly be unconservative to use the smooth drag coefficients for these cases.

Figure 3.2.64 gives coefficients for various rolled sections. In some cases a steady lift force transverse to the flow direction occurs as well as the in line force. This is not part of Morison's Equation. The equation: $F_l = 0.5C_l\rho DU^2$ gives this transverse force, where C_l is the lift coefficient. The data in Figure 3.2.64 is given in terms of the Drag-Lift coefficients C_{dl1} and C_{dl2} which are related to the member axes instead of the flow direction.

Values of C_d and C_l may be derived from C_{dl1} and C_{dl2} as described in the figure but the data is probably more useful in the given form.

c. Inertia coefficients

Inertia coefficients are given for some cases of prisms and plates in Figures 3.2.62 and 3.2.63. These have been based on the added mass values tabulated by Sarpkaya and Isaacson (1981). The values are based on potential flow theory.

Figure 3.2.65 gives first approximation estimates of added mass values and hence inertia coefficients for various built up sections. For flow at some angle to the directions given in the figure, the accelerations may be resolved into the given directions and the total inertia force determined by vector addition.

Figure 3.2.65 refers to Figure 3.2.66 for the added mass of tandem rectangles which is based on Sarpkaya (1960).

d. Consistency

It is important to ensure, when using these, or other, tables of coefficients that the C_d value is consistent with the definition of member width: D and that the C_m value is consistent with the definition of member cross sectional area: A .

Also when using tables of inertia coefficients it is necessary to determine whether the values given are the full inertia coefficients: C_m as defined in 3.2.1 or just the added mass coefficient C_a . Some authors use C_m for the added mass coefficient and C_M for the full inertia coefficient.

Shape	Direction of Flow	ρA	Added Mass (M)	C_a (M/ ρA)	C_m (1+C _a)	C_D
Flat Strip		ρDT	$\frac{\rho \pi D^2}{4}$	$\frac{\pi D}{4T}$	$1 + \frac{\pi D}{4T}$	1.9
Rectangular prisms		B/D				
		0.1 ρDB	$1.14 \rho \pi D^2/4$	8.95	9.95	1.9
		0.2 ρDB	$1.21 \rho \pi D^2/4$	4.75	5.75	2.0
		0.5 ρDB	$1.36 \rho \pi D^2/4$	2.14	3.14	2.5
		1 ρDB	$1.51 \rho \pi D^2/4$	1.19	2.19	2.2
		2 ρDB	$1.70 \rho \pi D^2/4$	0.67	1.67	1.5
		5 ρDB	$1.98 \rho \pi D^2/4$	0.31	1.31	1.2
10 ρDB	$2.23 \rho \pi D^2/4$	0.18	1.18	1.2		
		ρD^2	$1.52 \frac{\rho \pi D^2}{4}$	1.19	2.19	2.1
Rectangular prisms with rounded edges		$0.98 \rho D^2$	$1.51 \rho \pi D^2/4$	1.21	2.21	*1
		$0.91 \rho D^2$	$1.51 \rho \pi D^2/4$	1.30	2.30	*2

Notes : 1) ρA = Froude Krylov force per unit acceleration in the fluid

2) Morison's Equation $F/L = \frac{1}{2} C_D \rho D |U|U + C_m \rho A \dot{U}$ (F/L = Force per unit length of member)

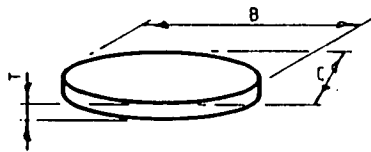
*1 C_D values for a rectangular prism with $r/d = 0.17$ should be taken as no less than 1.2 times the value for a circular cylinder of the same roughness.

*2 C_D values for a rectangular prism with $r/d = 0.33$ should be taken as no less than the value for a circular cylinder of the same roughness.

Figure 3.2.62. Drag and inertia coefficients for various prismatic shapes

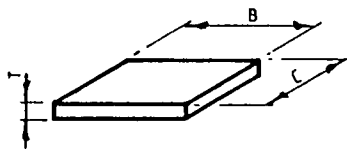
Shape	Direction of Flow	ρAT	Added Mass (M)	C_a (M/ ρV)	C_m (1+ C_a)	C_D
-------	-------------------	-----------	----------------	----------------------	-------------------	-------

Elliptical Plate



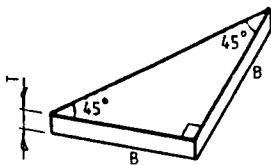
B/C	$\rho \pi BCT/4$	1.0 $\rho \pi BC^2/6$	C/T	1+C/T	
∞	-	0.98 $\rho \pi BC^2/6$	0.65C/T	1+0.65C/T	1.86
12.75	-	0.97 $\rho \pi BC^2/6$	0.65C/T	1+0.65C/T	1.36
7.0	-	0.90 $\rho \pi BC^2/6$	0.60C/T	1+0.60C/T	1.24
3.0	-	0.74 $\rho \pi BC^2/6$	0.49C/T	1+0.49C/T	1.17
1.5	-	0.63 $\rho \pi BC^2/6$	0.42C/T	1+0.42C/T	1.14
1.0	-				

Rectangular Plate



B/C	$\rho BCT/4$	1.0 $\rho \pi BC^2/4$	0.79C/T	1+0.79C/T	
∞	-	1.0 $\rho \pi BC^2/4$ <td>0.79C/T <td>1+0.79C/T <td>1.86</td> </td></td>	0.79C/T <td>1+0.79C/T <td>1.86</td> </td>	1+0.79C/T <td>1.86</td>	1.86
3	-	0.84 $\rho \pi BC^2/4$ <td>0.66C/T <td>1+0.66C/T <td>1.17</td> </td></td>	0.66C/T <td>1+0.66C/T <td>1.17</td> </td>	1+0.66C/T <td>1.17</td>	1.17
2	-	0.68 $\rho \pi BC^2/4$ <td>0.53C/T <td>1+0.53C/T <td>1.15</td> </td></td>	0.53C/T <td>1+0.53C/T <td>1.15</td> </td>	1+0.53C/T <td>1.15</td>	1.15
1.5	-				1.14
1.0	-				

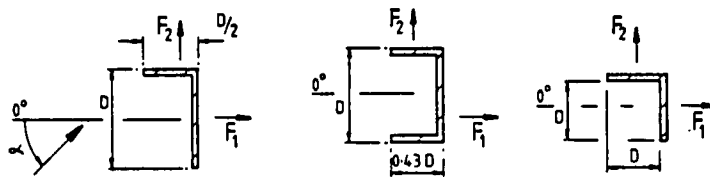
Triangular Plate



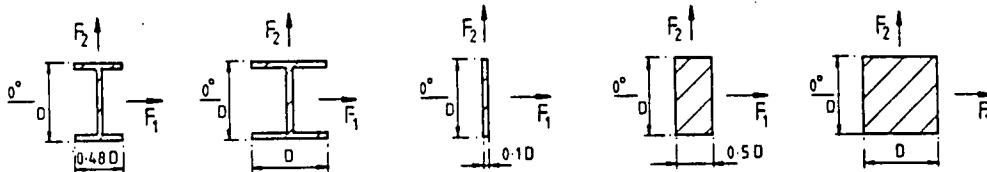
0.5 $\rho B^2 T$	0.3 ρB^3	0.6 B/T	1+0.6B/T	1.15
------------------	----------------	---------	----------	------

- Notes : 1) A = Area of plate T = Thickness of plate
 2) ρAT = Froude Krylov force per unit acceleration in the fluid
 3) Morison's Equation $F = \frac{1}{2} C_D \rho A |U| U + C_m \rho A T \dot{U}$

Figure 3.2.63. Drag and inertia coefficients for various plates



Degrees	C_{dl1}	C_{dl2}	C_{dl1}	C_{dl2}	C_{dl1}	C_{dl2}
0	+1.9	+0.95	+2.05	0	+2.1	+1.8
45	+1.8	+0.8	+1.85	+0.6	+1.8	+1.8
90	+2.0	+1.7	0	+0.6	+1.8	+2.1
135	-1.8	-0.1	-1.6	+0.4	-1.9	-1.0
180	-2.0	+0.1	-1.8	0	-2.0	+0.3
225					-1.4	-1.4



Degrees	C_{dl1}	C_{dl2}	C_{dl1}	C_{dl2}	C_{dl1}	C_{dl2}	C_{dl1}	C_{dl2}	C_{dl1}	C_{dl2}
0	+2.05	0	+1.6	0	+2.0	0	+2.1	0	+2.0	0
45	+1.95	+0.6	+1.5	+1.5	+1.8	+0.1	+1.4	+0.7	+1.55	+1.55
90	0	+0.9	0	+1.9	0	+0.1	0	+0.75	0	+2.0

Notes : 1) If U is the incident velocity at angle α
 then $F_1 = \frac{1}{2} C_{dl1} \rho DU^2$ $F_2 = \frac{1}{2} C_{dl2} \rho DU^2$

2) If the lift force is positive as shown :

then $C_d = C_{dl1} \cos \alpha + C_{dl2} \sin \alpha$ $C_l = -C_{dl1} \sin \alpha + C_{dl2} \cos \alpha$

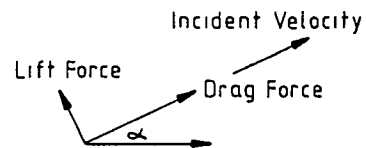
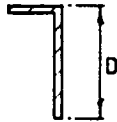





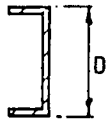





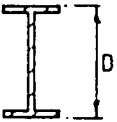




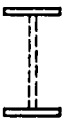


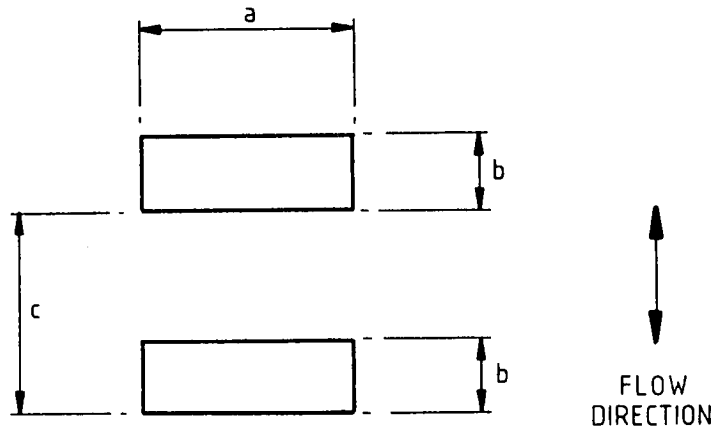
Figure 3.2.64. Drag-lift coefficient for prismatic shapes at various incidence angles

<u>Section</u>	<u>Flow Direction</u>	<u>Simplification For Added Mass Calculation</u>	<u>Added Mass</u>
			* $\frac{\rho \pi D^2}{4}$
			* $\frac{\rho \pi D^2}{4}$
			* $\frac{\rho \pi D^2}{4}$
			Use Fig. 3.2.66 as an approximation
			* $\frac{\rho \pi D^2}{4}$
			Use Fig. 3.2.66

Notes :

- 1) * In these cases the added mass may be taken as that for the equivalent flat plate shown by solid lines.
- 2) In each case the added mass coefficient ' C_a ' is $\frac{\text{Added Mass}}{\rho \times \text{cross section}}$
- 3) The cross section required for calculating C_a is the shaded area in column 1.
- 4) The inertia coefficient ' C_m ' is $(1 + C_a)$
- 5) These values are first approximations only.

Figure 3.2.65. Recommendations for calculating C_m values for rolled sections



Ca							
b/a							
c/a	0.1	0.2	0.4	0.6	1.0	1.5	2.0
0.1	4.8	-	-	-	-	-	-
0.2	4.5	2.6	-	-	-	-	-
0.6	4.7	2.8	1.4	1.0	-	-	-
1.0	5.3	3.2	1.6	1.1	0.7	-	-
1.5	5.8	3.6	2.0	1.3	0.8	0.5	-
2.0	6.4	4.0	2.3	1.6	1.0	0.6	0.4
3.0	7.1	4.6	2.5	1.8	1.2	0.9	0.6

$$\text{Added Mass} = 2 \rho C_a ab$$

Note : Similar diagram in Sarpkaya and Isaacson (1981) is incorrect

Figure 3.2.66 Added mass of tandem rectangular prisms (Sarpkaya 1960)

3.3 VORTEX SHEDDING INDUCED OSCILLATION

3.3.1 General

In currents and most wave flows members shed vortices. The member is subject to longitudinal and transverse load fluctuations as the vortices are shed. If the loading frequency corresponds to a natural frequency of the member large and potentially damaging vibrations may occur. This section describes the characteristics of vortex shedding in steady flow and waves and gives guidance on assessing and avoiding member oscillations. Lift forces in steady flow without member oscillation are discussed in Section 3.3.2. Member oscillation is introduced in Section 3.3.3. Lift forces in oscillatory flow are discussed in Section 3.3.5 and the corresponding member oscillations in Section 3.3.6. The final Sections of 3.3 contain recommendations and conclusions. Other useful general references include Blevins (1977), Hallam et al (1977), King (1977), Sarpkaya (1979a, b), Sarpkaya and Isaacson (1981) and Griffin (1981).

Most work on vortex shedding oscillations has been performed on circular cylinders and this is reflected in this section. For other shapes reference should be made to Blevins (1977) and Hallam et al (1977) where some results are presented for non circular cylinders in steady flow.

The observed characteristics of vortex shedding for the case of a steady current are shown in Figure 3.2.7. In wave flow the patterns are dependent on R_g , K_c and the presence of any currents. Some observed patterns of vortex shedding in oscillating flow are shown in Figure 3.3.1. These may be expected to be similar to the patterns for a vertical cylinder in waves but the pattern for a horizontal cylinder will be different (See Section 3.3.6d).

As each vortex forms it produces a suction on the member. In many cases vortices shed alternately from each side of the member. This results in an alternating transverse force with a period equal to the time taken to shed two vortices. If the member is symmetrical relative to the flow direction this transverse force will usually have a zero mean value. Otherwise there will also be a steady lift force as described in Section 3.2.13. The vortices also produce an alternating and steady in line or drag force. The alternating drag force usually has a period of half the alternating transverse force, because the drag force peaks as each vortex is shed. The steady drag force has been discussed extensively in Section 3.2.

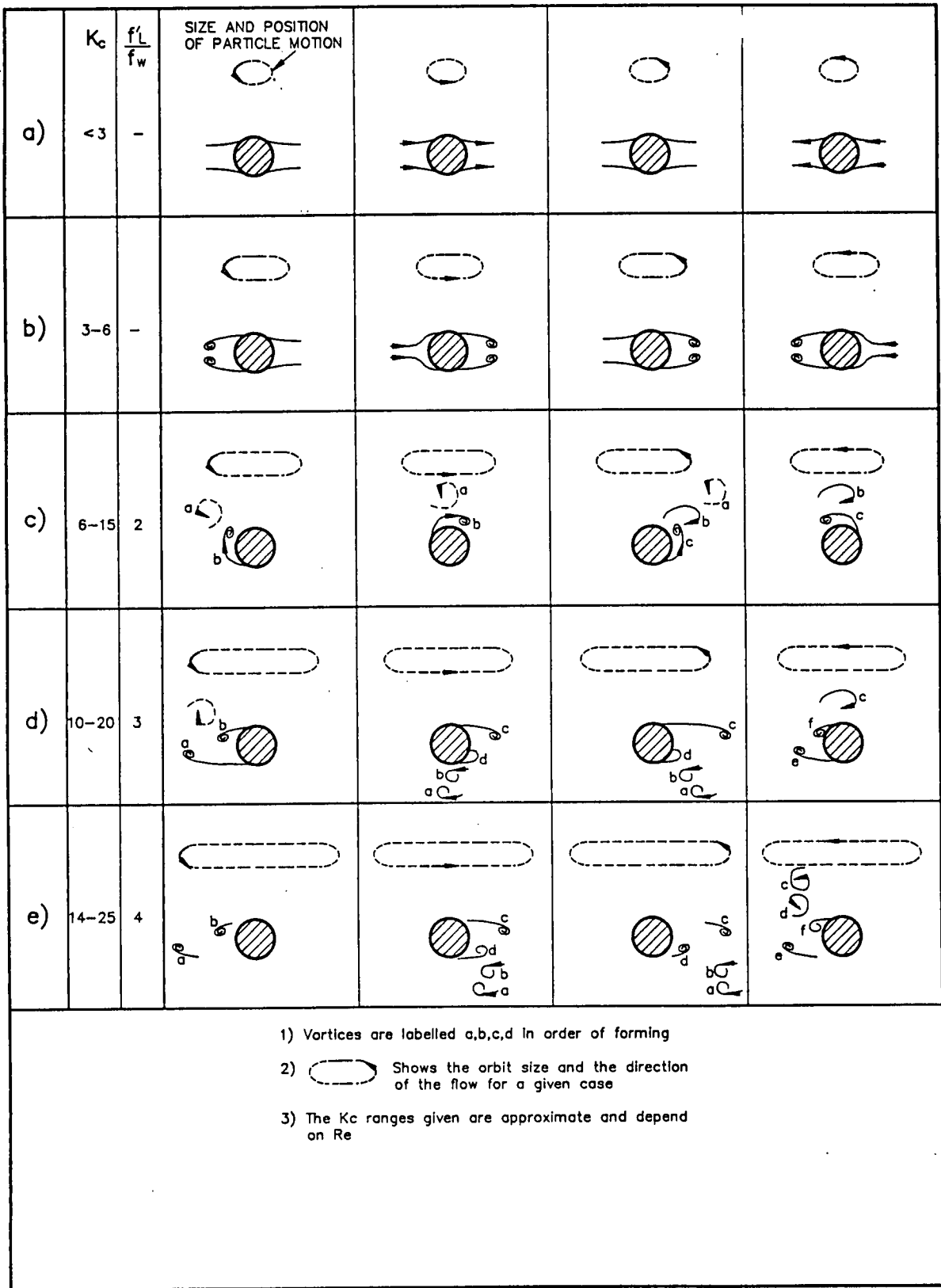


Figure 3.3.1. Visualisation of vortex shedding in oscillating flow
 (based on Sarpkaya (1976a,b), Sarpkaya and Isaacson (1981) and Grass et al (1984))

Mathematical models are now able to predict vortex-induced forces. Instead of solving the full Navier-Stokes equations, it is usually assumed that vorticity is shed and convected in vortex 'sheets' with inviscid flow outside these sheets. Numerical models of steady and oscillatory two-dimensional flow have been developed e.g. Stansby (1977) and Sarpkaya and Shoaff (1979). However at present these methods are still research orientated and the guidance given here is based on experimental measurements and very simple mathematical models.

Section 3.3.2 describes the vortex shedding phenomena for a member which is not oscillating in steady flow. Section 3.3.3 describes the changes in the fluid behaviour and the structural response when oscillations do occur. Sections 3.3.4 to 3.3.6 consider the same phenomena but in oscillating and wave flows.

3.3.2 Steady flow with no member oscillation

a. Alternating forces and frequencies

The alternating forces, excluding any steady component, may be characterised by their size F'_l , F'_d and by the Strouhal number relationship between vortex pair shedding frequency, incident velocity and member diameter.

$$\begin{aligned} F'_l &= 0.5 C'_l \rho D U^2 & F'_d &= 0.5 C'_d \rho D U^2 \\ S_t &= N_p D / U & \text{Typically } N_l &\approx N_p \text{ and } N_d \approx 2N_p \end{aligned}$$

Where:

		Typical units
F'_l	is the alternating lift force per length of member	N/m
F'_d	is the alternating drag force per unit length of member	N/m
C'_l	is the lift coefficient	-
C'_d	is the drag coefficient	-
ρ	is the density of water	Kg/m ³
D	is the member diameter or width perpendicular to the flow	m
U	is the velocity vector of the incidental flow resolved normal to the member	m/sec
N_p	is the frequency at which vortex pairs are shed	Hz
N_l	is the frequency of the fluctuating (transverse) lift force	Hz
N_d	is the frequency of the fluctuating (in line) drag force	Hz
S_t	is the Strouhal number	-

Note however that F'_l and F'_d vary randomly from one cycle of vortex shedding to another. The forces and the coefficients C'_l and C'_d may therefore define the rms or the maximum values. In principle the larger the number of cycles included in the time history the higher the likely peak value. It is therefore preferable to define C'_l and C'_d by an rms value and a probability distribution. We have not found any specific reference to distribution functions but if we assume a Rayleigh distribution of the force peaks then

$$C'_l \text{ (average maximum of 10 peaks)} \approx 2.5 C'_l \text{ (rms)}$$

$$C'_l \text{ (average peak value)} \approx 1.25 C'_l \text{ (rms)}$$

Where C'_l (rms) is calculated from the rms value of the alternating force about its mean value.

Figure 3.3.2 shows the range of C'_l (rms) obtained by various researchers and summarised by Sarpkaya and Isaacson (1981), Hallam et al (1977) and ESDU (1978). These results have been based on various C'_l (rms), peak and average peak values which have been converted to equivalent rms values using the relationships given above. The wide range of C'_l is probably caused by a number of factors which may include:

- a) The length of cylinder over which the lift forces are measured. (When the cylinder does not oscillate the length over which the lift forces are correlated may only be a few diameters, so, the shorter the measurement length the higher the C'_l).
- b) The turbulence in the incident flow (ESDU, 1978).
- c) The rigidity of the cylinder.
- d) The surface roughness of the cylinder (ESDU, 1978).
- e) The direction of the flow to the line of the cylinder (skew).
- f) The form of the end of the cylinder.

The broken line on Figure 3.3.2 corresponds to the average of the values reported by Hallam et al (1977) and this is recommended for design purposes. This would correspond to measurement lengths of a few cylinder diameters.

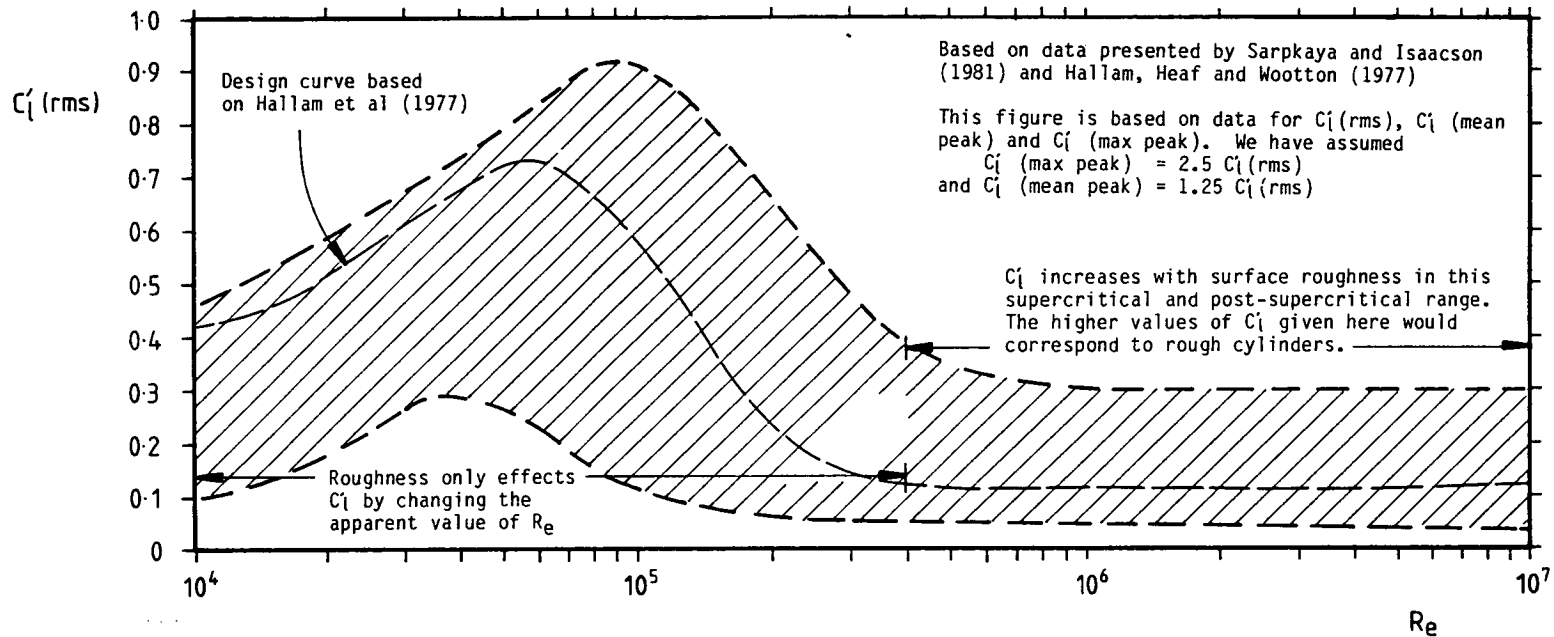


Figure 3.3.2. Range of measured values of C_l (rms) Vs Re for a smooth circular cylinder which does not oscillate

Figure 3.3.3 shows the range of C'_d (rms). This is based on Hallam et al (1977). Scatter in C'_d values will have similar origins to that in the C'_l values.

The frequency of the lift force, equal to that of shedding vortex pairs, is given by the Strouhal number relationship $N_l = S_t U/D$. In steady flow the Strouhal number for a cylinder is dependent on R_θ as shown by figure 3.3.4. (Lienhard, 1966). In subcritical flow and post-supercritical flow S_t is well defined. In critical and supercritical flow the wake is disorganised, vortices shed randomly and the Strouhal number can only define the peak vortex shedding frequency.

In the critical and supercritical regime Figure 3.3.4 shows a large range of measured peak frequencies. The Strouhal number of the peak frequency has been found to correspond to the lower values given by figure 3.3.4. when:

- i) The cylinder oscillates.
- or ii) The cylinder has a rough surface.
- or iii) The incident flow is turbulent (except for very low levels of turbulence).

The Strouhal number is also related to the spacing of adjacent vortices moving downstream in the wake. The time between shedding of single vortices T_s is $0.5/N_p$. Assuming that the vortices are convected away from the cylinder at the velocity, U , of the incident flow their spacing is $U/(2N_p) = D/(2S_t)$ i.e. individual vortices are spaced at about $0.5S_t^{-1}$ cylinder diameters. For S_t of about 0.2 the spacing of individual vortices is therefore about 2.5 cylinder diameters.

b. Correlation

The correlation of vortex shedding along the length of the cylinder is dependent on R_θ , the turbulence of the incident flow and any movement of the member. King (1977) summarises the very limited data on correlation for stationary members. At the Reynolds numbers of significance to offshore structures (generally greater than 10^4 for currents) the alternating vortex shedding induced loading, along a stationary member, is correlated over no more than 6 diameters and therefore, unless the member oscillates, the total force on a long member is small. Although not the subject of specific tests it is reasonable to assume the vortex shedding forces are unlikely to be correlated between different stationary members unless there is a specific mechanical or hydrodynamic coupling. It is therefore reasonable to ignore alternating vortex shedding forces when calculating total forces on braced structures such as jackets.

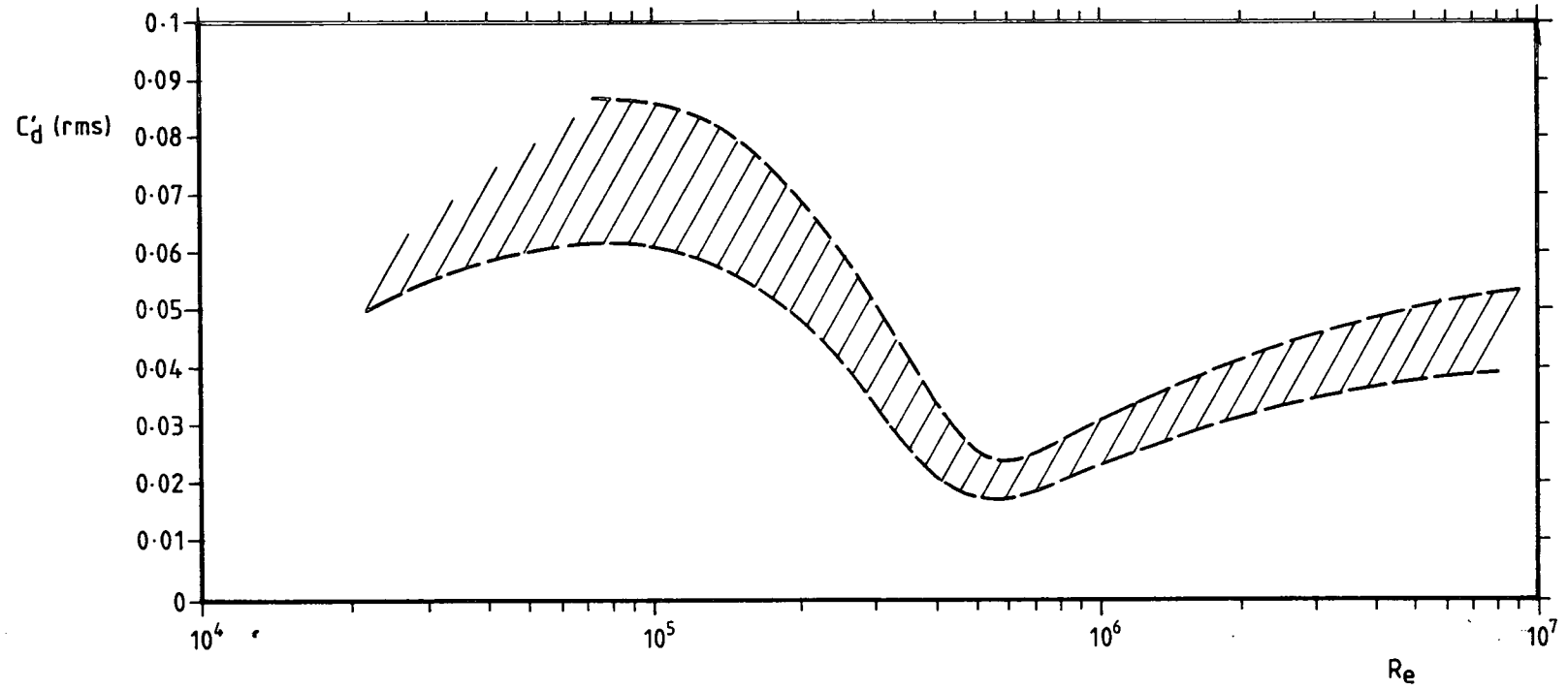


Figure 3.3.3. Range of measured values of $C_d \text{ (rms)}$ Vs Re for a smooth circular cylinder which does not oscillate, (Hallam, Heaf and Wootton, 1977)

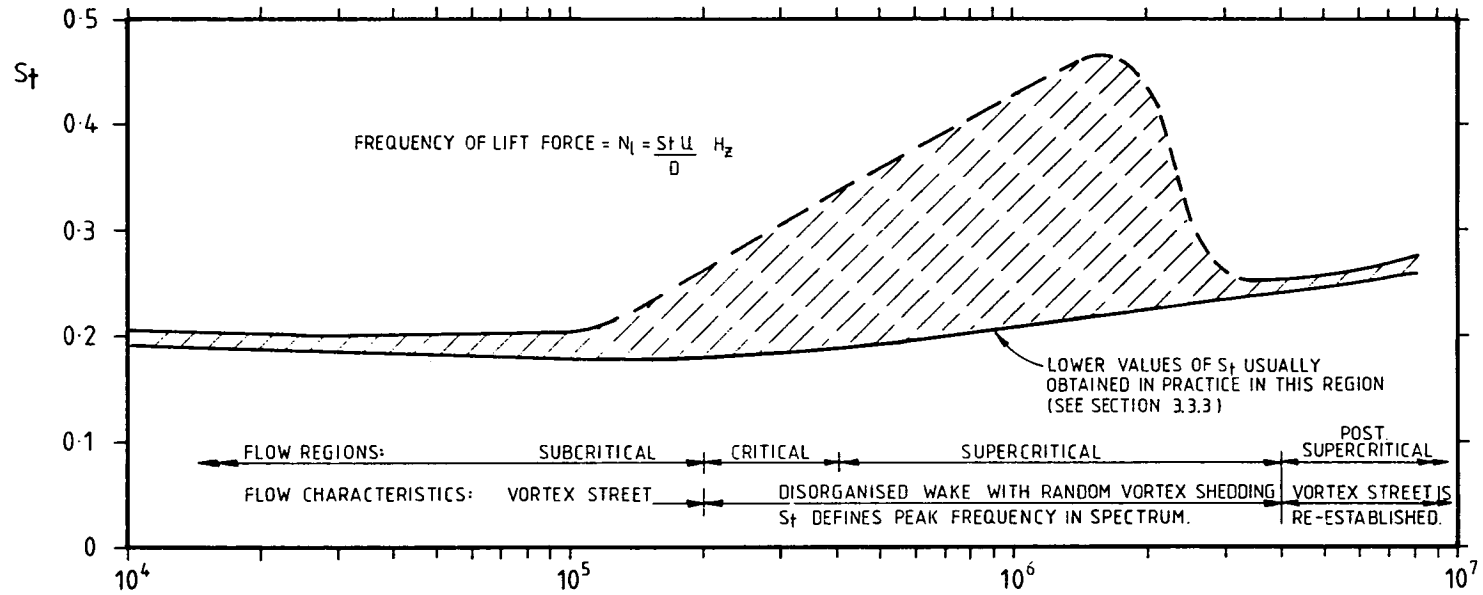


Figure 3.3.4. Strouhal number, of dominant lift frequency, versus Re for a circular cylinder which does not oscillate (Lienhard, 1966)

However a structure composed for example of vertical piles linked at the top but able to sway as a group, could be subject to a global effect from vortex shedding (Hallam et al, 1977).

c. Effect of surface roughness

Experimental data is limited but it is generally accepted that surface roughness changes the critical value of R_e as discussed in Section 3.2.3. Therefore the value of C'_l may, for R_e just less than critical, be reduced by surface roughness. In postcritical flow C'_l is not dependent on R_e . However in oscillating flow (see Section 3.3.4b) roughness has been found to increase the alternating lift force. It is therefore likely that the steady flow alternating forces are increased by surface roughness. We suggest that the smooth cylinder values should be increased by $C_d/0.7$ where C_d is the rough cylinder steady flow drag coefficient obtained from Figure 3.2.59. There is also some evidence that roughness increases correlation lengths (Wolfram, 1987, private communication).

d. End effects

Short stubby cylinders and the end one or two diameters of longer cylinders tend to have less strong vortex shedding than the centre portion of a long cylinder. This is the case whether the end is free or a nodal connection to another member.

e. Inclination

The vortex shedding forces on cylinders inclined to the flow direction may be calculated approximately using the independence principle, discussed for Morison loading in Section 3.2.4c. The lift force and vortex shedding frequency will be approximately dependent on the velocity normal to the cylinder. For further discussion and a review of the research see Sarpkaya and Isaacson (1981).

3.3.3 Steady flow with vortex induced member oscillation

a. Member oscillation

Wootton et al (1972) give an example (Figure 3.3.5) of the response of a flexible member to vortex shedding.

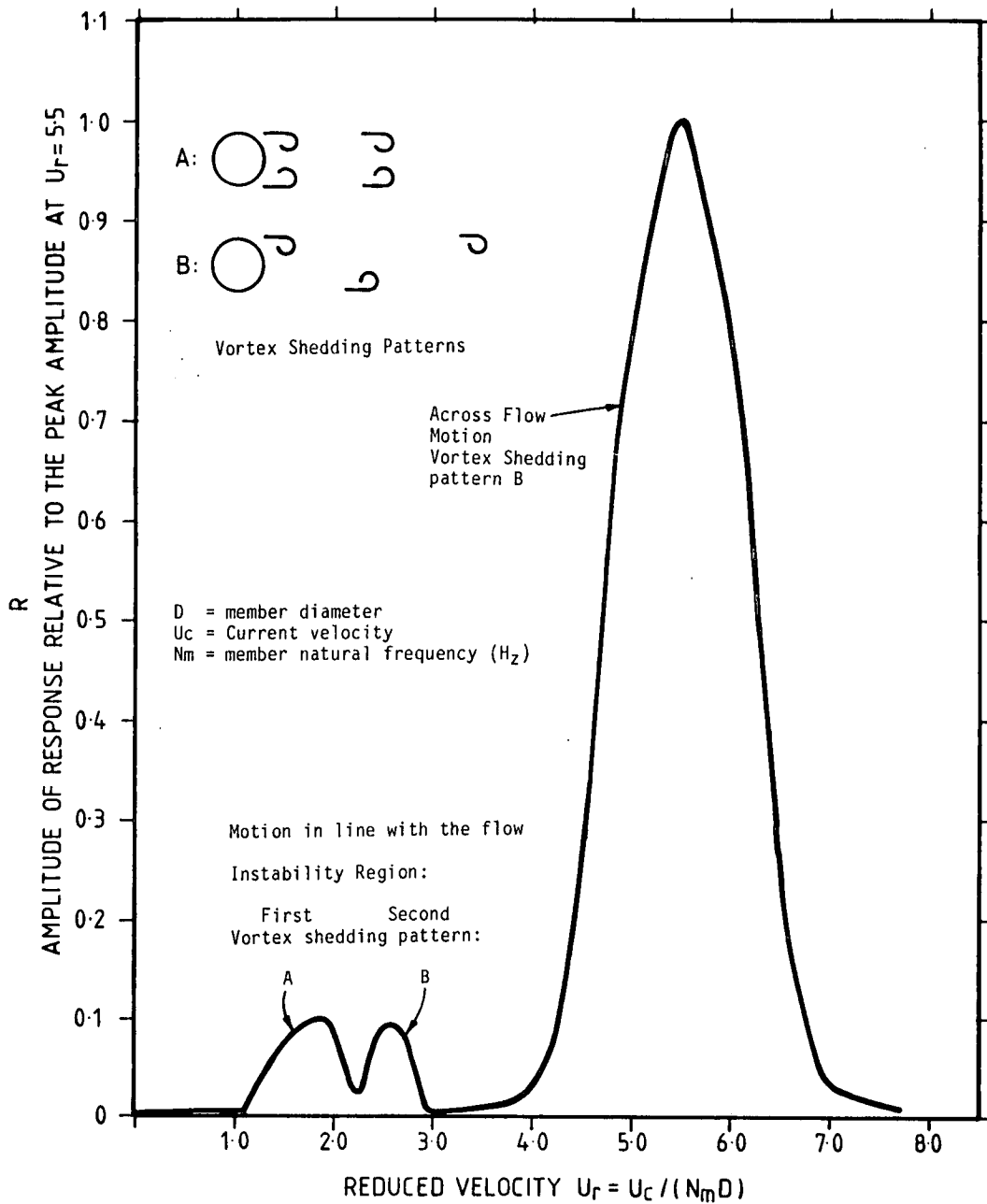


Figure 3.3.5. Typical response of a single member to vortex shedding in steady flow (Wootton et al, 1972 and King et al 1973)

The response is presented as a function of reduced velocity U_r .

Where:

$$U_r = U_c / N_m D$$

$$U_c = \text{flow velocity}$$

$$N_m = \text{natural frequency of the member}$$

$$D = \text{diameter of the member.}$$

Three peaks in the response are found where the vortex shedding becomes locked-on to the member's lowest natural frequency. The first two peaks correspond to in line motion of the member and the third corresponds to the transverse motion. The pattern of the response is repeated for each natural frequency which has mode shape deflections in line or across the flow. The peaks occur when one of the vortex shedding frequencies corresponds to the natural frequency, N_m of the member as discussed in Section 3.3.1. The two peaks in the in-line response (when only one might have been expected) are caused by the two different vortex shedding modes shown in Figure 3.3.5.

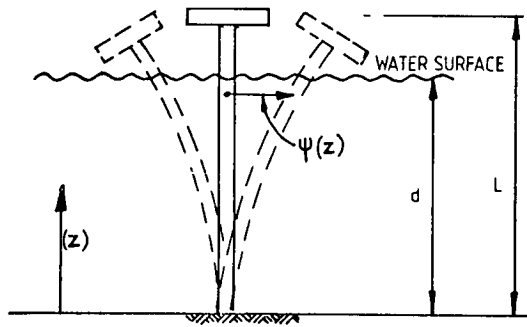
The amplitude of the dynamic response is determined by the properties of the member and the flow as characterised by a response parameter. Different authors use slightly different forms of the response parameter. In this report we have used a parameter which is also known as the Scruton number:

$$R_p = \frac{2M_e \delta}{\rho D^2}$$

Where

	<u>Typical Unit</u>
M_e is the effective mass per unit length of the member including the external added mass for the excited mode (see Figure 3.3.6)	kg/m
δ is the log decrement of structural damping in air ($\delta = 2\pi\xi$ where ξ = damping ratio) See Appendix J.	-
ρ is the density of sea water	kg/m ³
D is the member diameter	m

The amplitude of the locked-on response is a function of the response parameter as shown by Figure 3.3.7 for transverse motion and Figure 3.3.8 for in-line motion. These results for a cantilever cylinder were obtained experimentally by Wootton (1969) and for a spring mounted cylinder by Iwan (1975). Iwan also showed how the relative amplitudes of different mode shapes may be related to the results for the cantilever case (Table 3.3.1).



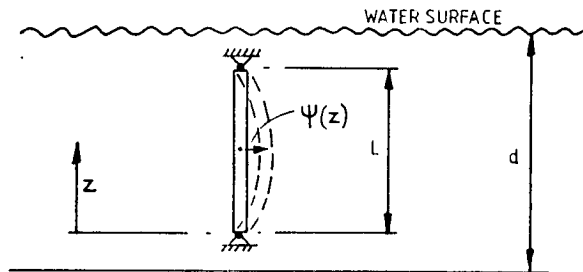
$$M_e = \frac{\int_0^L M(z) \Psi^2(z) dz}{\int_0^d \Psi^2(z) dz}$$

Case 1 Member only partly immersed

Notes

$M(z)$ is the actual mass per unit length at z

$\Psi(z)$ is the ordinate of the mode shape at z



$$M_e = \frac{\int_0^L M(z) \Psi^2(z) dz}{\int_0^L \Psi^2(z) dz}$$

Case 2 Member completely immersed

Figure 3.3.6. Calculation of equivalent mass per unit length for the response parameter (Hallam et al, 1977)

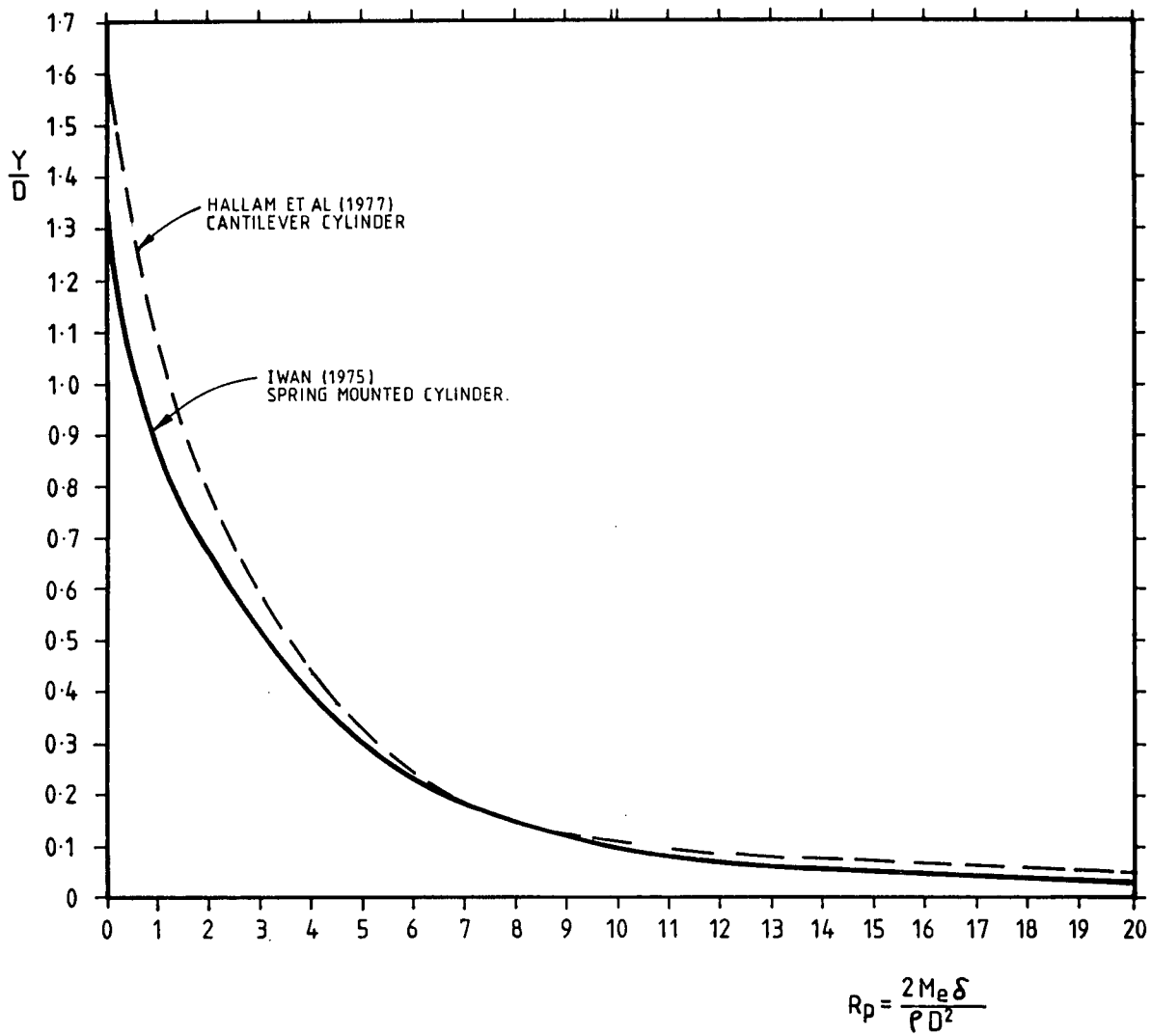


Figure 3.3.7. Amplitude of response of a cylinder to vortex excitation in steady flow

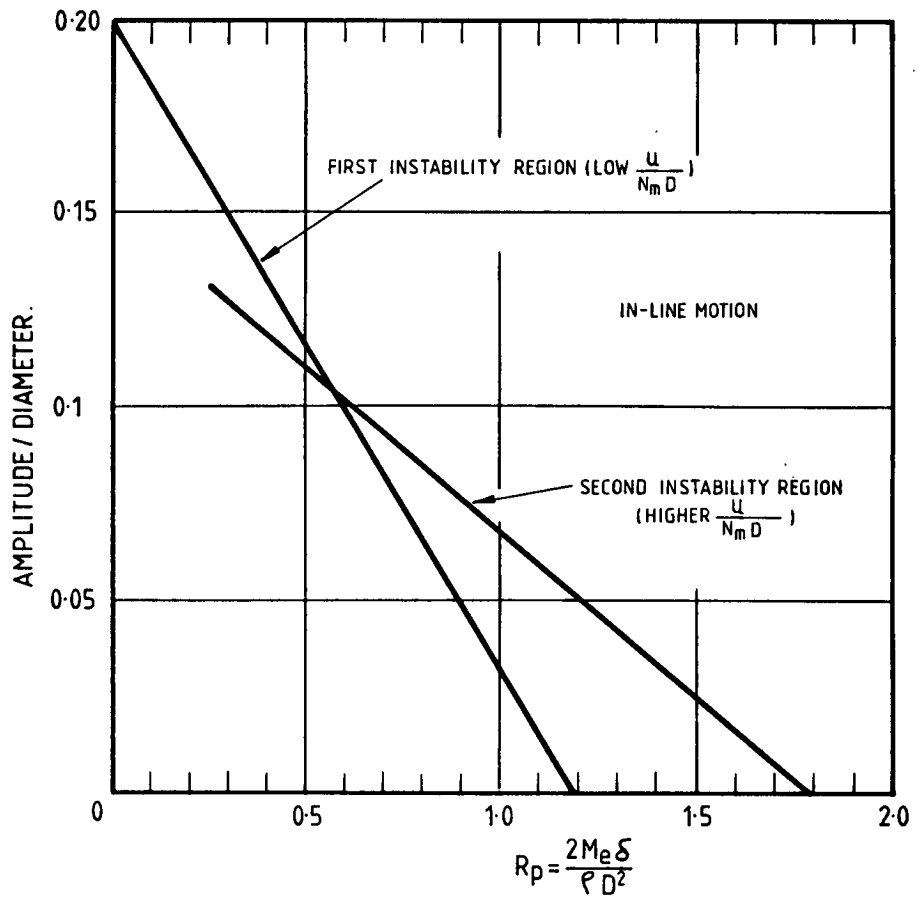


Figure 3.3.8. Amplitude of response of a cantilever cylinder for in-line motion (Hallam et al, 1977)

Table 3.3.1 - Relative amplitudes of response to vortex shedding for various vibration modes. (The response is the maximum within the mode shape)
Iwan (1975)

Cylinder Vibration Mode	Relative Amplitude of Response
Rigid Spring Mounted Cylinder	0.77
Pivoted Rod	0.99
String and Cable	0.89
Simply Supported Beam	0.89
Cantilever (1st mode)	1.00
Cantilever (2nd mode)	1.15
Cantilever (3rd mode)	1.18

It should be noted that the response parameter is not a rigorous parameter for use in defining the response of structures in water because it consists of two independent parameters, $2M_e/\rho D^2$ and δ . The use of this parameter, strictly, depends on the following two conditions being satisfied.

- 1) The form of the input force must be single frequency and sinusoidal. The relationship between amplitude and damping is $A \propto 1/\delta$ for such a force whilst for a wide band force spectrum of uniform power density $A \propto 1/(\delta)^{0.5}$ for example (Hallam et al, 1977). At very small deflection amplitudes, where the force due to vortex shedding is not enhanced by structural response, the overall force is closer to a wide band force. At resonance and at larger amplitudes the force more closely matches the sinusoidal condition.
- 2) The frequency of the response of the cylinder must not be affected by the force due to vortex shedding. This requires that the vortex shedding force is wholly in phase with the velocity : there being no component in phase with the displacement (or acceleration) of the cylinder. In practice it is known that this condition is only satisfied when the vortex shedding frequency and the natural frequency of the member (measured in still water) match exactly. There are indications that this requirement is not fully satisfied in many flow conditions and therefore care must be taken in the use of the response parameter.

It should also be noted that in cases such as risers the curvatures and hence stress levels are much greater in the higher modes than the lower modes for the same amplitude of response. Thus although the deflection response amplitude in higher modes may be reduced, because in general structural damping increases with increased mode, the stress levels and fatigue damage may not be dominated by the fundamental mode. In the case of risers it is common for fatigue damage to be attributable to the third or fourth mode.

An insight and first approximation to the response parameter - amplitude relationship can be obtained by using 'wake oscillator models' in which the cylinder is analysed as a damped mass-spring system subject to a fluctuating load at the cylinder's natural frequency.

Sarpkaya (1979b) assumes a simple sinusoidal loading. Blevins (1977) calculates the loading allowing for the relative motion of the cylinder and the flow. Blevins (1977) also develops a 'correlation' model which assumes a random loading that is correlated along the length of the cylinder. In Appendix K a simple wake oscillator model based on Sarpkaya (1979b) is developed and compared with Hallam (1977) and Iwan (1975). The model is shown to give a reasonable first approximation to the experimental data.

b. Effect of transverse oscillation on drag force, in steady flow

When a member oscillates transverse to the flow the steady drag force may considerably increase. This effect has been considered by Mercier (1973), Skop et al (1977), Patrikalakis and Chryssostomidis (1983) and Basu et al (1987). For locked-on oscillations the C_d value increases above the value for no oscillation: C_{d0} , as shown in Figure 3.3.9. Most of this data is for low R_e .

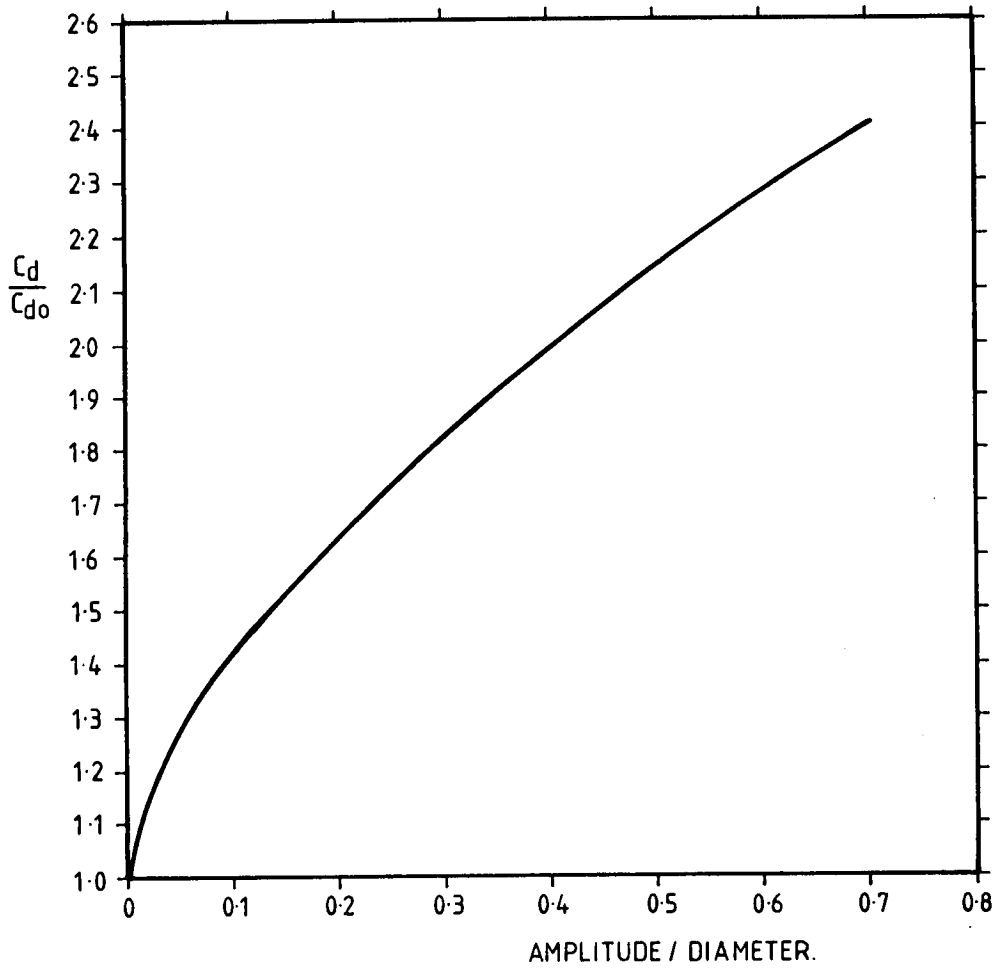


Figure 3.3.9. Amplification of drag coefficient by transverse locked on oscillation (Skop et al, 1977)

c. Effect of in line oscillation on the in line time varying drag force, in steady flow

The in line time varying drag force is affected by in line oscillation (King, 1977). In the first instability region

$$C'_d = 0.12 + 3.8 (A/D)$$

In the second instability region

$$C'_d = 0.08 + 2.66 (A/D)$$

where A is the amplitude of oscillation and D is the member diameter.

3.3.4 Lift forces in planar oscillating flow and waves with no member oscillation

a. Smooth cylinders

Lift forces have been measured in these types of flow by Sarpkaya (1976a,b and 1986), Chaplin (1985) and Bearman et al (1985). Their results for the lift coefficient are given in Figure 3.3.10. The lift coefficient we have used is defined by Sarpkaya (1976a) in terms of the rms force but the maximum velocity:

$$F'_l \text{ (rms)} = 0.5C'_l \text{ (rms)}\rho DU^2(\text{max})$$

Other definitions of C'_l include an alternative rms value, in terms of the rms velocity, used by Bearman et al (1985):

$$F'_l \text{ (rms)} = 0.5C'_l \text{ (a)} \rho DU^2(\text{rms})$$

A maximum C'_l is also used by Sarpkaya:

$$F'_l (\text{max}) = 0.5 C'_l (\text{max}) \rho D U^2 (\text{max})$$

For sinusoidal variation of U , $U^2(\text{rms}) = 0.5U^2(\text{max})$ therefore $C'_l (\text{rms}) = 0.5C'_l (\text{a})$

For a Rayleigh distribution of the peaks in F'_l , and taking an average of the maximum of 10 peaks $C'_l (\text{max}) = 2.5C'_l (\text{rms})$. This ratio is consistent with the results presented by Sarpkaya (1976a).

Figure 3.3.10 shows that Sarpkaya's (1976b) oscillating flow values of C'_l were similar to those obtained by Bearman et al (1985) in the De Voorst Flume. Chaplin (1985) obtained rather larger C'_l at the same R_e : as shown in Figure 3.3.11. Sarpkaya measured lift forces over 5 to 18 diameters of member length whereas Chaplin and Bearman measured pressures on one ring of pressure transducers. This difference between Sarpkaya and Chaplin may therefore be caused by a lack of correlation of the lift force over the length of Sarpkaya's cylinder. This in turn suggests that the average lift forces measured over the length of a typical brace member would be less in the ocean than in oscillating flow. The experiments showed that lift forces were negligible for K_c less than about 3.

Every (1980) measured $C'_l (\text{rms})$ values in combined wave and current for vertical cylinders in a wave flume. Reynolds numbers up to 1.4×10^4 and K_c^+ up to 20 were obtained. C'_l and K_c^+ were defined:

$$F'_l (\text{rms}) = 0.5 \rho C'_l (\text{rms}) D (U_c + U_w)^2$$

$$K_c^+ = (U_c + U_w) T / D$$

where

U_c = current velocity

U_w = maximum wave particle velocity

He found that the highest value of C'_l were about 1.0 and occurred at K_c^+ of 5 to 12. At K_c^+ of 20, C'_l was typically about 0.3.

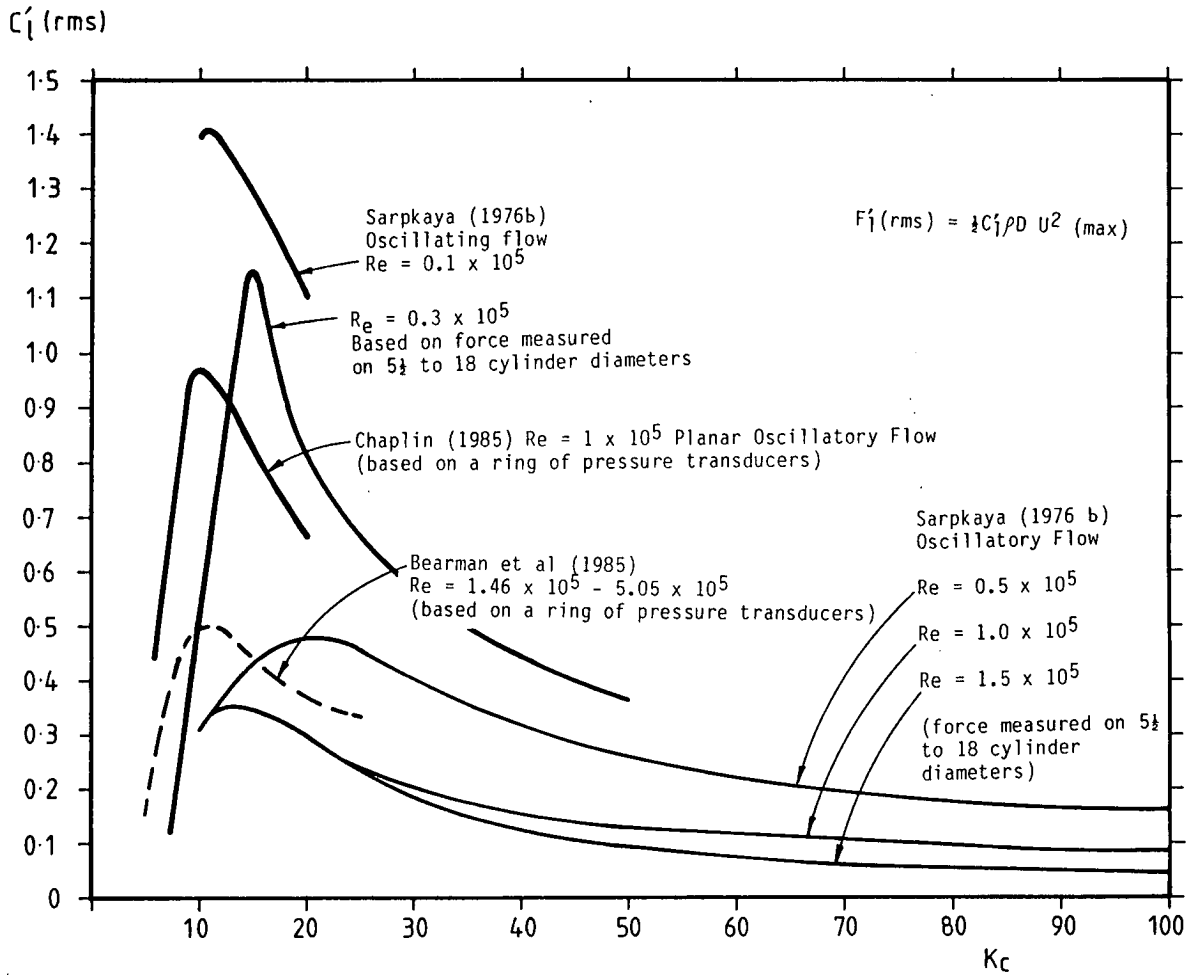
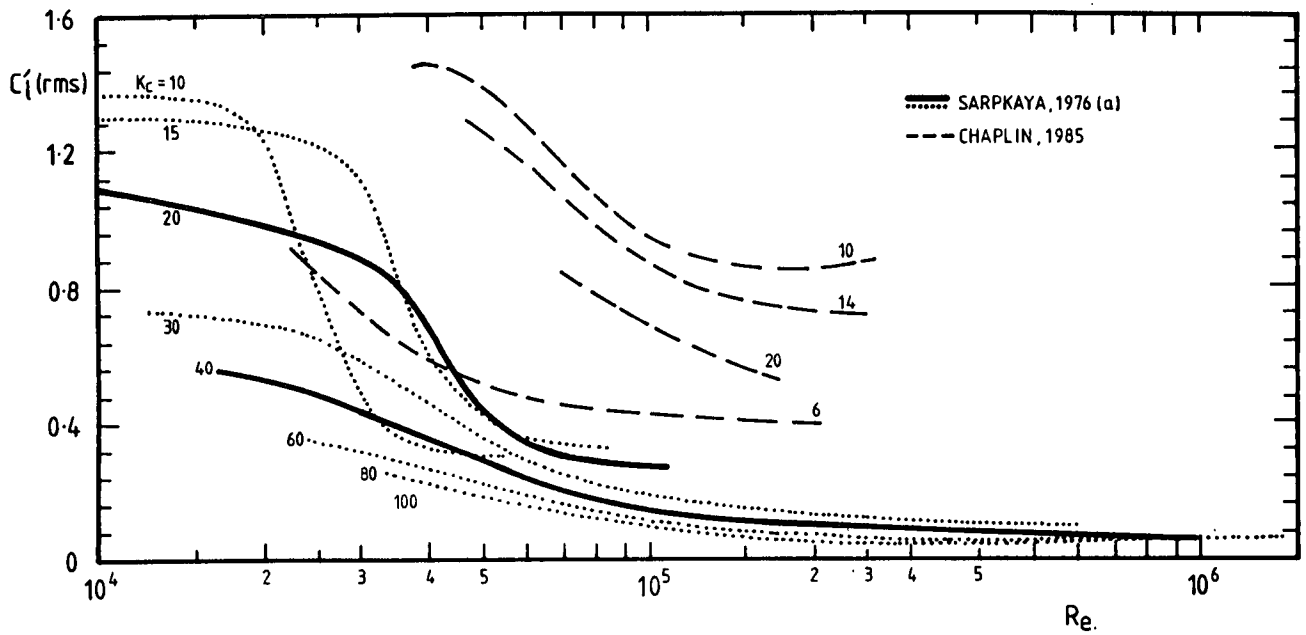


Figure 3.3.10 Lift coefficients for rigid cylinders in planar oscillatory and wave flow



Note: This graph has been based on $C_l'(max)$ assuming $C_l'(rms) = 0.4 C_l'(max)$.

Figure 3.3.11. Smooth cylinder C_l' versus Re for various values of K_c

b. Rough cylinders

Sarpkaya (1976a, b and 1986) has measured lift forces on rough and smooth cylinders in planar oscillating flow. Roughness considerably increases the lift force especially at K_c greater than 15. However these high lift forces are related to the high drag forces found in oscillating flow experiments and it is unlikely that as large an increase would occur in the sea. Some increase in C'_l with roughness is however likely and it is tentatively recommended for post-supercritical flow (R_e greater than about 5×10^4) that the smooth cylinder value of C'_l should be increased by $C_{d,0.7}$ where $C_{d,0}$ is the rough cylinder steady flow drag coefficient from Figure 3.2.59.

c. Empirical model of vortex shedding in oscillating flow

Bearman, Graham and Obasaju (1984) have produced a model of transverse loading in oscillating flow based on observations of the flow characteristics and the vortex shedding behaviour in steady flow. Their model fits the experimental data best, at K_c greater than 25, where a vortex street develops in each half wave cycle.

3.3.5 Frequency of vortex shedding in oscillating flow and waves

a. Oscillatory Flow

The characteristics of vortex shedding in this type of flow have been described by Isaacson (1974), Sarpkaya (1976 a,b) and Grass et al (1984).

Vortex shedding phenomena are considerably complicated by the flow oscillation and the interaction with previously shed vortices.

Figure 3.3.1 shows how the vortex shedding pattern varies with K_c for R_e of about 10^5 . As K_c increases more vortices form per wave cycle. The number can be determined approximately from:

- 1) The Strouhal number - individual vortex spacing relationship, given in Section 3.2.2 : $S_v = 0.5 S_t^{-1} D$

2) The particle orbit diameter relationship with K_c : $K_c = \pi b/D$

Therefore the number of vortices per wave cycle is approximately:

$$2b/S_v = (2K_c D/\pi)/(0.5S_t^{-1}/D) = 4K_c S_t/\pi$$

At K_c less than 3 the flow displaces by less than a cylinder diameter and vortices do not form. In the K_c range 3–6 vortices form but only shed occasionally.

At K_c of about 6 to 15 two vortices form and shed per wave cycle. Each vortex is influenced by the previously shed vortex and this causes the vortices to always pass the same side of the cylinder. This in turn leads to a lift force cycle for each vortex shed whereas in steady incident flow a lift force cycle occurs for each pair of vortices shed. Large lift and drag forces result from this type of behaviour and it is possible that the vortex shedding may be highly correlated by the action of the wave.

K_c in the range 10–20 results in 3 vortices being shed per wave cycle. Two vortices shed during one half cycle (a and b in Figure 3.3.1d) but vortex b inhibits one vortex (d) from shedding during the following half cycle. The resulting time history has harmonics at 1, 2, 3, 4 and 5 lift force cycles per wave period but the third harmonic is the largest so that again the dominant number of lift force cycles equals the number of vortices, and not vortex pairs, shed.

Further increase in K_c results in more vortices being shed per wave cycle and a lift force cycle per pair of vortices shed.

Sarpkaya (1976a,b and 1986) has analysed the frequency content of the lift force. Figure 3.3.12 shows the highest vortex shedding frequency that occurs during a wave cycle. Figure 3.3.13 shows the dominant frequency associated with the lift force. For a rigid smooth cylinder only the 2nd and 4th harmonics are significant. However roughness considerably increases the importance of the higher order harmonics.

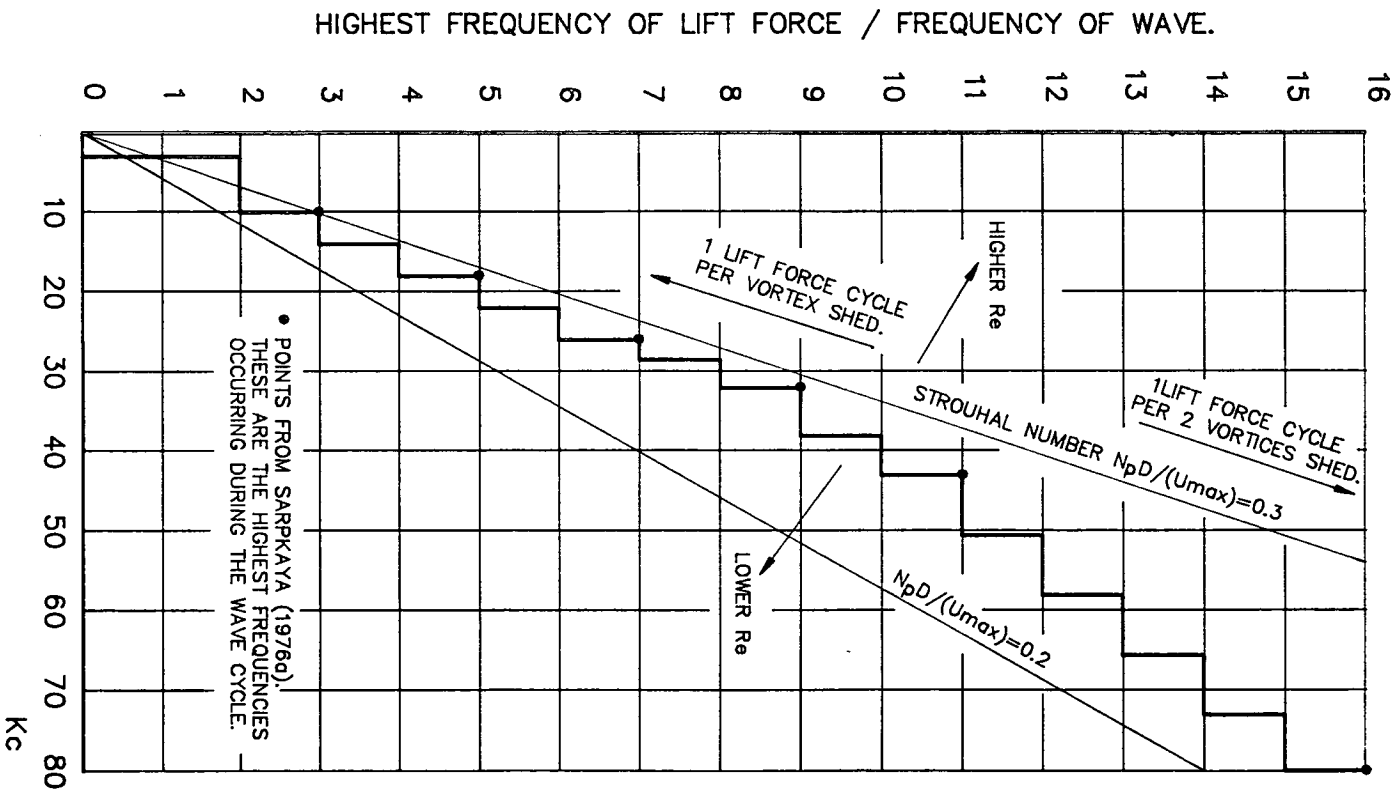


Figure 3.3.12. Highest frequency of vortex shedding during a wave cycle. Oscillatory flow at $Re = 1 \times 10^5$

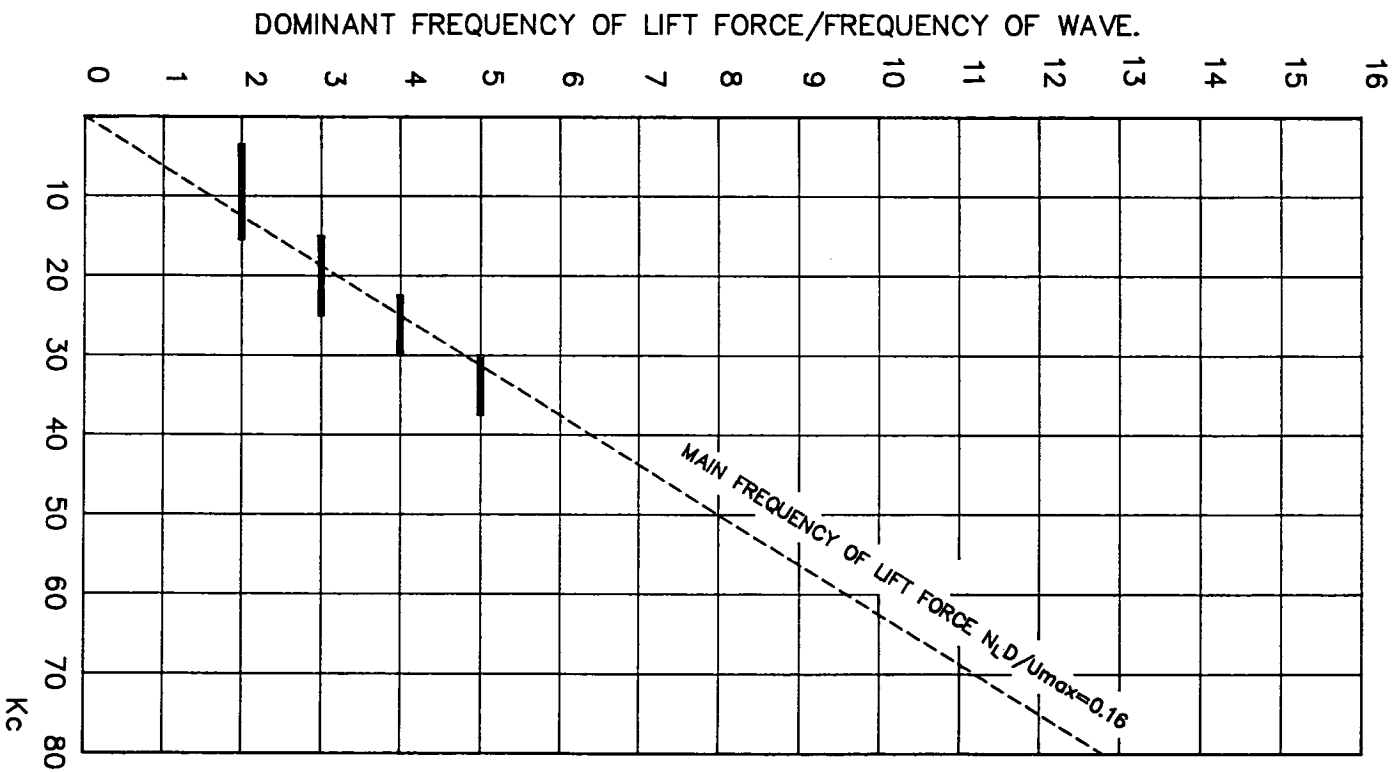


Figure 3.3.13. Dominant frequency of lift force oscillatory flow at $R_e / K_c = 6836$
 (based on Sarpkaya, 1986)

b. Wave flow

Every (1980) measured lift forces and frequencies on vertical cylinders in waves and current at K_c of 3 to 20 for subcritical R_e . At $K_c = 10$ and with no current he obtained a frequency spectrum dominated by 2 lift force cycles/wave cycle. As the current was increased the response at 1 lift force cycle/wave cycle increased and eventually became larger than the original peak when the current velocity exceeded about half the maximum wave particle velocity.

3.3.6 Planer oscillating and wave flow with vortex induced member, oscillation

a. Experimental results

Verley and Every (1977) conducted experiments on cylinders in waves at low K_c . Vibrations both in line and transverse were found to occur for U_r greater than 1.0. Steady flow conditions would only have led to in line oscillations for U_r less than 3.5 but the transverse oscillations can be explained by the shed vortices always passing the same side of the cylinder as described in Section 3.3.5. It was also found that the cylinder response was insensitive to the amount of damping. Verley and Every suspect that this was caused by the vortices being shed irregularly and so not building up a resonant response. The response to this type of intermittent vortex induced loading is less sensitive to the damping but should be less than that predicted by a response parameter curve.

The appropriate response parameter curve for use when vortices regularly pass one side of the member only has not been the subject of any research. However this is discussed in Appendix K where it is suggested that the amplitude of oscillation may be controlled providing R_p is greater than about 5.

Rajabi (1979) used the U tunnel apparatus of Sarpkaya (1976a) to determine the transverse response of spring mounted cylinders in planar oscillating flow. Rough and smooth cylinders were used in the experiment and it was found that the response parameter fitted the data better if C'_1 (rms) was introduced:

$$R_{pc} = 2M_e S / (\rho D^2 C'_1 \text{ (rms)}).$$

The peak response was found to occur at the mean frequency of the lift force (see figure 3.3.13). This corresponds to a Strouhal number of 0.16 based on the maximum velocity during the wave cycle or 0.25 based on the average particle speed.

Sarpkaya (1979b) discusses these results and presents response amplitude curves for R_p based on (1) structural mass with structural damping and (2) structural plus hydrodynamic added mass with structural plus hydrodynamic damping. To be consistent with the steady flow data we have adjusted the results to allow approximately for hydrodynamic added mass but no hydrodynamic damping. The resulting response curves are given in Figure 3.3.14. In comparison with the steady flow response curve (Iwan, 1975 plotted for C'_l (rms) = 0.33) the oscillating flow produces a lower response at low R_{pc} .

The highest values of R_{pc} given by Rajabi do not result in a very low amplitude of cylinder oscillation and it is difficult to extrapolate the curve to lower values. Also it is not certain that the U tunnel response parameter curve will be more applicable to wave flow than the steady flow response parameters. This is particularly the case at high K_c where wave drag forces are more closely related to steady flow drag than to oscillating flow drag. We therefore tentatively recommend that the steady flow response parameter - amplitude relationship is also applied to wave flow except for the case of one sided vortex shedding described above.

b. Intermittent lock-on

In wave flow the particle velocities over the whole wave cycle are not necessarily sufficiently high for continuous vortex shedding excitation to occur. Instead a repeating pattern of excitation followed by damped reducing oscillation is likely to occur. This is discussed further in Appendix L.

c. Effect of transverse oscillation on the drag force

No experimental results showing the effects of transverse oscillation on the drag force have been found for wave flow. It would be reasonable to assume that the effect would be similar to that found in steady flow. (See Figure 3.3.9)

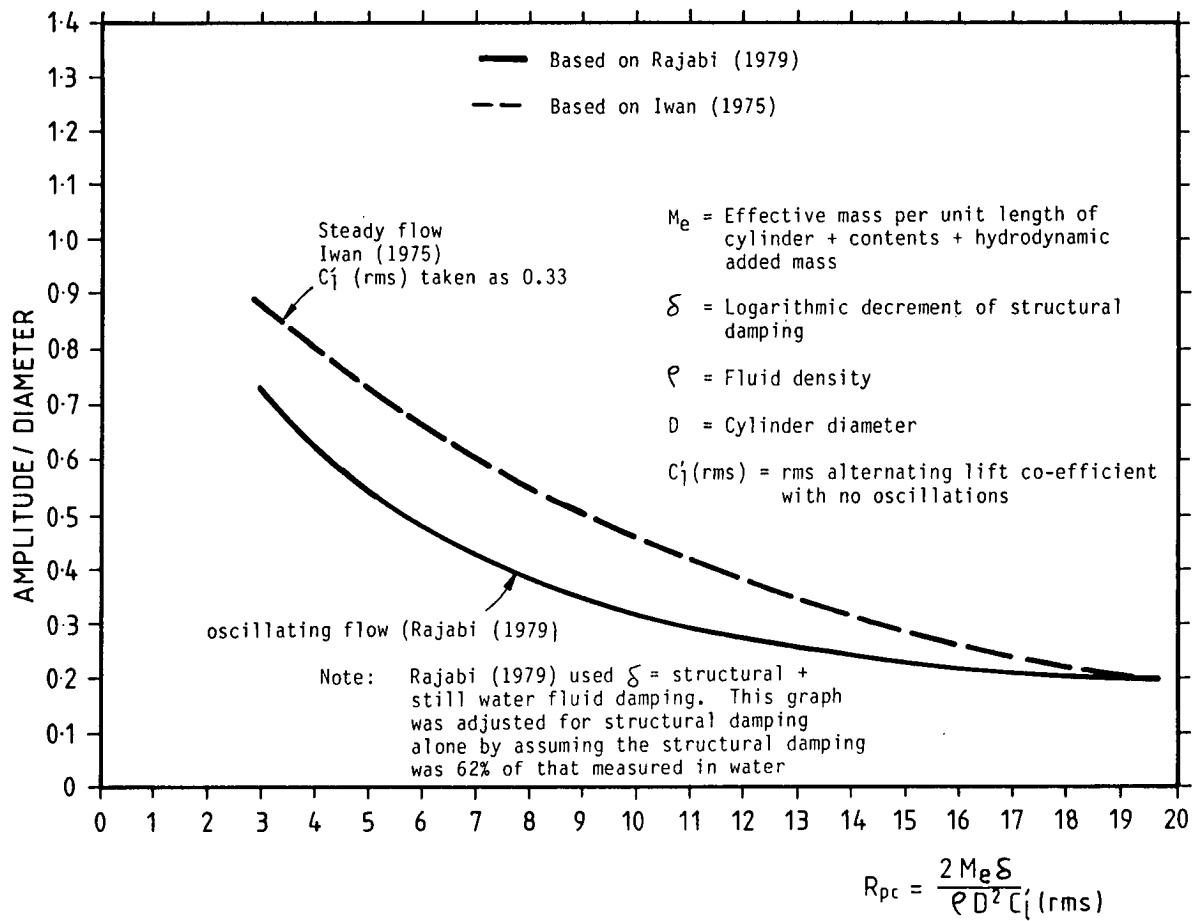


Figure 3.3.14 Amplitude of response of a spring mounted cylinder to vortex shedding excitation in oscillating flow

d. Cylinder Orientation

The vortex shedding behaviour of a vertical cylinder in waves and a cylinder in oscillating flow are expected to be similar by the independence principle discussed in 3.2.4. A horizontal cylinder will exhibit a different vortex shedding behaviour in which the vortices are convected around the cylinder as they are shed.

3.3.7 Recommendations for avoiding vortex induced member oscillation

a. Steady flow

In line oscillations should be avoided providing U_r , the reduced velocity: $U_c/(N_m D)$ is below 1.2. Transverse oscillations should be avoided provided U_r is below 3.5. If U_r is between 1.2 and 3.5 the amplitude of any (in-line) oscillation should be no more than 0.05D providing R_p , the response parameter: $2M_e \delta / (\rho D^2)$ is greater than about 1.8. If U_r is greater than 3.5 the amplitude of any (transverse) oscillation should be no more than 0.05D providing R_p is greater than about 20.

The above procedure controls but does not eliminate vortex induced oscillations. The small amplitude oscillations may still cause fatigue damage. A method for estimating fatigue damage from vortex shedding is given in Section 3.3.8.

b. Wave and current flow - vertical cylinders - (1)

If K_c is less than 4 waves alone will not cause vortices to shed. The combination of waves, with K_c less than 4, and current should be investigated as described in Section c below. (Note K_c should be calculated for the wave particle velocity alone).

If K_c is in the range 4 to 15 and the current is less than half the maximum wave particle velocity two vortices are shed per wave cycle and they may always pass the same side of the member. Large oscillations may occur if the natural frequency of the member is twice the wave frequency unless the response parameter: $R_p = 2M_e \delta / (\rho D^2)$ exceeds about 5 (estimated value not checked by experiment).

When K_c is in the range 4 to 15 and the current is less than half the maximum wave particle velocity, it is also possible to obtain large oscillations at the wave frequency, even when this does not correspond to a natural frequency. In this case the oscillation is caused by the particularly large drag and lift coefficients that occur in this range of K_c . The drag coefficient (see 3.2) may be further increased as described in 3.3.3b. The large lift coefficient is shown in Figure 3.3.10. In these cases it is necessary to perform a structural analysis to determine the response, which is no longer related to the response parameter.

If K_c is in the range 4 to 15 but the current exceeds half the maximum wave particle velocity the stability of the cylinder should be investigated as described in Section c.

If K_c is greater than 15 the stability of the member should be checked as described in Section c.

c. Wave and current flow - vertical cylinders - (2)

Section b defines certain cases for which this section is applicable. In these cases the criteria for vortex shedding induced oscillation may be taken as the same as for steady flow. However if the flow velocity is only in the critical range of reduced velocity for part of the wave cycle the value of the response parameter: R_p may be taken as $2M_g \delta / (\rho D^2 P)$ where P is given in Table 3.3.2.

d. Wave and Current Flow - Horizontal Cylinders

The vortex shedding pattern for a horizontal cylinder will be very different from that for a vertical cylinder. Vortices will however be shed at a similar frequency and, in the absence of any experimental data we would recommend that a horizontal cylinder is treated as in Section 3.3.7(b and c). The flow velocity to be used should be that normal to the cylinder and in the plane of the mode corresponding to the natural frequency being checked for lock-on.

Table 3.3.2 - Oscillation amplitude as a proportion (P) of the steady flow amplitude for intermittently locked-on vortex shedding.

	number of forcing cycles : f						
	0	1	2	5	10	20	999
	P						
	0	0	1	1	1	1	1
number of	1	0	0.38	0.56	0.77	0.88	0.95
decay cycles	2	0	0.24	0.39	0.63	0.79	0.90
m	5	0	0.12	0.22	0.42	0.61	0.79
	10	0	0.07	0.14	0.29	0.47	0.68
	20	0	0.05	0.09	0.20	0.36	0.57
	999	0	0.03	0.06	0.14	0.26	0.45

$\delta = 0.03$ during forcing cycles ($\xi = 0.5\%$)

$\delta = 0.05$ during decay cycles ($\xi = 0.8\%$)

f is the number of forcing cycles per wave where $U_r > U_{r\text{crit}}$

m is the number of decay cycles per wave where $U_r < U_{r\text{crit}}$

Note:

1. This table is applicable to a member continuously immersed in water. For members in the splash zone and subject to decay cycles in air $\delta = 0.03$ throughout and table L.3 should be used instead.
2. This table is based on an approximate calculation which assumes that:
 - a) locked on vortex shedding occurs as soon as the reduced velocity exceeds the critical value
 - b) damped reducing oscillations occur when the velocity is less than the critical value
3. For derivation see Appendix L

3.3.8 Fatigue analysis of members excited by vortex shedding

A fatigue analysis of a member subject to vortex shedding in a wide range of sea states is very difficult to perform. This is because a) the likely range of behaviour varies from full lock on to very little excitation and b) the presence of other types of wave loading complicates the stress range cycle counting.

An estimate of fatigue sensitivity could be made by performing a semi-probabilistic analysis (see Section 4.4.3) in which the sea conditions are split up into a large number of deterministic combinations of current and wave height, period and direction. Each deterministic case is analysed using the response parameter (Figure 3.3.7) in conjunction with Table 3.3.1 to determine the amplitude of oscillation of the cylinder for continuous excitation at the reduced velocity corresponding to perfect lock-on. The amplitude can be reduced by the factor P from Table 3.3.2 to allow for intermittent lock-on during a wave cycle.

The amplitude can be further reduced by a factor from Figure 3.3.5 to allow for the reduced velocity of most cases not corresponding to the peak response. This factor will be R for transverse oscillations (U_r greater than 3.5) or 10R for in line oscillations (U_r less than 3.5).

Having obtained the amplitude of oscillation these can be applied to the mode shape of the oscillation in order to calculate the member curvature and hence, from beam bending theory, the stress amplitude. This should be doubled to determine the stress range which may be taken to occur $T.N_m$ times during the wave cycle (where: T is the wave period (sec) and N_m is the members excited natural frequency (H_z)).

Hence the damage per wave and the cumulative fatigue damage for all waves from vortex shedding effects can be estimated.

The difficulty in adding the fatigue damage from vortex shedding alone to the fatigue damage from other e.g. Morison loading is discussed in 4.4.1b.

3.3.9 Vortex Shedding - Conclusion

Vortex shedding can excite resonant oscillations particularly in flexible members such as conductors and risers. This may result in large internal stresses with consequences for the member strength and fatigue life.

In a structure consisting of many small members having different natural frequencies, the shedding from different members is not usually synchronized and there will not usually be any global resonance effect.

However structural carry over effects from one member to another may be important. Also the natural frequency of a member is determined by the properties of adjacent members. Therefore it is not always satisfactory to calculate a natural frequency on the basis of a single member with idealised boundary conditions.

Response amplitudes under conditions of resonant 'lock-on' can be limited as described in Section 3.3.7. Fatigue damage can be estimated as described in Section 3.3.8.

Vortex shedding oscillations can most easily be avoided by increasing member diameter and natural frequencies. This will have the effect of decreasing U_r .

If that is not possible an increase in mass may increase R_p and help to prevent vortex shedding oscillations providing neither the diameter is increased nor the member natural frequency decreased. Therefore decreasing the span or increasing the structural wall thickness of a tubular member will make it less susceptible to vortex shedding.

Should neither of the above options be an acceptable solution it may be necessary to consider artificially increasing damping (see Walshe and Wootton, 1970) or to attach, for example, helical strakes to break up the flow (see Walshe and Wootton, 1970; Hallam et al, 1977, Zdravkovich, 1981 and Singh et al, 1984).

3.4 DIFFRACTION LOAD EVALUATION

3.4.1 Introduction

When structural members are larger in diameter than about $1/5$ of the wavelength it becomes necessary to analyse the manner in which the structure modifies or 'diffracts' the wave field (Standing, 1978). The analysis required is similar to a wave theory with additional boundary conditions of no flow through the structure. Diffraction theory is based on inviscid irrotational flow and therefore does not include any drag force in the estimate of loading. Fortunately when diffraction effects are important then the drag component of the total wave frequency loading tends to be small.

For a single member, as the wave length reduces to about twice the member diameter, the effect of diffraction is usually equivalent to a reduction in the inertia coefficient and a change in the phase of the inertia loading. The modification of the waves by a member may increase the wave height in the vicinity of the member. This is known as wave 'run up' or upwelling and should be taken into account when calculating the air gap (Eatock Taylor, 1987). The modified wave pattern also affects and is affected by other members. This may significantly increase or decrease the loading according to the characteristics of the modified wave pattern.

Various single and multiple body diffraction problems have been solved: see Hogben and Standing (1975) and Sarpkaya and Isaacson (1981). These will provide initial guidance on the likely effect of wave diffraction but it will frequently be necessary to perform a diffraction analysis using a general purpose computer program.

Some examples of the effect of diffraction on the loading on vertical cylinders are given in figures 3.4.1 to 3.4.4.

3.4.2 Analytical and numerical methods

The theoretical basis of diffraction theory is described in many texts, e.g. Sarpkaya and Isaacson (1981). Relatively simple problems e.g. of a vertical cylinder, may be solved analytically. More complex shapes may generally only be solved using numerical methods on a computer.

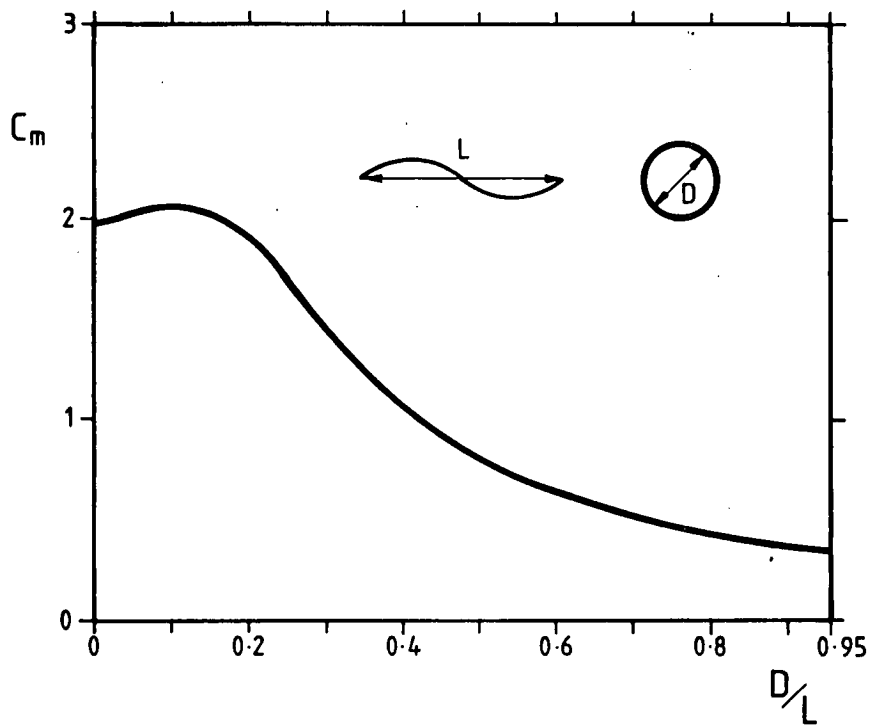


Figure 3.4.1. Effective inertia coefficient in diffracting conditions (Mogridge and Jamieson, 1976)

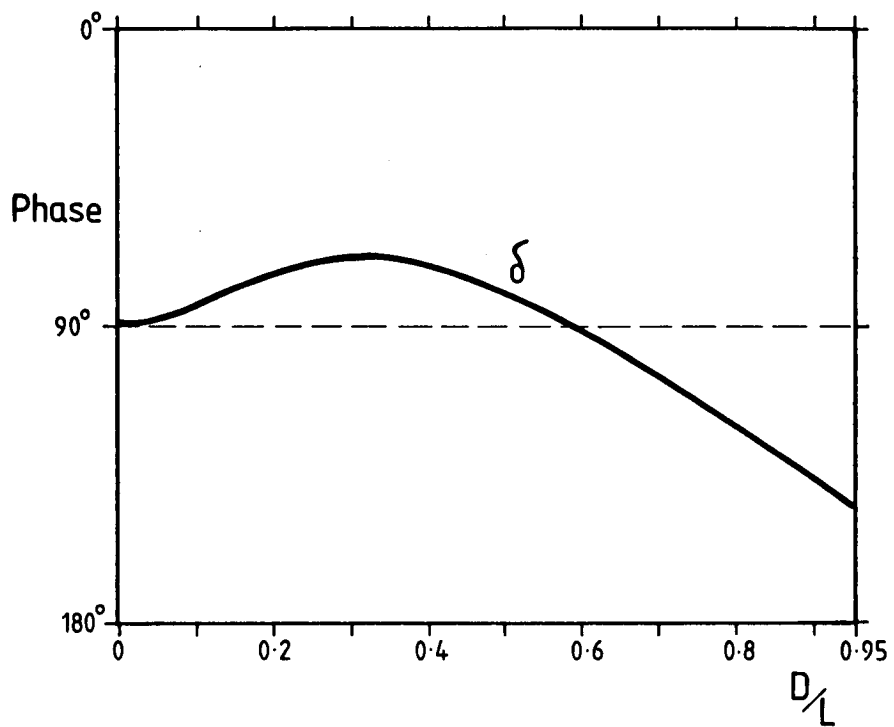


Figure 3.4.2. Phase of diffraction loading (Mogridge and Jamieson, 1976)

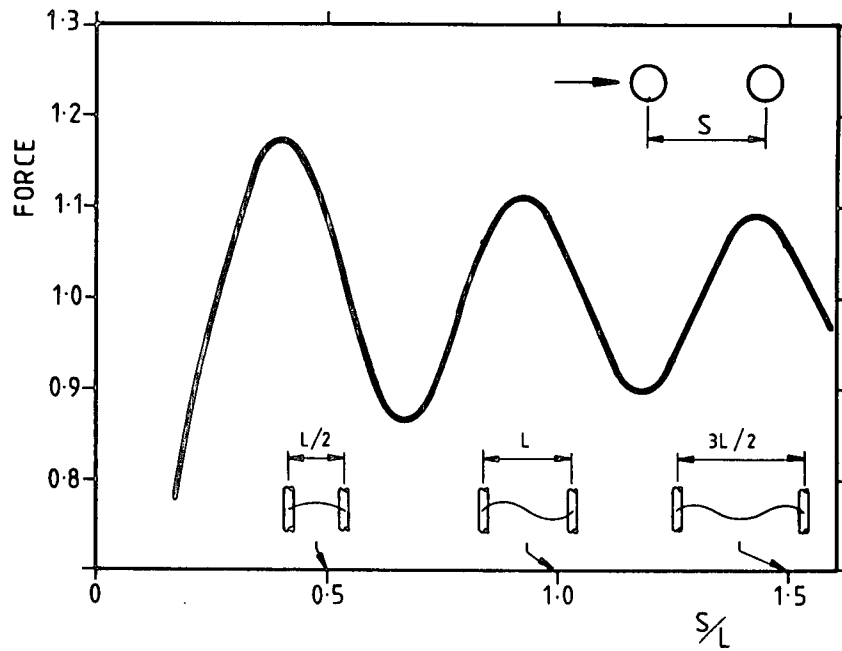


Figure 3.4.3. In-line force on upwave cylinder
(Spring and Monkmeier, 1974)

THE FORCE IS NORMALISED BY THE FORCE ON AN ISOLATED CYLINDER
 S = CYLINDER SPACING L = WAVELENGTH
 WAVELENGTH = $15.7 \times$ CYLINDER DIAMETER

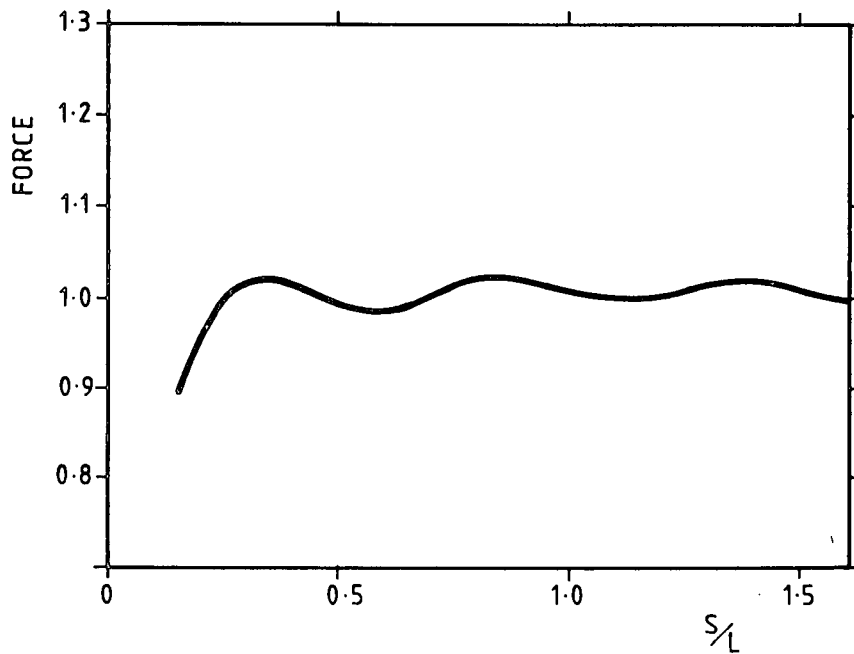


Figure 3.4.4. In-line force on downwave cylinder
(Spring and Monkmeier, 1974)

The finite element method has been used for treating wave diffraction problems see Zienkiewicz (1977) and Shen (1977). Source-sink methods are also commonly used at present. They only require a discretisation of the surface of the structure whereas the finite element method requires a three dimensional mesh of solid elements to represent the sea in the vicinity of the structure: see Hogben and Standing (1974). In either case mesh refinement studies or previous experience are needed in order to select a suitable mesh which should avoid numerical ill conditioning, be sufficiently fine to produce satisfactory answers but not so fine that excessive computer time is used.

The diffraction method is usually only applied to first or second order based on the assumptions of Stokes wave theory. Isaacson (1977) has solved the case of cnoidal wave diffraction by a vertical cylinder and (1981) describes a time stepping procedure for steep non linear waves interacting with arbitrary shapes of structure.

3.4.3 Effects of currents

The effect of currents on the loading on large bodies has been summarised by Hogben and Standing (1975) who mention three possible modes of influence on the wave force.

- 1) The incident wave motion may itself be altered in the presence of a current as described in Section 2.3.
- 2) Although drag forces are not taken into account in the diffraction approach, they are nevertheless liable to be significant in the presence of an appreciable current, this effect would normally be predicted on the basis of Morison's equation.
- 3) When a surface-piercing structure is subjected to a steady current, a surface wave pattern is set up which gives rise to an additional force, the so-called 'wave-making resistance' acting on the body. This may be taken into account by some diffraction theory programs. (Inglis and Price, 1980).
- 4) Diffracted and radiated wave patterns are also affected by current.

3.4.4 Differences between diffraction and the inertia term in Morison's equations

In section 3.1.3 the inertia loading on a member in accelerating flow is shown to be the sum of:

- a) The incident wave or Froude Krylov force : $\rho V \dot{U}$
- b) An added mass force associated with the modification to the flow by the stationary member: $C_a \rho V \dot{U}$
- c) Also if the member itself accelerates there is an additional inertia force or added mass force: $-C_a \rho V \dot{U}_m$

In the above equations:

- ρ = water density
- V = member volume
- \dot{U} = flow acceleration
- \dot{U}_m = member acceleration

There are a number of differences between the case of accelerating flow and diffracting conditions:

- 1) The three forces are no longer in phase with the acceleration at the centre of the member.
- 2) The Froude Krylov force no longer equals $\rho V \dot{U}$
- 3) Owing to 1) and 2) it is no longer possible to define $C_m = 1 + C_a$
- 4) The added mass force for flow acceleration is no longer equal to the added mass force for member acceleration.

3.4.5 Influence of diffracting members on other members

In many structures large diameter diffracting members will modify the wave loading on nearby non diffracting members for which Morison's equation would be applicable. A typical example (Standing, 1978) is the tower of a gravity platform which may be subject to drag and inertia loading conditions in a wave field modified by the presence of a large diameter base. This interaction affect may be taken into account by some diffraction programs.

3.4.6 Comparison of diffraction theory with experiment

Many comparisons have been made between diffraction theory calculations, model tests and real structures. In general diffraction theory is found to predict forces quite well.

Skjelbreia (1979) compares model test results and theoretical calculations for a concrete gravity structure and concludes that existing theories have a fair accuracy, that loads acting above MWL should not be ignored and that in some circumstances, dependent on the soil conditions, pressure loads acting on the underside of the base may need to be taken into account.

3.4.7 Jarlan walls

Some large diameter structures include perforated 'Jarlan Walls'. The analysis of these structures should account for wave diffraction and head loss in the flow through the perforations. Advice from hydrodynamic specialists should normally be sought before attempting either mathematical analysis or model test of these structures.

3.5 WAVE SLAM AND WAVE SLAP

3.5.1 General

As a wave surface immerses a member some water is rapidly accelerated to make way for the member. If the member enters the water at an angle the slam force amounts to a small force which moves along the member at the point of contact with the water surface. If the member enters the water with a face parallel to the water surface then the force acts along the whole length of the member at the same instant. This results in a short duration force which may be much larger than that from drag or inertia loading.

The force is known as a slam force if a horizontal member is immersed by a rising wave surface or if the member moves down into the wave, e.g. during transportation of a jacket on a barge.

The force is known as a slap force if an approximately vertical surface of a breaking or near breaking wave immerses a member.

In addition to the slam or slap forces buoyancy is applied to a member as it is immersed. Also a cavity forms behind the member which results in a suction force on the member until the cavity fills. This cavity effect is however not as important as the acceleration effect (Ridley, 1982). The relative importance of the Morison, buoyancy and slamming contributions to the total load was examined by Miller (1978) who found that the slamming term is the largest component if the Froude number $U/(gD)^{0.5}$ is greater than about 0.6.

Slamming affects local loads and fatigue lives of individual members. It does not usually increase the total design load on e.g. a jacket structure by an appreciable amount.

Roughness or fouling of a member will influence the slamming mechanism. Fouling changes the time history of the slam force and this might increase or decrease the slam load. The member's dynamic response is always important during wave slam and this is affected by any change in the time history of the force or any additional weight of marine growth attached to the member. The interaction of slam force time history and dynamic response has been considered by Ridley (1982).

3.5.2 Slam coefficients for cylinders

a. Equation for slam force

Present design practice is to calculate the slam force using an equation similar to that used for the calculation of drag force but with a slam coefficient in place of the drag coefficient. (It should be noted however that slam is an inviscid flow phenomenon which is hardly affected by viscosity or vortex shedding and that the similarity in the form of the equations is coincidental). The overall slam force on the cylinder is a maximum when the axis of the cylinder is parallel to the water surface. The slamming force per unit length is expressed in the form:-

$$F_s/L = 0.5 C_s \rho D U_p |U_s| \quad \text{or} \quad F_s/L = 0.5 C_s \rho D U |U|$$

where :

U_p is the velocity of the water particles resolved normal to the cylinder

U_s is the velocity of the normal to the surface resolved normal to the cylinder

For most cases of slamming $U_p = U_s = U$. For wave slap, particularly of vertical or inclined members in spilling breakers U_p and U_s may be very different.

D is the member's local effective diameter, ρ is water density and C_s is the slamming coefficient.

b. Theoretical time average slam coefficient

An insight into the slam phenomenon can be gained from the following simple analysis. During a wave slam an added mass per unit length of $C_a \rho \pi D^2/4$ is decelerated from a velocity of U_p to 0 in a time equal to D/U_s .

Force = rate of change of momentum therefore

$$\text{Force} = (C_a \rho \pi D^2/4) U_p / (D/U_s) = 0.5 (C_a \rho \pi/2) D U_p U_s$$

By comparison with the slam force equations in terms of C_s , C_s average = $C_a \pi/2$.

For a cylinder $C_a = 1$ and the average C_s would therefore be $\pi/2$.

However experiments have shown that the rate of change of momentum is not uniform over the immersion time but is very high just as the water surface touches the member.

Some recent tests on cylinders are described below:

c. Experimental measurements of slam coefficients

Faltinsen et al (1977) measured slam coefficients between 4.1 and 6.4 on rigid cylinders and found higher values on flexible cylinders.

Sarpkaya (1978) measured slam coefficients between 1.6 and 5.3 using the oscillating flow water tunnel (Fig. 3.2.10) but with the cylinder at the top of one of the vertical legs. He noted the importance of the dynamic response of the member and found that roughness increased the force rise time but tended to decrease the dynamic response of the member.

Kaplan (1979) estimated slam coefficients of between 1.9 and 5.1 based on measurements taken on the OTS structure. Sampling rate and data filtering problems prevented peak forces from being obtained and the estimates were made by comparing the actual measured time histories with similarly sampled and filtered theoretical time histories.

Campbell and Weynberg (1980) measured slam coefficients of 5.1 for perpendicular slamming into calm water, 4.1 for slightly disturbed water, 2.9 for aerated disturbed water and 4.1 for soft fouled cylinders. The variation in slam coefficient seems to be caused by a number of factors :-

1. the surface roughness
2. the shape of the water surface as it hits the member
3. the dynamic response of the member

Item 3 probably has a small effect on the peak slam force applied to a member. However, if the slam force is inferred from the response of the slammed member then the dynamic response of the member is important (see Section 3.5.3).

When the water surface is not parallel to the surface of the member the effect of the slam is that of a point load traversing the member. This produces lower slam coefficients. However, the smooth cylinder/calm water coefficients are reduced more than the fouled cylinder or disturbed water coefficients.

The time histories of the slam forces as measured by Campbell and Weynberg were :

$$5.15 / (1 + 19 Ut/D) + 0.55 Ut/D \text{ for the smooth cylinder}$$

and

$$4.1 / (1 + 8.3 Ut/D) + 0.45 Ut/D \text{ for the fouled cylinder}$$

where t = the time from the commencement of the slam

d. Theoretical estimates of slam force time histories and coefficients

Impact with a flat still water surface has been studied extensively because of its importance for ship hull slamming, seaplane landing and spacecraft touchdowns in the sea. Mathematical models have been developed for cases of simple geometry, such as spheres and wedges: Szébehely (1959), and cylinders: Kaplan and Gilbert (1976).

Various methods have been used to estimate the time history. A simple approach for a cylinder assumes that the added mass is equal to that of a flat plate of width equal to the instantaneous wetted width of the member. The slam force is then estimated from the rate of change of added mass. This gives a C_s value of π for a cylinder.

More detailed hydrodynamic analyses, taking into account the generation of spray, have produced higher values.

Gallagher and McGregor (1985) show the importance of trapped air during wave slamming by using a finite difference analysis which models the air flow as well as the behaviour of the water.

3.5.3 Member response to slam

Slam occurs over a very short period of time. This produces a dynamic response in the member which may increase or decrease the effect of the slam loading.

Miller (1980) accepts that high C_s values are possible but notes that the ideal conditions necessary have a low likelihood of occurrence in the real sea. By taking into account the directional and frequency spread of the waves and typical response characteristics of members, he suggested that a constant slamming coefficient $C_s = 3.5$ is usually conservative for estimating both extreme stresses and fatigue life.

Ridley (1982) extended Miller's (1980) work and, based on the time histories from Campbell (1982) produced graphs which enable the peak dynamic response of members to slam loading to be easily calculated. The dynamic amplification factor may be as high as two. The angle between the water surface and the member as the slam occurs is allowed for in the calculation and is shown to have a significant effect. Figures 3.5.1-3.5.2 are based on Ridley's work. Figure 3.5.1 shows the dynamic amplification factor, i.e.

(Dynamic peak response)/(peak response if the slam load were to be applied slowly).

Figure 3.5.2 shows the dynamic range factor, i.e.

(Dynamic max-min response)/(peak response if the slam load were to be applied slowly).

A 'response' may be deflection, moment or bending stress.

The figures are presented in terms of θ L/D and $U/f_n D$.

Where :

θ^c = angle between member axis and water surface (radians)

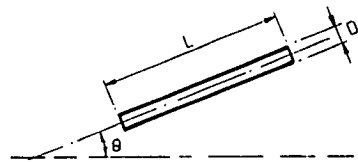
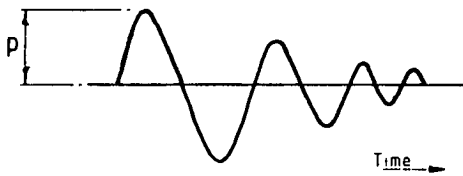
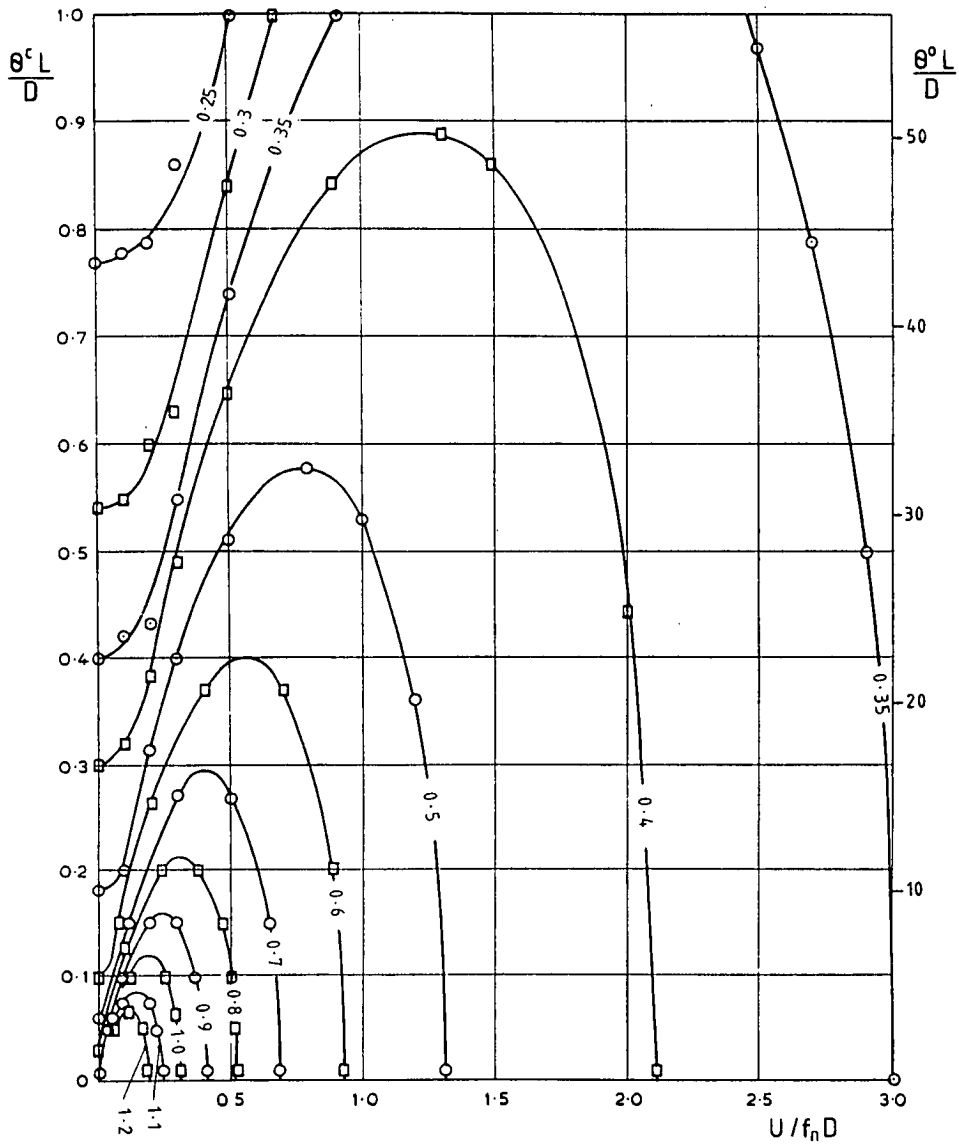
θ^o = angle between member axis and water surface (degrees)

L = member length

D = member diameter

U = velocity of impact measured normal to the cylinder (the possibility of different values of U_p and U_s was considered but not included in the final results)

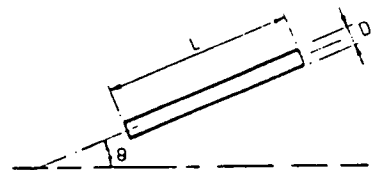
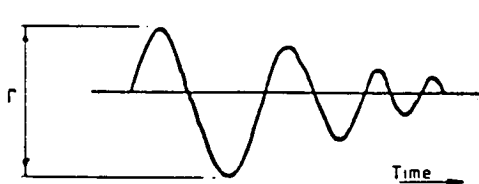
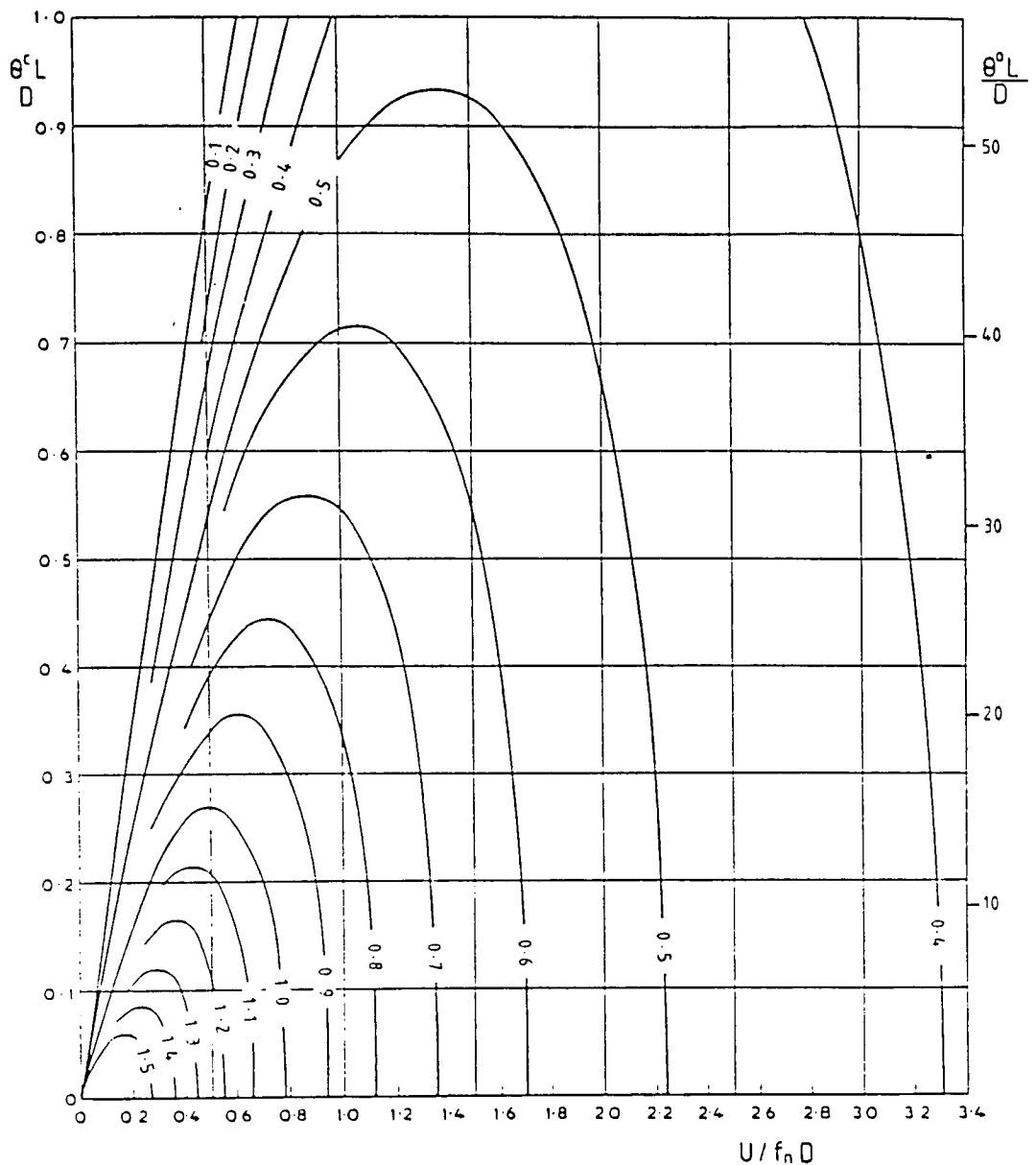
f_n = natural frequency of the member (H_z)



Notes

- D = diameter of member
- L = length of member
- f_n = natural frequency of member (excluding hydrodynamic added mass)
- U = velocity resolved normal to cylinder
- θ^c = angle between member and water surface (radians)
- θ^o = angle between member and water surface (degrees)

Figure 3.5.1. Initial peak slam response (p)/peak quasi static response



Notes

- D = diameter of member
- L = length of member
- f_n = natural frequency of member (excluding hydrodynamic added mass)
- U = velocity resolved normal to cylinder
- θ^c = angle between member and water surface (radians)
- θ^0 = angle between member and water surface (degrees)

Figure 3.5.2 Dynamic slam response range (r)/peak quasi static response

Because wave slam leads to a dynamic response in the slammed member a large number of cycles of oscillation occur for each slam. The oscillations will decay according to the damping characteristics of the member. The effect of these oscillations is to considerably increase the fatigue damage from wave slam effects. Ridley (1982) provides guidance on the form of the oscillations corresponding to assuming a logarithmic decrement of 0.05.

3.5.4 Probability of wave slam

Probabilities of wave slamming were discussed by Miller (1980) and further considered by Ridley (1982). They allowed for:

- a. The distribution of wave heights within a sea state.
- b. The distribution of mean water level.
- c. The distribution of wave directions.

The method is based on probability theory applied to water surface elevation within each sea state.

An alternative and conceptually much simpler method for calculating the probability of wave slams is to use the semi-probabilistic approach. This is described in 4.3.3 (for strength analysis) and 4.4.3 (for fatigue analysis) of Morison and diffraction loading effects. It is however easily adapted to wave slam and may be used in conjunction with Ridley's (1982) dynamic analysis of the response of a member to slam.

3.5.5 Slam coefficients for non-cylindrical members

a. Flat sided members

Slam coefficients for flat sided members will be very dependent on the angle of the sides to the water surface and the flatness of the water surface. Should a slam occur where a flat wave surface is nearly parallel with the member surface then very large values of slam coefficient may be expected.

However, the probability of flatness and perfect alignment will usually be very small and it is tentatively proposed that for non critical members a slam coefficient of 3 should be used with a dynamic amplification factor of 2.

Flat sided members which are subject to slamming and are critical (for overall structural safety or for other reasons) should be justified by model tests or by reference to the available literature. Broughton and Horn (1987) calculated the overall vertical slam forces on the underside of a platform deck using an added mass analogy. The calculated forces were compared with experimental results and were found to be reasonable estimates for 0.56m overlap, of this platform deck and wave crest, but the force was overestimated for 1.86m of overlap. Miller (1978) provides a useful bibliography.

b. Curved sided members

Members having a variable curvature, may be assumed to be subject to the same peak slam force per unit length as a cylinder having the same radius as the member at location of the wave impact.

$$\text{i.e. } F = 0.5 C_s \rho (2R) u^2$$

where R is the radius of curvature at the point of impact.

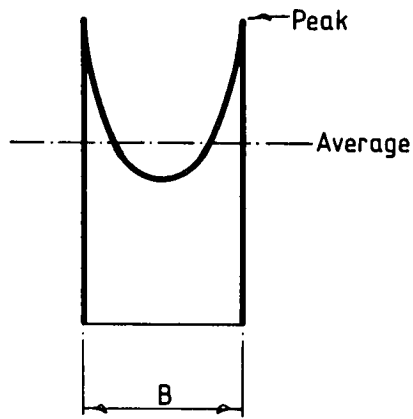
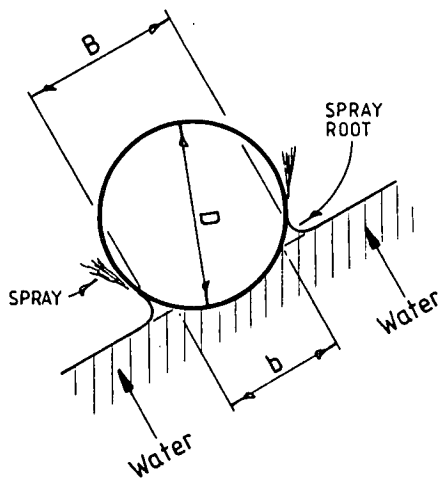
3.5.6 Pressure distributions from wave slam

For some members the high local pressures caused by wave slam may need to be considered. Campbell and Weynberg (1980) have measured pressures on cylinders subject to slamming. Figure 3.5.3 has been based on their results. This figure shows the width of the cylinder subject to the pressure, and the average pressure over that width, at any given time. The results are given in terms of the pressure coefficient C_p where:

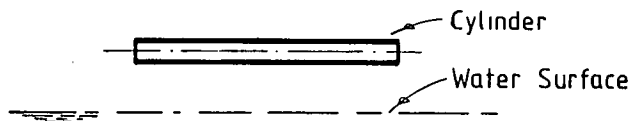
$$P = 0.5 C_p \rho U_p U_s.$$

Using this data a time history of the pressure loading on a panel of a cylinder may be calculated.

The initial peak pressure is very dependent on the 'rise time' and this in practice varies from one impact to another. Most experimental work seems to produce rise times of 0.001 to 0.01 seconds for nominally parallel impact. This limits the peak pressure, usually quite considerably. It is not clear whether there is any scale effect associated with the rise time. Results from tests at various scales seem to produce similar values of rise time which suggests that it may be independent of scale.



TYPICAL PRESSURE DISTRIBUTION C_p IS GIVEN FOR THE AVERAGE PRESSURE



Slam Pressure $P = \frac{1}{2} C_p \rho U_p U_s$

Basis of Graph

the force time history:

$$C_s = 5.15 / (1 + 19 Ut/D) + 0.55 Ut/D$$

and B vs $U_s t/D$ from Campbell and Weynberg (1980) Figure 6

$$\frac{U_s t}{D} = \frac{1}{2} \left(1 - \cos \left(\sin^{-1} \left(\frac{B}{1.5D} \right) \right) \right)$$

from geometry of cylinder and spray roots

U_N is the particle velocity of the flow resolved normal to the cylinder

U_s is velocity of the normal to the water surface resolved normal to the cylinder

- 1) Determine rise time: t_R take 0.001 sec if no other data available
- 2) Calculate $U_s t_R/D$
- 3) Locate point P corresponding to $U_s t_R/D$,
- 4) Joint point P to the origin
- 5) The C_p time history is then given:

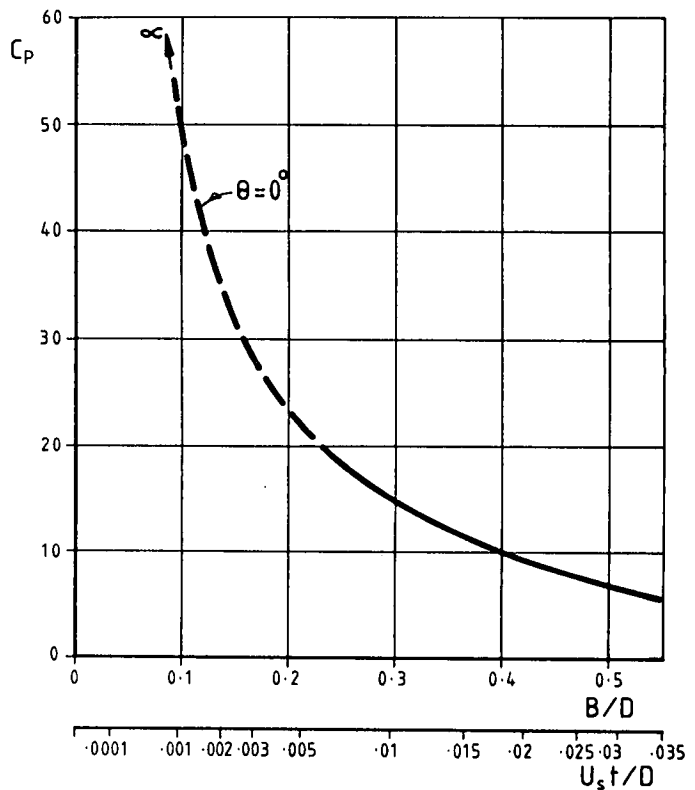
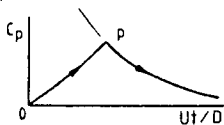


Figure 3.5.3. Slam pressure coefficient time history

Note that the rise time for the pressure in a localised area will not necessarily be the same as the rise time for the total force.

3.5.7 Wave slap

a. General

Wave slap occurs when a breaking or near breaking wave immerses a member. The physics of the slap force is exactly the same as that of wave slam, therefore the calculation methods for slam forces and pressures may also be used for wave slap on members.

Slap pressure measurements include those by Denny (1951) which are related to sea walls, Kjeldsen (1981) for impacts on flat plates in deep water conditions (Figure 3.5.4) and Ochi and Tsai (1984) for breaking and recently broken deep water waves.

The results of these measurements have been presented in non dimensional form related to either the wave height or the wave particle velocity. Approximate relationships between these results and the C_p defined in Section 3.5.6 are derived in Appendix M and used in the remainder of this section.

Damage to offshore structures corresponding to slam pressure in excess of 1 MN/m^2 has been recorded by the Department of Energy. Higher extreme pressures may be expected on the basis of model test results although actual values are very difficult to predict.

b. Slap pressures on cylinders and curved surfaces

Ochi and Tsai (1984) measured slap forces on cylinders from just breaking and recently broken deep water waves. In Appendix M4 we have estimated that their measurements correspond to a C_p of about 9 for the broken wave and 13 for the breaking wave. We also show that these values are reasonably consistent with the slam pressure time history given in Figure 3.5.3. It is therefore recommended that wave slap is treated as wave slam for the calculation of pressure loading.

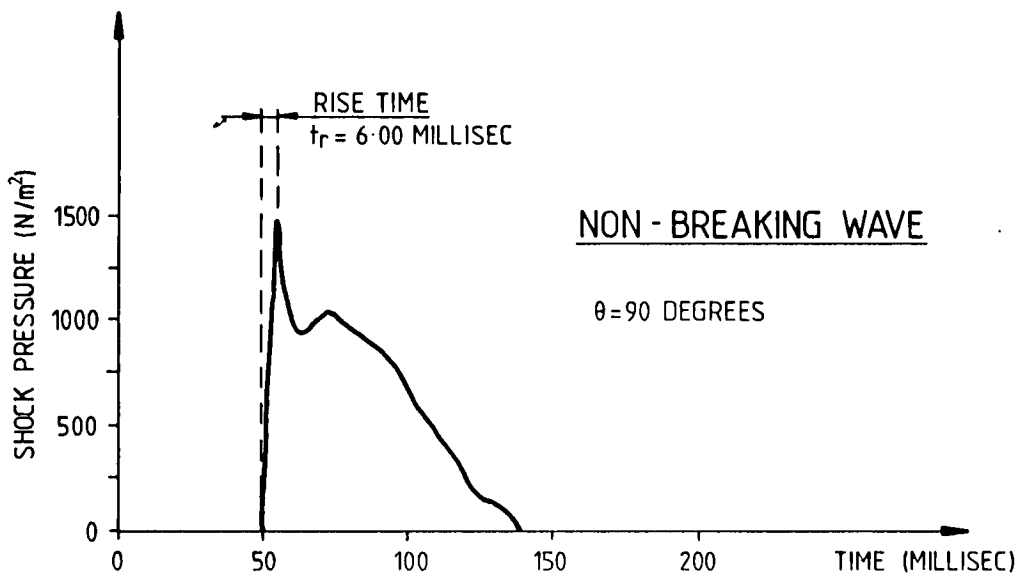


Figure 3.5.4. Shock pressure time history from a deepwater spilling wave (Kjeldson, 1981)

c. Slap Pressures on flat areas

This problem is similar to that of a steep wave hitting a sea wall or the side of a ship.

An average slap pressure coefficient can be calculated for this case based on the rate of change of momentum.

If a flow having a velocity U is assumed to be stopped by a perpendicular wall the momentum change per unit area per unit time is ρU^2 .

The average slap pressure is given by $0.5 C_p \rho U^2$.

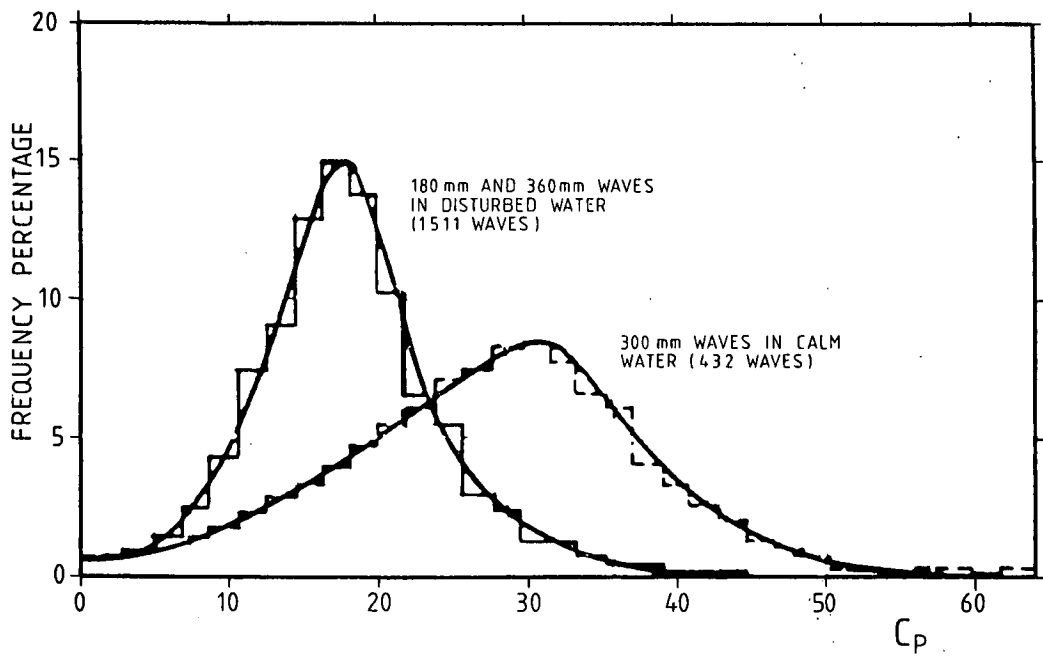
Therefore C_p (average) = 2.

Broughton and Horn (1987) used a similar approach for estimating the horizontal forces on a platform deck with inadequate air gap. They estimated the pressure as ρcU , where c is the celerity of the wave, and compared the result with model tests. They found that the force was reasonably estimated for a 0.56m overlap of wave and platform deck but whereas the calculated force increased considerably when the overlap was 1.96m the model test predicted an increase of only 10%.

As for the case of wave slam on a cylinder a wave impact on a vertical face produces an initial peak pressure many times the average value.

Wiegel (1964) reviews some of the early research associated with waves breaking on sea walls. Some of the most interesting work was by Bagnold (1939) and Denny (1951). Denny presented ratios of pressure head to wave height for plunging waves. These were carefully set up to give the highest pressures on sea wall. The spread of values is seen to be considerable and dependent on the surface characteristics of the water: measured pressures were considerably less when there were 'wavelets' of about one tenth of the main wave height superimposed on the main wave. Denny's results, adjusted to C_p values, as discussed in Appendix M4, are shown in Figure 3.5.5. For rough wave surfaces the average value of C_p is about 18.

Denny also shows where, in the wave height, the maximum pressures were found to occur (Figure 3.5.6).



Note: The C_p values have been estimated from pressure head/wave height data - see Appendix M.2

Figure 3.5.5. Frequency of impact pressures on a model sea wall (Denny, 1951)

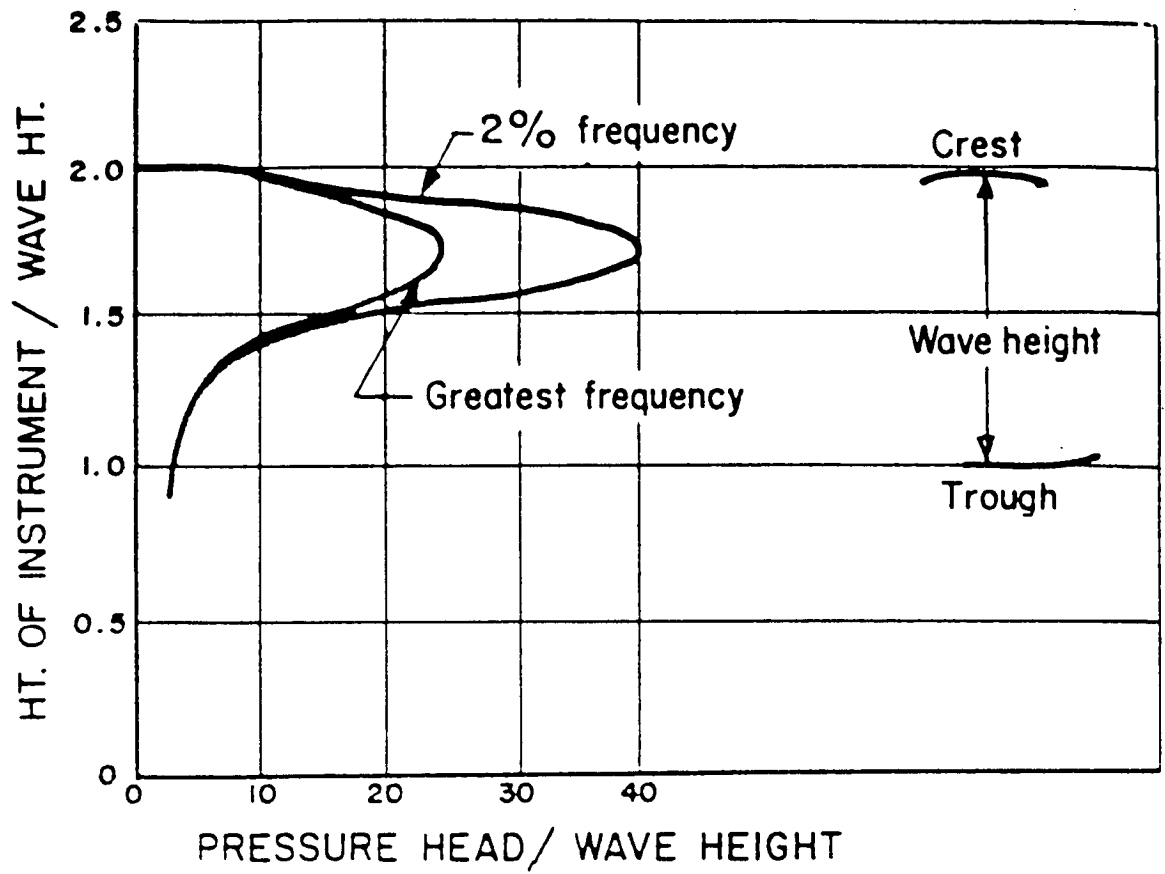


Figure 3.5.6. Pressure distribution on a model sea wall (Denny, 1951)

Slap pressures on a vertical plate in deep water waves have been measured by Kjeldsen (1981). In Appendix M3 we have estimated that his measurements correspond to a C_p of about 7.

Kawakami, Michimoto and Kobayashi (1977) performed slamming experiments with a model ship, having a flat bottom, in regular waves. The C_p values determined for various locations on the bottom had average values of 19 to 47 and maximum values of 25 to 73.

Rask (1986) compares a number of formulae for slamming pressures on ships hulls. These are based on theoretical and experimental studies of wedges impacting a water surface. For a wedge whose faces make angles of 10° with the water surface the predicted C_p values varied from 17 to 70.

3.5.8 Probability of wave slap from breaking waves

a. Probability of wave breaking in deep water

This is difficult to determine. Estimates can be made on the basis of individual wave scatter diagrams, e.g. Ochi and Tsai (1984) but they depend on the shape of the extreme part of the diagram which is probably not very reliable.

Kjeldsen et al (1981) and Myrhaug and Kjeldsen (1987) have made predictions of breaking wave occurrence on the basis of measurements taken around the Norwegian coast.

b. Probability of wave breaking in shoaling conditions

The probability may be determined by using an individual wave scatter diagram for the waves in deep water and before they approach the shallow water. The waves which break at any given location and their breaking characteristics can be estimated using the method given in 2.4.2.

3.5.9 Recommendations for the calculation of wave slam and slap forces and pressures

a. General

In this section wave forces are given for overall member analysis and wave pressures are given for local analysis of, for example, individual plates and stiffeners.

Both forces and pressures are subject to scatter but the pressures are much more variable than the total forces.

b. Slam and slap forces

Ridley's (1982) method described in Section 3.5.3 should be used.

c. Slam and slap pressures

Overall the various experiments show that slamming and slapping pressures can vary considerably. Further research is required particularly on slapping pressures and slapping wave probabilities. Ideally reliability techniques would then be used to determine satisfactory design criteria.

Slam and slap pressures may be tentatively estimated using Figure 3.5.3. This figure gives a time history of the pressure and a time history of the chord width 'B' over which the pressure acts. Large areas of plating can therefore be designed for much lower pressures than small areas of plating.

The highest pressure on the smaller areas of plating is limited by a 'rise time' effect which is probably associated with the compressibility of trapped air. In the worst cases the highest pressure occurs about .001 second after the wave and member first touch.

Wave slam and slap pressures will be reduced by the presence of small wavelets on the surface of the main wave. This should result in a reduction in pressure, perhaps to about one half the value predicted by the graph in Figure 3.5.3.

For wave slam calculation the water surface of the main wave (on which the wavelets are superimposed) may reasonably be assumed flat. For wave slap calculations the assumption of a flat surface is likely to be too conservative as the breaking wave will almost certainly be curved both in plan and elevation. This overall curvature should lead to a further reduction in slap pressure, especially for members whose diameter is greater than the wave height.

We give a tentative method for estimating slap pressures allowing for wave surface curvature, along with some examples, in Appendix N.

d. Statistics of wave slam and slap

The statistics of wave slam and wave slap occurrence are discussed in Section 3.5.7 and 3.5.10. In addition to the probability of occurrence of a particular impact velocity it is necessary to consider the probability distribution of the impact coefficient (C_s or C_p). However, it is unlikely that both will have extreme values in the same event.

For fatigue calculations it is also necessary to consider the range of impact coefficients that occur. Again using the maximum values will be conservative.

3.6 HYDROSTATIC AND HYDRODYNAMIC PRESSURE

3.6.1 Hydrostatic pressure

The global effect of hydrostatic pressure is simply that of buoyancy and a calculation based on immersed volume is satisfactory. However, in order to calculate the stresses in a member immersed in water, a more complicated calculation, based on the actual pressure distribution, is required. It is occasionally necessary to consider the influence of internal and external pressure on the global behaviour of slender beam members. There is an interaction between the pressure along the length of an immersed member and the curvature of the member. This results in external pressure reducing bending deflections and an internal pressure increasing bending deflections. This interaction may be analysed using the effective tension approach (Sparks 1980). The effect is typically only important when the difference between the internal and external pressure exceeds 100m of water.

3.6.2 Hydrodynamic pressure

The distribution of hydrodynamic pressure on a body immersed in an inviscid fluid can be calculated from potential theory for steady or uniformly accelerating flow (see Sarpkaya and Isaacson, 1981) or from diffraction theory for wave flow (see Section 3.4). A body in sea water will shed vortices and this will change the pressures calculated from diffraction theory.

The order of magnitude of the inviscid flow hydrodynamic pressures may be estimated by calculating the so called Incident, Froude Krylov or Excess Pressure under the waves. This is the cyclic pressure, caused by the waves, that would occur if there was no structure present. (see Appendix A, Table A1). The presence of the structure will modify the incident pressure and result, in theoretical inviscid flow, in total hydrodynamic pressures of typically 0.5 to 2.0 times the incident values.

The pressures associated with flow separation may be determined approximately from the time averaged and fluctuating drag and lift forces, which may be assumed to act on the projected area of the member.

Pressures caused by wave slam and slap are discussed in 3.5.

3.7 INTERFERENCE BETWEEN MEMBERS

3.7.1 General

Members of offshore structures do not occur in isolation. The effect of the wake of one member on another and the alteration of the velocity field may significantly change the resultant forces from those predicted.

Flow interference between circular cylinders in various arrangements has been reviewed by Zdravkovich (1977, 1985) and Sarpkaya and Isaacson (1981). Most of this work has been performed in subcritical flow but the results show that there is generally only a moderate change in the drag forces acting on the members providing the centreline spacing is greater than 3 to 4 diameters. Changes in drag force when one cylinder is in the wake of another become very small at a spacing of 10 to 15 diameters but lift forces may still be affected significantly up to a spacing of 20 diameters. For spacings of less than 3 diameters interference effects may become very large.

When performing experimental work on arrays a significant proportion of the width of the tank or tunnel may be occupied by the members. This 'blockage effect' may cause higher forces on the members than would occur in the open sea.

Sections 3.7.2 to 3.7.8 deal with rectangular arrays of 2 or more cylinders having approximately equal diameters. Sections 3.7.8 to 10 deals with attachments and Section 3.7.11 discusses joints.

3.7.2 Forces on arrays of cylinders in steady flow

Pearcey et al (1982) measured drag forces on groups of smooth cylinders in simulated post critical steady flow (by using trip wires and an actual Reynolds number of 4×10^4 to 8×10^4).

They found that for a pair of cylinders at a centreline spacing of $5D$ the drag coefficient for the downstream cylinder was considerably affected by the angle of incidence of the flow. When the flow is in line with the cylinders the drag force on the rear cylinder reduced to 64% of the isolated cylinder value. However, when the flow is at 18.5° to the plane through the axes of both cylinders the drag force on the rear cylinder increased to 128% of the isolated cylinder value. In both cases the force on the front cylinder remained at the isolated cylinder value.

Pearcey et al (1982) also measured forces on cylinders in 2 x 2, 3 x 3, and 4 x 4 arrays with a centreline spacing to diameter ratio of 5. Figures 3.7.1 and 3.7.2 show the effect of interference on the 2 x 2 and 3 x 3 cylinder arrays. Table 3.7.1 shows the increased in line forces on individual members and thw whole group which are important for the analysis of strder increased to 128% of the isolated cylinder value. In both cases the force on the front cylinder remained at the isolated cylinder value.

Pearcey et al (1982) also measured forces on cylinders in 2 x 2, 3 x 3, and 4 x 4 arrays with a centreline spacing to diameter ratio of 5. Figures 3.7.1 and 3.7.2 show the effect of interference on the 2 x 2 and 3 x 3 cylinder arrays. Table 3.7.1 shows the increased in line forces on individual members and thw whole group which are important for the analysis of structures.

Table 3.7.1 - Increased in line force on arrays of cylinders in steady simulated post critical flow

S/D = 5	Force on group	Force on single member
2 x 2	1.07	1.18
3 x 3	1.12	1.27

Pearcey et al did not attempt to measure steady lift forces but suggest that these will occur and result in a further increase in the forces.

Pearcey et al suggested three interference effects on drag loads:

The first effect tends to reduce the drag for any individual member that lies directly downstream of others, because the incident velocity is reduced in the wake of the upstream cylinders.

The second effect tends to increase the drag for any individual member that lies to the side of the wake of an upstream one, where the presence of the upstream cylinder and its wake leads to an increased velocity to the side of the wake.

The third effect is that the increased vorticity of the incident flow on a downstream cylinder moves the position of the transition to turbulence downstream. This may increase or decrease the loading on the downstream cylinder according to the Reynolds Number.

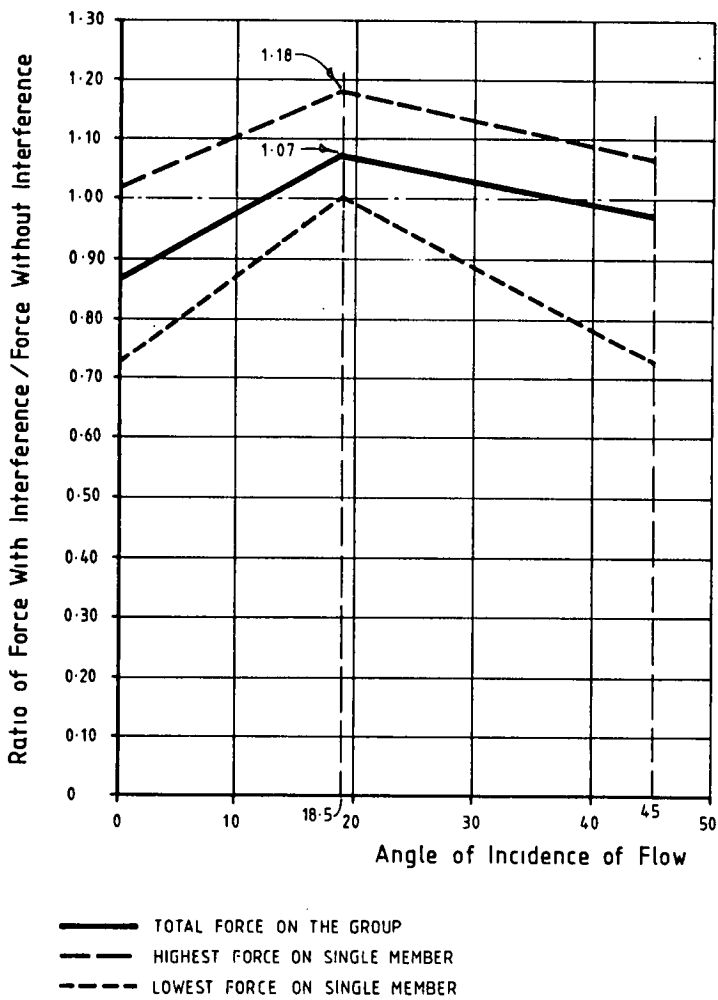
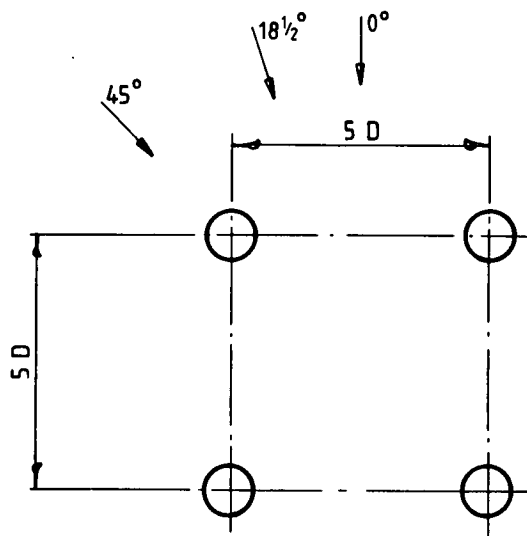


Figure 3.7.1. Changes in loading on a group of 4 cylinders caused by interference (simulated post critical steady flow, $S/D = 5$, Pearcey et al, 1982)

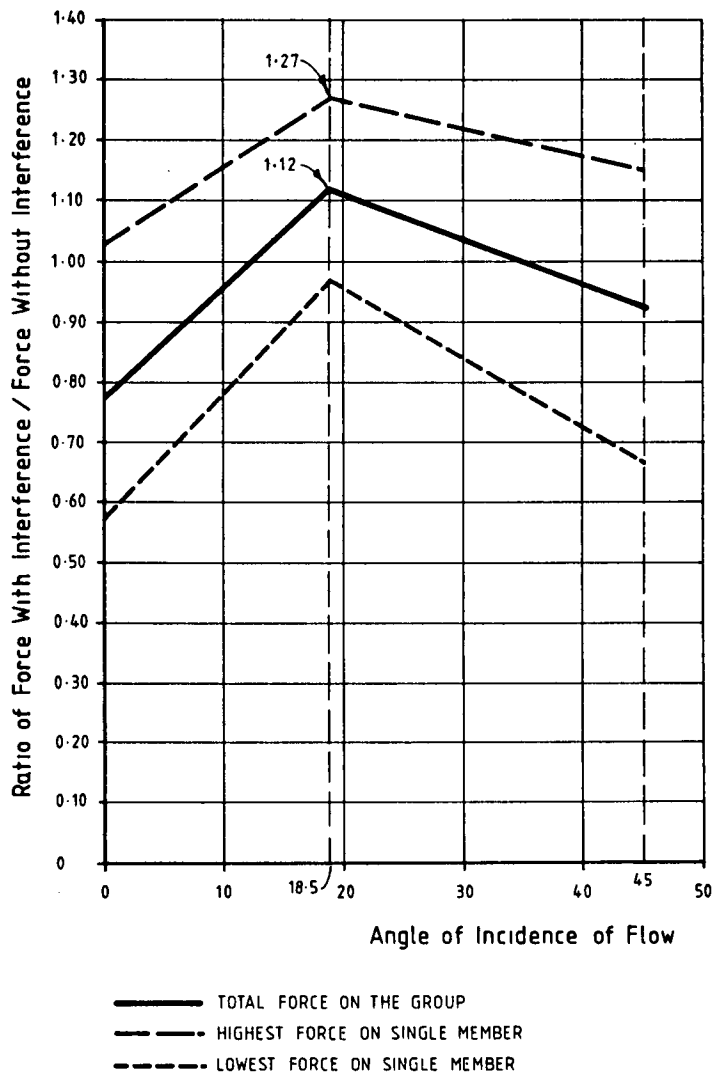
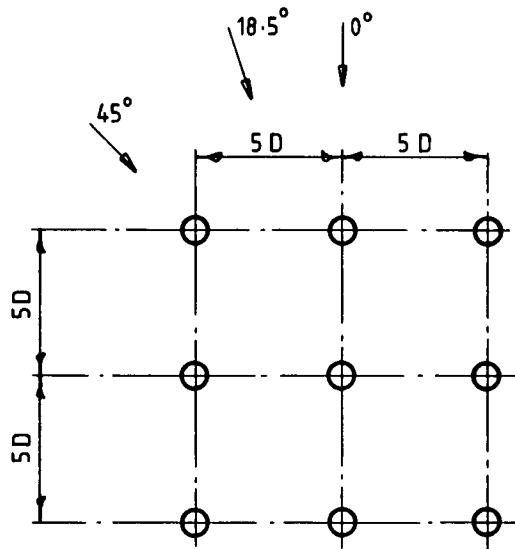


Figure 3.7.2. Changes in loading on a group of 9 cylinders caused by interference (Pearcey et al, 1982)

Heideman and Sarpkaya (1985) performed experiments on a square 5 x 5 array of cylinders of S/D = 2 and a rectangular 5 x 5 array with S/D = 2 and 5 (see Table 3.7.2). For comparison they also measured the forces on solid 'bounding' prisms which had the same overall external dimensions as the arrays, and on an isolated cylinder. Measurements were made in both steady and oscillating flow. All cylinders were sand roughened with a k/D of 1/50.

In steady flow the loading on the 'bounding prism' was less than the total load on the cylinders except when the incident flow was parallel to the edge of the square prism, when the loading on the prism was nearly 50% greater than that on the array.

The loading on a single member was always found to be higher than the average for the arrays, see Table 3.7.3. The shielding factor varied from 0.8 to 1.0 for the rectangular array and 0.5 to 0.7 for the square array.

Table 3.7.2 - Spacing to diameter ratios - (Heideman and Sarpkaya, 1985)

	Rectangular Array	Square Array
Across 0° Flow	2	2
Along 0° Flow	5	2

Table 3.7.3 - Shielding effect for arrays in steady flow $R_e = 2 \times 10^4$ (Heideman and Sarpkaya, 1985)

Flow Angle	Single Member	Rectangular Array	Square Array
0°	1	0.8	0.5
15°	1	0.9	0.6
20°	1	1.0	0.7

3.7.3

In line forces on arrays of cylinders in oscillating flow

Heideman and Sarpkaya (1985) found that in oscillating flow the loading on the 'bounding prism' was higher than the loading on the cylinder array except when the incident flow was parallel to the edge of the rectangular prism. An 'opposite' conclusion to that found for steady flow.

At $K_c = 10$ there was a blockage effect in the array and the isolated cylinder forces were lower than the average for the array, by up to 30%. However at higher K_c there was a shielding effect and the single member force was always higher than the average array member force, see Tables 3.7.4 and 3.7.5.

Table 3.7.4 - Total force for arrays in oscillating flow $R_e = 1300$
blockage effect at $K_c = 10$ (Heideman and Sarpkaya, 1985)

Flow Angle	Single Member	Rectangular Array	Square Array
0°	1	1.4	1.2
15°	1	1.4	1.1
20°	1	1.3	1.0

Table 3.7.5 - Total force for arrays in oscillating flow $R_e = 13000$ shielding effect at $K_c = 100$ (Heideman and Sarpkaya, 1985)

Flow Angle	Single Member	Rectangular Array	Square Array
0°	1	0.3	0.5
15°	1	0.6	0.6
20°	1	0.8	0.7

Bushnell (1976) performed experiments on pairs of cylinders and a 3 x 3 array of smooth cylinders, at a spacing of 4D. The oscillating flow conditions were : R_e of 2×10^4 to 8.6×10^4 and K_c from 31 to 126. The experiments were performed with and without trip wires which were intended to simulate post critical flow conditions.

The results for the array tests are given in Tables 3.7.6 and 3.7.7. These showed that there was generally minimal interference effect until the K_c value became greater than 30. This corresponds to a water particle double amplitude/cylinder spacing of 2.5.

Table 3.7.6 - Increased in line force on array of cylinders in oscillating critical flow ($R_e = 4 \times 10^4$) (S/D = 3) (Bushnell, 1976)

Angle	K_c	b/s	Force on group	Force on single member
0°	31	2.5	1.00	1.0
0°	62	5.0	0.75	1.0
0°	126	10.0	0.75	1.1
20°	31	2.5	1.0	1.1
20°	62	5.0	0.95	1.1
20°	126	10.0	0.85	1.2

b = 2x amplitude of flow oscillation

s = centreline spacing of cylinders

Table 3.7.7 - Increased in line force on array of cylinders in oscillating simulated post critical flow ($R_e = 4 \times 10^4$) (with trip wires) (S/D = 3) (Bushnell, 1976)

Angle	K_c	b/s	Force on group	Force on single member
0°	31	2.5	1.15	1.20
0°	62	5.0	0.95	1.15
0°	126	10.0	0.85	1.10
20°	31	2.5	1.15	1.25
20°	62	5.0	0.25	1.65
20°	126	10.0	0.30	1.75

The increased loading was not separated into drag and inertia effects but at the higher K_c value of 62 to 126 it is likely that all the changes were dominated by drag effects.

The applicability of these results to true post-critical flow is unclear. It is possible that the results are valid, in which case large increases in loading on cylinder arrays should be expected. However, the drag coefficient determined by Bushnell for a single cylinder with trip wires was 0.9 at high K_c . This is higher than the post-critical oscillating flow value of 0.65 and more consistent with a rough cylinder value. If the single cylinders with trip wires were behaving like rough cylinders in critical oscillating flow then it is possible that the increases measured for the arrays are caused partly by the increased turbulence in the flow moving the flow pattern around each cylinder into the supercritical region. This effect will significantly increase the drag coefficients in the tests but not cause any increase in true post-critical flow.

The results for the 0° incidence suggest that this effect could amount to 15% for the group and 20% for the most highly loaded member. This leaves an increase of 13% for the force on the group and 46% for the force on an individual member. These results (for a 3D spacing of members) are then comparable with the steady flow results of Pearcey et al (1982) which, for a 5D spacing of members, gave increases of 12% for the group and 27% for the force on a single member of the group.

Beckmann and Merwin (1979) analysed data from the OTS structure which had a 7 x 3 group of members simulating conductors. The spacing to diameter ratio was 5.4 along the three member lines and 3.6 along the seven member lines. The average drag coefficient for the (smooth) cylinders in large waves was 0.6. This coincided with the value for no interference. The spread of C_d values was large but no consistent interference or shielding effects could be identified either for the total force on the array or for the forces on 5 separately instrumented conductors.

Vortex shedding caused the cylinders to vibrate transverse to the flow, at a frequency corresponding to the Strouhal number. The moments induced by vortex shedding were at times greater than the drag force. No effect of the transverse vibration on the drag force could be determined.

Chakrabarti (1979) performed experiments on lines of cylinders in waves at R_o of 10^4 to 4×10^4 and K_c of 3 to 50. The arrangement of cylinders included:

Number of Cylinders : 2, 3 and 5

Centreline spacing of cylinders : 1.1, 1.33, 2 and 5 diameters

Orientation of line : 0° , 45° and 90° for the wave direction.

Chakrabarti does not present results for a single cylinder but the difference between the results for 5 diameter spacing and 2 diameter spacing is generally small. Therefore at 5 diameters spacing the interference effects would seem to be negligible.

For the cylinders at 0° (in line with the wave direction) there was found to be a shielding effect as the spacing decreased.

When five cylinders were positioned at 90° to the wave the force on the end cylinders increased by 2.75 times as the spacing decreased from 5D to 1.1D. The force on the other cylinders increased by about 4.5 times resulting in a 3.8 times increase in the total load on the group.

With the cylinders at 45° to the wave direction the forces were similar to the 90° case with a general increase in force as the spacing reduced.

3.7.4 Inertia and diffraction forces on arrays of cylinders in inviscid flow

Inertia coefficients have been calculated for groups of cylinders using potential flow theory by Yamamoto and Nath (1976) and Dalton and Helfinstine (1971). Spring and Monkmeyer (1974) have used diffraction theory. However Sarpkaya and Isaacson (1981) suggest that coefficients determined by these methods may not be appropriate to arrays of small cylinders (e.g. conductors) because of modification of the pressure distribution by the eddies.

It is therefore recommended that inertia forces for cylindrical arrays are determined experimentally where they are important.

For cylinders of diameter greater than one fifth of the wavelength the effect of the cylinders individually or in groups diffracting the waves must be taken into account and any vortex shedding effects will be very small. Diffraction is associated with the structure modifying the incident wave pattern. The interference is then transferred as a wave and can travel over longer distances than interference from drag and inertia effects which are approximately limited to the orbit radius. The interference effect will reduce approximately as:

$$(\text{spacing} / \text{diameter})^{-0.5}$$

This produces a slow reduction of the interference effect with distance.

3.7.5 Lift forces on arrays of cylinders

a. Fluctuating lift forces

Bushnell (1976) also measured lift forces on the cylinder pairs and arrays. At the critical R_e values of the tests lift forces were much larger than in post critical flow. In the two cylinder tests lift forces were modified from the isolated cylinder values as shown in Table 3.7.8. The angle given is the angle between the flow direction and the plane containing the axes of the two cylinders.

Table 3.7.8 - Factors by which lift forces were modified in 2 cylinder tests in simulated post critical oscillating flow $S/D = 3$, $R_e = 2 \times 10^4$ to 8.6×10^4 , with trip wires

K_c	Angle		
	0°	20°	40°
31	0.8	0.9	0.8
62	2.0	1.9	1.2
126	2.9	3.1	1.9

Larger increases in lift force were found for the 3 x 3 array. The largest lift force of 5 times the single cylinder value was obtained from the cylinder with trip wires which also had the largest drag force of 1.75 times the single cylinder value. This would

imply a peak force increased to about 2.1 times the single cylinder value. However, this increase may have been partly caused by a failure of the trip wires to act as intended. Without trip wires the largest lift force was 3.7 times the single cylinder value.

Verley and Every (1977) have also compared the lift forces and dynamic response of single cylinders and a 4 x 3 array of cylinders with $S/D = 2.0$ at K_c up to 30. They found that there was no increase in the lift forces measured in the array. This is consistent with the low K_c results of Bushnell (1976).

b. Steady lift forces

Large lift forces can occur when a line of cylinders is not exactly parallel or perpendicular to the flow direction. Bokaian and Geoola (1985) demonstrate this for two cylinders in steady flow at $Re = 2900$ and 5900.

3.7.6 Conclusion for arrays of cylinders

a. Drag and inertia forces - total force on an array

The experiments show that the force is dependent on the angle the flow makes with the array. Figure 3.7.3 shows a typical change in total force with incident flow direction. In the range of centreline spacing to diameter (S/D) of most interest for conductor arrays ($S/D = 3$ to 5) the force may increase or decrease but will probably remain within about 20% of that predicted without allowing for any interaction.

At smaller spacing the interaction effect can be much greater: a line of 5 cylinders across the flow at $(S/D) = 1.1$ resulted in an increase to about 3.8 times the total force for 5 isolated cylinders.

Since these changes for typical conductor spacings are relatively small and the loading on the conductors is only part of the total loading on a jacket structure it may often be reasonable to ignore any interference effects in the calculation of the total force on a conductor array.

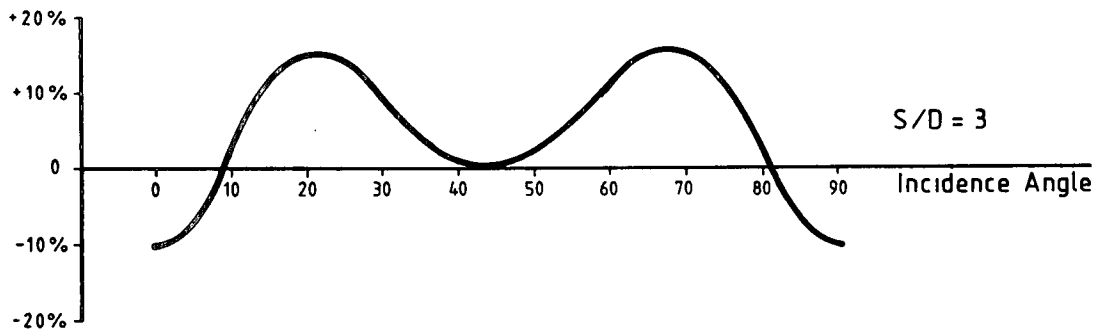
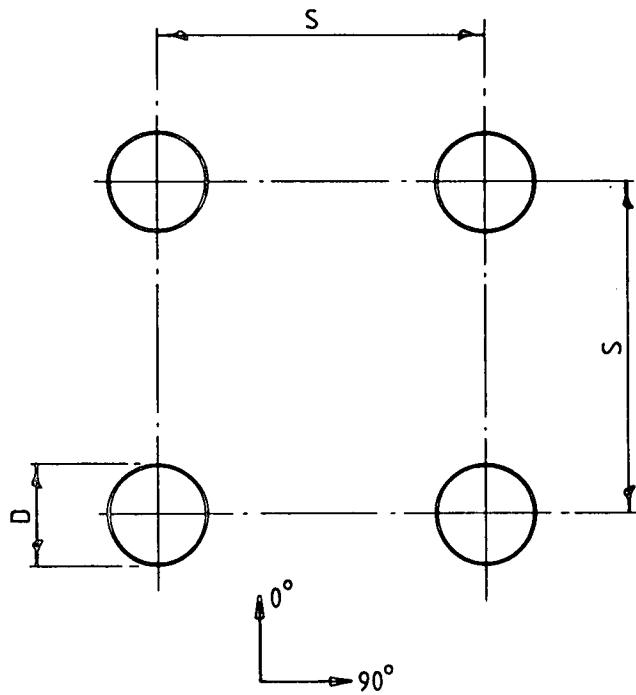


Figure 3.7.3. Interference effect on total in-line force on a rectangular array with $S/D = 3$

b. Drag and inertia forces - force on individual members

In steady flow, oscillating flow and laboratory waves the forces on members within arrays are highly sensitive to interaction effects. At $S/D = 5$ increases of 27% were obtained for a 3 x 3 array. At $S/D = 3$ increases of up to 75% were obtained, again on a 3 x 3 array. Five cylinders across the flow at $S/D = 1.1$ resulted in an increase, for the cylinder with the highest loading, to 4.5 times the single cylinder force.

Analysis of data from the OTS structure in the sea (S/D 3.6 and 5.3) did not identify any increase in the loading on the conductors which were instrumented.

Nevertheless the results from steady flow and oscillating flow experiments demonstrate that some cylinders in arrays are likely to be subject to significantly higher loads than would be estimated for a single cylinder. We would tentatively recommend, for members in arrays with spacing between 3D and 5D, that the extreme local loading on any individual member should be taken as 1.5 times the loading calculated without allowing for interference. For lower member spacing reference should be made to relevant experimental data. For larger member spacing interference effects may be ignored.

c. Fluctuating lift forces

There is some evidence from oscillating flow experiments that lift forces on members in arrays may be much higher than single member lift forces for K_c greater than 30. However, in this range of K_c oscillating flow may not correspond very well with real sea conditions so until more data is available cylinders in arrays should be checked for vortex shedding induced oscillation assuming no interference.

d. Steady lift forces

These can occur and are most significant for small member spacing.

e. Diffraction forces

When members span more than one fifth of a wavelength they modify the wave. This may effect other members at large distances from the diffracting member. See Section 3.7.4.

3.7.7 Interference between non cylindrical shapes

Little data is available. In the diffraction regime the diffraction calculation should account for a member shape.

In the absence of specific data for the drag/inertia regimes then the interference factors obtained for smooth cylinders may be used.

3.7.8 Attachments

Attachments to the members of an offshore structure take many forms, e.g. sacrificial anodes, pile guides, walkways and risers. Little data exists concerning the effect of these attachments on the wave loading of the parent members. In some cases the phenomena involved may be expected to be similar to those described in Sections 3.7.2 to 3.7.8. In other cases the effect of the attachment is to change the shape of the member.

3.7.9 Total load on a member with attachments

a. General

Sacrificial anodes are used in large numbers on steel members of offshore structures to control or reduce corrosion. These anodes are manufactured commercially in a range of shapes and sizes, and are fitted by a variety of methods.

The effect of the anodes on the total wave loading of members to which they fitted can be expected to vary with several parameters for instance:

- i. Anode shape.
- ii. The method of fixing and the gap between the anode and the member to which it is fitted.
- iii. The length of the member covered by anodes.
- iv. The incidence angle of the anode relative to the wave.
- v. The orientation of the member to which the anode is fitted.

Singh et al (1982) fitted one square cross section shape of anode to circular cylinders which were either vertical or horizontal and parallel to the wave crests. Stand off distance and incidence angle were varied in these experiments. The anode width was one quarter of the cylinder diameter. The Reynolds number was less than 10^5 but the flow was thought to be post critical. Keulegan Carpenter number range was from 1 to 12.

They concluded that :

1. The effect of anodes varies considerably with orientation of the member in which the anodes are fitted.
2. On vertical cylinders the anodes always increase the loading. Increasing the incidence, defined as the angle between the radius to the anode and the flow direction, results in an increase in force. As an example, at an incidence of 90° , with the stand off distance equal to one anode width, a load of 2 times that on a plain cylinder was recorded. At a similar orientation, reducing the stand off distance to zero caused a further increase in loading, to about 3 times that on the smooth cylinder. However, an increase in stand off distance from one anode width to two anode widths caused only a slight change in loading.
3. On vertical cylinders the wave loading penalty appeared to be increasing with K_c .
4. On horizontal cylinders, the effect of anodes is more complex. Anodes mounted on a horizontal plane through the member caused a reduction in the in line forces but generated large transverse forces. An increase in load of almost twice that on a plain cylinder was observed at K_c greater than 10.
5. Stand off distance is also important on horizontal cylinders. Generally, decreasing stand off distance increased the total force, however for K_c greater than about 8 the effect of stand off distance is reduced.

b. Recommended method of estimating total forces on members with attachments standing off from the member

1. In line forces:

Analysis of the results of Singh et al suggests that the maximum forces on members with attachments standing off from the member may be underpredicted if no interference effects are allowed for, see Table 3.7.9.

Table 3.7.9 - C_d and C_m Values for anode of size $D/4$ by $D/4$, standing off by $D/4$, on a Cylinder of diameter D . Experimental values compared with values calculated without allowing for interference effects ($R_e = 10^5$, K_c 1 to 12)

Note:		Measured Singh et al (1982)		Calculated assuming no interference		Blockage effect
		(1)	(2)	(1)	(2)	
(1) Coefficients for use with member dimensions						
(2) Coefficients for use with member + anode dimensions		(1)	(2)	(1)	(2)	
Vertical cylinder	C_d (max. value)	1.4	1.1	1.2	1.0	1.2
Horizontal cylinder	C_d (max. value)	1.2	1.0	1.2	1.0	1.2
Vertical cylinder	C_m (max. value)	2.7	2.5	2.2	2.0	1.2
Horizontal cylinder	C_m (max. value)	2.2	2.0	2.2	2.0	1.0

Note: Singh et al calculate C_d and C_m for D and A in Morison's equation corresponding to the member alone.

The calculated values are seen to be approximately correct for the horizontal cylinders and a little low for the vertical cylinders.

However, the experimental values given are for the worst incidence angle of the flow. For anodes and other appurtenances scattered over a structure the assumption of no interference would therefore be reasonable.

2. Lift forces:

The anode attached to one side of the cylinder was found to produce a lift force of similar size to the drag force.

Lift forces on smooth cylinders are much higher at the low Reynolds Number of the experiments than they are at the high Reynolds Numbers of the prototype flows. However, the attachments almost certainly generated a post critical flow in the experiments and therefore the results may be applicable to offshore structures.

It is therefore recommended that members with attachments should, over the length of the attachment, be capable of taking an additional steady lift force equal to the drag force on the attachment and member. This force need not be included in the total global load.

- c. Recommended method of estimating total forces on members having attachments mounted with no gap.

For appurtenances attached to the surface of cylinders with no stand off distance higher forces were measured, see Table 3.7.10. In this case the C_a value when the appurtenance is orientated at right angles to the flow should be calculated for an approximate added mass force of:-

$$\frac{\rho \pi (D + d)^2 \dot{U}}{4} \text{ and a Froude Krylov Force of } \frac{\rho \pi (D^2 + d^2) \dot{U}}{4}$$

where D is the diameter of the member and d is the width of the appurtenance. The C_m value appropriate for use with the total area of the member and the attachment (see Section 3.2.13) is therefore $((D + d)^2 + D^2 + d^2)/(D^2 + d^2) = 2.4$ for the dimensions used by Singh et al. The drag force should allow for the extra width and also for the higher C_d caused by forcing boundary layer separation to occur at the appurtenance which leads to a wider wake. The C_d value for the cylinder with the appurtenance may then be taken as the average value for a cylinder and a plate, e.g. $(1.0 + 2.0)/2 = 1.5$ and the width in Morison's equation should be taken as $D + d$.

Table 3.7.10 - C_d and C_m Values for anode of size $D/4$ by $D/4$, mounted with no gap on a Cylinder of diameter D . Experimental values compared with calculated values for the modified member

Note:	Measured		Calculated	
	Singh et al (1982)		assuming no interference	
(1) Coefficients for use with member dimensions alone	<hr/>			
(2) Coefficients for use with member + anode dimensions i.e. $D \leftarrow D + d$, $A_e \leftarrow \pi(D^2 + d^2)/4$	(1)	(2)	(1)	(2)
Vertical cylinder C_d (max. value)	2.2	1.8	1.9	1.5
Horizontal cylinder C_d (max. value)	2.0	1.6	1.9	1.5
Vertical cylinder C_m (max. value)	2.9	2.7	2.6	2.4
Horizontal cylinder C_m (max. value)	2.6	2.4	2.6	2.4

The recommended method is seen to be quite good for the horizontal cylinder but to underestimate the loading on the vertical cylinder.

3.7.10 Force on Attachments to Members

No data is available for calculating the force on attachments themselves. It is common practice to use potential flow theory to allow for an increased force on attachments caused by the disturbance to the flow from the presence of the member.

For cylindrical members the increased flow velocity in a plan through the axis of the member and at 90° to the normal flow is given by: $(1 + 0.25D^2/R^2)U$ where D is the diameter of the cylinder, R is the radial distance from the centre of the cylinder (R is therefore always greater than $D/2$) and U is the incident velocity. (See Figure 3.7.4.)

It is proposed that this formula is used to magnify the drag, inertia and lift coefficients

for the calculation of local loading on the appurtenance when the appurtenance is attached normal to the flow.

This magnification need not be applied for the calculation of global forces or forces on a member and attachment together.

For attachments at other angles to the incident flow the potential flow speed and direction is given in Figures 3.7.4 and 3.7.5.

The real interaction between the members is rather more complicated than these diagrams suggest : lift forces will be present, buffeting of the attachment by the turbulence in the wake of the member may occur and theoretically there is an additional inertia force which results from a convective acceleration which is in phase with the velocity and proportional to the $(\text{incident flow velocity squared})/(\text{Diameter of the main member})$. The amplitude and direction of this force is shown in Figures 3.7.6 and 3.7.7. Figures 3.7.4 to 3.7.7 are derived in Appendix O.

3.7.11 Joints

The structural joints of a steel framed offshore structure present several complications from a fluid loading point of view. End effects of a finite length member are likely to be noticeable in this region as will be the interference of one member end on another. The various members concerned are likely to have differing diameters and, to increase local structure strength, members may be increased in diameter as they approach the joint.

It is not yet possible to take into account interference effects despite the possibility that forces may be changed.

In calculating wave loads on joints, present industrial practice takes account of the various diameter increases.

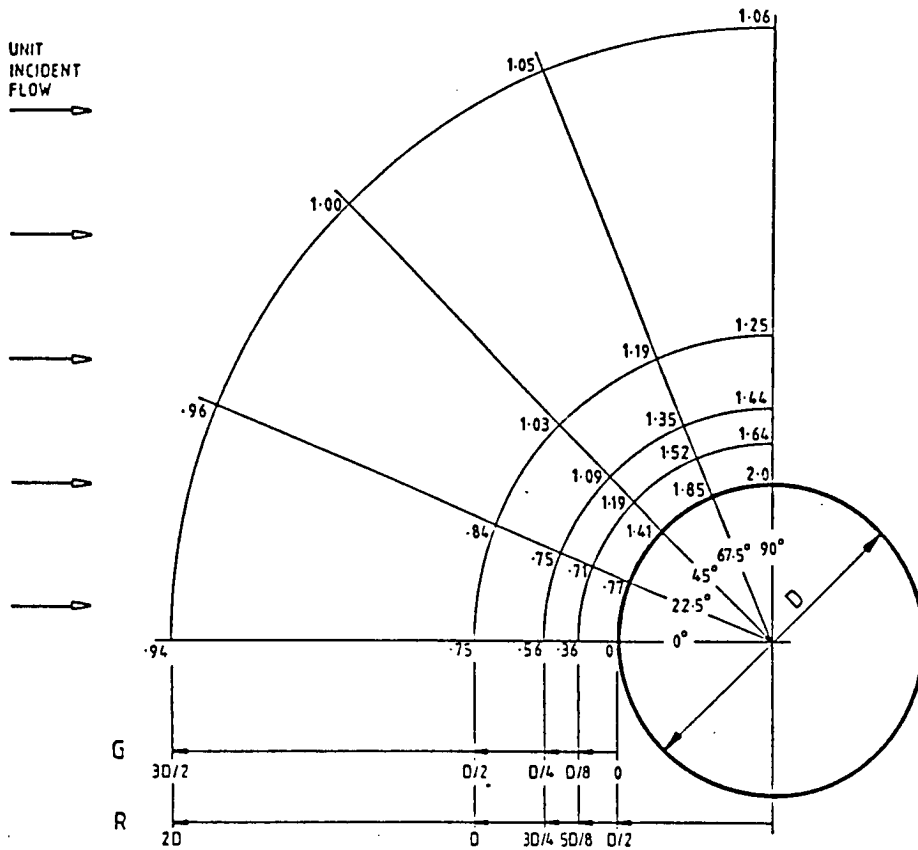


Figure 3.7.4. Flow speed around a cylinder for a unit incident velocity

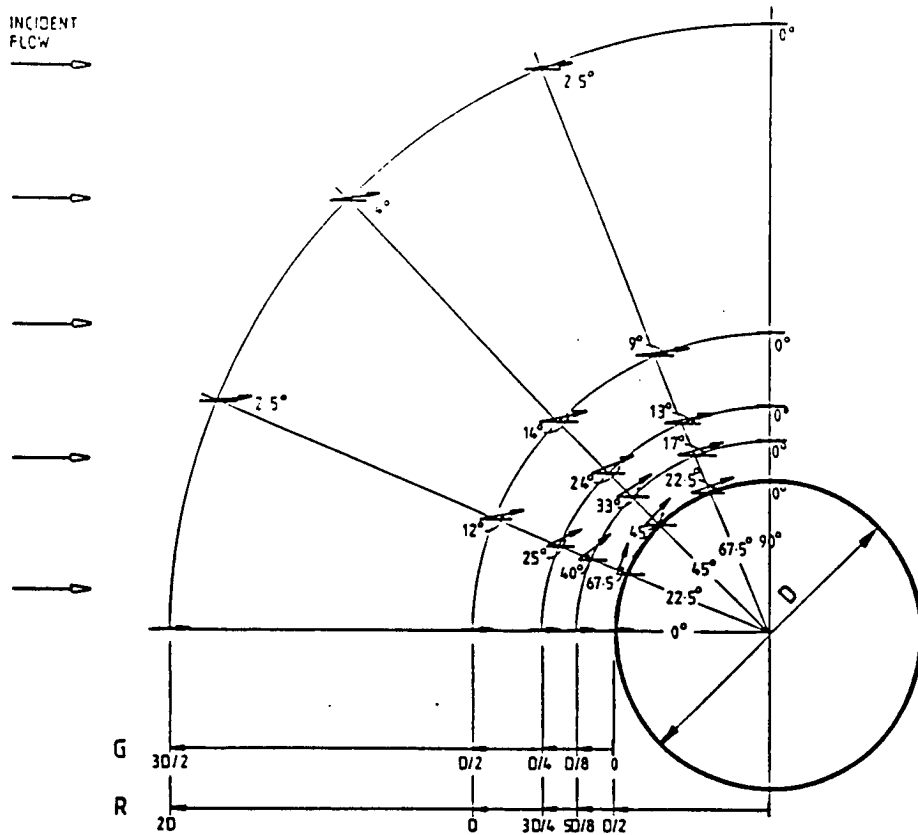


Figure 3.7.5. Direction of flow around a cylinder

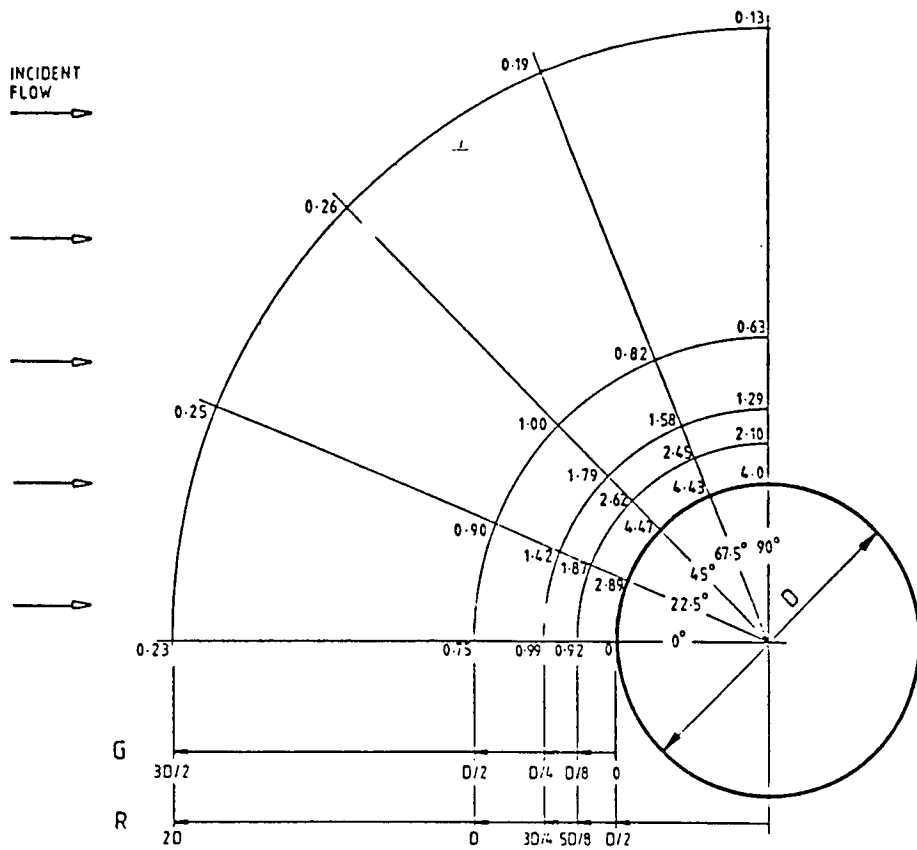


Figure 3.7.6. Convective acceleration around a cylinder
(Multiply above values by $(\text{incident velocity})^2 / D$)

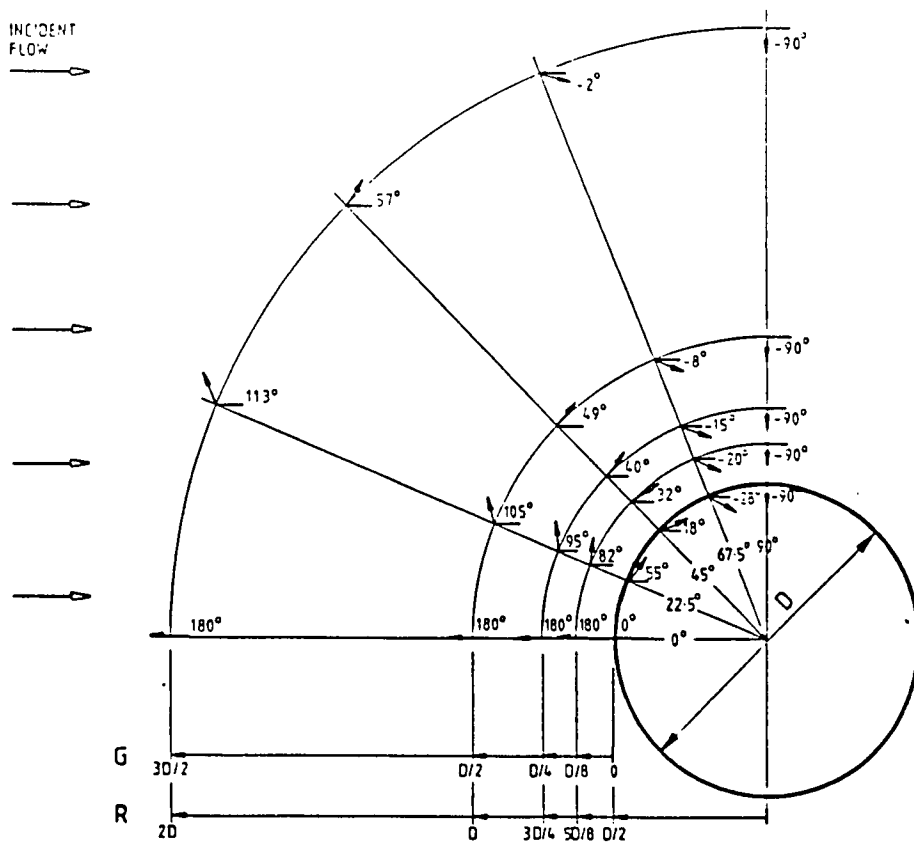


Figure 3.7.7. Direction of convective acceleration around a cylinder

3.7.12 Interference : Conclusions

a. General

This is a summary of the more detailed recommendations and conclusions given in Section 3.7.6 for arrays and in Sections 3.7.9 and 3.7.10 for attachments.

b. Total loading on arrays

Interference will probably change the total loading on cylinder arrays, such as conductor arrays by less than 20%, providing the spacing to diameter ratio is greater than 3. It may often be reasonable to take the loading as the sum of the Morison loading for each cylinder separately.

When the centre line spacing to diameter is less than 3, large increases or reductions in load may occur and reference should be made to the detailed discussion in 3.7 and experimental data.

c. Loading on individual members in arrays

Loading on individual members of arrays can, for certain wave directions, be significantly greater than that on an isolated member. For cylinder spacings in the region 3D to 5D it is tentatively recommended that extreme member loading be considered to be increased by 50%. For lower member spacing reference should be made to experimental data.

Individual members in arrays may also be subject to steady lift forces especially at small member spacings and increased fluctuating forces from vortex shedding at the higher values of K_c .

d. Total loading on members with attachments

When attachments stand off from the member and the gap is not filled with marine growth, the total in-line loading, calculated assuming no interference, should be correct to about 20%. Therefore it may often be acceptable to ignore the interference effect. The

member may also be subject to a significant lift force of similar size to the drag force on the member. The member should be capable of taking this lift force but it need not be considered when calculating the total force on the structure.

When there is no gap between the member and the attachment the loading should be calculated for the modified member shape, see Section 3.7.9c.

e. Loading on attachments

Attachments may be subject to flow velocities of up to twice that of the flow incident on the member. The largest effect would be to quadruple drag forces and to double inertia forces. In addition convective accelerations in the flow will lead to an extra inertia force which is in phase with the velocity, proportional to velocity squared, and up to twice the no interference drag force. Fortunately the largest drag forces occur at different locations to the largest convective acceleration inertia forces. Figures 3.7.4 to 3.7.7 are provided for estimating the effects.

3.8 REFERENCES

References in 3.2

- Achenbach E. 1971. Influence of Surface Roughness on the Cross-flow Around a Circular Cylinder, JFM, Vol 46, pp 321-335.
- Atkins, 1979, Wave Force Investigation at Forties Field Platform FB, Final Report of Results, WS Atkins Consultants, Epsom.
- Bearman P, Chaplin J, Graham J, Kostense J, Hall P and Klopman G, 1985, The Loading on a Cylinder in Post-Critical Flow beneath Periodic and Random Waves, Proc of BOSS Conference, Delft.
- Bishop JR, 1980, A New Coefficient for Total Wave Forces, OT-R-8017, NMI R77.
- Bishop JR, 1984, Wave Force Investigation at the Second Christchurch Bay Tower, Summary Report, OT-0-82100, NMI R177.
- Bishop, 1987, Wave force coefficients for horizontal and vertical cylinders with kelp fouling, measured at the Christchurch Bay Tower, OTH 87268, HMSO.
- Borgman LE and Yfantis E, 1979, Three Dimensional Character of Waves and Forces, Civ Eng in the Oceans IV, pp 791-804, San Francisco.
- Bullock GN, 1983, Wave Loading on a Generally Orientated Small Diameter Cylinder, Dept Civ Eng., University of Salford, Report 83/190, UK.
- Bursnall WJ and Loftin LK, 1951, Experimental Investigation of the Pressure Distribution about a Yawed Circular Cylinder in the Critical Reynolds Number Range, NACA Tech Note 2463.
- Chakrabarti SK, 1982, Wave Force Coefficients for Rough Vertical Cylinders, J Waterway Port Coastal and Ocean Eng Div, ASCE, Vol 108, No 4, pp. 445-455.
- Chaplin JR, 1981, Boundary Layer Separation from a Cylinder in Waves, Proc Int Symp on Hydrodynamics in Ocean Eng, pp 645-666, Trondheim.

Chaplin JR, 1985a, Morison Inertia Coefficients in Orbital Flow, J Waterway Port Coastal and Ocean Eng Div, ASCE, Vol 111 No 2, pp 201-215.

Chaplin JR, 1985b, Loading on a Cylinder in Uniform Elliptical Orbital Flow, Liverpool University Civil Engineering Report, MCE/JUL/85.

Chiu WS, 1966, The Boundary-Layer Formation and Vortex Shedding on Yawed Cylinders, Washington State Univ, College of Eng, Bull 299.

Cotter DC and Chakrabarti SK, 1984, Wave Force Tests on Vertical and Inclined Cylinders, J Waterway Port Coastal and Ocean Eng Div, ASCE, Vol 110, No 1.

Delany NK and Sorenson NE, 1953, Low-Speed Drag of Cylinders of Various Shapes, Technical Note 3038. National Advisory Committee for Aeronautics, USA.

Gaston JD and Ohmart RD, 1979, Effects of Surface Roughness on Drag Coefficients, Civil Eng in the Oceans IV, ASCE, pp 611-621.

Garrison CJ, 1985, Comments on Cross-Flow Principle and Morison's Equation. J Waterway Port Coastal and Ocean Eng Div, ASCE, Vol, 111, No 6, pp 1075-1079.

ESDU, 1981, Mean Forces, Pressures and Flow Field Velocities for Circular Cylindrical Structures : Style Cylinder with two-dimensional flow, Engineering Sciences Data Unit, Item 80025, London.

Grace RA and Casciano FM, 1969, Ocean Wave Forces on a Subsurface Sphere, Waterways and Harbours and Coastal Eng Div, ASCE, Vol 95, No 3, pp 291-317.

Grass AJ, Simons EE and Cavenagh NJ, 1984, Fluid Loading on Horizontal Cylinders in Wave Type Orbital Flow, Proc Int Symp Offshore Mech and Arctic Eng, Paper No 262, ASME.

Guyen O, Patel VC and Farrell C, 1975, Surface Roughness Effects on the Mean Flow Past Circular Cylinders, Iowa Institute of Hydraulic Research Report No 175, Iowa City, IA.

Hanson AR, 1966, Vortex Shedding from Yawed Cylinders, AIAA Journal, Vol 4, pp 738-740.

Heideman JC, Olsen OA and Johannson PI, 1979, Local Wave Force Coefficients, Civ Eng in the Oceans IV, pp 684-699, San Francisco.

Heideman JC and Sarpkaya T, 1985, Hydrodynamic Forces on Dense Arrays of Cylinders, OTC 5008, Houston.

Hoerner SF, 1965, Fluid-Dynamic Drag, 3rd Ed. Published by the Author, New Jersey.

Holmes P and Chaplin JR, 1978, Wave Loads on Horizontal Cylinders, Proc 16th International Conf on Coastal Eng, Vol 3, p 2449, Hamburg.

Isaacson M, 1979, Non Linear Inertia Forces on Bodies, J Waterways Harbours and Coastal Eng Div, ASCE, No 3, pp 213-227.

Keulegan GH and Carpenter LH, 1958, Forces on Cylinders and Plates in an Oscillating Fluid, Research of the National Bureau of Standards, Vol 60, No 5.

Miller BLP, 1976, The Hydrodynamic Drag of Roughened Circular Cylinders, National Physical Laboratory Report, R147.

Norton DJ, Heideman JC and Mallard WW, 1981, Wind tunnel Tests of Inclined Cylinders, OTC 4122, Vol IV, pp 67-75, Houston.

Novak M, 1975, Discussion of 'Yaw Effects on Galloping Instability' by R Starecky J, Eng Mechs Div, ASCE, EM4, p 745.

O'Brien MD and Morison JR, 1952, The Forces exerted by Waves on Objects, Trans of the American Geophysical Union, Vol 33, No 1.

Ohmart RD and Gratz RL, 1979. Drag Coefficients from Hurricane Wave Data, Civil Eng in the Oceans IV, ASCE, pp 260-272.

Paape A and Breusers HNC, 1967, The Influence of Pipe Dimension on Forces exerted by Waves, 10th Coastal Eng Conf, Chapter 48, ASCE.

Pearcey HH, 1979, The Effects of Surface Roughness on the Wave Loading for Cylindrical Members of Circular Cross Section, National Maritime Institute, NMI R65, OT-R-7960.

Pearcey HH, Singh S, Cash R and Matten R, 1985, Fluid Loading on Roughened Cylindrical Members of Circular Cross-Section, BMT Report 191, OT-0-8411.

Pearcey HH, Matten RB and Singh S, 1986, Fluid forces for Cylinders in Oscillating Flow Waves and Currents when Drag and Inertia effects are present together, BMT Report, OT-0-86-011.

Sarpkaya T, 1960, Added Mass of Lenses and Parallel Plates, Eng Mechs Div ASCE, Vol 86, EM3, pp 141-152.

Sarpkaya T, 1975, Forces on Cylinders and Spheres in Oscillating Fluid, J Applied Mech, ASME, Vol 42.

Sarpkaya T, 1976a, Vortex Shedding and Resistance in Harmonic Flow About Smooth and Rough Circular Cylinders at High Reynolds Numbers, Report No NPS-59SL76021, Naval Postgraduate School, Monterey, CA.

Sarpkaya T, 1976b, In-Line and Transverse Forces on Smooth and Sand-Roughened Cylinders in Oscillatory Flow at High Reynolds Numbers, Report No. NPS-69SL76062, Naval Postgraduate School, Monterey, CA.

Sarpkaya T and Garrison CJ, 1963, Vortex Formation and Resistance in Unsteady Flow, J Applied Mech, Vol 30, Series E, No 1, pp 16-24.

Sarpkaya T and Isaacson M, 1981, Mechanics of Wave Force on Offshore Structures, Van Nostrand Reinhold.

Sarpkaya Raines TS and Trytten DO, 1982, Wave Forces on Inclined Smooth and Rough Circular Cylinders. OTC 4207, pp 731-736, Houston.

Sarpkaya T and Cakal I, 1983, A Comprehensive Sensitivity Analysis of the OTS Data, OTC 4616, Houston.

Sarpkaya T and Storm M, 1985, In-line Force on Cylinder Translating in Oscillatory Flow, Applied Ocean Res, Vol 7, No 4, pp 188-195.

Sarpkaya T, 1986, In-line and Transverse Forces on Smooth and Rough Cylinders in Oscillatory Flow at High Reynolds Numbers, Report No. NPS-69-86-003.

Starsmore N, 1981, Consistent Drag and Added Mass Coefficients from Full Scale Data, OTC 3990, Houston.

Teng C and Nath JH, 1985. Forces on Horizontal Cylinder Towed in Waves, J Waterway Port Coastal and Ocean Eng Div, ASCE, Vol 111, No 6.

Torum A, 1985, Wave Forces on a Pile in the Surface Zone, Regular Non Breaking Waves, Progress Report No 2, Report No 1.9, Marintek, Trondheim, Norway.

Wolfram J and Theophanatos A, 1985, The Effects of Marine Fouling on the Fluid Loading of Cylinders- Some Experimental Results, OTS 4954, Houston.

References in 3.3

Basu Ak, Robinson RW, Adam DA and Clarke CSJ, 1987, Some Recent Tests on Vortex Shedding Behaviour of Model Risers under Uniform Current - Comparison with Theory, Proc 4th Offshore Mech and Arctic Eng Symp, ASME, pp 191-201, Houston.

Bearman PW, Graham JMR and Obasaju ED, 1984, A Model for the Transverse Forces on Cylinders in Oscillatory Flows, Applied Ocean Res. Volume 6 No 3, pp 166-172.

Bearman PW, Chaplin JR, Graham JMR, Kostense JK, Hall PF and Klopman G, 1985, The Loading of a Cylinder in Post Critical Flow Beneath Periodic and Random Waves, Behaviour of Offshore Struc, Amsterdam.

Blevins RD, 1977, Flow Induced Vibration, Van Nostrand Reinhold, New York.

Chaplin JR, 1985, Loading on a Cylinder in Uniform Elliptical Orbital Flow, Liverpool University Civ Eng Rep, MCE/JUL/85.

ESDU, 1978, Across-Flow Response Due to Vortex Shedding: Isolated Circular Cylindrical Structures in Wind or Gas Flows, Engineering Sciences Data Unit, Item 78006, Amend A, London.

Every MJ, 1980, Lift Forces Acting on Circular Elements Subjected to Wave and Currents, OT-R-8054, BHRA, England.

Grass AJ, Simons RR and Cavanagh NJ, 1984, Fluid Loading on Horizontal Cylinders in Wave Type Orbital Flow, Proc Int Symp Offshore Mech and Arctic Eng, Paper No 262, ASMI.

Griffin OM, 1981, OTEC Cold Water Pipe Design for Problems caused by Vortex-Excited Oscillations, Ocean Eng Volume 8, No 2, pp 129-209.

Hallam MG, Heaf NJ and Wootton LR, 1977, Dynamics of Marine Structures: Methods of Calculating the Dynamic Response of Fixed Structures Subject to Wave and Current Action, Report UR8. Construction Industry Research and Information Association Underwater Engineering Group, London.

Isaacson M, 1974, The Forces on Circular Cylinders in Waves, Phd Thesis Univ of Cambridge.

Iwan WD, 1975, The Vortex Induced Oscillation of Elastic Structural Elements, J Eng Industry, Vol 97, pp 1378-1382.

King R, 1977, A Review of Vortex Shedding Research and its Applications, Ocean Eng, Vol 4, pp 141-171.

Lienhard JH, 1966, Synopsis of Lift, Drag and Vortex Frequency Data for Rigid Circular Cylinders, Washington State Univ, Coll of Eng, Res Div Bull 300.

Mercier JA, 1973, Large Amplitude Oscillations of a Circular Cylinder in a Low-Speed Stream, PhD Dissertation, Stevens Institute of Technology.

Patrikalakis NM and Chryssostomidis C, 1983, Theoretical and Experimental Prediction of the Response of a Marine Riser Model in a Uniform Stream, MIT Sea Grant Program Report 83-15.

Rajabi F, 1979, Hydroelastic Oscillations of Smooth and Rough Cylinders in Harmonic Flow, PhD Thesis, Naval Postgraduate School, Monterey, CA, Reported by Sarpkaya and Isaacson (1981) and Sarpkaya and Rajabi (1979).

Sarpkaya T, 1976a, Vortex Shedding and Resistance in Harmonic Flow About Smooth and Rough Circular Cylinders at High Reynolds Numbers. Report No NPS-59SL76021, Naval Postgraduate School, Monterey, CA.

Sarpkaya T, 1976b, In-Line and Transverse Forces on Smooth and Sand-Roughened Cylinders in Oscillatory Flow at High Reynolds Numbers, Report No NPS-69SL76062, Naval Postgraduate School, Monterey, CA.

Sarpkaya T and Shoaff RL, 1979, Numerical Modelling of Vortex-Induced Oscillations, Proc Conf Civ Eng in Oceans IV, ASCE, San Francisco.

Sarpkaya T, 1979a, Vortex Induced Oscillations, A Selective Review, J App Mech, Vol 46, pp 241-258.

Sarpkaya T, 1979b, Lateral Oscillations of Smooth and Sand-Roughened Cylinders in Harmonic Flow, Mech of Wave Induced Forces on Cylinders, Edited by Shaw TL, Pitman, London.

Sarpkaya T and Rajabi F, 1979, Dynamic Response of Piles to Vortex Shedding in Oscillating Flows, OTC 3647, Houston.

Sarpkaya T and Isaacson M, 1981, Mechanics of Wave Forces on Offshore Structures, Van Nostrand Reinhold.

Sarpkaya T, 1986, In-Line and Transverse Forces on Smooth and Rough Cylinders in Oscillatory Flow at High Reynolds Number, Report No NPS69-86-003, Naval Postgraduate School, Monterey, CA.

Singh S, Cash RF, Boribond LA, Salter J, Wheatley JH, Miller NS, 1984, The Effect of Slats, Strakes and Other Vortex Suppression Devices on Wave Loads, NMI 159, OT/0/8412.

Skop RA, Griffin OM and Ramberg SE, 1977, Strumming Predictions for the Seacon II Experimental Mooring, OTC 2884, pp 61-66, Houston.

Stansby PK, 1977, An Inviscid Model of Vortex-Shedding from a Circular Cylinder in Steady and Oscillatory Far Flows, Proc Inst Civ Eng, Vol 63, pp 865-880, London.

Verley RLP and Every MJ, 1977, Wave Induced Vibrations of Flexible Cylinders, OTC 2899, Houston.

Walshe DE and Wootton LR, 1970, Preventing Wind Induced Oscillations of Structures of Circular Section, Proc Inst Civ Eng, London.

Wootton LR, 1969, The Oscillation of Large Circular Stacks in Wind, Proc Inst Civ Eng, Vol 43, pp 573-598.

Wootton LR, Warner MH, Sainsbury RN and Cooper DH, 1972, Oscillation of Piles in Marine Structures - A Description of the Full-Scale Experiments at Immingham, Technical Note 40, Construction Industry Research and Information Association, London.

Zdravkovich MM, 1981, Boundary Layer Devices, Review and Classification of Various Aerodynamic and Hydrodynamic Means for Suppressing Vortex Shedding, J Wind Eng and Ind Aerodynamics, Vol 7, pp 145-189.

References in 3.4

Eatock Taylor R, Compliant Structures Programme Continues Success, Offshore Research Focus, No 59, June, Department of Energy.

Hogben N and Standing RG, 1974, Wave Loads on Large Bodies, Proc Int Symp on the Dynamics of Marine Vehicles and Structures in Waves, Univ College, London.

Hogben N and Standing RG 1975, Experience in Computing Waves Loads on Large Bodies, OTC 2189, Houston.

Inglis RB and Price WG, 1980, Calculation of the Velocity Potential of a Translating Pulsating Source, Trans RINA, pp 163-173.

Isaacson M, 1977, Shallow Wave Diffraction Around Large Cylinder, J Waterway Port Coastal and Ocean Div, ASCE, Vol 103, WW1.

- Isaacson M, 1981, Steep Wave Forces on Large Offshore Structures, OTC 3955, Houston.
- Sarpkaya T and Isaacson M, 1981, Mechanics of Wave Forces on Offshore Structures, Van Nostrand Reinhold.
- Shen SF, 1977, Finite Element Methods in Fluid Mechanics, Ann Rev Fluid Mech, Vol 9.
- Skjelbreia M, 1979, Wave Forces on Large North Sea Gravity Structures, Civ Eng in the Oceans IV, pp 137-160, San Francisco.
- Standing RG, 1978, Applications of Wave Diffraction Theory, NMT E32, OT-M-7801, London.
- Spring BH and Monkmeyer PL, 1974, Interaction of Plan Waves with Vertical Cylinders, Proc 14th Coastal Eng Conf ASCE, Vol 111, pp 1828-1847, Copenhagen.
- Zienkiewicz OC, 1977, The Finite Element Method, 3rd edition, McGraw-Hill, London.

References in 3.5

- Bagnold RA, 1939, Interim Report on Wave-Pressure Research, J Inst Civ Eng, pp 202-226, London.
- Broughton P and Horn E, 1987, Ekofisk Platform 2/4C: Re-analysis Due to Subsidence, Proc Inst Civ Eng, Part 1, 82, October, pp 949-979.
- Campbell IMC and Weynberg PA, 1980, Measurement of Parameters Affecting Slamming, Wolfson Unit for Marine Technology, Report No 440 OT-R-8042.
- Campbell IMC, 1982, Response of a Tubular beam to an inclined Slam Impact, Wolfson Unit of Marine Technology. Report 488/1, University of Southampton.
- Denny DF, 1951, Further Experiments on Wave Pressures, J Inst Civ Eng, February, pp 330-345.
- Faltinsen OM, Kjaerland O and Nottveit A, 1977, Water Impact Loads and Dynamic Response of Horizontal Circular Cylinders in Offshore Structures, OCT 2741, Houston.

Gallagher P and McGregor RC, 1985, Slamming Simulations : An Application of Computational Fluid Dynamics, Fourth Conf Num Ship Hydrodynamics, Nat Acad Sci, Washington.

Kaplan P, and Gilbert MN, 1976, Impact Forces on Platform Horizontal Members in the Splash Zone, OTC 2498, Houston.

Kaplan P, 1979, Impact Forces on Horizontal Members, Civ Eng in the Oceans IV, ASCE, Vol II, pp 716-731.

Kawakami M, Michimoto J, Kabayashi K, 1977, Prediction of Long Term Whipping Vibration Stress Due to Slamming of Large Full Ship in Rough Seas, Int Shipbuilding Prog, 24, pp 83-110.

Kjeldsen SP, Lystad M and Myrhaug D, 1981, Forecast of Breaking Waves on the Norwegian Continental Shelf. Norwegian Met Inst and Norwegian Hydrodynamic Lab.

Kjeldsen SP, 1981, Shock Pressures from Deep Water Breaking Waves, J of Fluids Eng, Vol 99, pp 567-584.

Miller BL, 1978, Wave Slamming Loads on Horizontal Circular Elements of Offshore Structures, Trans Roy Inst Nav Archit, Vol 120, London.

Miller BL, 1980, Wave Slamming on Offshore Structures, National Maritime Institute, Report No NMI-R81.

Myrhaug D and Kjeldsen SP, 1987, Prediction of Occurrences of Steep and High Waves in Deep Water, J Waterways Port Coast and Ocean Eng, Vol 113, No 2, pp 122-138.

Ochi MK and Tsai CH, 1984, Prediction of Impact Pressures by Breaking Waves on Vertical Cylinders in Random Seas, Applied Ocean Research, Vol 6, No 3, pp 157-165.

Rask I, 1986, Slamming Pressure in Short Crested and and Oblique Seas, No 105, Chalmers University of Technology, Goteborg, Sweden

Ridley JA, 1982, A Study of Some Theoretical Aspects of Slamming, NMI R158, OT-R-8482113.

Sarpkaya T, 1978, The Hydrodynamic Resistance of Roughened Cylinders in Harmonic Flow, Trans Roy Inst Nav Archit, Vol 120, London.

Szebehely VG, 1959, Hydrodynamic Impact, Applied Mechanics Reviews, Vol 12, No. 5.

Wiegel RL, 1964, Oceanographical Engineering, Prentice-Hall International.

References in 3.6

Sarpkaya T and Isaacson M, 1981, Mechanics of Wave Forces on Offshore Structures, Van Nostrand Reinhold.

Sparks CP, 1980, Mechanical Behaviour of Marine Risers Mode of Influence of Principal Parameters, J of Energy Resources Technology, ASME, Vol 102, pp 214-222.

References in 3.7

Beckmann H and Merwin JE, 1979, Wave Forces on Conductor Pipe Group, Civ Eng in the Oceans IV, pp 700-715, San Francisco.

Bokaian A and Geoola F, 1985, Hydrodynamic Forces on a Pair of Cylinders, OTC 5007, Houston.

Bushnell MJ, 1976, Wave Forces on Cylinder Arrays, HRS Report EX 752, OT-R-7613.

Chakrabarti SK, 1979, Wave Forces on Vertical Array of Tubes, Civ Eng in the Oceans IV, pp 241-259, San Francisco.

Dalton C and Helfinstine RA, 1971, Potential Flow Past a Group of Cylinders, of Basic Engineering, ASME, pp 636-642.

Heideman JC and Sarpkaya T, 1985, Hydrodynamic Forces on Dense Arrays of Cylinders, OTC 5008, Houston.

Pearcey HH, Cash RF, Salter IJ and Boribund A, 1982, Interference Effects on the Drag Loading for Groups of Cylinders in Uni-Directional Flow, NMI R-130, OT-R-8256.

Sarpkaya T and Isaacson M, 1981, Mechanics of Wave Forces on Offshore Structures, Van Nostrand Reinhold.

Singh S, Cash R, Harris D and Boribond LA, 1982, Wave Forces on Circular Cylinders with Large Excrescences at Low Keulegan and Carpenter Numbers, NMI R 133, OT-R-8209.

Spring BH and Monkmeyer PL, 1974, Interaction of Plane Waves with Vertical Cylinders, Proceedings of the 14th Coastal Eng Conf, ASCE, Vol III, pp 1828-1827.

Verley RLP and Every MJ, 1977, Wave Induced Vibrations of Flexible Cylinders, OTC 2899, Houston.

Yamamoto T and Nath JH, 1976, Hydrodynamic Forces on Groups of Cylinders, OTC 2499, Houston.

Zdravkovich M, 1977, Review of Flow Interference Between Two Circular Cylinders in Various Arrangements, J of Fluids Engineering, ASME, Vol 99, Ser 1, No 4, pp 618-633.

Zdravkovich M, 1985, Forces on Pipe Clusters, Separated Flow around Marine Structures, pp 201-226, Trondheim.



ISBN 0 11 413324 7
Volume 1 of 2 Volumes
Not sold separately

HMSO publications are available from:

HMSO Publications Centre
(Mail and telephone orders only)
PO Box 276, London, SW8 5DT
Telephone orders 071-873 9090
General enquiries 071-873 0011
(queuing system in operation for both numbers)

HMSO Bookshops
49 High Holborn, London, WC1V 6HB 071-873 0011 (counter service only)
258 Broad Street, Birmingham, B1 2HE 021-643 3740
Southey House, 33 Wine Street, Bristol, BS1 2BQ (0272) 264306
9-21 Princess Street, Manchester, M60 8AS 061-834 7201
80 Chichester Street, Belfast, BT1 4JY (0232) 238451
71 Lothian Road, Edinburgh, EH3 9AZ 031-228 4181

HMSO's Accredited Agents
(see Yellow Pages)

and through good booksellers

£80.00 net (package price, two publications)

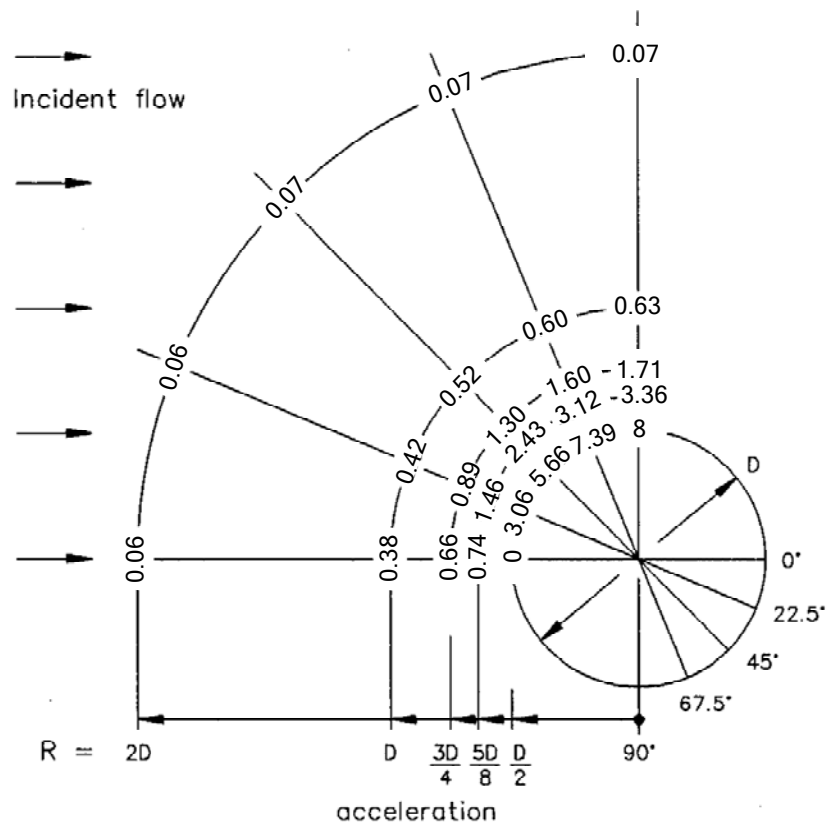


Figure 3.7.6. Convective acceleration around a cylinder (multiply above values by $(\text{incident velocity})^2 / D$)

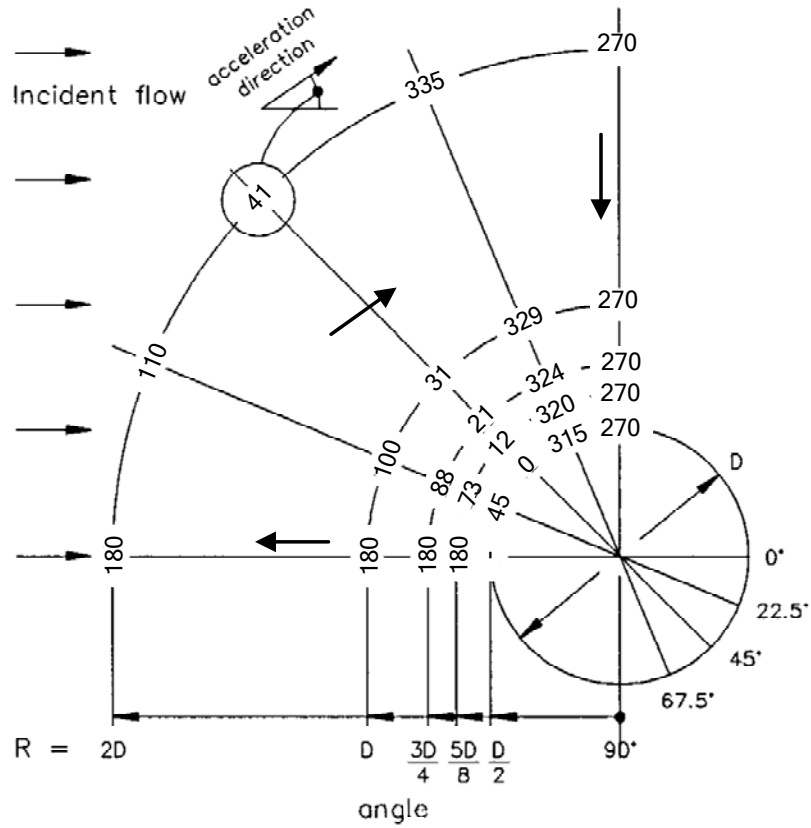


Figure 3.7.7. Direction of convective acceleration around a cylinder (degrees)

Note this page has been corrected: September 2008